

**STRUCTURAL AND BIOPHYSICAL INSIGHTS FROM TARGETING
MELANOMA USING GENETICALLY MODIFIED T-CELL
RECEPTORS**

**A Thesis Submitted in Requirement of
Cardiff University for the Degree of Doctor of Philosophy**

**Florian Madura
2013
School of Medicine**

A Papy et Tata

ACKNOWLEDGEMENTS

I would like to thank the Tenovus cancer charity for funding the research documented in this thesis.

To my main supervisor, Professor Andy Sewell, I would like to express my sincerest gratitude for giving me the opportunity to carry out this interesting project and to learn so many things. Thank you for the time you dedicated to me, for spending nights on proofreading my thesis and for helping me to develop as an independent scientist.

To my co-supervisor, Dr Dave Cole, thank you so much for your patience, your constant support and the good fun we had throughout my 3 years in Cardiff. It was good being one of your first students and I learnt a lot from you. Thanks for your dedication on proofreading my thesis, I owe you a lot!

Special thanks to Dr Pierre Rizkallah for his involvement in my work and for teaching me crystallography, to Kim Miles for being such a good teacher and to Dr John Bridgeman for his huge help regarding the tissue culture project. Many thanks to all those who participated in any way in the realization of this work. Thanks to all members of the “T-cell group” and all my PhD student friends, past and present, for making my time in Cardiff so enjoyable.

My last thanks “in English” goes to my friend Chris Holland, we had such a good time in Cardiff! Thanks for the Fish & Chips nights, the laugh and the support during the tough times and for spending so much time with me even if I was moaning a lot.

Merci à Bruno Laugel, ami et ancien coloc, parce qu'on s'est quand même bien marré !


Merci à Fabien Blanchet pour les pauses-café, les franches parties de rigolade, les longues discussions (scientifiques ou pas) ainsi que pour m'avoir accueilli pendant deux bonnes semaines à la fin de ma thèse.

Un grand merci à ma famille et future belle-famille, et plus particulièrement à mes parents. Papa et Maman vous avez toujours été là pour moi, toujours été présents dans ma vie et tout au long de ma scolarité. Votre soutien, qu'il soit moral, affectif ou financier, a été un facteur déterminant de ma réussite.

Enfin, merci à toi Emilie Charles, ma future femme. Les trois années passées loin de toi n'ont pas été faciles mais on y est arrivé. Tu as toujours cru en moi et m'as toujours soutenu, tu as su trouver les mots quand ça n'allait pas et je pouvais toujours compter sur toi. Maintenant c'est fini et une nouvelle vie commence pour nous deux.


DECLARATION

This work has not previously been accepted in substance for any degree and is not concurrently submitted in candidature for any degree.

Signed.....(candidate) Date:08/04/2013.....


Statement 1:

This thesis is being submitted in partial fulfilment of the requirements for the degree of PhD.

Signed.....(candidate) Date:08/04/2013.....

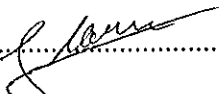
Statement 2:

This thesis is the result of my own independent work/investigation, except where otherwise stated. Other sources are acknowledged by explicit references.

Signed.....(candidate) Date:08/04/2013.....

Statement 3:

I hereby give consent for my thesis, if accepted, to be available for photocopying and for inter-library loan, and for the title and summary to be made available to outside organisations.

Signed.....(candidate) Date:08/04/2013.....

ABSTRACT

CD8⁺ T-cells recognise pathogens and cancer through a specific interaction between the T-cell receptor (TCR) and a 8-14 amino-acid residue peptide presented by class I major histocompatibility complex (pMHC) molecules expressed on the target cell surface. The first structures of murine and human TCR/pMHC complexes, published in 1996, revealed a number of important features of the TCR/pMHC interface. Currently, <25 unique human TCR/pMHC complexes are reported in the literature. This is a relatively low number compared with the number of antibody or unligated pMHC structures. The lack of structural information regarding human TCR/pMHC complexes has compromised the determination of a comprehensive and accepted set of rules that govern T-cell antigen recognition. Difficulties in generating TCR/pMHC complex crystals partly explain the low number of these structures. The first part of this thesis reports the development of a new crystallization screen (TOPS) designed specifically for the generation of such protein crystals. I also had access to MART-1-specific TCRs, the MART-1 protein being expressed by virtually all fresh melanoma tumour specimens. Different human leukocyte antigen (HLA)-A*0201-restricted peptides from this protein are presented at the melanoma cell surface. As TCRs are known to bind to cancer-derived “self” peptides with weak affinity, there is considerable interest in designing enhanced affinity TCRs for the recognition of HLA-A*0201-MART-1. My work concentrated on the MART-1-specific TCR MEL5 and its affinity-enhanced variant selected by phage display, α 24 β 17. I analysed the biophysical properties of α 24 β 17 and determined that it bound HLA-A*0201-MART-1 with >30,000-fold enhanced affinity and distinct thermodynamics. Comparison of TCR/HLA-A*0201-MART-1 complex structures solved with TOPS and binding biophysics showed that: (i) TCR affinity can be enhanced by increasing interactions between the TCR and the MHC surface; (ii) soluble α 24 β 17 retains the peptide specificity by a novel mechanism involving interactions with solvent molecules; and, (iii) MEL5 interaction with the physiologically relevant MART-1₂₇₋₃₅ nonameric antigen led to a peptide anchor residue switch, a TCR-induced modification that has never been observed before. I also initiated a preliminary study on the generation of genetically modified Jurkat cells and CD8⁺ T-cells expressing a range of affinity-enhanced TCRs directed against melanoma for adoptive cell therapy. These results suggested that melanoma specificity is retained after MEL5 transduction and that there is no need to optimize beyond a TCR affinity threshold to obtain optimal T-cell activation. Collectively, these data shed light on the complex and unpredictable nature of T-cell antigen recognition.

PUBLICATIONS

Miles KM, Miles JJ, **Madura F**, Sewell AK and Cole DK. *Real time detection of peptide-MHC dissociation reveals that improvement of primary MHC-binding residues can have a minimal, or no effect on complex stability*. Molecular Immunology. 2011 Jan;48(4):728-32.

Bulek AM*, Cole DK*, Skowera S, Dolton G, Gras S, **Madura F**, Fuller A, Miles JJ, Gostick E, Price DA, Drijfhout JW, Knight RR, Huang GC, Lissin N, Molloy PE, Wooldridge L, Jakobsen BK, Rossjohn J, Peakman M, Rizkallah PJ and Sewell AK. *Structural basis of human β -cell killing by CD8+ T cells in Type 1 diabetes*. Nature Immunology. 2012 Jan 15;13(3):283-9.

Bulek AM*, **Madura F***, Fuller A, Holland CJ, Schauenburg AJA, Sewell AK, Rizkallah PJ and Cole DK. *TCR/pMHC Optimized Protein crystallization Screen*. Journal of Immunological Methods. 2012 Aug 31;382(1-2):203-10.

Holland CJ, Rizkallah PJ, Vollers S, Calvo-Calle JM, **Madura F**, Fuller A, Sewell AK, Stern LJ, Godkin A and Cole DK. *Minimal conformational plasticity enables TCR cross-reactivity to different MHC class II heterodimers*. Scientific Reports. 2012 Sep 4, 2:629.

Ekeruche-Makinde J*, Clement M*, Cole DK*, Edwards ESJ, Ladell K, Miles JJ, Wynn K, Fuller A, Lloyd K, **Madura F**, Dolton GM, Pentier J, Lissina A, Gostick E, Baxter TK, Baker BM, Rizkallah PJ, Price DA, Wooldridge L and Sewell AK. *TCR optimized peptide skewing of the T-cell repertoire*. Journal of Biological Chemistry. 2012 Oct 26, 287(44):37269-81.

Submitted/under preparation

Madura F*, Rizkallah PJ*, Miles KM, Holland CJ, Bulek AM, Fuller A, Schauenburg AJA, Miles JJ, Liddy N, Malkit S, Li Y, Hossain M, Baker BM, Jakobsen BK, Sewell AK and Cole DK. *Specificity of an enhanced affinity T-cell receptor maintained by altered thermodynamics*. 2013 (Manuscript submitted)

Madura F et al. *A melanoma specific TCR induces a peptide anchor residue switch*. 2013 (Manuscript in preparation)

*Shared first authorship

TABLE OF CONTENTS

ACKNOWLEDGEMENTS.....	3
DECLARATION.....	4
ABSTRACT.....	5
PUBLICATIONS.....	6
TABLE OF CONTENTS.....	7
LIST OF FIGURES.....	16
ABBREVIATIONS.....	21
1 CHAPTER 1 INTRODUCTION.....	24
1.1 General concepts of adaptive immunity.....	26
1.2 T-cells.....	27
1.2.1 Conventional T-cells.....	27
1.2.2 Unconventional T-cells.....	30
1.3 The shaping of the T-cell repertoire.....	32
1.3.1 TCR gene assembly.....	32
1.3.2 T-cell selection.....	34
1.3.3 T-cell activation and differentiation.....	37
1.3.4 Immunological synapse.....	38
1.4 Peptide processing and presentation by MHCI molecules.....	39
1.5 Structural basis of TCR/pMHC recognition.....	42
1.5.1 Introduction to X-ray crystallography.....	42
1.5.2 Structure of pMHCI.....	45
1.5.3 Structure of $\alpha\beta$ TCR.....	47
1.5.4 General features of TCR binding revealed from TCR/pMHC structures..	49

1.6 Biophysical basis of TCR/pMHC recognition	53
1.6.1 Introduction to Surface Plasmon Resonance and biophysics.....	53
1.6.1.1 Basis of SPR.....	54
1.6.1.2 Kinetic and affinity parameters.....	56
1.6.1.3 Thermodynamic parameters.....	57
1.6.2 TCRs bind to pMHCs with weak affinity and relatively slow kinetics	60
1.6.3 Thermodynamic features of TCR/pMHC interaction	61
1.7 TCR triggering models	62
1.8 Improving TCR affinity.....	65
1.8.1 Selection of high-affinity TCRs using allo-restriction.....	65
1.8.2 Rational design of high-affinity TCRs.....	67
1.8.3 Display technologies	68
1.9 Aims of the thesis.....	72
2 CHAPTER 2 MATERIALS AND METHODS.....	73
2.1 Bacterial cell culture	76
2.1.1 Culture medium and bacterial strains.....	76
2.1.2 Transforming competent cells.....	76
2.2 Molecular biology.....	77
2.2.1 Plasmids	77
2.2.1.1 Vectors for protein expression	77
2.2.1.2 Vectors for the production of lentivirus.....	78
2.2.2 Cloning of a range of different affinity TCRs toward melanoma into a lentiviral vector	78
2.2.3 Enzymatic digestion.....	80
2.2.4 Agarose gel purification and ligation.....	80

2.3 Protein chemistry	81
2.3.1 Protein expression as inclusion bodies.....	81
2.3.2 Refolding of pMHCI.....	82
2.3.3 Refolding of soluble TCR.....	83
2.3.4 Fast Protein Liquid Chromatography (FPLC) purification.....	84
2.3.5 Sodium dodecyl sulphate – Polyacrylamide gel electrophoresis and SimplyBlue™ staining.....	85
2.3.6 Biotinylation of pMHCI and manufacture of pMHCI tetramer.....	85
2.4 Surface Plasmon Resonance.....	86
2.4.1 Equilibrium-binding analyses	87
2.4.2 Kinetic analyses	87
2.5 Crystallography.....	89
2.5.1 Crystallisation conditions for $\alpha 24\beta 17$, A2-ELA-4A and $\alpha 24\beta 17$ /pMHCI complexes.....	89
2.5.2 Crystallisation conditions for MEL5/A2-AAG and MEL5/A2-EAA complexes.....	89
2.5.2.1 MEL5/A2-AAG: different TCR/pMHCI complexes mixing.....	89
2.5.2.2 MEL5/A2-EAA: seeding from MEL5/A2-AAG	91
2.5.3 X-ray diffraction data collection, molecular replacement and model refinement	91
2.6 Mammalian cell culture.....	92
2.6.1 Mammalian cell culture medium	92
2.6.2 Cell lines	93
2.6.3 Cryopreservation and storage of cell lines.....	96
2.6.4 Cell counting by Trypan exclusion	96

2.7	Generation of transduced Jurkat and CTL lines	96
2.7.1	Lentivirus production	96
2.7.2	Jurkat TCR negative GLuc transduction and sorting	97
2.7.3	CTL transduction	98
2.7.3.1	CTL sorting from peripheral blood mononuclear cells (PBMCs)	98
2.7.3.2	CTL transduction, sorting and expansion	99
2.8	Flow cytometry analysis	100
2.9	Jurkat activation assay	100
2.10	CTL effector function assays	101
2.10.1	Peptide titration assay	101
2.10.2	Peptide library screen	101
2.10.2.1	A description of positional scanning combinatorial peptide libraries (PS-CPLs)	101
2.10.2.2	Peptide library screen assay	102
2.10.3	ELISA (Enzyme-linked immunosorbent assay) for MIP1 β	102
2.10.4	Chromium release assay	103
3	CHAPTER 3 DEVELOPMENT OF A TCR/pMHC OPTIMIZED PROTEIN CRYSTALLIZATION SCREEN	105
	Chapter background	106
3.1	Introduction	106
3.1.1	Methods for producing recombinant TCRs	107
3.1.2	Methods for improving TCR stability	108
3.1.3	Generating crystals for high resolution X-ray diffraction	109
3.1.4	Aim	111
3.2	Results	111

3.2.1	Design of a TCR/pMHC Optimized Protein crystallization Screen	111
3.2.2	Comparison of TOPS efficiency with commercially available screens...	115
3.2.3	Optimal conditions for the generation of TCR/pMHC complex crystals	120
3.2.4	TOPS efficiency correlated to the datasets obtained in this screen	123
3.3	Discussion.....	126
4	CHAPTER 4 T-CELL RECEPTOR HIGH AFFINITY AND SPECIFICITY BASED ON FAVOURABLE ENTROPY	128
	Chapter background.....	130
4.1	Introduction	130
4.1.1	Therapeutic application of monoclonal antibodies	132
4.1.1.1	“Naked” or unconjugated monoclonal antibody therapy	132
4.1.1.2	Conjugated monoclonal antibody therapy	133
4.1.1.3	Bispecific antibody therapy.....	134
4.1.2	Monoclonal TCRs	135
4.1.3	Aim.....	138
4.2	Results	138
4.2.1	Production and purification of soluble TCRs and pMHCs for this study	138
4.2.2	$\alpha 24\beta 17$ TCR binds to A2-ELA with high affinity due to an extended off-rate	143
4.2.3	MEL5 and $\alpha 24\beta 17$ TCRs use a similar binding mode to engage A2-ELA	143
4.2.4	Enhanced TCR-MHC interactions govern the high affinity binding of the $\alpha 24\beta 17$ TCR.....	151
4.2.5	The $\alpha 24\beta 17$ TCR is highly sensitive to peptide substitutions.....	154

4.2.6	Peptide substitutions do not alter the overall conformation of the $\alpha 24\beta 17/A2$ -ELA complex.....	157
4.2.7	Peptide substitutions do not directly alter the contact interface between the $\alpha 24\beta 17$ TCR and A2-ELA	158
4.2.8	Peptide substitutions do not alter the overall conformation of unligated A2-ELA molecules.....	161
4.2.9	Peptide specificity is governed by a distinct thermodynamic signature and a reduction in water bridges	164
4.3	Discussion.....	171
5	CHAPTER 5 STRUCTURAL AND BIOPHYSICAL COMPARISON OF TCR BINDING TO NATURAL VARIANT HLA-A2-RESTRICTED MELANOMA PEPTIDES.....	175
	Chapter background.....	177
5.1	Introduction.....	177
5.1.1	Conformational changes observed upon TCR recognition	178
5.1.1.1	TCR flexibility on pMHC engagement.....	179
5.1.1.2	MHC flexibility on pMHC engagement	179
5.1.1.3	Peptide flexibility on pMHC engagement.....	180
5.1.2	Structural observations of the common HLA-A2-restricted melanoma antigens	180
5.1.3	Aim.....	183
5.2	Results	183
5.2.1	Production and purification of soluble TCRs and pMHCs	183
5.2.2	MEL5 and $\alpha 24\beta 17$ TCR binding to natural MART-1 antigens.....	185
5.2.3	Protein crystallization.....	188

5.2.4	Structures of MEL5 and $\alpha 24\beta 17$ complexed to A2-EAA and A2-AAG	190
5.2.5	The high affinity of $\alpha 24\beta 17$ toward MART-1 _{26/27-35} is due to an increase in the interaction between the TCR and the MHC	190
5.2.6	Binding mechanisms of two melanoma-specific TCRs to the HLA-A2-restricted EAAGIGILTV MART-1 antigen	193
5.2.7	The MEL5 TCR distinguishes EAA with ELA due to an enhanced flexibility of the natural decamer	195
5.2.8	TCR binding to A2-AAGIGILTV induces a peptide anchor switch	197
5.2.9	Different binding mechanisms of recognition for MEL5/AAG _{bulged} and MEL5/AAG _{stretched}	203
5.2.10	Reduction in interactions between MEL5 TCR and A2-AAG results in weaker binding affinity	205
5.2.11	The binding of MEL5 and $\alpha 24\beta 17$ to A2-AAG leads to a gain of enthalpy and entropy compared to the binding to A2-EAA	207
5.3	Discussion	213
6	CHAPTER 6 ENGINEERING T-CELLS WITH AN OPTIMIZED TCR AGAINST MELANOMA	218
	Chapter background	220
6.1	Introduction	220
6.1.1	TCR gene transfer	221
6.1.2	Vectors for transfer of TCR genes	223
6.1.3	Optimised transfer of an $\alpha\beta$ TCR	224
6.1.3.1	Choosing a transgene cassette	224
6.1.3.2	Choosing a transfer vector	225
6.1.4	Choosing a tumour antigen to target	228

6.1.5	Enhanced affinity TCRs	228
6.1.6	Potential problems with TCR gene transfer of enhanced TCRs	229
6.1.6.1	TCR chain mispairing	229
6.1.6.2	Engineered TCRs bypass thymic editing	231
6.1.6.3	TCRs exhibit an affinity/dwell time optimum for T-cell activation	232
6.1.7	Aim.....	233
6.2	Results	233
6.2.1	Testing of MEL5 TCR transduction in Jurkat cells	233
6.2.2	Transduction of primary HLA A2 ⁺ CD8 ⁺ T-cells with MEL5 TCR	236
6.2.3	Peptide specificity of HLA A2 ⁺ CD8 ⁺ T-cells transduced with MEL5 TCR	240
6.2.4	Transduction of Jurkat TCR negative GLuc with a panel of affinity- enhanced TCRs	244
6.2.5	Jurkat TCR negative GLuc cells transduced with enhanced affinity melanoma-specific TCRs reveal an unexpected glycosylation site	248
6.2.6	An affinity optimum for T-cell activation in the MEL5 system	250
6.3	Discussion.....	250
7	CHAPTER 7 GENERAL DISCUSSION.....	256
7.1	Implications of my results	257
7.1.1	New crystallization screening improves study of TCR/pMHC recognition	257
7.1.2	Enhanced MHC contacts mediate TCR high affinity without loss of specificity	260
7.1.3	A novel thermodynamic mechanism mediates high-affinity TCR specificity	261

7.1.4	A new molecular mechanism of TCR/pMHC recognition	261
7.1.5	Heteroclitic peptides can alter T-cell antigen specificity due to changes at the atomic level	263
7.1.6	MEL5 TCR gene transfer generates melanoma-specific T-cells	265
7.1.7	Detrimental motifs can be introduced during TCR affinity maturation...	265
7.1.8	An optimal TCR affinity for TCR gene therapy against melanoma	267
7.2	Perspectives.....	268
7.3	Summary.....	269
	REFERENCES.....	270
	APPENDICES.....	294

LIST OF FIGURES

Figure 1.1. Simplified schematic representation of thymocyte development from the double negative (DN) to the single positive (SP) stages.....	36
Figure 1.2. Class I MHC antigen processing pathway.....	40
Figure 1.3. Schematic representation of the phase and energy diagrams for crystallization of proteins.....	43
Figure 1.4. Crystal structure of HLA-A2 in complex with an heteroclitic melanoma peptide (FLTGIGITV) to represent the overall structure of pMHCI..	46
Figure 1.5. Crystal structure of melanoma specific TCR DMF5 to represent the overall structure of $\alpha\beta$ TCR.	48
Figure 1.6. Crystal structure of the type 1 diabetes autoreactive 1E6 TCR complexed to HLA-A2 presenting the preproinsulin (PPI) self peptide PPI ₁₅₋₂₄ to represent the overall structure of $\alpha\beta$ TCR/pMHCI complex.....	50
Figure 1.7. Schematic representation of Surface Plasmon Resonance.	55
Figure 1.8. Schematic representation of the different display technologies to increase TCR affinity.	69
Figure 3.1. Schematic representations of the different methods to increase soluble TCRs stability.	110
Figure 3.2. Analysis of the crystallization conditions of 16 previously published TCR/pMHC complexes.....	114
Figure 3.3. Comparison of TCR/pMHC structures obtained in my laboratory in TOPS and TOPS screen-derived versus commercially available screens.	119
Figure 3.4. Analysis of crystallization conditions obtained from 25 TCR/pMHC complexes.....	122

Figure 3.5. Analysis of the frequency of appearance of a particular condition. ..	124
Figure 3.6. Representation of the expected TOPS efficiency correlated to the datasets obtained with that screen based on the implemented scoring system.	125
Figure 4.1. Differences in antigen recognition between mAbs and TCRs.....	137
Figure 4.2. Example of inclusion bodies purity and anion exchange purification step.	140
Figure 4.3. Gel filtration examples and purity of proteins for crystallography and biophysical analysis.	141
Figure 4.4. Gel filtration, protein crystal and high-resolution diffraction pattern of the $\alpha 24\beta 17/A2$ -ELA complex.....	142
Figure 4.5. Binding affinity and kinetic analysis of the HLA A2-ELAGIGILTV specific wildtype MEL5 TCR and the high-affinity TCR, $\alpha 24\beta 17$	144
Figure 4.6. 2Fo-Fc electron density maps for all structures reported in this chapter.	146
Figure 4.7. Structural analysis of the binding mode implemented by MEL5 <i>versus</i> $\alpha 24\beta 17$ when interacting with A2-ELA.....	149
Figure 4.8. Structural differences between the MEL5 TCR <i>versus</i> $\alpha 24\beta 17$ TCR when interacting with A2-ELA.....	150
Figure 4.9. The $\alpha 24\beta 17$ mutated residues make an increased number of contacts with the MHC surface compared to MEL5 wildtype residues.....	153
Figure 4.10. $\alpha 24\beta 17$ is extremely sensitive to alanine substitutions within the ELAGIGILTV peptide.	156
Figure 4.11. Structural comparison of the binding mode implemented by $\alpha 24\beta 17$ when interacting with A2-ELA, A2-ELA4A and A2-ELA7A.	159

Figure 4.12. Interactions between $\alpha 24\beta 17$ and modified residues in the ELAGIGILTV peptide at positions 4 and 7.....	160
Figure 4.13. Alanine substitutions do not alter the overall conformation of the unligated A2-ELA related pMHCs.	163
Figure 4.14. Thermodynamic analysis of the $\alpha 24\beta 17$ /A2-ELA interaction.	165
Figure 4.15. Thermodynamic analysis of the $\alpha 24\beta 17$ /A2-ELA4A interaction. ..	166
Figure 4.16. Thermodynamic analysis of the $\alpha 24\beta 17$ /A2-ELA7A interaction. ..	166
Figure 4.17. Thermodynamic analysis of $\alpha 24\beta 17$ binding to A2-ELA, A2-ELA4A and A2-ELA7A.	167
Figure 4.18. $\alpha 24\beta 17$ undergoes large TCR CDR movement during ligand engagement.	168
Figure 4.19. $\alpha 24\beta 17$ makes more water bridges with A2-ELA than with A2-ELA4A and A2-ELA7A.	170
Figure 5.1. Atomic structures of AAGIGILTV and EAAGIGILTV complexed to HLA-A2.	182
Figure 5.2. Binding affinities of the MEL5 and $\alpha 24\beta 17$ TCRs with A2-EAA and A2-AAG.	186
Figure 5.3. Co-purification by gel filtration of $\alpha 24\beta 17$ /A2-EAA and $\alpha 24\beta 17$ /A2-AAG complexes for crystallography.	189
Figure 5.4. Structural differences in the TCR V α domain between MEL5 and $\alpha 24\beta 17$ bound to A2-AAG and A2-EAA.	194
Figure 5.5. Peptide contacts between the MEL5 TCR and A2-EAA.	194
Figure 5.6. Binding mechanism of $\alpha 24\beta 17$ /A2-EAA.	196
Figure 5.7. Structural differences between MEL5/A2-EAA and MEL5/A2-ELA.	196

Figure 5.8. 2Fo-Fc peptide electron density maps for all structures reported in this chapter.....	198
Figure 5.9. Stretched and bulged conformations of AAG during MEL5 binding.	200
Figure 5.10. AAG peptide anchor residue switch during MEL5 binding.....	201
Figure 5.11. Structural differences in the peptide conformation between the unligated A2-AAG and $\alpha 24\beta 17$ /A2-AAG structures.....	202
Figure 5.12. Different mechanisms of recognition for MEL5/AAG _{bulged} and MEL5/AAG _{stretched}	204
Figure 5.13. Structural differences in the MEL5 interaction with the first peptide residue of EAA, AAG _{stretched} and AAG _{bulged}	206
Figure 5.14. Thermodynamic analysis of the MEL5 interaction with A2-AAG and A2-EAA.	208
Figure 5.15. Thermodynamic analysis of the $\alpha 24\beta 17$ interaction with A2-AAG.	209
Figure 5.16. Thermodynamic analysis of the $\alpha 24\beta 17$ interaction with A2-EAA.	210
Figure 5.17. Thermodynamic analysis of the MEL5 and $\alpha 24\beta 17$ interactions with A2-EAA and A2-AAG.....	211
Figure 6.1. Schematic representation of adoptive cell therapy process.	222
Figure 6.2. Schematic representation of the “third generation” lentivirus system used in this study.....	226
Figure 6.3. Schematic representation of $\alpha\beta$ TCR mispairing after TCR gene transfer.....	230

Figure 6.4. Schematic representation of the vectors and transgene cassette for the production of lentivirus.	234
Figure 6.5. Transduction of Jurkat TCR negative GLuc cells with a lentivirus for the expression of rCD2 and MEL5 TCR.	235
Figure 6.6. Transduction of primary HLA A2 ⁺ CD8 ⁺ T-cells with a lentivirus for the expression of rCD2 and MEL5 TCR	237
Figure 6.7. MEL5 TCR transduced primary T-cells recognise HLA A2 ⁺ targets pulsed with cognate peptide and natural levels of antigen presented on the surface of melanoma cells.	239
Figure 6.8. Decameric peptide PS-CPL activation assay of the MEL13 clone. ...	241
Figure 6.9. Decameric peptide PS-CPL activation assay of the MEL5 transduced A2 ⁺ CD8 ⁺ T-cells.	242
Figure 6.10. Box plot summary of the PS-CPL activation assays for MEL13 clone and MEL5 transduced A2 ⁺ CD8 ⁺ T-cells.....	243
Figure 6.11. Transduction of Jurkat J.RT3-T3.5 GLuc cells with a lentivirus for the expression of six MEL5 TCR mutants.....	247
Figure 6.12. Threshold of melanoma-specific TCR affinity for maximum T-cell activation.....	249

ABBREVIATIONS

A2: HLA*0201
ACT: Adoptive cell therapy
ADCC : Antibody-dependent cell-mediated cytotoxicity
AIRE: Autoimmune regulator
AML: Acute myeloid leukaemia
APC: Allophycocyanin
APC: Antigen-presenting cell
BCR: B-cell receptor
BiTE : Bispecific T-cell Engaging
BSA : Buried surface area
CAR: Chimeric antigen receptor
CD (number): Cluster of differentiation (number)
CDD: Charge-coupled device
CDR: Complementarity determining region
CMV: Cytomegalovirus
cPPT : Central polypurine tract
CTL: Cytotoxic T lymphocyte
DC: Dendritic cell
DLS: Diamond Light Source
DN: Double negative
DNA: Deoxyribonucleic acid
DNA-PK: DNA-dependent protein kinase
DP: Double positive
DTT: Dithiothreitol
E. coli: Escherichia coli
EDC: 1-ethyl-3-(3-dimethylpropyl)-carboiimide
EF-1 : Elongation factor-1
ELISA: Enzyme-linked immunosorbent assay
EpCAM : Epithelial cell adhesion molecule
ER: Endoplasmic reticulum
ERAAP: Endoplasmic reticulum aminopeptidase associated with antigen processing
Fab: Fragment antigen binding
FACS : Fluorescence activated cell sorting
FCS: Foetal calf serum
FDA : Food and Drug Administration
FITC: Fluorescein isothiocyanate
FPLC: Fast Protein Liquid Chromatography
FW: Framework region
GO : Gemtuzumab ozogamicin
GOI: Gene of interest
H-bond: Hydrogen bond
HIV: Human immunodeficiency virus
HLA: Human leukocyte antigen
HTLV: Human T-lymphotropic virus
HV4: Hypervariable region 4
IB: Inclusion body

IFN- γ : Interferon γ
 Ig: Immunoglobulin
 IL (number) : Interleukine (number)
 ImmTAC : Immune-mobilizing monoclonal TCR against cancer
 iNKT: Invariant Natural Killer T-cell
 IPTG : Isopropyl β -D-1-thiogalactopyranoside
 IRES : Inter-ribosomal entry site
 ISP: Immature single positive
 ITAM: Immunoreceptor tyrosine-based activation motif
 ITC: Isothermal Titration Calorimetry
 K_A : Equilibrium association constant
 K_D : Equilibrium dissociation constant
 k_{off} / k_d : Dissociation rate constant
 k_{on} / k_a : Association rate constant
 KP: Kinetic proofreading
 LB: Luria-Bertani
 LTR: Long terminal repeat
 LV: Lentiviral vector
 mAb: Monoclonal antibody
 MAIT: Mucosal-associated invariant T-cell
 MART-1: Melanoma antigen recognized by T-cells 1
 Mdm2: Murine double-minute 2
 Melan-A: Melanoma antigen A
 MHC I: Class I major histocompatibility complex
 MHC II: Class II major histocompatibility complex
 MIP: Macrophage inflammatory protein
 MM-GBSA : Molecular Mechanics-Generalized Born Surface Area
 MR1: MHC-related molecule 1
 MWCO : Molecular weight cut-off
 NFAT: Nuclear Factor of Activated T-cells
 NHS: N-hydroxysuccinimide
 NK: Natural Killer
 NKT: Natural Killer T-cells
 NOD/SCID : nonobese diabetic–severe combined immunodeficiency
 OD₂₈₀: Optical density at 280 nm
 OD₆₀₀: Optical density at 600 nm
 PAGE: Polyacrylamide gel electrophoresis
 PBMC: Peripheral blood mononuclear cell
 PBS: Phosphate Buffer Saline
 PCR: Polymerase chain reaction
 PE: R-phycoerythrin
 PEG: Polyethylene glycol
 PHA: Phytohaemagglutinin
 pMHC: Peptide-MHC complex
 PS-CPL : Positional scanning combinatorial peptide libraries
 R factor: Reliability factor
 RAG: Recombinase-activating gene
 rCD2: Rat CD2
 RNA: Ribonucleic acid
 rpm: Revolutions per minute

RRE : Rev response element
RSV : Rous sarcoma virus
RT : Room temperature
RU: Response or Resonance Unit
RV: γ -retroviral vector
SB: Salt bridge
SC: Shape complementarity
scTCR : Single-chain TCR
SDM: Site-directed mutagenesis
SDS: Sodium dodecyl sulfate
SIN : Self-inactivating
siRNA : Small interfering RNA
SMAC: Supramolecular activation clusters
SP: Single positive
SPR: Surface Plasmon Resonance
ST: Serial triggering
SV40: Simian virus 40
 $t_{1/2}$: Half-life
TAA: Tumour-associated antigen
TAP: Transporter associated with antigen processing
TCR: T-cell receptor
TdT: terminal deoxynucleotidyl transferase
TGF β : Tumour growth factor β
 T_H : Helper T-cell
TIL: Tumour-infiltrating lymphocyte
TNF- α : Tumour necrosis factor α
TOPS: TCR/pMHC Optimized Protein crystallisation Screen
TOPSORT: TCR-optimized peptide skewing of the repertoire of T-cells
 T_{reg} : Regulatory T-cell
TSA : Tumour-specific antigen
vdW : van der Waals
VSV-G : Vesicular stomatitis virus glycoprotein
WPRE : Woodchuck Hepatitis Post-transcriptional Regulatory Element
wt: Wild-type
WT1: Wilms tumour antigen-1
ZFN : Zinc-finger nuclease
 $\beta 2m$: $\beta 2$ -microglobulin
 ΔC_p° : Specific heat capacity
 ΔG° : Standard Gibbs free energy
 ΔH° : Enthalpy
 ΔS° : Entropy

CHAPTER 1

INTRODUCTION

1.1	General concepts of adaptive immunity	26
1.2	T-cells	27
1.2.1	Conventional T-cells	27
1.2.2	Unconventional T-cells	30
1.3	The shaping of the T-cell repertoire	32
1.3.1	TCR gene assembly.....	32
1.3.2	T-cell selection.....	34
1.3.3	T-cell activation and differentiation.....	37
1.3.4	Immunological synapse.....	38
1.4	Peptide processing and presentation by MHCI molecules	39
1.5	Structural basis of TCR/pMHC recognition	42
1.5.1	Introduction to X-ray crystallography.....	42
1.5.2	Structure of pMHCI	45
1.5.3	Structure of $\alpha\beta$ TCR.....	47
1.5.4	General features of TCR binding revealed from TCR/pMHC structures ..	49
1.6	Biophysical basis of TCR/pMHC recognition	53
1.6.1	Introduction to Surface Plasmon Resonance and biophysics.....	53
1.6.1.1	Basis of SPR.....	54
1.6.1.2	Kinetic and affinity parameters	56
1.6.1.3	Thermodynamic parameters	57
1.6.2	TCRs bind to pMHCs with weak affinity and relatively slow kinetics	60
1.6.3	Thermodynamic features of TCR/pMHC interaction	61

1.7 TCR triggering models	62
1.8 Improving TCR affinity.....	65
1.8.1 Selection of high-affinity TCRs using allo-restriction.....	65
1.8.2 Rational design of high-affinity TCRs.....	67
1.8.3 Display technologies	68
1.9 Aims of the thesis.....	72

1.1 GENERAL CONCEPTS OF ADAPTIVE IMMUNITY

The human immune system provides defence against pathogens by triggering two broadly defined types of immunity: innate immunity and adaptive immunity. Both types of immunity usually work together for effective pathogen clearance (Medzhitov and Janeway, 2000). Innate immunity relies on phagocytes (monocytes, macrophages and neutrophils), cells that release inflammatory mediators (basophils, mast cells and eosinophils), natural killer (NK) cells as well as components of the complement system and lies behind most inflammatory responses (Delves and Roitt, 2000a). My work focussed on adaptive immunity which general concepts are discussed herein.

Adaptive immunity is controlled by immune cells called lymphocytes. There are two types of lymphocyte, B and T lymphocytes. Lymphocytes express antigen-binding receptors that are manufactured by gene rearrangement of germline gene segments. This process, described in detail below, has the capacity to produce huge numbers of individual receptors that each exhibit a different binding specificity (Davis and Bjorkman, 1988). The principal roles of B-cells are to secrete immunoglobulins (Igs), the antigen-specific antibodies responsible for the suppression of extracellular micro-organisms, and to perform antigen exposure to T-cells when specialized into antigen-presenting cells (APCs) (Delves and Roitt, 2000a; Delves and Roitt, 2000b). The principal roles of T-cells are to: (i) promote immunity against intracellular and extracellular pathogens by activating innate immunity cells and B-cells (helper T-cells, T_{HS}) (Cavani et al., 2012; King et al., 2008; Ma et al., 2010; Zelante et al., 2009); (ii) promote immunosuppression to avoid autoimmunity and to prevent immune response from becoming uncontrolled (regulatory T-cells, T_{RegS}) (Boehm,

2011; Dong and Martinez, 2010); and, (iii) eliminate pathogens by killing virally infected cells and cancer cells (cytotoxic T-cells, CTLs) (Boehm, 2011; Laugel et al., 2011). One of the most important aspects of adaptive immunity is its ability to generate immunological memory, the capacity to “recall” previous infections and to react more rapidly upon subsequent antigen exposure (Delves and Roitt, 2000a). The process of vaccination where a deliberate exposure to a harmless version of a pathogen, or a specific antigen from a pathogen, is used to generate memory cells that can provide immediate protection to future infections is dependent on this important recall function (Medzhitov and Janeway, 2000).

1.2 T-CELLS

As my work has focussed on a particular aspect of adaptive immunity mediated by T-cells, the rest of my thesis will focus on these important cells. T-cells develop in the thymus from common lymphoid progenitors arising from the bone marrow or foetal liver. Broadly speaking, T-cells can be divided into “conventional” T-cells and “unconventional” T-cells.

1.2.1 Conventional T-cells

Most T-cells bearing an $\alpha\beta$ TCR, made from the $V\alpha$ and $V\beta$ genes, and expressing a co-receptor (CD4 or CD8) are conventional T-cells that recognise protein antigens in the form of short peptides (Lefranc, 1990) (**Table 1.1**). The vast majority of T-cells in human or mouse peripheral blood or lymphoid organs are conventional T-cells and it is this subset that has received most attention to date. Conventional T-cells recognise protein antigens that have been processed and presented in a binding groove of molecules called Major Histocompatibility Complex (MHC) molecules.

Table 1.1. Conventional T-cell classes adapted from (Dong and Martinez, 2010; Murphy, 2012)

Class	Subset	Co-receptor expressed on T-cell membrane
Helper T-cell (T_H)	T_{H1} , T_{H2} , T_{H3} , T_{H9} , T_{H17} , T_{H22} and T follicular helper cell (T_{FH})	CD4
Regulatory T-cell (T_{Reg})	T_{R1} , natural T_{Reg} , inducible T_{Reg} (iT_{Reg}) and CD8 $\alpha\alpha$ T-cell	CD4 or CD8 $\alpha\alpha$
Cytotoxic T-cell (CTL)	CD8 $\alpha\beta$ T-cell	CD8 $\alpha\beta$

Thus, T-cells are said to exhibit “MHC restriction” (Zinkernagel and Doherty, 1974; Zinkernagel and Doherty, 1997). These peptide-MHC (pMHC) complexes are recognised by the TCR which engages both the peptide and MHC components of the bipartite antigen (Garboczi et al., 1996; Garcia et al., 1996; Townsend and Bodmer, 1989; Townsend et al., 1985).

The conventional $\alpha\beta$ T-cells lineage is divided into two subsets: $CD4^+$ T-cells restricted by class II MHC (MHCII) and $CD8^+$ T-cells restricted by MHCI (Bluestone et al., 2009; Laugel et al., 2011). The $CD4^+$ subset includes the T_{HS} and T_{RegS} whereas the $CD8^+$ subset usually represents the CTLs (Murphy et al., 2008). However, cytotoxic $CD4^+$ T-cells have also been identified (Fleischer, 1984; Marshall and Swain, 2011) and some $CD8^+$ T-cells have regulatory functions (Laugel et al., 2011; Terry et al., 1990). $CD8^+$ T-cells can be divided into two subsets depending on which form of the co-receptor they are expressing ($CD8\alpha\alpha$ homodimer or $CD8\alpha\beta$ heterodimer). $CD8\alpha\alpha$ intraepithelial T-cells have been found in the gut and can have regulatory functions through the production of IL-10 and TGF β (Leishman et al., 2001; Terry et al., 1990) but their role is less well-understood than $CD8\alpha\beta$ T-cells (Laugel et al., 2011). $CD8\alpha\beta$ T-cells (known as T_C or $CD8^+$ CTL) can kill infected and transformed cells via production of cytolytic molecules such as perforin and granzymes A and B (Delves and Roitt, 2000a). $CD8\alpha\beta$ T-cells can protect the host from cancer and viral infections (Laugel et al., 2011). $CD8\alpha\beta$ T-cells also secrete “type-1” (IL-2, TNF- α and IFN- γ) or “type-2” cytokines (IL-4, IL-5, IL-6, IL-10 and IL-13) (Croft et al., 1994; Inui et al., 2001; Seder et al., 1992), however these cytokine profiles were first described for $CD4^+$ T-cells (Mosmann et al., 1986). Although $CD8^+$ T-cells play an important role in suppressing viral infection, the

CD8⁺ T-cell mediated response to cancer is usually less effective (Miles et al., 2010). Moreover, CD8⁺ T-cells are also implicated in other health-related problems such as organ transplant rejection (Mannon et al., 1998) and autoimmunity (Agostini et al., 1993; Bulek et al., 2012a). Although my work has been focussed on conventional T-cells, I provide a description of unconventional T-cell types below for the sake of completeness.

1.2.2 Unconventional T-cells

There are various types of unconventional T-cells (Gapin, 2009). All $\gamma\delta$ T-cells are thought to recognise unconventional ligands and to fall in this category. The $\gamma\delta$ T-cell lineage represents a small percentage of the T-cell population in peripheral blood (~1-10%) but these cells are abundant in tissues, especially in epithelial layers (Pang et al., 2012; Plattner and Hostetter, 2011). $\gamma\delta$ T-cells express a heterodimeric TCR made from the V γ and V δ genes. $\gamma\delta$ T-cells have been conserved throughout vertebrate evolution and are therefore likely to perform a very important function. $\gamma\delta$ T-cells can recognize antigens such as phospho-antigens, lipids and glycolipids presented by MHC complex-related proteins (“non-classic MHC”) (Hayday, 2009) but can also recognize antigens directly just as antibody molecules do (Bukowski et al., 1994; Johnson et al., 1992). Another unconventional T-cell subset, described as mucosal-associated invariant T-cells (MAIT) (Porcelli et al., 1993; Treiner et al., 2005), recognize microbial vitamin B metabolites presented by the MHCIIb molecule MR1 (MHC-related molecule 1) (Kjer-Nielsen et al., 2012; Treiner et al., 2003). MAITs bear an $\alpha\beta$ TCR made from the V α 7.2 and J α 33 variable genes in humans and V α 19 and J α 33 variable genes in mice (Gapin, 2009). The invariant TCR α chain has also been found to preferentially associate with a limited number of TCR β

chains (V β 2 and V β 13 in humans and V β 6 and V β 8 in mice) (Treiner et al., 2005). It has been suggested that MAIT cells could have a positive role in regulating Ig A secretion in the intestine (Treiner et al., 2003; Treiner and Lantz, 2006) or could have immunoregulatory functions in autoimmunity (Croxford et al., 2006). Other unconventional T-cells are recognizing antigens presented by an MHC I-related protein, the CD1 molecule. CD1 molecules present diverse lipid antigens and are classified into group 1 (comprising CD1a, CD1b and CD1c) and group 2 (containing only CD1d); CD1e molecule being considered intermediate (Murphy, 2012). T-cells that recognize lipids presented by CD1 express neither CD4 nor CD8. Among these T-cells, another known important unconventional T-cell subset is called natural killer T (NKT) cells (Kronenberg, 2005). The most commonly described group of NKT cells is the Type 1 or invariant NKT (iNKT) subset that is involved in immunity to infectious disease, autoimmunity and in tumour surveillance (Gapin, 2010; Juno et al., 2012). Human iNKT cells use an invariant TCR V α 24-J α 18 chain associated with variant TCR V β 11 chains to recognize lipid antigens presented by the non-polymorphic MHC Ib molecule CD1d (Brennan et al., 2012; Davodeau et al., 1997; Porcelli and Modlin, 1999). Bacterial (Kinjo et al., 2006) and self (Brennan et al., 2012) iNKT ligands have been described but no viral-associated ligands have been reported so far despite iNKT activation during viral infection (Juno et al., 2012). Finally, a glycolipid not produced by mammals that strongly activate iNKT cells, namely α -galactosylceramide (α -GalCer), is one the best characterized iNKT TCR ligand due to its potential as a vaccine adjuvant and is widely used in the study of iNKT TCRs/CD1d interactions (Borg et al., 2007; Gadola et al., 2002; Gadola et al., 2006; Juno et al., 2012).

1.3 THE SHAPING OF THE T-CELL REPERTOIRE

1.3.1 TCR gene assembly

The recombination mechanism leading to the assembly of antigen receptors is common for both B-cells and T-cells and was first described for antibodies (Tonegawa, 1983). The initial observation, that the sequences of Ig genes in mature B-cells were different of that from embryonic tissues (Tonegawa, 1983), was crucial for the understanding of antigen receptor diversity generation. The process of functional B-cell receptor (BCR) and TCR gene assembly is called somatic recombination (or somatic rearrangement) and involves congregation of sequentially ordered random segmental germline DNA rearrangements of the variable (V), diversity (D) and joining (J) gene segments under the control of recombinase-activating genes 1 and 2 (RAG-1 and RAG-2) (Bonilla and Oettgen, 2010). The human germline TCR α locus (on chromosome 14) is constituted of 70-80 V, 61 J and 1 constant (C) segments whereas the TCR β locus (on chromosome 7) is constituted of 52 V, 2 D, 13 J and 2 C segments (Murphy et al., 2008). The overall variety of rearranged DNA fragments during somatic recombination is the result of both combinatorial and junctional diversity (Schatz, 2004). The combinatorial diversity relies on both the number of germline gene segments that can combine at either the TCR α or β locus and the pairing of the randomly generated α and β chains. However, the combination of germline gene segments is restricted by the facts that not all segmental gene rearrangements are equally likely to occur and that random pairing of the TCR chains does not always produce a functional TCR (Boehm, 2011). Junctional diversity can produce a “random” nucleotide region in each TCR chain using P-nucleotides (generating palindromic sequences) and N-nucleotides (non-templated nucleotides) absent in the germline DNA. This

randomisation process is active during the joining of VJ segments (α chain) or the joining of DJ segments followed by the joining of VDJ segments (β chain) (Schatz, 2004). Up to 20 N-nucleotides can be added by the TdT (terminal deoxynucleotidyl transferase) enzyme at the blunt ends before ligation of the DNA while the Artemis:DNA-PK (DNA-dependent protein kinase) complex mediates the insertion of P-nucleotides at the ends of asymmetrical DNA fragments generated during excision of the non-coding segments (Murphy et al., 2008; Schatz, 2004). The junctional diversity is considered to introduce most of the TCR genetic variability and it is believed that T-cells have the ability to generate 10^{15} - 10^{20} unique TCRs from a limited number of genes (Arstila et al., 1999; Davis and Bjorkman, 1988; Nikolich-Zugich et al., 2004).

The clonal selection theory (Jerne, 1955; Jerne, 1971) suggested that individual lymphocytes are specific for a single antigen only, an idea that was widely accepted. The ability of V(D)J rearrangements to produce a theoretical 10^{15} - 10^{20} unique TCRs meant that the TCR repertoire could be extensive enough to recognise the $>10^{15}$ potential foreign peptides (Sewell, 2012). Consequently, the clonal selection theory of T-cell recognition remained largely unchallenged prior to seminal work by Mason (Mason, 1998; Sewell, 2012). Mounting evidence now excludes theories based around a single TCR for each peptide antigen (Mason, 1998; Sewell, 2012). It has been estimated that the human naive T-cell pool is constituted by less than 10^8 distinct $\alpha\beta$ TCRs (Arstila et al., 1999) and it has been shown that the T-cell clone expressing the 1E6 TCR was able to respond to over 10^6 decameric peptides (Wooldridge et al., 2012). Hence, extensive T-cell cross-reactivity provides a

potential mechanism for how a limited TCR repertoire can provide broad antigenic cover (Sewell, 2012).

1.3.2 T-cell selection

T-cell progenitors originate from foetal liver and bone marrow stem cells and migrate to the thymus where they mature into T-cells before populating peripheral lymphoid organs (Delves and Roitt, 2000a). Thymic education is a spatially and temporally regulated process in which thymocytes undergo several morphological and genetic differentiation steps based on MHC restriction. The process is characterised by the differential expression of various phenotypic cell-surface markers and leads to the selection of T-cells expressing a functional TCR. Developing $\alpha\beta$ T-cells undergo an extensive selection that shapes the mature repertoire of T-cells to ensure self-MHC restriction as well as self tolerance in processes called positive and negative selection (Starr et al., 2003). The different stages of thymocyte development can be discriminated with the differential expression of the co-receptors CD4 and CD8.

First, progenitor cells differentiate into double negative (DN, CD4⁻ CD8⁻) thymocytes in the thymic stroma with the rearrangement of the germline DNA described in the previous section. Thymocyte precursors first rearrange their TCR β gene and the product of the rearranged allele is then expressed on the thymocyte surface as part of a pre-TCR complex consisting of the CD3 components and the pre-T α invariant chain that comprises only the constant region (Bosselut, 2004). The cells then migrate to the thymic cortex where the rearrangement of the TCR α chain occurs, and the product of the rearranged allele associates with the TCR β and the

CD3 complex potentially forming a functional $\alpha\beta$ TCR (Bosselut, 2004; Chaplin, 2010). DN thymocytes differentiate first into immature CD8 single positive (ISP) cells and then into double positive (DP) cells that express low levels of a clonotypic TCR and both the CD4 and CD8 co-receptors before positive selection (Bosselut, 2004; Murphy et al., 2008) (**Figure 1.1**). Cells are positively selected by receiving survival signals if they express a TCR with an intermediate affinity for self pMHCs expressed on epithelial cells in the thymic cortex and they mature into CD4 or CD8 single positive (SP) cells (Delves and Roitt, 2000a). Thymocytes expressing a TCR that has a very low or no affinity for pMHC complexes are thought to “die by neglect” as they are unlikely to be useful and do not receive a survival signal. It is believed that about 90% of T-cell precursors are not selected at this stage and therefore die by neglect in the thymus (Palmer and Naeher, 2009). At both the DP and SP stages, cells expressing a TCR with a high affinity for self pMHC molecules are deleted in the process called negative selection (Kappler et al., 1987). These potentially harmful self-reactive T-cells are eliminated by induction of apoptosis when they interact with dendritic cells and macrophages in the thymic medulla (Delves and Roitt, 2000a). Moreover, the expression of some, but not all, tissue-specific proteins in the thymic medulla is controlled by a gene called *AIRE* (autoimmune regulator) (Metzger and Anderson, 2011). Hence, intrathymic negative selection could apply even to proteins that are otherwise restricted to tissues outside the thymus. The autoimmune regulator protein AIRE, expressed in medullary stromal cells, interacts with several proteins involved in transcription and seems to lengthen transcripts from promoters that would otherwise terminate (Murphy, 2012).

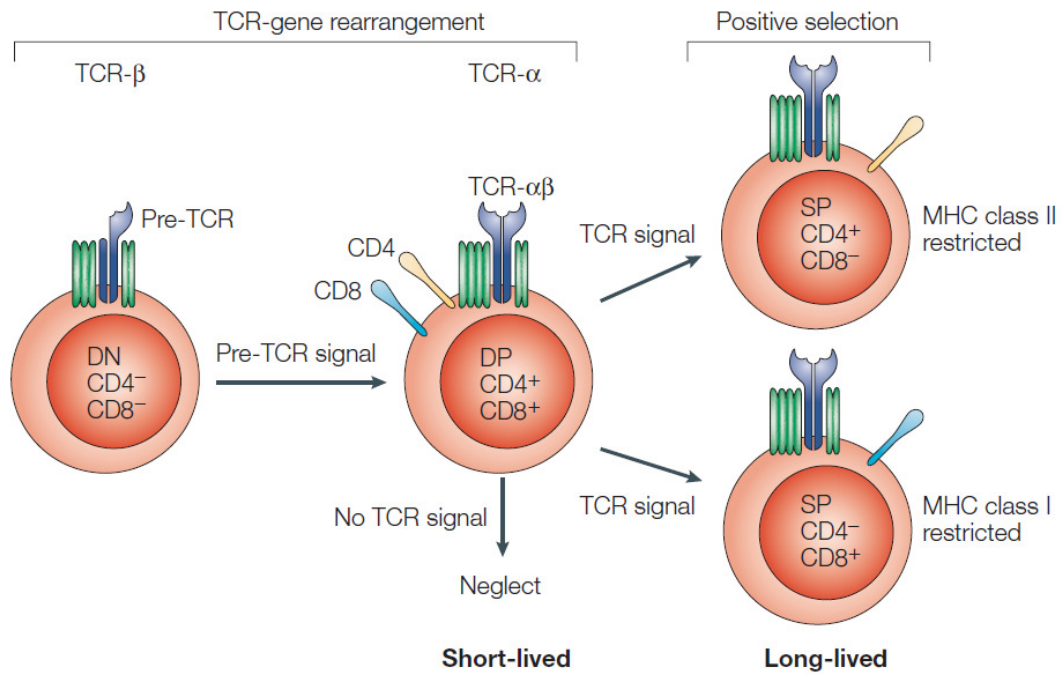


Figure 1.1. Simplified schematic representation of thymocyte development from the double negative (DN) to the single positive (SP) stages.

Thymocyte precursors enter the thymus and rearrange their TCR β gene. The product of the rearranged allele is then expressed on the thymocyte surface as part of a pre-TCR complex which also includes the pre-T α invariant chain and CD3 components. Cells differentiate into double positive (DP) thymocytes that rearrange their TCR α gene and express a clonotypic $\alpha\beta$ TCR. Cells with intermediate avidity for self pMHC complexes survive and differentiate into mature CD8⁺ T-cells and CD4⁺ T-cells while those with low or no avidity die by neglect (positive selection). Figure from (Bosselut, 2004).

These two processes of selection ensure that only T-cells with a relatively weak affinity for self-peptide/MHC populate the periphery (Alam et al., 1996; Liu et al., 1998).

1.3.3 T-cell activation and differentiation

Differentiation of CD4⁺ and CD8⁺ naïve T-cells into effector T-cells in the peripheral immune organs is initiated through signals from APCs. These signals may be contact-dependent through surface molecules or soluble factors like cytokines (Delves and Roitt, 2000a; Delves and Roitt, 2000b). The required signalling can be grouped into three types of signals: 1, 2 and 3 (Murphy, 2012). Signal 1, the antigen specific signal, is the interaction between the TCR and its cognate pMHC on the APC. Signal 1 alone leads to T-cell inactivation by anergy or apoptosis, often resulting in antigen tolerance (Murphy, 2012). APCs that can activate naïve T-cells bear cell-surface proteins known as co-stimulatory molecules or co-stimulatory ligands. These interact with naïve T-cell-surface receptors, known as co-stimulatory receptors, to transmit a signal that is required along with signal 1 for T-cell activation; this signal is called signal 2 (Delves and Roitt, 2000a). The best understood of these co-stimulatory receptors is the cell-surface protein CD28. CD28 is present on the surface of all naïve T-cells and binds the co-stimulatory ligands B7.1 (CD80) and B7.2 (CD86) which are expressed mainly on specialized APCs such as dendritic cells (Murphy et al., 2008). Signal 2 drives the T-cell towards an activation state referred to as T_H0 (Delves and Roitt, 2000a). This state is characterized by sustained proliferation, surface-marker up-regulation and a mixed cytokine expression profile. Signal 3, also transmitted by the APC, drives CD4⁺ and CD8⁺ T-cell differentiation into effector cells (Thomas, 2004). This signal conveys

crucial information on the pathogen and infected tissue. The different T-cell subtypes (**Table 1.1**) are associated with distinct signals that induce their formation, different transcription factors that drive their differentiation and unique cytokines and surface markers that define their identity (Murphy et al., 2008; Thomas, 2004).

1.3.4 Immunological synapse

In addition to the co-receptor CD4 or CD8, the $\alpha\beta$ TCR is associated on the T-cell surface with the CD3 complex. The main role of the CD3 machinery is to transduce signals to the interior of the cell when the TCR contacts its cognate pMHC (Delves and Roitt, 2000a; Delves and Roitt, 2000b). T-cell activation also involves antigen-independent cell-cell interactions including CD2 (LFA-2), CD40L, LFA-1 and CD28 located on the T-cell surface which contact CD58 (LFA-3), CD40, ICAM-1 and CD80 (B7.1)/CD86 (B7.2) on the surface of APCs, respectively (Murphy, 2012). On encounter of an APC, a T-cell initiates a process of cell surface molecular rearrangement culminating in the formation of organised cell-cell interfaces called “immunological synapse” or supramolecular activation clusters (SMAC) (Alarcon et al., 2011; Grakoui et al., 1999). The SMAC is organised into (i) a central area (cSMAC) in which the TCR/CD3 complex, its co-receptors CD4 or CD8 and the co-stimulatory protein CD28 are positioned for optimal interaction with pMHC, CD80 and CD86 on the APC; and (ii) a peripheral area (pSMAC) where LFA-1, CD43, CD45 and ICAM-1 are sequestered. These latter molecules located in the pSMAC regulate the activity initiated by the cSMAC members (Alarcon et al., 2011; Davis and Dustin, 2004).

1.4 PEPTIDE PROCESSING AND PRESENTATION BY MHCI MOLECULES

Human MHC molecules are called human leukocyte antigens (HLAs). These MHC glycoproteins bind peptide fragments of proteins that have been synthesized within the cell or that have been phagocytosed by the cell. Peptides derived from exogenous proteins are assembled with MHCII proteins on the surface of specialized antigen presenting cells (APCs) such as macrophages and dendritic cells (DC). Peptides from endogenous proteins are presented by MHCI that are found at the surface of almost all nucleated cells. This elegant system allows T-cells to inspect the internal proteome for anomalies. MHCI molecules are composed of a 44 kDa polymorphic transmembrane α heavy chain associated with the 12 kDa non-polymorphic β 2-microglobulin (β 2m) protein (Bjorkman, 1997). In humans, the heavy chain of the 3 major class I HLA molecules (HLA-A, HLA-B and HLA-C) and β 2m are encoded by distinct genes on chromosome 6 and chromosome 15, respectively. Protein fragments are generated from cellular proteins through the action of the proteasome, a proteolytic machinery composed of more than 25 subunits, and are presented in the context of MHCI molecules in a process referred as the MHCI antigen processing pathway (**Figure 1.2**) (Niedermann, 2002). The main role of the proteasome is the degradation of proteins as part of normal cellular homeostasis and it is therefore constitutively expressed in almost all cells (Tanaka et al., 2012; Zoeger et al., 2006). The proteasome contains multiple active protease sites spaced in such a way that they digest proteins into peptide fragments of different length (Mazza and Malissen, 2007; Probst-Kepper et al., 2004). If a pathogenic threat is detected, release of IFN γ by cells such as macrophages signals a transformation of the proteasome into an immunoproteasome (Kloetzel and Ossendorp, 2004).

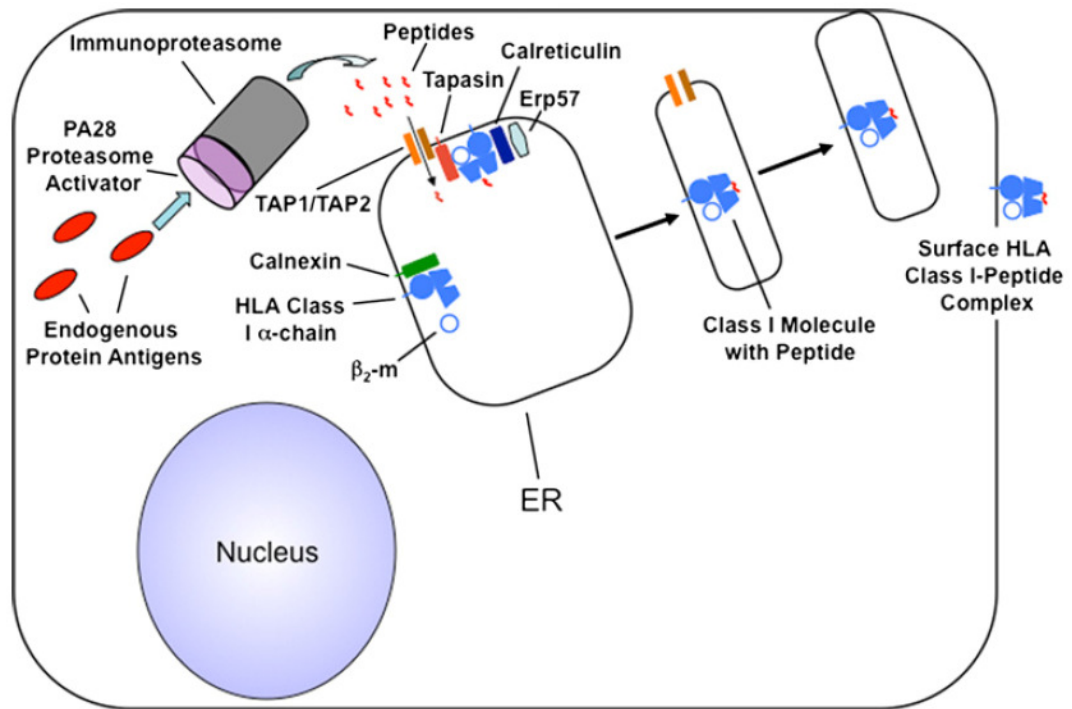


Figure 1.2. Class I MHC antigen processing pathway.

Antigenic proteins found within the cell (endogenous antigens) are degraded into peptides by the immunoproteasome and transported into the endoplasmic reticulum (ER) via the transporter associated antigen processing proteins (TAP 1 and TAP 2). Some of these peptides bind to class I MHC with the help of chaperone proteins calreticulin, Erp57 and calnexin and are transported to the cell surface for immune surveillance by CD8⁺ T-cells. Figure from (Chaplin, 2010).

The immunoproteasome differs from the proteasome in three catalytic subunits (LMP2, MECL1 and LMP) and it produces peptides of the appropriate length for transport into the endoplasmic reticulum (ER) and with carboxy-terminal residues that are preferred anchor residues for binding to most MHCI (Kloetzel and Ossendorp, 2004; Murphy, 2012). Proteasomal cleavage fragments are transported to the ER via a transporter system consisting of two ATP-binding cassette subunits, the transporter associated with antigen processing 1 and 2 (TAP 1 and TAP 2). Peptides in the ER might require further processing before loading onto MHCI and an ER-resident aminopeptidase ERAAP (Endoplasmic reticulum aminopeptidase associated with antigen processing, known as ERAP1 in humans) is implicated in this process (Kloetzel and Ossendorp, 2004). Studies have shown that ERAAP is required for the generation of the normal repertoire of MHCI peptides (Hammer et al., 2006) and that ERAP1 trims precursor peptides by a “molecular ruler” mechanism (Chang et al., 2005). 8-14 residue-long peptides are eventually generated and the loading of peptide into the peptide-binding groove of the class I HLA heavy chain inside the ER occurs under the direction of the protein tapasin with the help of chaperone proteins calreticulin and Erp57 (Garbi et al., 2006; Momburg and Tan, 2002). The peptide-MHCI (pMHCI) heavy chain complex is stabilized by the chaperone protein calnexin which dissociates when β 2m binds (Chaplin, 2010). The pMHCI complex is then transported through the Golgi apparatus to the cell surface in exocytic vesicles. Interestingly, despite “exogenous” antigens being presented by class II MHC, studies have shown that under certain circumstances these antigens can also be presented by class I MHC (Chaplin, 2010). This phenomenon, designated as “cross-presentation”, plays an important role in antiviral immunity as some viruses have the ability to suppress the class II MHC endogenous pathway of antigen presentation (Sigal et al.,

1999). Cell surface expressed pMHC I can then be sampled by CD8⁺ T-cells. Since my work was funded to focus on the recognition of MHC I-restricted peptides by tumour-specific TCRs, I will not go into further detail about MHC class II.

1.5 STRUCTURAL BASIS OF TCR/pMHC RECOGNITION

1.5.1 Introduction to X-ray crystallography

The resolution of light microscopy is limited by the wavelength of visible light. This makes mitochondria, at about 500 nm in diameter, the smallest cellular structures visible by light microscopy (Henze and Martin, 2003; McCoy, 2009). Proteins are even smaller, the majority ranging from 4 to 6 nm in diameter; over 100 times smaller than the wavelength of red visible light (approximately 1000 nm) (Polikarpov et al., 1997). Resolving structure at the atomic level requires the use of radiation with a wavelength in the X-ray range, about 1 Å (0.1 nm) (McCoy, 2009; Polikarpov et al., 1997). However, as X-rays cannot be focused by a lens in the same way as visible light to create an image of the object, obtaining a protein structure at atomic resolution using X-rays requires very different methodology. The first step involves generating crystals of the molecule of interest in order to obtain a well ordered arrangement of molecules that will provide a diffraction pattern when exposed to X-rays. Crystallization occurs when the concentration of protein in solution is greater than its limit of solubility. The limit of solubility can be reached by slowly increasing the concentration of precipitant (such as polyethylene glycol (PEG) or a salt) in a protein solution. Under most conditions the protein will precipitate when it reaches its limit of solubility. However, under some conditions, it can enter a supersaturated meta-stable phase and it is from this phase that crystals form (Asherie, 2004) (**Figure 1.3A**).

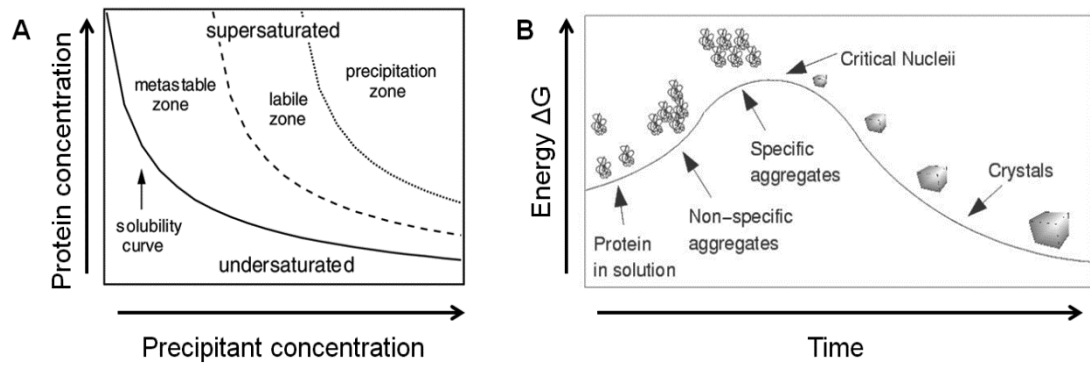


Figure 1.3. Schematic representation of the phase and energy diagrams for crystallization of proteins.

(A) Representation of a phase diagram showing the solubility of a protein in solution depending on the concentration of precipitant. Figure adapted from (Asherie, 2004).
 (B) Representation of an energy diagram showing that an activation barrier must be overcome for the crystallization of proteins to occur (nucleation). Figure adapted from (McCoy, 2009).

For a protein to crystallize, it must overcome an energy barrier analogous to that of conventional chemical reactions. The high-energy intermediate is the "critical nucleus" that seeds crystal growth (McCoy, 2009) (**Figure 1.3B**). Protein crystals are arranged as lattices containing several repeating units ("unit cells") organized and oriented in a regular fashion. After being grown, protein crystals are soaked in cryoprotectant (such as glycerol or ethylene glycol), cryo-cooled in liquid nitrogen (100K) and then brought to an X-ray beam facility such as a synchrotron (Garman, 1999; Zhao, 2011). When the X-ray beam hits the protein crystal, the molecular electron clouds scatter the X-rays to form a diffraction pattern (or reflections) that can be recorded on photographic film (Blundell and Johnson, 1976) or measured on a charge-coupled device (CCD) detector (Smyth and Martin, 2000). In order to collect a full set of diffraction patterns from every angle required to build a 3D picture, the protein crystal is rotated through 180 degrees. One obstacle that comes up from the use of X-ray crystallography is the "phase problem". Each reflection has an intensity and a phase angle, but only the intensities can be measured by the detector. In order to solve the three-dimensional protein structure, the phase information can be recovered by 2 methods: "experimental phasing" using heavy-atoms incorporated in the protein crystal (Garman and Murray, 2003; McCoy and Read, 2010) and "molecular replacement" using a known molecular model to solve the unknown crystal structure of a related molecule (Evans and McCoy, 2008). Electron density maps can be generated using both amplitude and phase information and are used to solve the three-dimensional structure of the protein. Once the initial structure of the protein has been modelled, the model undergoes rounds of refinement to ensure that the experimental data fit the observed data obtained from the new structure (Smyth and Martin, 2000). An indicator of model quality is the *R*

factor (or Reliability factor), which calculates the discrepancy (%) between the observed and calculated amplitudes (Smyth and Martin, 2000). An R factor near 20% is considered acceptable (Brunger, 1992). The final refined protein structure will allow the understanding of the physical mechanisms by which proteins perform their functions.

1.5.2 Structure of pMHCI

Human pMHCI is composed of the HLA α heavy chain non-covalently associated to β 2m and a peptide (**Figure 1.4**). The heavy chain comprises 3 extracellular domains (α 1, α 2 and α 3) (**Figure 1.4A**), a transmembrane domain and a short intracellular domain that anchors in the cell membrane. Structurally, α 1 and α 2 domains are formed of a long α helix and several anti-parallel β -sheets. The MHC α 1-helix and α 2-helix form the sides of the peptide-binding groove and the β -sheets form the base of the groove (**Figure 1.4A&B**). The α 3 domain forms an immunoglobulin-type fold that consists of 5 antiparallel β -sheets (**Figure 1.4A**). The β 2m molecule is mainly made of 6 anti-parallel β -sheets (**Figure 1.4A**) (Madden, 1995; Rudolph et al., 2006).

The peptide binding groove has been described in terms of “pockets” or “sub-sites” (A to F), with each pocket composed of diverse amino acid sequences that alter the shape and chemical composition of the groove (Saper et al., 1991) (**Figure 1.4B**). In HLA-A*0201 (the most common Caucasian allele), the MHC B pocket generally accommodates peptide positions 1 or 2, while the C-terminus of the peptide binds to the MHC F pocket.

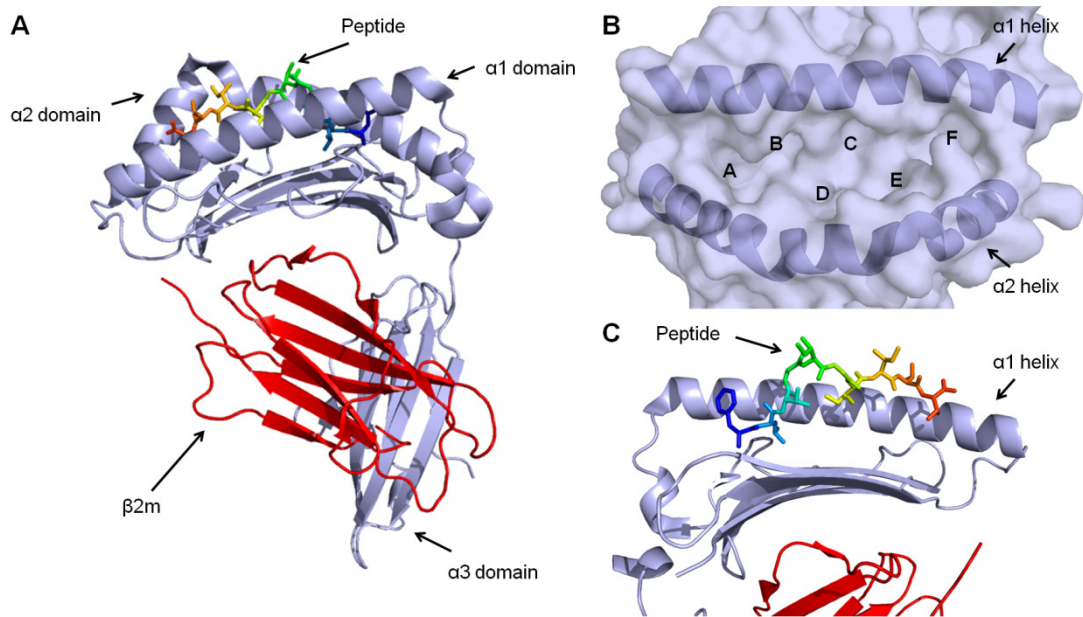


Figure 1.4. Crystal structure of HLA-A2 in complex with an heteroclitic melanoma peptide (FLTGIGITV) to represent the overall structure of pMHCI.

(A) pMHCI is composed of an α heavy chain (α 1, α 2 and α 3 domains in blue cartoon) non-covalently associated to β 2m (red cartoon). The peptide (rainbow stick) binds in the MHC binding groove formed by the α 1 and the α 2 domains. (B) Schematic representation from above the peptide binding groove showing the MHC binding pockets (A-F) as described in (Saper et al., 1991). (C) The peptide conformation in MHC is generally characterised by a prominent central bulge allowing TCR/peptide interaction. Figure adapted from the A2-FLT structure published in (Ekeruche-Makinde et al., 2012).

This anchoring is essential to stabilise pMHC at the cell surface during presentation, and allows other peptide residues to form the classical ‘peptide-bulge’ that generally contact the TCR during T-cell recognition of MHC I-restricted peptides (Borbulevych et al., 2007; Rudolph et al., 2006) (**Figure 1.4C**).

1.5.3 Structure of $\alpha\beta$ TCR

The $\alpha\beta$ TCR, an heterodimeric glycoprotein formed by a disulfide-linked α and β chain, is stabilized by an extracellular, membrane-proximal, inter-chain disulfide bond at the T-cell surface. The $\alpha\beta$ TCR is structurally similar to an antibody Fab fragment (**Figure 1.5A**) (Garcia et al., 1999; Rudolph et al., 2006). The α and β chains contain a constant (C) domain that anchors into the T-cell membrane (via a linker) and a variable (V) Ig-like domain that contacts the pMHC I. Each domain is constituted by several anti-parallel β -sheets linked together by short α -helices and intra-domain disulfide bonds allow the immunoglobulin fold (**Figure 1.5A**) (Garcia et al., 1999; Rudolph et al., 2006). The C domains are relatively conserved for all $\alpha\beta$ TCRs, with $C\alpha$ being more acidic and $C\beta$ being more basic, hence a highly polar $C\alpha/C\beta$ interface involved in TCR pairing (Garcia et al., 1999; Turner et al., 2006). The V domains are composed of 3 hypervariable complementarity determining regions (CDR1-3) loops and another loop on the V domains called the hypervariable region 4 (HV4) (Garcia et al., 1996) or framework region (FW) (Miles et al., 2010) that contact both the MHC and the peptide (**Figure 1.5B**). CDRs 1 and 2 are encoded within the V gene segments (as described in section 1.3.1), but CDR3 loops are also made from junctional diversity (Turner et al., 2006).

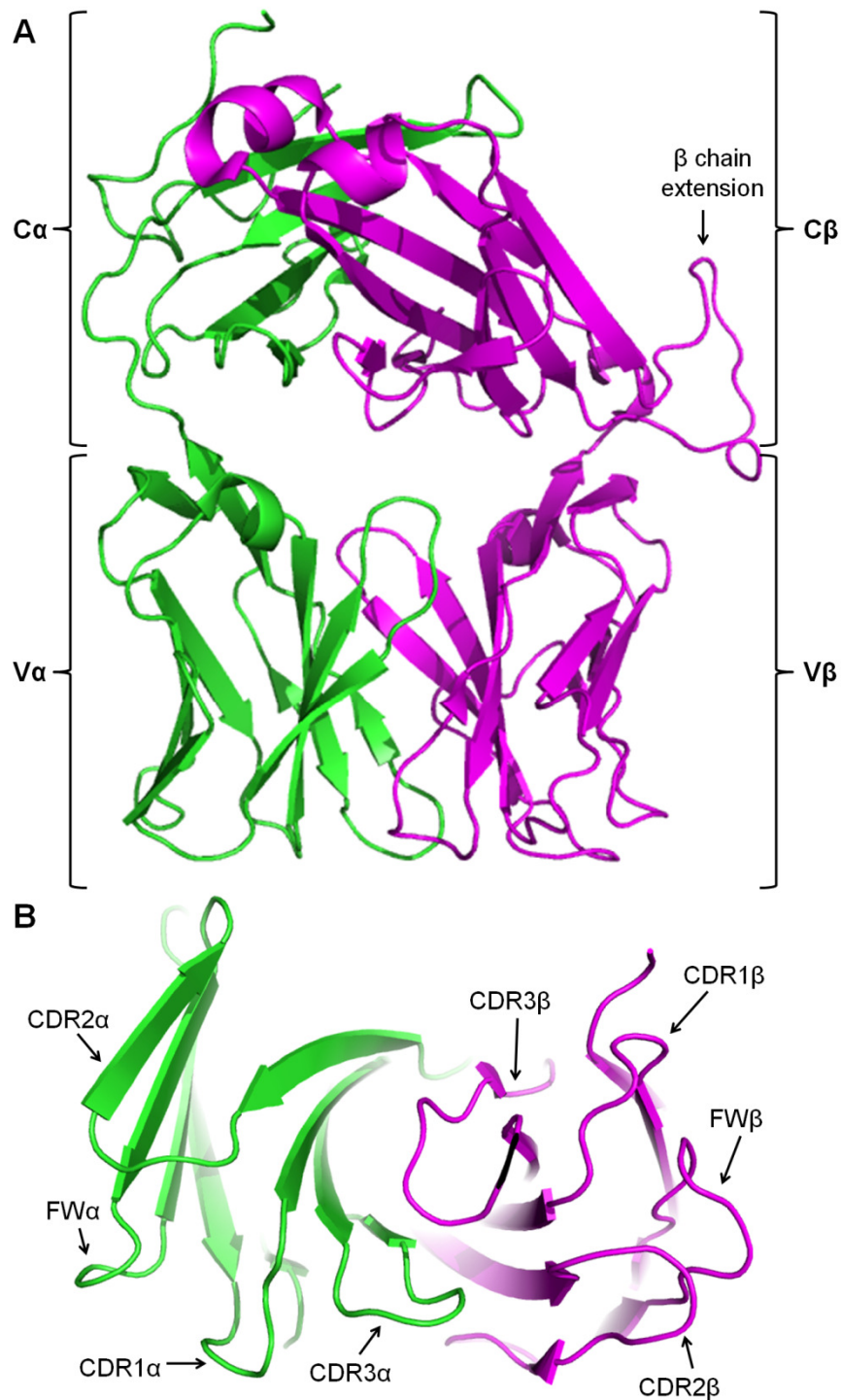


Figure 1.5. Crystal structure of melanoma specific TCR DMF5 to represent the overall structure of $\alpha\beta$ TCR.

(A) The $\alpha\beta$ TCR consists of a disulfide linked α (green cartoon) and β (pink cartoon) chain, with the CDR loops at the bottom of the V domains. The C domains (top) are relatively conserved for all $\alpha\beta$ TCRs with the C β domain presenting an extended loop. (B) View from below of the CDR and FW loops of the TCR variable region. Figure adapted from the DMF5 TCR structure published in (Borbulevych et al., 2011).

1.5.4 General features of TCR binding revealed from TCR/pMHC structures

The crystal structures of several TCR/pMHC complexes (**Figure 1.6A**) have been solved and reviewed (Rudolph et al., 2006; Turner et al., 2006). TCRs bind to pMHCs in a diagonal docking mode with a “crossing angle” ranging from 22° to 70° and a mean around 35° (**Figure 1.6B**). The V α domain mainly lies over the N-terminus of the peptide and the MHC α 2-helix whereas the V β domain lies mainly over the C-terminus of the peptide and the MHC α 1-helix (**Figure 1.6C**), this fixed polarity being common to all TCR/pMHC complexes reported to date (Garcia et al., 2009; Rudolph et al., 2006). The CDR loops have different roles during antigen recognition because of their position on the pMHC surface with the CDR2 loops contacting mainly the MHC helices, the more variable somatically rearranged CDR3 loops contacting mainly the peptide and the peptide-proximal regions of the MHC helices and the CDR1 loops in-between (Cole et al., 2009). HV4s have also been found to contact the MHC and/or the peptide (Borbulevych et al., 2011; Miles et al., 2010). Due to the fixed polarity, a number of TCR docking mode theories have been proposed (Colf et al., 2007; Mazza and Malissen, 2007) including the peptide-centric model where the TCR/peptide contacts determine the CDR1 and CDR2 footprint on the MHC helices and permits optimal contacts to be formed with the MHC surface (Sherman and Chattopadhyay, 1993) and the MHC-centric model where the shared structural determinants on MHC recognized by CDR1 and CDR2 determine the docking mode with disregard for the peptide or prior to peptide scanning by the hypervariable CDR3 loops (Daniel et al., 1998).

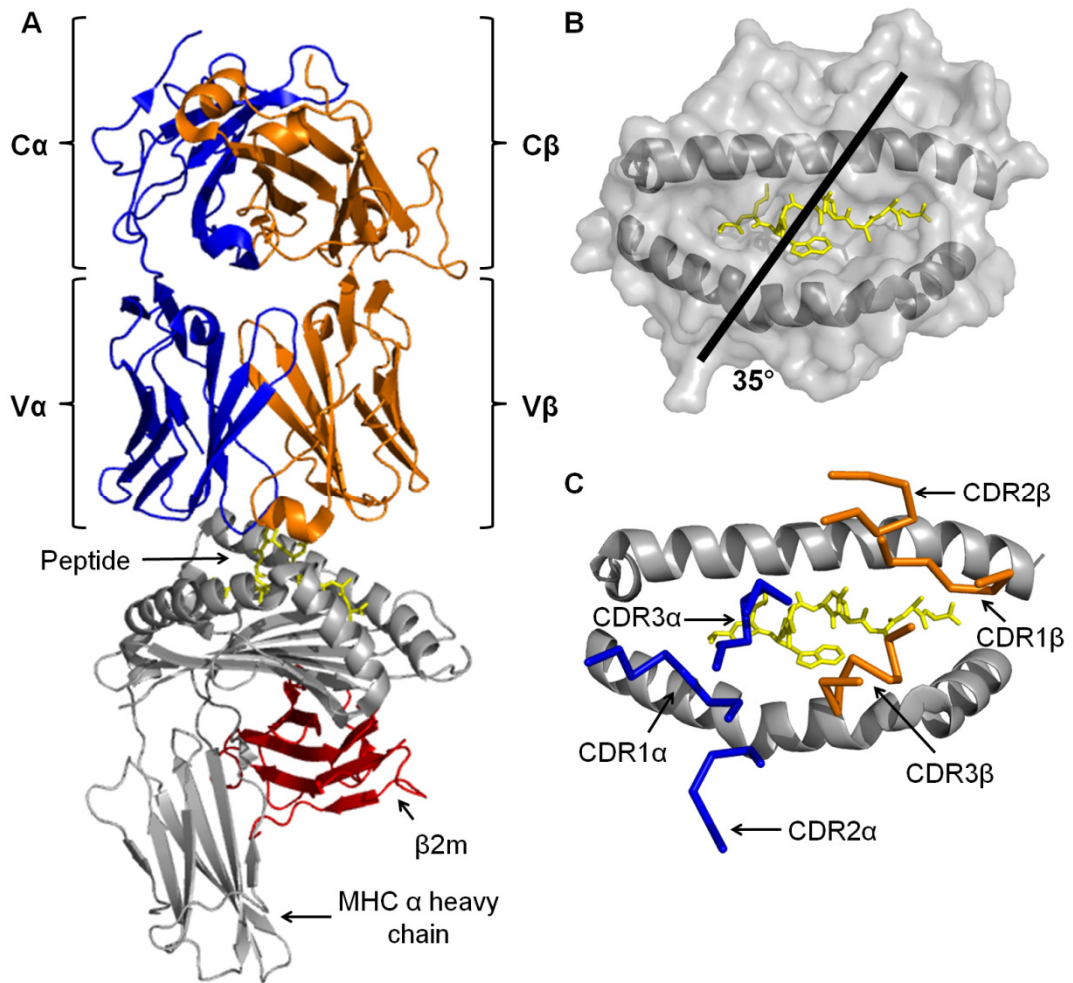


Figure 1.6. Crystal structure of the type 1 diabetes autoreactive 1E6 TCR complexed to HLA-A2 presenting the preproinsulin (PPI) self peptide PPI₁₅₋₂₄ to represent the overall structure of $\alpha\beta$ TCR/pMHC I complex.

(A) 1E6 (blue and orange cartoon) binds to PPI₁₅₋₂₄ (yellow sticks) presented by HLA-A2 (grey and red cartoon) in a diagonal docking mode. (B) The black diagonal line indicates the mean crossing angle of TCRs onto pMHCs ($\sim 35^\circ$) (Rudolph et al., 2006). (C) View down the center of the MHC binding groove showing the positions of the 1E6 TCR CDR loops (CDR α loops and CDR β loops in blue and orange ribbon, respectively) when binding to HLA-A2 (grey cartoon) presenting PPI₁₅₋₂₄ (yellow sticks). The V α domain mainly lies over the N-terminus of the peptide and the MHC $\alpha 2$ -helix whereas the V β domain lies mainly over the C-terminus of the peptide and the MHC $\alpha 1$ -helix. Figure adapted from the 1E6/A2-PPI₁₅₋₂₄ structure (Bulek et al., 2012a).

Some evidence supports the peptide-centric theory, notably the analysis of TCRs with long CDR3 β loops and pMHCs displaying bulged peptides (Borg et al., 2005; Housset and Malissen, 2003; Mazza and Malissen, 2007). Structure of a TCR bound to a MHCI displaying a 13-mer “super-bulged” peptide showed that the CDR2 loops made limited interactions with the MHC surface (Rudolph et al., 2006; Tynan et al., 2005). The structure of a TCR bound to MHCI displaying an 11-mer peptide showed that the peptide is “bulldozed”, or flattened, by the TCR CDR3 loops during binding, allowing the TCR CDR2 loops to contact the MHC surface (Tynan et al., 2007). A further study showed that the TCR CDR1 and CDR2 loops played a minimal energetic role, compared to the CDR3 loops, during the binding of the LC13 TCR to HLA-B*0801-FLRGRAYGL (Borg et al., 2005). Finally, re-investigation of the interaction between the A6 TCR and the B7 TCR with HLA-A*0201-LLFGYPVYV (A2-Tax) (Ding et al., 1999; Ding et al., 1998; Garboczi et al., 1996), that share the same V β -gene (V β 6-5) encoding their CDR1 and CDR2 loops, revealed that the A6 and B7 TCRs bound to the same N-terminal region of the A2-Tax complex. This comparison showed that the A6 and B7 TCR CDR3 loops shared a number of identical contacts with the Tax peptide, whilst their CDR2 loops bound to distinct regions of HLA-A*0201-LLFGYPVYV. However, a second MHC-centric model of TCR engagement, known as the “two-step model”, has also been proposed (Wu et al., 2002). In a biophysical study, Wu et al. evaluated the contribution of IE^k-MCC individual residues on the 2B4 TCR binding by mutating residues to alanine (alanine scan) and measuring the effects by surface plasmon resonance (Wu et al., 2002). The results suggested that MHC contacts dictated the initial association, guiding TCR docking in a way that was mainly independent of the peptide, whereas peptide contacts determined the stability of the binding. These authors concluded that this

two-step process facilitated the efficient scanning of diverse pMHC complexes on the surface of cells and also made TCRs inherently cross-reactive towards different peptides bound to the same MHC. Additionally, the murine 2C TCR was solved in complex with both self (L^d-QL9) and non-self (K^b-dEV8) antigens (Colf et al., 2007). These data showed that the 2C TCR binding to the two antigens with different conformational modalities was not simply a result of the peptide/CDR3 interactions, hence supporting the MHC-centric model. Moreover, another recent study involving four murine TCRs expressing the same TRBV gene (V β 8.2) suggested the existence of germline-encoded TCR/pMHC interaction “codons” allowing the TCRs to dock with an invariant modality by using “ancient” MHC anchor points (Feng et al., 2007). In support of this notion, some conserved residue interactions between a TCR and a MHCI have been observed elsewhere (Rudolph et al., 2006). Among them, three residues within MHCI (positions 65 and 69 on the α 1-helix and position 155 on the α 2-helix), described as the “restriction triad” (Burrows et al., 2009; Tynan et al., 2005), have shown the highest average number of contacts between the TCR and the MHCI in previously reported TCR/pMHCI structures (Rudolph et al., 2006). These fixed interactions support the idea that common TCR/MHC contacts could have an important role in conserving the diagonal docking mode (Bridgeman et al., 2012).

Another important feature of the TCR/pMHC interaction is the conformational flexibility of both the TCR and the pMHC upon binding. Currently, three main types of conformational changes have been observed and are described in more detail elsewhere (**Chapter 5**). First, TCR flexibility has been shown upon pMHC engagement (CDR loops and constant domain) (Armstrong et al., 2008b; Beddoe et al., 2009). Second, movements of the MHC α -helices have been described (Auphan-

Anezin et al., 2006). Finally, there have been reports that TCR binding can induce peptide conformational changes (Rudolph et al., 2006; Ruppert et al., 1993). This structural plasticity could be important for immune surveillance by allowing T-cells to cross-react with a large number of antigens (Housset and Malissen, 2003). The ability of TCRs to cross-react has been highlighted structurally with examples such as the BM3.3 TCR complexed to 3 pMHC ligands (Mazza et al., 2007; Reiser et al., 2003; Reiser et al., 2000), the 2C TCR complexed to 4 pMHC ligands (Colf et al., 2007; Degano et al., 2000; Garcia et al., 1998; Luz et al., 2002), the A6 TCR complexed to 5 pMHC ligands (Ding et al., 1999; Gagnon et al., 2006; Garboczi et al., 1996) and more recently the melanoma-specific TCRs DMF4 and DMF5 complexed to 2 different melanoma pMHC ligands (Borbulevych et al., 2011).

1.6 BIOPHYSICAL BASIS OF TCR/pMHC RECOGNITION

1.6.1 Introduction to Surface Plasmon Resonance and biophysics

It is possible to monitor the formation and the dissociation of complexes between biomolecules in real time using Surface Plasmon Resonance (SPR) biosensors. SPR biosensors have been used to characterise a diverse set of interaction partners (e.g. receptors, antibodies, enzymes, nucleic acids or viruses) and the information obtained from SPR analyses is both qualitative (e.g. epitope mapping or site specificity analyses) and quantitative (e.g. affinity, kinetic or thermodynamic analyses) (Karlsson, 2004). This section will briefly describe the physical basis of SPR and the different parameters obtained with this technique.

1.6.1.1 Basis of SPR

SPR physical principles are complex and beyond the scope of this introduction but a basic understanding is useful to understand the data. Essentially, SPR detects changes in refractive index in the aqueous layer close to a sensor chip surface which correlates to the changes in mass or buffer composition (**Figure 1.7A**). When a light beam passes from material with a high refractive index into material with a low refractive index (e.g. glass and water, respectively) some light is reflected from the interface. At an angle of incidence (θ) above a critical angle of incidence (θ_c), the polarized light is completely reflected (total internal reflection) and by coating the glass surface with a layer of metal (e.g. gold) some of the light is “lost” into the metallic film (van der Merwe, 2001). This “lost” light generates an electromagnetic component called an evanescent wave which excites electrons in the gold film resulting in the formation of surface plasmons (electron charge density waves) within the gold film (Jason-Moller et al., 2006). At θ , the energy transfer is concomitant with a drop in the intensity of the reflected light, the reflected light angle being called the surface plasmon resonance angle (θ_{spr} or SPR angle). The local refractive index can be influenced by both biomolecules adsorbed onto the thin metal layer (ligands) and analytes in a mobile phase running along a flow-cell and binding to the ligands. Thus, if binding occurs, the local refractive index changes and it leads to modification in energy transfer and shift of θ_{spr} (Pattnaik, 2005). A sensorgram depicts the changes ($\Delta\theta_{\text{spr}}$) which are monitored in real-time and measured in response or resonance units (RUs), 1 RU being the equivalent of a 10^{-4} ° θ_{spr} shift (Pattnaik, 2005; van der Merwe, 2001). SPR allows the determination of several ligand-receptor interaction parameters. The interaction between a TCR and a pMHC will be used to describe these parameters in the sections below.

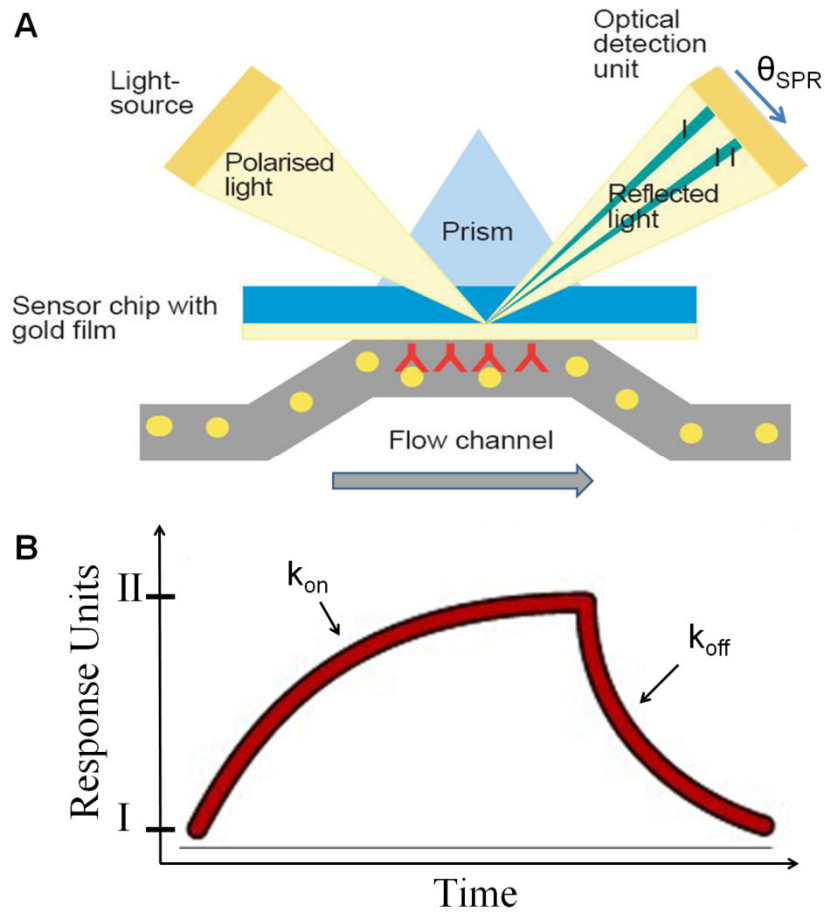
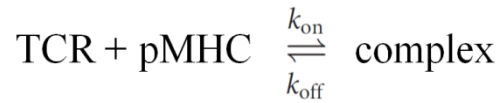


Figure 1.7. Schematic representation of Surface Plasmon Resonance.

(A) As the analyte (yellow) binds to the surface bound protein (red), the local refractive index shift and the SPR angle (θ_{spr}) moves from I to II. Figure adapted from (Homola, 2003). (B) Sensorgram representing the shift in θ_{spr} from I to II which is recorded as an increase in Response Units (RU) allowing the determination of the association (k_{on}) and dissociation (k_{off}) rate constants. Figure adapted from (Murphy et al., 2008).

1.6.1.2 Kinetic and affinity parameters

The interaction between a TCR and a pMHC can be described by:



Here, the kinetic parameters k_{on} (or k_a) and k_{off} (or k_d) are the association rate constant (or on-rate constant) and the dissociation rate constant (or off-rate constant) for the formation and the dissociation of the TCR/pMHC complex, respectively, and can be measured by SPR (Stone et al., 2009) (**Figure 1.7B**). k_{on} is a measure of the time that a TCR at a given concentration takes to reach an equilibrated state of binding to the pMHC. Therefore, k_{on} is measured in terms of complex formation per second in a 1 M solution of TCR and pMHC with its units being $\text{M}^{-1}\text{s}^{-1}$. k_{off} is a measure of the stability of the TCR/pMHC interaction and does not depend on the TCR and pMHC concentrations. Therefore, k_{off} is measured in terms of complex decay per second with its units being s^{-1} . A related parameter, the half-life of the TCR/pMHC interaction ($t_{1/2}$), can be derived from the k_{off} . It represents the time needed for half of the TCR molecules to dissociate from the pMHC and can be calculated as $t_{1/2} = \ln 2 / k_{\text{off}}$ (Irving et al., 2012). When the reaction has reached equilibrium, the affinity of the TCR/pMHC interaction can be represented by the equilibrium association constant (K_A) which is directly related to k_{on} and k_{off} . It is defined by the equation $K_A = k_{\text{on}} / k_{\text{off}}$ (Karlsson et al., 2006; van der Merwe, 2001) and thus has units M^{-1} . However, the affinity is more commonly expressed in terms of equilibrium dissociation constant (K_D), which is the inverse of K_A ($K_D = 1 / K_A$) with $K_D = k_{\text{off}} / k_{\text{on}}$ having units in M. Therefore, an interaction with a fast k_{on} and a slow k_{off} will be of higher affinity than the opposite (slow k_{on} and fast k_{off}) and a lower K_D equals a higher affinity. If the kinetic parameters are too fast to be

measured, these constants can be obtained using standard Scatchard approaches where at equilibrium

$$K_D = \frac{[TCR] \times [pMHC]}{[complex]}$$

with the brackets (e.g. [TCR]) indicating the concentration of the molecules (De Mol and Fischer, 2008; Stone et al., 2009). Thus, in a typical SPR experiment with immobilized pMHC (ligands), when the concentrations of ligated and unligated pMHC are equal (i.e. half maximal RU in an SPR titration with increasing TCR concentrations) the K_D is equal to the concentration of TCR required to reach this half saturation (Stone et al., 2009). Finally, the affinity can also be expressed in terms of “binding free energy” or standard Gibbs free energy (ΔG° in cal.mol^{-1}) from the affinity constants (van der Merwe, 2001) with units as follows:

$$\Delta G^\circ = RT \ln \frac{K_D}{C^\circ} = RT \ln \frac{1}{K_A \times C^\circ} = -RT \ln \frac{K_A}{C^\circ}$$

where R is the universal gas constant ($1.9872 \text{ cal.K}^{-1}.\text{mol}^{-1}$), T is the absolute temperature in Kelvin ($298.15 \text{ K} = 25^\circ\text{C}$), C° is the standard concentration (1 M), K_A or K_D are the equilibrium affinity constants in M^{-1} or M, respectively.

1.6.1.3 Thermodynamic parameters

Thermodynamic analysis of TCR/pMHC interactions has increased the understanding of the molecular determinants of TCR binding and specificity (Armstrong et al., 2008a). The binding free energy ΔG° of TCR/pMHC (or any protein-protein) interactions described in the previous section consists of a heat component taken up (endothermic reaction) or released (exothermic reaction) during the binding process, namely enthalpy (ΔH°) (Murphy and Freire, 1995). The other component is entropy (ΔS°), related to the variation in the degree of “order” during

binding (De Mol and Fischer, 2008). To obtain these thermodynamic parameters using SPR, K_D s first have to be measured over a range of temperatures. If it is assumed that ΔH° is independent of the temperature, the linear form of the van't Hoff equation can be applied:

$$\Delta G^\circ = RT \ln \frac{K_D}{C^\circ} = \Delta H^\circ - T\Delta S^\circ$$

By plotting $\ln(K_D/C^\circ)$ (or $\ln(K_D)$ only as $C^\circ=1$ M) against $1/T$ for each temperature, ΔH° and ΔS° will be deduced as the slope of the linear plot equals $\Delta H^\circ/R$ and the y-intercept equals $-\Delta S^\circ/R$. However, for most protein/ligand interactions ΔH° varies with the temperature (van der Merwe, 2001). In this case, the non-linear (integrated) form of the van't Hoff equation is fitted:

$$\Delta G^\circ = RT \ln K_D = \Delta H^\circ - T\Delta S^\circ + \Delta C_p^\circ(T - T_0) - T\Delta C_p^\circ \ln \frac{T}{T_0}$$

where T is the temperature in Kelvin (K) at which the K_D is measured, T_0 is the reference temperature (298.15 K = 25°C), ΔH° is the enthalpy change upon binding at T_0 (cal.mol⁻¹), ΔS° is the standard entropy change upon binding at T_0 (cal.mol⁻¹.K⁻¹) and ΔC_p° is the specific heat capacity (cal.mol⁻¹.K⁻¹) which is assumed to be temperature-independent and is a measure of the variation of ΔH° with temperature.

The variation of each parameter (ΔH° , ΔS° and ΔC_p°) reflects the structural modifications occurring during binding (Armstrong et al., 2008a; Armstrong et al., 2008b). ΔH° variation is caused by the formation and the disruption of non-covalent bonds (van der Waals (vdW), hydrogen and ionic bonds). A reaction with a negative ΔH° is enthalpically favourable. This can be due to conformational rearrangements during the binding process and involves bonds between the TCR and the pMHC, but also bonds of solvent and intramolecular bonds (van der Merwe, 2001). For example, it has been estimated that trapping of water in a protein-protein complex could

increase the enthalpy binding from -1.5 to -3 kcal.mol⁻¹ per water molecule (Cooper, 2005) and that the average energy for the formation of a salt bridge is ~ -3.7 kcal.mol⁻¹ (Kumar and Nussinov, 1999). ΔS° is generally interpreted in terms of the change in the order/disorder balance during complex formation. It comprises the restriction of conformational freedom and alternation of bonds involved during binding. A reaction with a positive ΔS° indicates that disorder increases during binding, which is entropically favourable. Hydration can be an important factor for ΔS° (e.g. in hydrophobic binding) as the burial of water-accessible surfaces can result in the expulsion of ordered water molecules and can contribute to the binding due to increases in entropy (De Mol and Fischer, 2008). ΔC_p° variation is almost entirely attributed to solvent effects and can be interpreted in terms of solvent-accessible polar (hydrophilic) and apolar (hydrophobic) surface areas buried during binding (Murphy and Freire, 1995). An increase in accessible apolar surface increases ΔC_p° whereas the burial of apolar surface decreases ΔC_p° . However it is important to note that if the standard errors of the measured K_{DS} are above 1%, ΔC_p° cannot be interpreted with statistical significance (Tellinghuisen, 2006; Zhukov and Karlsson, 2007). Indeed, as ΔC_p° is determined from the second derivative of ΔG° (directly related to K_D) with respect to temperature, van't Hoff ΔC_p° changes can vary with the exclusion of only a single data point or even a change in the error associated with a data point (Armstrong et al., 2008a; Zhukov and Karlsson, 2007). In a recent study, Zhukov and Karlsson assessed how uncertainty in K_D measurement propagates to the thermodynamic parameters and concluded that comparison of protein-protein interactions with regard to the magnitudes of ΔC_p° should generally be avoided (Zhukov and Karlsson, 2007).

1.6.2 TCRs bind to pMHCs with weak affinity and relatively slow kinetics

The biophysical data accumulated by techniques such as SPR or isothermal titration calorimetry (ITC) show that TCRs bind their cognate pMHCs with relatively weak affinity ($K_D = 0.1\text{-}270\ \mu\text{M}$) (Bridgeman et al., 2012; Cole et al., 2007) compared to other Ig-like proteins such as antibodies ($K_D = \text{nM-pM}$) (van der Merwe and Davis, 2003). MHCII-restricted TCRs seem to bind with a weaker affinity compared to MHCI-restricted TCRs with average K_{DS} around $92\ \mu\text{M}$ and $32\ \mu\text{M}$, respectively (Bridgeman et al., 2012; Cole et al., 2007). Likewise, anti-pathogen specific TCRs bind with a higher affinity compared to self-reactive TCRs (autoimmune or cancer-specific TCRs) with average K_{DS} around $8\ \mu\text{M}$ and $90\ \mu\text{M}$, respectively (Bridgeman et al., 2012; Cole et al., 2007). As it has been recently shown that weak TCR binding affinity is generally associated with a less sensitive/effective T-cell response (Irving et al., 2012; Schmid et al., 2010; Thomas et al., 2011), these differences in affinity correlate with the idea that CD8^+ T-cells recognizing the self-derived tumour-associated antigens (TAAs) have been subjected to immune tolerance mechanisms in order to prevent autoimmunity (Boon et al., 2006).

Kinetically, TCRs bind pMHCs with slow-to-moderate k_{on} s (generally between $10^3\ \text{M}^{-1}\cdot\text{s}^{-1}$ and $10^5\ \text{M}^{-1}\cdot\text{s}^{-1}$) (Bridgeman et al., 2012; Davis et al., 1998), slower than the $10^6\ \text{M}^{-1}\cdot\text{s}^{-1}$ expected for this kind of geometrically constrained protein-protein interaction (Janin, 1997; Vijayakumar et al., 1998). Slow k_{on} s support the idea of TCR, MHC and peptide conformational flexibility in the unligated state, with only a particular conformation among the several conformations being able to bind the pMHC (Rudolph et al., 2002; Rudolph et al., 2006). However, in some cases k_{on} s are only slightly below $10^6\ \text{M}^{-1}\cdot\text{s}^{-1}$, indicating that the conformational changes are most

likely small disorder-to-order transitions (Davis-Harrison et al., 2005). The range of the experimental k_{off} s measured for the interaction between TCRs and agonist pMHCs is narrow (0.01 s^{-1} to 0.73 s^{-1}), with an average k_{off} of 0.24 s^{-1} , which is consistent with TCR/pMHC structural data showing a similar number of bonds between the different complexes (Bridgeman et al., 2012; Rudolph et al., 2006). Interestingly, several studies suggest that the k_{off} most likely governs T-cell sensitivity. This tight kinetic window might allow T-cells to be really sensitive to a very low number of pMHCs because of T-cell activation by serial triggering or kinetic proofreading (see section 1.7 below) (Manz et al., 2011; Sewell, 2002) contrary to engineered T-cells expressing enhanced affinity TCRs displaying longer k_{off} s (below the kinetic window) that fail to recognise low density pMHC ligands (Thomas et al., 2011). This notion is further supported by studies showing that faster k_{off} s (above the kinetic window) can result in T-cell anergy and extremely fast k_{off} s can lead to T-cell antagonism (Boulter et al., 2007).

1.6.3 Thermodynamic features of TCR/pMHC interaction

While the kinetic parameters and the affinities of TCR/pMHC interactions determined to date fall into a narrow window, the enthalpies and entropies associated with each complex can vary dramatically. TCRs were presumed to bind pMHCs with a “thermodynamic signature” consisting of an unfavourable entropy variation ($\Delta S^\circ < 0$) and a favourable enthalpy variation ($\Delta H^\circ < 0$) (Willcox et al., 1999a; Willcox et al., 1999b). Together with the kinetic and structural data, the unfavourable entropy changes suggested that instead of only adjusting conformation upon binding, TCR CDR loops presented flexibility in the unbound state (Armstrong et al., 2008a). However, due to several observations of entropically favourable TCR/pMHC

interactions (Colf et al., 2007; Davis-Harrison et al., 2005; Ely et al., 2006), it is now clear that there is no enthalpic/entropic “signature” but rather different binding thermodynamic features depending on each particular TCR/pMHC complex. Currently, ΔH° varies from -30 to 18 kcal.mol⁻¹ and ΔS° varies from -80 to 80 cal.mol⁻¹.K⁻¹ (Armstrong et al., 2008a; Holland et al., 2012). Thermodynamic analysis, coupled to structural analysis, gives insight into how structural features contribute to binding energetics. Most of the thermodynamic data obtained so far correlates with the conformational changes and dynamics observed for TCR binding to pMHC, but unfortunately thermodynamic analyses are not available for all of the TCR/pMHC interactions for which both ligated and unligated TCR and/or pMHC structures are available (Armstrong et al., 2008b). Generally, data suggests that favourable enthalpy and unfavourable entropy can be linked to conformational changes (Willcox et al., 1999a) whereas unfavourable enthalpy and favourable entropy can be linked to the expulsion of solvent molecules upon binding (Cole et al., 2009).

1.7 TCR TRIGGERING MODELS

On the T-cell surface, the $\alpha\beta$ TCR associates non-covalently with a signalling complex which contains a number of invariant CD3 transmembrane proteins including γ , δ , ϵ and ζ chains. These subunits associate with each other, forming the CD3 $\zeta\zeta$ homodimer and CD3 $\epsilon\delta$ or CD3 $\epsilon\gamma$ heterodimers (Koning et al., 1990; Manolios et al., 1994). Immunoreceptor tyrosine-based activation motifs (ITAMs) are present in all CD3 subunits cytoplasmic domains and are phosphorylated by an intracellular tyrosine kinase called Lck upon T-cell antigen recognition (Barber et al., 1989). The phosphorylation of these tyrosine residues is known to be crucial in

TCR signalling leading to T-cell activation (Kersh et al., 1998a). The process by which TCR/pMHC interactions result in these biochemical changes is referred to as “TCR triggering” and there is currently no consensus on the mechanisms involved in this process (van der Merwe and Dushek, 2011). Several models of TCR triggering have been described including: (i) conformational change models (Alam et al., 1999; Reich et al., 1997), (ii) segregation/redistribution models (Davis and van der Merwe, 1996; Viola et al., 1999), (iii) aggregation models (Boniface et al., 1998; Irvine et al., 2002; Trautmann and Randriamampita, 2003), (iv) kinetic proofreading model (McKeithan, 1995; Rabinowitz et al., 1996) and (v) serial triggering model (Valitutti et al., 1995). The kinetic proofreading (KP) and serial triggering (ST) models are not mutually exclusive and are detailed below as they are relevant to the work presented in this thesis.

First, the KP model proposed to explain how small differences in the half-life of the TCR/pMHC interactions are translated into differences in TCR signalling (McKeithan, 1995; Rabinowitz et al., 1996). It suggested that TCR signalling requires a series of sequential steps that are fully reversed upon dissociation of the TCR/pMHC complex (McKeithan, 1995; Rabinowitz et al., 1996). This model was notably supported by the partial phosphorylation of CD3 subunits occurring when a suboptimal ligand is presented to the TCR (Kersh et al., 1998b). The initial KP model proposed that a TCR must bind to a pMHC long enough to initiate the phosphorylation events that lead to T-cell activation, hence only the half-life/off-rate dictates the T-cell response (or absence of response) (McKeithan, 1995). However, the KP model was initially confronted by the ST model (or equilibrium affinity model (Jansson, 2011)) where T-cell activation is related to the K_D of the

TCR/pMHC interaction (hence related to k_{on} and k_{off}) (Stone et al., 2009; Tian et al., 2007). The ST model is based on the fact that small numbers of agonist pMHCs can trigger a large number of TCRs (Valitutti et al., 1995) and it has been shown that a single specific pMHC is sufficient for TCR triggering (Irvine et al., 2002). Contrary to the KP model, it stated that the on-rate was also involved in T-cell activation as the fast k_{on} s and relatively short half-lives of TCR/pMHC interactions would increase the number of engaged TCRs (Valitutti, 2012; Valitutti et al., 1995). Moreover, it was supported by the fact that T-cells expressing TCRs with an half-life/affinity beyond a certain threshold (or “affinity ceiling”) might become less effective (Sewell, 2002). Indeed, by transducing $CD8^+$ T-cells with different TCRs presenting a range of affinity for NY-ESO-1, Schmid et al. showed in a recent study that above a certain affinity threshold T-cell avidity and function were not further enhanced (Schmid et al., 2010). Finally, a theoretical study has recently shown support for both models (Dushek et al., 2009). Dushek et al. refined the initial KP model and suggested a new model in which fast k_{on} allowed a single TCR to rebind to the same pMHC before diffusing apart and the rebinding was assumed to be fast enough to allow the activation steps. Thus, a fast on-rate can compensate a short half-life. Also, in a mathematical model based on TCR down-regulation for an array of TCR mutants, Coombs et al. suggested an optimal half-life of TCR/pMHC interaction by combining the KP and the ST models (Coombs et al., 2002). A short half-life led to TCRs failure to achieve the active proofreading step whereas a long half-life prevented serial engagement of the TCRs.

1.8 IMPROVING TCR AFFINITY

As described earlier in this Chapter, TCRs bind their cognate pMHCs with relatively weak affinity ($K_D = 0.1\text{-}270\ \mu\text{M}$) and TCRs bind with a weaker affinity to tumour-associated antigens compared to pathogenic antigens. As it has been shown that T-cell sensitivity can be related to TCR affinity (Holler et al., 2001; Schmid et al., 2010), extended research has been undertaken in order to enhance the affinity of the TCR/pMHC interaction. TCRs with improved affinity could be used for soluble therapy (described in **Chapter 4**) or for adoptive cell therapy (ACT) (described in **Chapter 6**). A number of different methods have been described to modulate TCR affinity such as direct isolation of high-affinity T-cell clones or genetic engineering of the TCR antigen-binding region (using *in silico* modelling or display technologies).

1.8.1 Selection of high-affinity TCRs using allo-restriction

High-affinity TCRs can be obtained by using alloreactive T-cells as such cells have undergone thymic selection in the absence of the restricting HLA molecule (Kronig et al., 2009; Sadovnikova and Stauss, 1996). Sadovnikova et al. published in 1996 a study where they isolated mouse CTLs specific for the Mdm2 (murine double-minute 2) protein, an ubiquitously expressed self protein which is frequently over-expressed in tumours and presented by allogenic H-2K^b class I molecules, using the allo-restricted T-cell repertoire of H-2^d mice (Sadovnikova and Stauss, 1996). Thus, allo-restricted CTLs were generated by stimulating naive H-2^d splenocytes with H-2K^b APCs pulsed with mdm100 (an Mdm2-derived peptide). Approximately 50% of the CTL clones were of “high avidity” (meaning that they recognised low densities of antigenic peptide at the cell surface) and efficiently recognized Mdm2-expressing

tumour cells. Using similar allo-restricted approaches, several groups have isolated T-cell clones and TCRs (Kronig et al., 2009; Schuster et al., 2007; Wilde et al., 2009) against different cancer-associated antigens. Using this method, Xue et al. isolated a TCR and CTL clones specific for an HLA-A2 restricted peptide epitope of the Wilms tumour antigen-1 (WT1) which could selectively kill immature human leukemia progenitor and stem cells *in vitro* (Xue et al., 2005). They isolated high-avidity CTLs specific for WT1 peptide presented by HLA-A2 from HLA-A2 negative (HLA-A2⁻) donors and CTLs from HLA-A2 positive (HLA-A2⁺) donors which were then transduced with the WT1-specific TCR using a retroviral vector. The gene-transduced T-cells acquired WT1 peptide specificity and showed stable long-term TCR expression. They also demonstrated that TCR-transduced human CTLs are functionally active *in vivo*, highlighted by the elimination of leukemia cells in the nonobese diabetic–severe combined immunodeficiency (NOD/SCID) mice (Xue et al., 2005).

Instead of generating T-cells using an allo-restricted approach from HLA-mismatched donors, a second option to avoid tolerance to self inducing low-affinity T-cells is to use TCRs from xenogenic T-cells that have matured in a non-tolerant host (Kieback and Uckert, 2010). HLA-A2 transgenic mice have been generated and can be immunized with a human antigenic peptide which is homologous to the mouse amino acid sequence (eg MDM2₃₃₋₄₁) or that differs from the mouse in critical positions (eg MDM2₈₀₋₈₈) (Stanislowski et al., 2001). Thus, it is possible to expand T-cells restricted to human MHC from a xenogenic repertoire. Using this method, several murine TCRs specific for human tumour associated antigens (eg MDM2, p53, gp100) have been isolated (Cohen et al., 2005; Morgan et al., 2006;

Stanislowski et al., 2001). However, the immunogenicity of fully murine or partially humanized mouse TCRs cannot be excluded if such proteins were used in human patients.

1.8.2 Rational design of high-affinity TCRs

Zoete et al. used a rational *in silico* design approach for the generation of high-affinity TCRs (Zoete et al., 2010) that optimized the interaction between the TCR and the pMHC based on Molecular Mechanics-Generalized Born Surface Area (MM-GBSA) free energy calculations and crystal structures of TCR/pMHC complexes (Zoete and Michielin, 2007). For example, the MM-GBSA approach was applied to the BC1 TCR, this TCR being closely related to the 1G4 TCR (four amino acid differences between 1G4 and BC1) specific for NY-ESO-1, to estimate the contribution of individual amino acids to the binding energy with NY-ESO-1 (using 1G4/A2-NY-ESO-1 crystal structure) and identify amino acid replacements in the BC1 TCR that would enhance or reduce the TCR/pMHC interaction (Irving et al., 2012). By combining optimized BC1 TCR α and β chains they developed a panel of A2-NY-ESO-1 specific TCRs with up to 150-fold increase in affinity compared to the wild type BC1.

Another rational design recently performed by Alli et al. involved the mutation of a glycine to serine at position 107 within the CDR3 β stalk of TCRs. This group used structural analyses to identify a glycine-serine variation in the TCR that modulated antigen sensitivity (Alli et al., 2011). Glycine at position 107 (G107) is unique to TRBV13-2 in mice (among 23 TRBV) and to TRBV12-5 in humans (among more than 54 TRBV). The alignment of the TRVB revealed that most CDR3 β displayed a

serine at position 107 (S107) both in mice (18/23 TRBV sequences) and humans (45/54) (Alli et al., 2012; Turner et al., 2006). Structural analyses revealed that the hydroxymethyl side chain of the S107 was positioned to intercalate into the core of the CDR3 β loop and created a network of van der Waals bonds. On the contrary, G107 did not have any side chain and left a gap. They hypothesized that the gap present in TRBV13-2 CDR3 β was energetically unfavourable and that a mutation into S107 would increase the stability and hence enhance the affinity. Experimentally, the mutation with a serine led to a ~10-1000 fold enhanced antigen sensitivity in 3 of 4 TRBV13-2 TCR tested but biophysical analyses was not performed to measure the affinity of the TCRs for their ligands and to evaluate the mechanism of their enhanced reactivity (Alli et al., 2011).

1.8.3 Display technologies

Despite being applied successfully for the development of monoclonal antibodies, initial efforts using a method to display and to select high affinity TCRs showed limited success (Weidanz et al., 1998). This was probably because of the difficulty in expressing TCRs in a soluble form, notably due to the reduced abilities of the TCR α and β chains to associate compared to the heavy and light chains of the antibodies (Rudolph et al., 2006). However, this problem was overcome with recent strategies using yeast, T-cell, or phage display (**Figure 1.8**) coupled to some of the methods described in **Chapter 3** to improve TCR stability. Typically, in all three different display technologies, a T-cell clone that is specific for the desired pMHC antigen was used as a source for cloning the genes that encode the TCR α and β chains. After random or site-directed mutagenesis, these genes were cloned into the display system and selected for pMHC binding (Richman and Kranz, 2007).

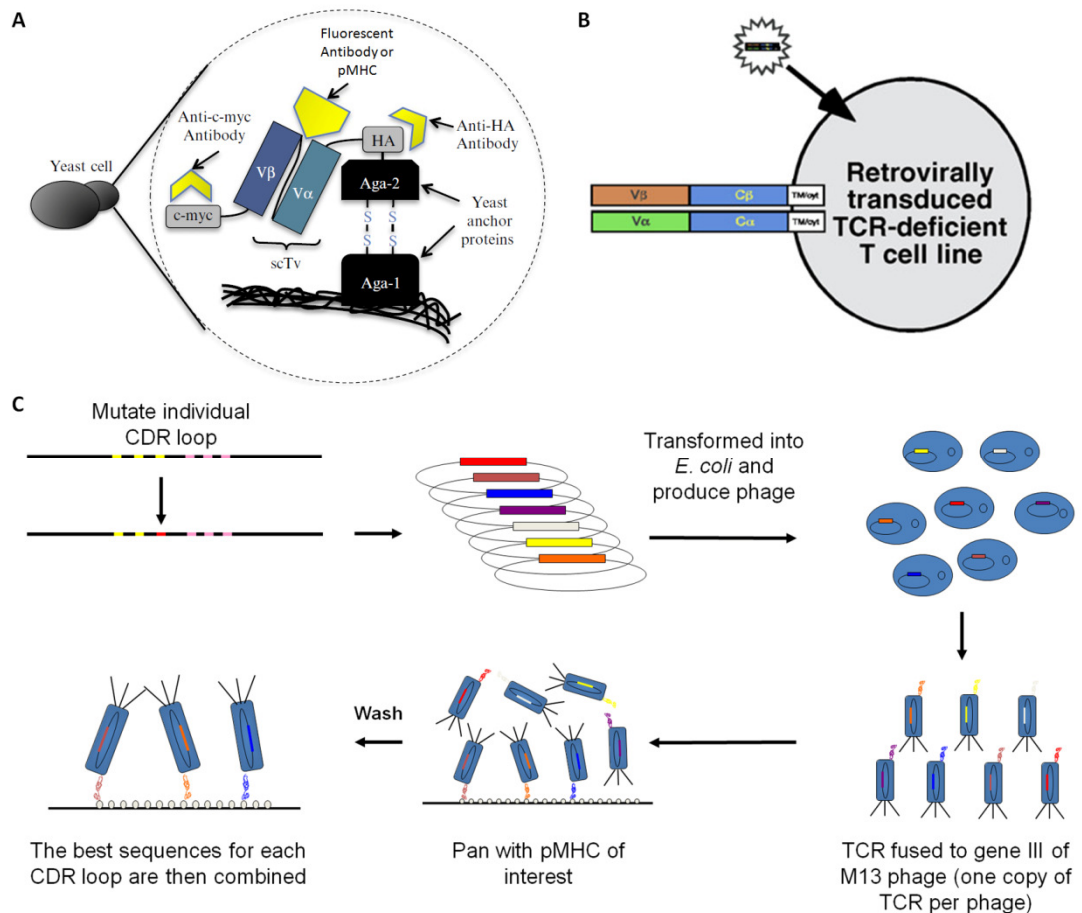


Figure 1.8. Schematic representation of the different display technologies to increase TCR affinity.

(A) Cartoon showing yeast display of a scTCR construct, including N- (HA) and C-terminal (c-myc) expression tags, by fusion to the yeast mating protein Aga-2 which is, in turn, linked by disulfide bonds to the integral yeast cell wall protein Aga-1. The scTCR expression can be monitored by antibodies against the expression tag and the variable domains or with the specific pMHC (Figure adapted from (Stone et al., 2012)). (B) T-cell display of a full-length TCR expressed on the surface of a TCR deficient T-cell hybridoma after transduction with a retrovirus (Figure adapted from (Richman and Kranz, 2007)). (C) Representation of the phage display process to engineer TCR affinity, the method used for the generation of the high-affinity TCRs used during my PhD. Individual CDR loops were mutated and inserted into three cistronic vector pEX746 with the TCR β chain fused to phage coat protein pIII and the TCR α chain targeted to the periplasm to allow its association with the β chain after transformation into *E. coli*. The produced phages, expressing a single TCR, were screened with the pMHC of interest and the best sequences for each loop were then combined.

The yeast display technology targets the TCR to the yeast cell surface by fusing the coding sequence to that of a native yeast mating protein Aga-2 (Stone et al., 2012) (**Figure 1.8A**). While this system has been successful in the isolation and affinity maturation of antibodies (Bowley et al., 2007; Siegel, 2009), TCRs have posed a more formidable challenge. In this display system, the TCR has been displayed as a stabilized single-chain TCR (scTCR), in the V β -linker-V α form described in **Chapter 3**. Two mouse TCRs were engineered for higher affinity using this system: 3.L2 TCR (MHC class-II restricted) which binds the foreign antigen I-E^k-Hb (Persaud et al., 2010) and 2C TCR (MHC class-I restricted) which binds an alloantigen H2-L^d-QL9, a foreign antigen H2-K^b-SIYR and a self-antigen H2-K^b-dEV8 (Richman and Kranz, 2007). The major limitation in using this display technology for the generation of high-affinity TCRs is the need to mutate the TCR variable domains in order to allow the scTCR to be expressed on the yeast surface before affinity maturation. To date, the only TCRs that have been obtained with this yeast surface display are those with clonotypic antibodies that allowed for the stabilization and display of the single-chain format (Chervin et al., 2008).

TCRs have also been engineered by T-cell display using a retroviral vector to introduce the TCR α and β chains into a TCR deficient T-cell hybridoma (Kessels et al., 2000) (**Figure 1.8B**). The introduced TCR was expressed on the surface in its native conformation, complexed with the CD3 subunits, allowing for a fully functional T-cell. Although TCRs have not been engineered for higher affinity using this method, Kessels et al. reported an alteration of the F5 TCRs specificity, the parental F5 TCR being specific of the influenza A epitope (ASNENMDAM) whereas one of the mutants had acquired a specificity for a different influenza A

strain epitope (ASNENMETM). A drawback of T-cell display is the more limited potential for combinatorial library diversity. This is related to low retroviral transduction efficiency. Even though Kessels et al. estimated that after optimization of transduction and sorting strategies it could be possible to achieve a retroviral TCR display libraries 10^6 - 10^7 in size (Kessels et al., 2000), mammalian cell libraries are more likely in the range of $\sim 10^4$ (Richman and Kranz, 2007) while yeast and phage display technologies reliably produce libraries of $\sim 10^7$ and $\sim 10^{10}$ transformants, respectively (Li et al., 2005b; Stone et al., 2012).

A third system, phage display, preceded the development of the yeast display system by almost a decade and has been used extensively to identify and affinity mature antibodies (Richman and Kranz, 2007). It targets the protein of interest on the surface of the phage by fusion to the N-terminus of a viral coat protein (**Figure 1.8C**). As with yeast display and for the reasons described above (TCR stability), TCR engineering by phage display initially yielded limited success (Stone et al., 2012). However, the stabilisation of the TCR α and β chain pairing described in **Chapter 3** ('Boulter-disulphide' method for "dsTCRs", section 3.2.1) has helped to solve these issues and allowed affinity maturation of TCRs by phage display (Boulter et al., 2003; Li et al., 2005b). Individual CDR loops were mutated and "dsTCRs" were cloned into a three cistronic vector (pEX746) for phage display, with the TCR β chain fused to phage coat protein pIII and the TCR α chain targeted to the periplasm to allow its association with the β chain (Li et al., 2005b). Vectors were then transformed into *E. coli* and the produced phage, expressing a single dsTCR, were screened with the pMHC of interest. The best CDR sequences for each loop (from TCRs displaying enhanced affinities) were then combined to create high-

affinity TCRs. Li et al. generated more than ten different high-affinity TCRs using phage display and this affinity maturation method has generated the highest TCR/pMHC binding affinity to date ($K_D = 26$ pM) (Li et al., 2005b). For example, a variant of the A6 TCR specific for the HTLV-1 Tax peptide displayed a binding affinity ($K_D = 2.5$ nM) 720 times stronger than the wild type TCR ($K_D = 1.8$ μ M) (Li et al., 2005b) and high-affinity variants of the SL9 TCR specific for the HIV Gag peptide were recently used to design artificial HIV specific T-cells with an enhanced ability to kill HIV infected cells (Varela-Rohena et al., 2008). Finally, the high-affinity variants of MEL5 TCR used during my PhD were generated with this method.

1.9 AIMS OF THE THESIS

The work reported within this thesis aims to further improve our knowledge of the interaction between the T-cell receptor (TCR) and the peptide-major histocompatibility complex (pMHC). Specifically, I aimed to:

1. Develop an optimized screen for the crystallization of TCR/pMHC complexes
2. Analyse the specificity of a high-affinity TCR directed against a melanoma antigen
3. Investigate the structural and biophysical differences between TCRs with different affinities in the recognition of melanoma antigens
4. Determine the optimal TCR affinity for adoptive cell therapy directed against melanoma

CHAPTER 2

MATERIALS AND METHODS

2.1 Bacterial cell culture	76
2.1.1 Culture medium and bacterial strains.....	76
2.1.2 Transforming competent cells.....	76
2.2 Molecular biology.....	77
2.2.1 Plasmids	77
2.2.1.1 Vectors for protein expression	77
2.2.1.2 Vectors for the production of lentivirus.....	78
2.2.2 Cloning of a range of different affinity TCRs toward melanoma into a lentiviral vector	78
2.2.3 Enzymatic digestion.....	80
2.2.4 Agarose gel purification and ligation.....	80
2.3 Protein chemistry	81
2.3.1 Protein expression as inclusion bodies.....	81
2.3.2 Refolding of pMHCI.....	82
2.3.3 Refolding of soluble TCR.....	83
2.3.4 Fast Protein Liquid Chromatography (FPLC) purification.....	84
2.3.5 Sodium dodecyl sulphate – Polyacrylamide gel electrophoresis and SimplyBlue™ staining.....	85
2.3.6 Biotinylation of pMHCI and manufacture of pMHCI tetramer.....	85
2.4 Surface Plasmon Resonance.....	86
2.4.1 Equilibrium-binding analyses	87
2.4.2 Kinetic analyses	87

2.5 Crystallography.....	89
2.5.1 Crystallisation conditions for $\alpha 24\beta 17$, A2-ELA-4A and $\alpha 24\beta 17/pMHCI$ complexes.....	89
2.5.2 Crystallisation conditions for MEL5/A2-AAG and MEL5/A2-EAA complexes.....	89
2.5.2.1 MEL5/A2-AAG: different TCR/pMHCI complexes mixing.....	89
2.5.2.2 MEL5/A2-EAA: seeding from MEL5/A2-AAG	91
2.5.3 X-ray diffraction data collection, molecular replacement and model refinement	91
2.6 Mammalian cell culture.....	92
2.6.1 Mammalian cell culture medium	92
2.6.2 Cell lines	93
2.6.3 Cryopreservation and storage of cell lines	96
2.6.4 Cell counting by Trypan exclusion	96
2.7 Generation of transduced Jurkat and CTL lines.....	96
2.7.1 Lentivirus production.....	96
2.7.2 Jurkat TCR negative GLuc transduction and sorting.....	97
2.7.3 CTL transduction	98
2.7.3.1 CTL sorting from peripheral blood mononuclear cells (PBMCs)	98
2.7.3.2 CTL transduction, sorting and expansion	99
2.8 Flow cytometry analysis	100
2.9 Jurkat activation assay	100
2.10 CTL effector function assays	101
2.10.1 Peptide titration assay	101
2.10.2 Peptide library screen.....	101

2.10.2.1	A description of positional scanning combinatorial peptide libraries (PS-CPLs)	101
2.10.2.2	Peptide library screen assay	102
2.10.3	ELISA (Enzyme-linked immunosorbent assay) for MIP1 β	102
2.10.4	Chromium release assay.....	103

2.1 BACTERIAL CELL CULTURE

2.1.1 Culture medium and bacterial strains

Luria-Bertani (LB) medium: 10 g/L tryptone (Fisher Scientific), 5 g/L yeast extract (Fisher Scientific) and 5 g/L NaCl (Fisher Scientific).

LB agar medium: 15 g/L agar bacteriological (Oxoid), 10 g/L tryptone (Fisher Scientific), 5 g/L yeast extract (Fisher Scientific), 5 g/L NaCl (Fisher Scientific) and supplemented with 30 mg/L kanamycin (Sigma-Aldrich®) or 50 mg/L carbenicillin (Sigma-Aldrich®) for the selection of transformants.

TYP medium: 16 g/L tryptone (Fisher Scientific), 16 g/L yeast extract (Fisher Scientific), 5 g/L NaCl (Fisher Scientific) and 2.5 g/L potassium phosphate dibasic (Acros organics).

Freezing medium: LB medium mixed with 25% glycerol (Sigma-Aldrich®).

E. coli One Shot® TOP10 (Invitrogen™) competent cells were used as host for all DNA manipulations except with lenti vectors pELNSxv and grown in LB medium. *E. coli* XL10-Gold® (Stratagene) competent cells were used as host for lenti vectors and grown in LB medium. *E. coli* Rosetta 2(DE3)pLysS (Novagen®) competent cells were used for protein expression and grown in TYP medium. All cells were grown at 37°C.

2.1.2 Transforming competent cells

Transformation was performed as described by the vendors (Invitrogen™, Stratagene and Novagen®). Briefly, 25 µL of competent cells were thawed on ice for

5 min and 1 μ L (approximately 50 ng to 100 ng) of plasmid DNA was added to the aliquot. After 10 min incubation on ice, cells were incubated in a water bath at 42°C for 30 sec. After a 2 min recovery period on ice, 125 μ L of room temperature (RT) S.O.C. media (Invitrogen™) was added and the mix was incubated at 37°C and 220 revolutions per minute (rpm) for 1 hour in an Orbi-Safe New Orbit incubator (Sanyo). Bacterial cells were then streaked out on LB agar medium plates supplemented with antibiotics and grown overnight at 37°C. Several of the colonies that grew were then picked, cultured overnight into LB medium supplemented with 30 mg/L kanamycin or 50 mg/L carbenicillin and cells were centrifuged and re-suspended in freezing medium for storage.

2.2 MOLECULAR BIOLOGY

2.2.1 Plasmids

All the plasmids were purified using a QIAprep spin Miniprep Kit (Qiagen), Zippy™ Plasmid Miniprep Kit (Zymo Research) or PureLink HiPure Plasmid Filter Purification Kit (Invitrogen™) following the manufacturer's recommendations and DNA concentration was measured using a NanoDrop ND1000 (Thermo Scientific).

2.2.1.1 Vectors for protein expression

The pGMT7-plasmid (Banham and Smith, 1993) was used as the vector for protein expression, conferring a resistance to ampicillin/carbenicillin. It contains a sequence encoding the protein of interest inducible with IPTG (Isopropyl β -D-1-thiogalactopyranoside) under the control of the T7 promoter, the sequence being cloned between BamHI and EcoRI restriction sites. These vectors, initially generated

by PCR mutagenesis and PCR cloning, were used to produce the α -chain and the β -chain soluble domains of MEL5 and α 24 β 17 TCRs, HLA-A2 heavy chain, biotin tagged HLA-A2 heavy chain and β 2m (**Appendix 1**).

2.2.1.2 Vectors for the production of lentivirus

Eight sequences encoding different proteins for the lentiviral expression of TCRs with different affinities toward a melanoma antigen were designed. After being chemically synthesized by GeneArt, plasmids rCD2-pMA, MEL5-pMA, Mel α wt β 5-pMA, Mel α wt β 9-pMA, Mel α wt β 12-pMA, Mel α wt β 13-pMA, Mel α wt β 15-pMA and Mel α wt β 17-pMA were generated. All plasmids conferred a resistance to kanamycin (**Table 2.1**). These plasmids were used as starting vectors in the cloning strategy (section 2.2.2) and sequences were inserted into the lenti vector pELNSxv (Dull et al., 1998) to obtain 7 different lenti vector listed in **Table 2.1**. Packaging plasmids for the production of lentiviruses were pRSV.REV, pMDLg/p.RRE and pVSV-G (Dull et al., 1998) and, as well as pELNSxv, conferred a resistance to ampicillin/carbenicillin.

2.2.2 Cloning of a range of different affinity TCRs toward melanoma into a lentiviral vector

All the different cassettes cloned into pELNSxv were based on the same model. The 2A-like sequences (T2A and P2A) were utilized to construct a tricistronic vector bearing the TCR α chain along with the TCR β chain and the rCD2 reporter gene. Restriction sites XbaI and BspEI, SmaI and XhoI, and NsiI and Sall, flanked the TCR α chain, TCR β chain and rCD2, respectively (**Chapter 6 Figure 6.4**).

Table 2.1. List of the different lenti vectors generated during my PhD.

Starting vector	MEL5-pMA	Mel α wt β 5-pMA	Mel α wt β 9-pMA	Mel α wt β 12-pMA	Mel α wt β 13-pMA	Mel α wt β 15-pMA	Mel α wt β 17-pMA
Destination vector	rCD2-pMA						
Cloning sites	XbaI/XhoI						
Intermediate cloning vector	MEL5 rCD2-pMA	Mel α wt β 5 rCD2-pMA	Mel α wt β 9 rCD2-pMA	Mel α wt β 12 rCD2-pMA	Mel α wt β 13 rCD2-pMA	Mel α wt β 15 rCD2-pMA	Mel α wt β 17 rCD2-pMA
Destination vector	pELNSxv						
Cloning sites	XbaI/SalI						
Final lenti vector	pELNSx v MEL5 rCD2	pELNSx v Mel α wt β 5 rCD2	pELNSx v Mel α wt β 9 rCD2	pELNSx v Mel α wt β 12 rCD2	pELNSx v Mel α wt β 13 rCD2	pELNSx v Mel α wt β 15 rCD2	pELNSx v Mel α wt β 17 rCD2

First, the cassettes TCR α chain-T2A-TCR β chain were excised from the GeneArt starting vectors using XbaI and XhoI restriction enzymes and cloned into the linearized rCD2-pMA destination vector (**Table 2.1**). *E. coli* One Shot® TOP10 (Invitrogen™) competent cells were transformed with the new pMA intermediate plasmids (**Table 2.1**). Plasmids were then purified and sequences were confirmed by automated DNA sequencing (Lark Technologies). The TCR-rCD2 cassettes were then excised from positive intermediate plasmids using XbaI and SalI restriction enzymes and cloned into linearized pELNSxv to obtain 7 different lenti vectors (**Table 2.1**).

2.2.3 Enzymatic digestion

All restriction endonucleases and enzymatic digestion buffers were purchased from New England Biolabs. Enzymatic digestion of plasmid DNA was performed in a final volume of 20 μ L with 2 μ g of plasmid and a restriction enzyme volume maintained at less than 10% of the total volume. After a 2h00 incubation at 37°C, restriction fragments were separated by electrophoresis.

2.2.4 Agarose gel purification and ligation

The enzymatic digestion sample was mixed with 5 μ L of DNA Loading Buffer (Bioline) and restriction fragments were separated by electrophoresis for 1h00 at 100 V in a 1% agarose (Invitrogen™) gel containing 1X SYBR safe DNA gel stain (Invitrogen™) in 100 mL of Tris-acetate-EDTA buffer. A molecular weight marker (HyperLadder™ I, Bioline) was loaded at the same time as the samples to estimate the size of the restriction fragments and they were visualised with a Transilluminator (Modern Biology Inc). Inserts and vector backbones of interest were then extracted

and purified from the agarose gel using QIAquick Gel Extraction Kit (Qiagen) according to the manufacturer's recommendations and DNA concentration measured using NanoDrop ND1000 (Thermo Scientific). The ligation of inserts into vector backbones was performed using 1 μ L of T4 DNA ligase (New England Biolabs) and 50 ng of vector backbone with a molecular ratio of vector to insert of 1:1 and 1:3 in a final volume of 10 μ L of DNA ligase buffer (New England Biolabs) at RT for 30 min. Ligation product was then used to transform competent *E. coli* as described in section 2.1.2.

2.3 PROTEIN CHEMISTRY

2.3.1 Protein expression as inclusion bodies

E. coli Rosetta 2(DE3)pLysS transformed with a pGMT7-derived plasmid vector containing the sequence encoding the protein of interest were grown overnight at 37°C on LB agar plate supplemented with 50 mg/L carbenicillin. A starter culture of the clone producing the most protein of interest was first prepared. In order to do so, individual colonies were picked and grown at 37°C and 220 rpm in 30 mL of TYP supplemented with carbenicillin until the suspension reached an optical density at 600 nm (OD_{600}) between 0.4 and 0.6. The protein production was induced in a 5 mL aliquot using 0.5 mM IPTG (Fisher Scientific) for 3h00. 20 μ L of suspension with and without induction were subjected to SDS-PAGE analysis and the gel was stained with SimplyBlue™ SafeStain (Invitrogen™) as described in section 2.3.5. Starter cultures were then added to 1 L of TYP, supplemented with 100 μ M carbenicillin, and cells were grown as described above until the suspension reached an OD_{600} between 0.4 and 0.6. Protein expression was induced for 3h00 with 0.5 mM IPTG and cells were then centrifuged for 20 min at 4000 rpm in a Legend RT centrifuge

(Sorvall®) with a Heraeus 6445 rotor. The pellet was dissolved in 40 mL of lysis buffer (10 mM Tris pH 8.1 (Fisher Scientific), 10 mM magnesium chloride (MgCl₂) (Acros organics), 150 mM NaCl (Fisher Scientific), 10% glycerol (Sigma-Aldrich®)), sonicated on ice for 30 min at 60% power using a 2 sec interval with a Sonopuls HD 2070 coupled to a MS73 probe (Bandelin) and incubated at RT for 30 min with 0.1 g/L DNase (Fisher Scientific). The suspension containing proteins in the form of inclusion bodies (IB) was treated twice with 100 mL of wash buffer (0.5% Triton® X100 (Sigma-Aldrich®), 50 mM Tris pH 8.1 (Fisher Scientific), 100 mM NaCl (Fisher Scientific), 10 mM EDTA pH 8.1 (Fisher Scientific)) and 20 min of centrifugation at 4°C and 10 000 rpm with an Evolution RC centrifuge and a SLA-1500 rotor (Sorvall®). The pellet was re-suspended in 100 mL of re-suspension buffer (50 mM Tris pH 8.1 (Fisher Scientific), 100 mM NaCl (Fisher Scientific), 10 mM EDTA pH 8.1 (Fisher Scientific)) and centrifuged as before at 10 000 rpm. Finally, the pellet was dissolved in 10 mL of guanidine buffer (6 M guanidine (Fisher Scientific), 50 mM Tris pH 8.1 (Fisher Scientific), 2 mM EDTA pH 8.1 (Fisher Scientific), 100 mM NaCl (Fisher Scientific)) and the protein concentration was determined by measuring the optical density at 280 nm (OD₂₈₀) using NanoDrop ND1000 (Thermo Scientific). A 20 µL fraction of the suspension in lysis buffer, washing buffer and re-suspension buffer was subjected to SDS-PAGE and stained with SimplyBlue™ SafeStain (Invitrogen™) (described in section 2.3.5) during this process in order to check the quality of the IB production.

2.3.2 Refolding of pMHCI

Approximately 30 mg of HLA-A2 (or HLA-A2 with a biotin tag) heavy-chains IB preparation, 30 mg of β2m IB preparation and 4 mg of peptide (ProImmune) were

mixed and denatured for 30 min at 37°C in a final volume of 6 mL of guanidine buffer supplemented with 10 mM dithiothreitol (DTT) (Sigma-Aldrich®). Protein refolding was initiated by diluting the previous mix in 1 L of a pre-chilled MHC redox buffer (50 mM Tris pH 8.1 (Fisher Scientific), 400 mM L-arginine (SAFC®), 2 mM EDTA pH 8.1 (Fisher Scientific), 6 mM cysteamine (Sigma-Aldrich®) and 4 mM cystamine (Sigma-Aldrich®)). Protein refolds were then left stirring at 4°C for 3h00, transferred into 12.4 kDa MWCO (molecular weight cut-off) dialysis tubing (Sigma-Aldrich®), dialysed twice for 24h00 against 20 L of 10 mM Tris pH 8.1 (Fisher Scientific) and finally filtered on Metricel® 0.45 µm membrane filter (Pall) and purified by anion exchange and gel filtration (described in section 2.3.4).

2.3.3 Refolding of soluble TCR

Approximately 30 mg of TCR α chain IB preparation and 30 mg of TCR β chain IB preparation were denatured separately for 30 min at 37°C in 3 mL of guanidine buffer supplemented with 10 mM DTT (Sigma-Aldrich®). Protein refolding was initiated by diluting the denatured TCR α chain in 1 L of a pre-chilled TCR redox buffer (50 mM Tris pH 8.1 (Fisher Scientific), 2.5 M urea (Sigma-Aldrich®), 2 mM EDTA pH 8.1 (Fisher Scientific), 6 mM cysteamine (Sigma-Aldrich®) and 4 mM cystamine (Sigma-Aldrich®)) for 30 mins. The denatured TCR β chain was then added to the TCR redox buffer and TCR refolds were then left stirring at 4°C for 3h00. Refolds were transferred into 12.4 kDa MWCO dialysis tubing (Sigma-Aldrich®), dialysed twice 24h00 against 20 L of 10 mM Tris pH 8.1 (Fisher Scientific), filtered on Metricel® 0.45 µm membrane filter (Pall) and purified by anion exchange and gel filtration methods described below.

2.3.4 Fast Protein Liquid Chromatography (FPLC) purification

Refolded proteins were purified first by anion exchanged and then by gel filtration using Fast Protein Liquid Chromatography (FPLC). The filtered refold preparation was loaded onto a 7.9 mL POROS® 10/100 HQ 50 µm column (Applied Biosystems™) pre-equilibrated with 20 mL of 10 mM Tris pH 8.1 (Fisher Scientific). Proteins were then eluted at 5 mL/min with a salt gradient (0-500 mM NaCl in 10 mM Tris pH 8.1) and 1 mL fractions were collected. Fractions corresponding to the protein of interest were analysed by SDS-PAGE (described in section 2.3.5) and fractions containing the protein of interest were pooled together and concentrated down to 500 µL with 10 kDa MWCO Vivaspin 20 (Sartorius) or 10 kDa MWCO Vivaspin 4 (Sartorius) by centrifugation for 20 min at 4000 rpm and 4°C in a Legend RT centrifuge (Sorvall®) with a Heraeus 6445 rotor. Proteins were stored at 4°C before gel filtration. Concentrated protein preparations were then loaded with a 2 mL injection loop onto a 24mL Superdex 200 10/300 GL column (GE Healthcare) pre-equilibrated with the appropriate elution buffer (Phosphate Buffer Saline (PBS, Oxoid), BIAcore buffer HBS (10 mM HEPES pH 7.4, 150 mM NaCl, 3.4 mM EDTA and 0.005% surfactant, GE Healthcare) or crystal buffer (10 mM Tris pH 8.1 (Fisher Scientific) and 10 mM NaCl (Fisher Scientific))). Elution was performed at a flow-rate of 0.5 mL/min and 1 mL fractions containing the protein of interest were analysed by SDS-PAGE and concentrated down, as described above, to 100 µL. Protein concentration was measured by UV spectrophotometry on spectrophotometer Biomate 3 (Thermo Spectronic). Absorbance value at 280 nm was used to calculate the protein concentration ($C_{protein}$) using the Beer-Lambert law $C_{protein} = \frac{OD_{280}}{\epsilon_{protein} \times l_{cuvette}}$ where the distance the light travels through the cuvette ($l_{cuvette}$) is 1 cm and the molar extinction

coefficient ($\epsilon_{protein}$) obtained with ProtParam software (Wilkins et al., 1999) equals 95800 $M^{-1}.cm^{-1}$ for pMHCI complexes, 77350 $M^{-1}.cm^{-1}$ for the MEL5 TCR and 86860 $M^{-1}.cm^{-1}$ for the $\alpha 24\beta 17$ Mel TCR. Pure protein sample was then kept at 4°C if used within two days or frozen at -20°C for short-term storage and -80°C for long-term storage.

2.3.5 Sodium dodecyl sulphate – Polyacrylamide gel electrophoresis and SimplyBlue™ staining

Proteins were separated by Sodium dodecyl sulphate - Polyacrylamide gel electrophoresis (SDS-PAGE) using the NuPAGE® system (Invitrogen™). A 20 μL aliquot of protein sample was mixed with 5 μL of 5X Laemmli buffer (Laemmli, 1970) (315 mM Tris pH 6.4 (Fisher Scientific), 10% glycerol (Sigma-Aldrich®), 2% SDS (Sigma) and 0.0125% Bromophenol Blue (Sigma)) and denatured at 95°C for 5min (non-reducing conditions). For reducing conditions, 50 mM DTT (Sigma-Aldrich®) was added prior to denaturation. Samples were analysed on NuPAGE® Novex® 4-12% Bis-Tris gels in 1X NuPAGE® MES running buffer at 200 V for 45 min and 10 μL of SeeBlue Plus 2 Pre-stained Standards (Invitrogen™) or 5 μL of BLUEye Prestained Protein Ladder (GeneDirex®) was used as molecular weight marker. The gels were stained with SimplyBlue™ SafeStain (Invitrogen™) and destained with Milli-Q water (Millipore™) following the manufacturer's instructions.

2.3.6 Biotinylation of pMHCI and manufacture of pMHCI tetramer

For the multimerization of pMHCI molecules, biotin-tagged pMHCI complexes were first biotinylated. An aliquot of biotin-tagged pMHCI complexes, previously gel

filtrated in PBS, was adjusted to 700 μ L with PBS and mixed with 100 μ L of Biomix A (0.5 M Biocine buffer pH 8.3) (Avidity), 100 μ L of Biomix B (100 mM ATP, 100 mM MgOAc, 500 μ M d-Biotin), 100 μ L of d-Biotin (500 μ M) (Avidity) and 1 μ L of BirA enzyme (Biotin Protein Ligase) (Avidity) at 3 mg/mL. The mix was incubated for 2h00 at 37°C and gel filtrated in BIAcore buffer as described above in order to remove the excess of biotin. Biotinylated monomers were used for BIAcore experiments and, after multimerization, as tetramers in cell assays.

Multimerization of the pMHCI molecules was performed by adding R-phycoerythrin (PE) conjugated streptavidin (Invitrogen™) or allophycocyanin (APC) conjugated streptavidin (Invitrogen™) in aliquots to saturate the biotin binding sites to a molar ratio pMHCI:conjugate of 4:1. Tetramer names are formed with the first 3 letters of the peptide followed by the chromophore name (eg for a tetramer presenting the peptide ELAGIGILTV and coupled to the R-phycoerythrin the name will be ELA-PE).

2.4 SURFACE PLASMON RESONANCE

For both Surface Plasmon Resonance (SPR) methods, equilibrium-binding analysis and kinetic analysis, experiments were performed with a BIAcore 3000, or T100® (GE Healthcare) equipped with a CM5 sensor chip (GE Healthcare). Briefly, CM5 chip coupling solutions (GE Healthcare) containing 100 μ L of 100 mM NHS (N-hydroxysuccinimide) and 100 μ L of 400 mM EDC (1-ethyl-3-(3-dimethylpropyl)-carboiimide) were used to activate the chip prior to streptavidin binding. Approximately 5000 response units (RU) of streptavidin (110 μ L of 200 μ g/mL in 10 mM acetate pH 4.5 (Sigma-Aldrich®)) was covalently linked to the chip surface in

all four flow-cells and 100 μL of 1 M ethanolamine hydrochloride was used to deactivate any remaining reactive groups.

2.4.1 Equilibrium-binding analyses

For the equilibrium-binding analyses, biotinylated pMHCI at $\sim 1 \mu\text{M}$ in BIAcore buffer was coupled to the streptavidin-coated chip. Approximately 500-2000 RU of pMHCI was attached to the CM5 sensor chip at a slow flow-rate of 10 $\mu\text{L}/\text{min}$ to ensure uniform distribution on the chip surface. The surface was then saturated with 1 mM biotin (Avidity) in BIAcore buffer. Ten serial dilutions ($1/2$ dilutions) of soluble TCRs (MEL5 or Mel $\alpha 24\beta 17$) in BIAcore buffer were injected over the relevant flow-cells at a high flow-rate of 45 $\mu\text{L}/\text{min}$ at the concentrations indicated and at 25°C. For the thermodynamics experiments, this method was repeated at the following temperatures: 5°C, 10°C (MEL5 only), 13°C ($\alpha 24\beta 17$ only), 15°C, 20°C, 25°C, 30°C. Results were analysed using BIAevaluation 3.1 (GE Healthcare), Excel (Microsoft) and Origin 6.0 (Microsoft) software. The equilibrium binding constant (K_D) values were calculated assuming a 1:1 interaction ($A + B \leftrightarrow AB$) by plotting specific equilibrium-binding responses against protein concentrations followed by non-linear least squares fitting of the Langmuir binding equation $AB = \frac{B \times AB_{max}}{K_D + B}$.

The thermodynamic parameters were calculated using the non-linear van't Hoff equation ($RT \ln K_D = \Delta H^\circ - T\Delta S^\circ + \Delta C_p^\circ(T - T_0) - T\Delta C_p^\circ \ln(T/T_0)$) with $T_0 = 298 \text{ K}$.

2.4.2 Kinetic analyses

Two different methods were used to obtain the kinetics (k_{on} and k_{off}): “single injection kinetics” and “single cycle kinetic” (Karlsson et al., 2006). Approximately

200 RU of biotinylated pMHCI at $\sim 1 \mu\text{M}$ in BIAcore buffer was coupled to the streptavidin-coated chip at a slow flow-rate of $10 \mu\text{L}/\text{min}$ and the chip was then saturated with biotin (Avidity). $\alpha 24\beta 17$ soluble TCR was injected at a high flow-rate of $45 \mu\text{L}/\text{min}$ in order to limit the effects of mass-transport on binding association measurements and re-binding effects on the measurement of TCR dissociation.

For the “single injection kinetics” method, the $\alpha 24\beta 17$ soluble TCR at approximately 430 nM was injected for 240 sec (association time) over the four flow-cells and then the BIAcore buffer was injected for 1200 sec at the same flow-rate (dissociation time) at 25°C . Responses were measured in real-time and association rate constant (k_{on}), dissociation rate constant (k_{off}) and equilibrium binding constant ($K_D = \frac{k_{\text{off}}}{k_{\text{on}}}$) were estimated by fitting of the data using BIAevaluation 3.1 (GE Healthcare) software.

For the “single cycle kinetic” method, five serial dilutions ($1/3$ dilutions) of the $\alpha 24\beta 17$ soluble TCR from approximately 460 nM to approximately 6 nM was injected for 200 sec at 25°C . The dissociation time between each injection was 120 sec and the dissociation time after the last injection was 3600 sec . Constants (k_{on} , k_{off} and K_D) were estimated by global fitting of the data using BIAevaluation 3.1 (GE Healthcare) software. For the thermodynamics experiments, this method was repeated at the following temperatures: 5°C , 7°C , 12°C , 15°C , 19°C , 22°C , 25°C , 30°C , 32°C , 35°C , 37°C and 40°C . The thermodynamic parameters were calculated using the non-linear van't Hoff equation with Origin 6.0 software.

2.5 CRYSTALLOGRAPHY

2.5.1 Crystallisation conditions for $\alpha 24\beta 17$, A2-ELA-4A and $\alpha 24\beta 17/pMHCI$ complexes

All protein crystallisation trials were set up in-house on a Phoenix (Art Robbins Instruments) crystallisation robot. Crystals were grown by vapour diffusion at 18°C via the sitting drop technique in 96-well Intelli-plate (Art Robbins Instruments) with a reservoir containing 60 μ L of crystallisation buffer (mother liquor).

For $\alpha 24\beta 17$ TCR and A2-ELA-4A pMHCI crystallisation, the soluble TCR and pMHCI were concentrated down to approximately 10 mg/mL (0.2 mM) in crystal buffer. For the $\alpha 24\beta 17/pMHCI$ complexes crystallisation, TCR and pMHCI were mixed with a 1:1 molar ratio to obtain a protein solution at approximately 10 mg/mL (0.1 mM). Proteins were mixed with crystallisation buffers at a volume ratio of 1:1 (0.2 μ L protein and 0.2 μ L mother liquor) from screens presented in **Chapter 3**. Crystallised proteins and optimal crystallisation buffers are detailed in **Table 2.2**.

2.5.2 Crystallisation conditions for MEL5/A2-AAG and MEL5/A2-EAA complexes

2.5.2.1 MEL5/A2-AAG: different TCR/pMHCI complexes mixing

The crystallisation method presented above was slightly modified in order to obtain crystals for MEL5/A2-AAG complex. The protein solution of MEL5/A2-AAG complex at 0.1 mM in crystal buffer was supplemented with 1 μ M of $\alpha 24\beta 17/A2$ -AAG complex in crystal buffer. Crystallisation trial was then performed as described above.

Table 2.2. Crystallised proteins and optimal crystallisation buffer.

Crystal	Buffer (Molecular Dimensions)	Polyethylene glycol (PEG) (Molecular Dimensions)	Ammonium sulphate (Sigma-Aldrich®)	Glycerol (Sigma-Aldrich®)
α 24 β 17	0.1 M sodium cacodylate pH 6.5	20% PEG 8000	0.2 M	
A2-ELA-4A	0.1 M sodium cacodylate pH 6.0	20% PEG 8000	0.2 M	
α 24 β 17/A2-ELA	0.1 M HEPES pH 7.0	20% PEG 4000	0.2 M	
α 24 β 17/A2-EAA	0.1 M HEPES pH 7.5	15% PEG 4000	0.2 M	8.7%
α 24 β 17/A2-AAG	0.1 M HEPES pH 7.0	20% PEG 4000		15%
α 24 β 17/A2-ELA-4A	0.1 M Tris pH 7.5	15% PEG 4000		17.4%
α 24 β 17/A2-ELA-7A	0.1 M Bis Tris propane pH 7.0	20% PEG 4000	0.2 M	17.4%
MEL5/A2-AAG	0.1 M HEPES pH 7.5	25% PEG 4000		15%
MEL5/A2-EAA	0.1 M Tris pH 7.5	15% PEG 4000		15%

Table 2.3. Beamlines, wavelengths of detection and detectors used for each crystal at DLS.

Crystal	DLS beamline	Wavelength of detection (Å)	Detector
α 24 β 17	I24	0.978	Rayonix MX300
A2-ELA-4A	I03	0.976	ADSC Q315 CCD
α 24 β 17/A2-ELA	I03	0.976	ADSC Q315 CCD
α 24 β 17/A2-EAA	I02	0.979	ADSC Q315r
α 24 β 17/A2-AAG	I03	0.976	ADSC Q315 CCD
α 24 β 17/A2-ELA-4A	I03	0.976	ADSC Q315 CCD
α 24 β 17/A2-ELA-7A	I03	0.976	ADSC Q315 CCD
MEL5/A2-AAG	I04-1	0.916	Marmosaic 300mm CCD
MEL5/A2-EAA	I04-1	0.916	Marmosaic 300mm CCD

Optimal crystals were obtained in 0.1 M HEPES pH 7.5 (Molecular Dimensions), 15% glycerol (Sigma-Aldrich®) and 25% PEG 4000 (Molecular Dimensions) (**Table 2.2**).

2.5.2.2 MEL5/A2-EAA: seeding from MEL5/A2-AAG

The seeding kit Seed Bead™ (Hampton Research) was used to obtain crystals of MEL5/A2-EAA complex as no crystals were obtained with the methods described above. Crystals of MEL5/A2-AAG complex obtained in section 2.5.2.1 were used as seeds for MEL5/A2-EAA complex. In order to do so, the 0.4 µL drop containing the MEL5/A2-AAG crystals and 50 µL of mother liquor (0.1 M Tris pH 8.0, 15% glycerol, 25% PEG 4000) from the reservoir was added to the Seed Bead™ eppendorf and it was vortexed for 90 sec. This seeding mix was then serially diluted ($1/10$ and $1/100$ dilutions) into the same buffer and 35 µL of MEL5/A2-EAA complex solution around 1 mM was supplemented with 1 µL of seeding mix or 1 µL of seeding mix dilution. Crystallisation trials were then performed as described above. Optimal crystals were obtained in 0.1 M Tris pH 8.5 (Molecular Dimensions), 15% glycerol (Sigma-Aldrich®) and 15% PEG 4000 (Molecular Dimensions) (**Table 2.2**).

2.5.3 X-ray diffraction data collection, molecular replacement and model refinement

Crystals were harvested in-house and cryo-cooled in liquid nitrogen (100 K). Data were collected in a stream of nitrogen gas at 100 K on different beamline at the Diamond Light Source (DLS), Oxfordshire, UK. The **Table 2.3** compiles the beamlines, wavelength of detection and detectors used for each crystal. Reflection

intensities were estimated with the MOSFLM package (Leslie, 1992) and the data were scaled, reduced and analysed with SCALA and the CCP4 package (Ccp, 1994). Structures were solved with Molecular Replacement using PHASER (McCoy et al., 2007). The model sequence was adjusted with COOT (Emsley and Cowtan, 2004) and the model refined with REFMAC5 (Murshudov et al., 1997). Graphical representations were prepared with PYMOL (Delano, 2002).

2.6 MAMMALIAN CELL CULTURE

2.6.1 Mammalian cell culture medium

RPMI-PSG: RPMI-1640 medium (Invitrogen™) supplemented with 100 IU/mL penicillin (Invitrogen™), 100 IU/mL streptomycin (Invitrogen™) and 2 mM L-glutamine (Invitrogen™).

R2: RPMI-PSG medium containing 2% of heat-inactivated foetal calf serum (FCS, Invitrogen™).

R10: RPMI-PSG medium containing 10% FCS (Invitrogen™).

D10: DMEM medium (Invitrogen™) supplemented with 100 IU/mL penicillin (Invitrogen™), 100 IU/mL streptomycin (Invitrogen™), 2 mM L-glutamine (Invitrogen™), 2 mM Na pyruvate (Invitrogen™) and containing 10% FCS (Invitrogen™).

CK medium: R10 supplemented with 2.5% Cellkines (Helvetica Healthcare), 200 IU/mL IL-2 (Pharmacy) and 25 ng/mL IL-15 (Peprotech).

Freezing medium: 40% R10, 10% DMSO (Sigma-Aldrich®) and 50% FCS (Invitrogen™).

2.6.2 Cell lines

293T: 293T cells are a highly transfectable derivative of the HEK293 cells (Demaison et al., 2002) which constitutively express the simian virus 40 (SV40) large T antigen. These cells were grown in D10 at 37°C / 5% CO₂ and used to produce the lentiviruses.

HLA-A2 C1R: C1R is a human B-cell lymphoblastoid line lacking surface HLA-A and HLA-B antigens. C1R was derived from Hmy.2 B-LCL by gamma irradiation followed by selection for class I monoclonal antibodies and complement (Storkus et al., 1989). Hmy.2 CIR B-cells expressing wild type HLA-A*0201 were generated previously (Purbhoo et al., 2001; Wooldridge et al., 2005). Briefly, cells were transfected with pcDNA3.1 mammalian expression vector (Invitrogen™) containing an insert encoding wild type full length HLA-A*0201 and cells were then cloned by limiting dilution. These cell lines, maintained in R10 medium at 37°C / 5% CO₂, show 100% HLA-A2 expression and were used for the Jurkat activation assays, the peptide titration assays, the peptide library assay and the chromium release assays.

Mel526 and Mel624: Mel526 and Mel624 cells lines are HLA-A2 positive melanoma cell lines established from cryopreserved single cell suspensions of metastatic deposits from patients and were identified as pure tumour cell populations by cytologic and immunocytochemical analysis (Topalian et al., 1990; Topalian et

al., 1989). These cell lines were maintained as monolayer cultures in D10 medium at 37°C / 5% CO₂ and were used as target cells for the chromium release assay.

Jurkat TCR negative GLuc: Jurkat TCR negative J.RT3-T3.5 cells (ATCC[®] number TIB-153[™]) derived from Jurkat E6.1 cells (Weiss and Stobo, 1984) were grown in R10 at 37°C / 5% CO₂. These cells lack the β chain of the TCR and do not express either CD3 or the $\alpha\beta$ TCR on the surface (Liu et al., 2000). These cells have been transfected in-house by Dr John Bridgeman with a NFAT-luc construct (Stratagene, via Dr Reno Debets) containing NFAT (Nuclear Factor of Activated T-cells) responsive elements from the IL2 promoter driving the expression of *Gaussia* Luciferase.

MEL5/MEL13: These CD8⁺ T-cell clones are expressing a TCR specific for the heteroclitic version of the melanoma antigen Melan-A/MART-1₂₆₋₃₅ (ELAGIGILTV) in complex with HLA-A*0201 (Cole et al., 2009). Cells were grown in CK medium at 37°C / 5% CO₂. These two clones were generated at the same time from the same CD8⁺ T-cell line by Professor Andrew Sewell and have a TCR that is identical at the nucleotide level. MEL5 and MEL13 are therefore considered to be an identical clone.

Jurkat transduced and CTL transduced: these cells are respectively Jurkat TCR negative cells GLuc or CD8⁺ T-cells transduced with the different lentiviruses. They are expressing MEL5 TCR or a modified version of MEL5 and rCD2 on the surface and were grown in R10 or CK medium at 37°C / 5% CO₂, respectively. **Table 2.4** lists the different transduced cell lines.

Table 2.4. List of the different transduced cell lines generated during my PhD.

Cell type	Transduced						
Jurkat TCR negative GLuc	Jurkat MEL5 rCD2	Jurkat MEL5 β 5 rCD2	Jurkat MEL5 β 9 rCD2	Jurkat MEL5 β 12 rCD2	Jurkat MEL5 β 13 rCD2	Jurkat MEL5 β 15 rCD2	Jurkat MEL5 β 17 rCD2
HLA-A2 positive CD8 ⁺ T-cells	A2 ⁺ CD8 ⁺ MEL5 rCD2						

2.6.3 Cryopreservation and storage of cell lines

Cells for cryopreservation were generally stored in 1ml of freezing medium in cryovials (Nunc) at cell concentrations of 5×10^6 or 10×10^6 cells/ml. Cryovials were stored in cryo-freezing containers (Nalgene) at -80°C for 48 hours and then transferred to liquid nitrogen containers. Cryopreserved cells were thawed at 37°C in a water bath and transferred gently using a Pasteur pipette (Fisher Scientific) into cool (4°C) RPMI-PSG. Cells were centrifuged for five minutes at 500 g then resuspended in the appropriate media.

2.6.4 Cell counting by Trypan exclusion

Cell counting was carried out by mixing 10 μl of cell suspension with an equal volume of Trypan blue (STEMCELL™ Technologies). 10 μl of this mixture was then transferred onto a clean Neubauer haemocytometer (Weber Scientific International Ltd). Viable cells were identified by the absence of Trypan staining at a 100 times magnification on a light microscope (Olympus CK40 model).

2.7 GENERATION OF TRANSDUCED JURKAT AND CTL LINES

2.7.1 Lentivirus production

For the production of a lentivirus batch, $15\text{-}30 \times 10^6$ 293T cells were seeded one day prior to transfection into a 75 cm^2 flask (Greiner Bio-One) in 25 mL of D10. Cells were transfected with a plasmid mix (15 μg pELNSxv containing the insert of interest, 18 μg pRSV.REV, 7 μg pVSV-G and 18 μg pMDLg/p.RRE) using 174 μL of Express-in™ (Open Biosystems) reagent in 3 mL of D10 supplemented with 10 mM HEPES pH 7.4 (Invitrogen™). After 1 min incubation at RT with the

transfection mix, 22 mL of D10 supplemented with 10 mM HEPES was added and transfected cells were incubated. One day post-transfection, the supernatant was collected, kept at 4°C and 25 mL of fresh D10 medium was added in order to collect a 48h00 post-transfection supernatant. Both supernatant batches (24h00 and 48h00) were filtered separately with 0.22 µm filters (Miller®-GP, Millipore) into a 38.5 mL thin-wall ultracentrifuge tube (Ultra-Clear™, Beckman), ultracentrifuged for 2h00 at 26000 g and 4°C (Optima™ L-100 XP with SW28 rotor, Beckman Coulter). Each pellet was dissolved in 2mL of D10 supplemented with 10 mM HEPES and 200 µL aliquots of the lentivirus suspensions were stored at -80°C.

2.7.2 Jurkat TCR negative GLuc transduction and sorting

For the transduction of the Jurkat TCR negative GLuc with a lentivirus, cells were seeded one day prior to transduction into 6-well plate (Greiner Bio-One) at 4×10^5 cells/well in 4 mL of R10. Cells were transduced with 5 µL of the lentivirus suspension and were analysed two days post-transduction by fluorescence activated cell sorting (FACS) (section 2.8). In order to obtain a pure population expressing the TCR of interest, Jurkat transduced cells were magnetically sorted using MS Columns (Miltenyi Biotec) and MiniMACS™ (Miltenyi Biotec), following the manufacturer's instructions. Briefly, up to 1×10^7 cells were resuspended in 400 µL of cold MACS buffer (PBS supplemented with 0.5% heat-inactivated FCS and 2 mM EDTA) and incubated on ice in the dark for 20 min with 10 µL of anti-CD3 FITC (fluorescein isothiocyanate) conjugated antibody (AbD Serotec). Cells were then washed twice with 2 mL of cold MACS buffer, resuspended in 400 µL of cold MACS buffer and incubated on ice for 20 min with 20 µL of anti-FITC microbeads (Miltenyi Biotec). Cells were magnetically sorted in cold MACS buffer, centrifuged for 5 min at 1500

rpm (PK 131 centrifuge with T516 rotor, ALC®), resuspended in R10 and incubated at 37°C / 5% CO₂ in a 24-well plate (Greiner Bio-One).

2.7.3 CTL transduction

2.7.3.1 CTL sorting from peripheral blood mononuclear cells (PBMCs)

CTLs were isolated from peripheral blood mononuclear cells (PBMCs). Buffycoats from 500 mL blood from healthy donors were purchased from the Welsh Blood Service or 50 mL samples were collected by venepuncture into a sterile container with preservative free heparin (LEO Laboratories Ltd) at a final concentration of 100 IU/ml of blood. PBMCs were isolated on a Ficoll-Hypaque (Lymphoprep™, Axis-Shield) density gradient centrifugation of blood diluted 1 to 1 with sterile PBS in sterile 50 mL Falcon™ centrifuge tubes (BD Biosciences) for 20 min at 2000 rpm (Sorvall RT 6000D centrifuge) without breaks. Buffy coat was aspirated from the gradient interface with a Pasteur pipette and placed in sterile 50 mL Falcon™ centrifuge tubes (BD Biosciences). Cells were then washed twice with RPMI-PSG and resuspended in RPMI-PSG. CTLs were magnetically sorted from PBMCs mainly as described in previous section. Briefly, PBMCs were centrifuged at 1300 rpm for 10 min (PK 131 centrifuge with T516 rotor, ALC®) and the pellet was resuspended in 80 µL of cold MACS buffer per 1×10^7 cells. The cell suspension was mixed with 20 µL of anti-CD8 microbeads (Miltenyi Biotec) per 1×10^7 cells, incubated on ice for 20 min, and cells were magnetically sorted in cold MACS buffer. CTLs were washed twice with R10 and resuspended in CK medium at 5×10^5 cells/mL. For the activation of these CTLs, 1×10^6 cells per well were seeded in a 24-well plate with 75 µL of Dynabeads® Human T-Expander CD3/CD28 (Invitrogen™) and cells were incubated overnight at 37°C / 5% CO₂. Non-sorted

PBMCs were also used as feeders (PBMCs irradiated with Cesium-137) for transduced CTLs expansion.

2.7.3.2 CTL transduction, sorting and expansion

Activated CTLs were transduced with 1 mL of the lentivirus suspension and analysed two days post-transduction by FACS for rCD2 and/or MEL5 TCR expression (section 2.8). In order to obtain a pure population expressing MEL5, transduced CTLs were magnetically sorted twice; first using an anti-rCD2-PE conjugated antibody (rCD2-PE) (AbD Serotec) and then using an ELA-PE tetramer as described above in section 2.3.6. Briefly, transduced CTLs were first incubated for 20 min on ice in the dark with 10 μ L of rCD2-PE followed by a sorting using 20 μ L of anti-PE microbeads (Miltenyi Biotec). rCD2 positive transduced cells were then grown and maintained for 2 weeks in a 25 cm² flask (Greiner Bio-One) with 1×10^7 feeders in CK medium supplemented with 1 μ g/mL phytohaemagglutinin (PHA, Alere Ltd) in order to expand them. This single positive population was then incubated for 20 min on ice in the dark with 12 μ L of ELA-PE in MACS buffer supplemented with 50 nM dasatinib (Axon) in order to avoid induced cell death. Double positive cells (cells expressing rCD2 and the TCR of interest) were sorted using 20 μ L of anti-PE microbeads (Miltenyi Biotec). Cells were grown first for a week with feeders in CK medium supplemented with 1 μ g/mL PHA and they were then maintained in CK medium.

2.8 FLOW CYTOMETRY ANALYSIS

The expressions on the cell surface of the TCR of interest, rCD2, CD3 or CD8 were detected by FACS. Cells were washed once in PBS and resuspended in 50 μ L of PBS staining mix containing 5 μ L of antibody conjugated to FITC, APC or PE. Staining mix was supplemented with 1 μ L of pMHCI tetramer for the detection of expression of a specific TCR. Cells were incubated on ice in the dark for 20 min, washed twice with cold PBS and resuspended in 300 μ L of cold PBS. Analysis were performed on a BD FACSCanto™ II (BD Biosciences) flow cytometer using BD FACSDiva 6.0 software (BD Biosciences). Results were analysed with FlowJo 7.6 software (Tree Star, Inc).

2.9 JURKAT ACTIVATION ASSAY

In the wells of a 96-well round bottomed plate (Greiner Bio-One), 1×10^5 CIR cells (in 45 μ l volume) expressing wild type HLA-A*0201 were pulsed in duplicate with 5 μ L peptide at 1 mM or 5 μ L of PHA at 1mg/mL at 37°C / 5% CO₂ for 2 hours. Jurkat TCR negative GLuc were then washed once in PSG and resuspended in R10. 1×10^5 Jurkat TCR negative GLuc (in 50 μ l) were then added per well of pulsed targets and plates were incubated for 5h00 at 37°C / 5% CO₂. Cell supernatant was collected and 50 μ L of GLuc substrate (BioLux® *Gaussia* Luciferase Assay Kit, New England Biolabs) was added to 20 μ L of supernatant in a 96-well Microfluor® 2 plate (Thermo Scientific). Luminescence at 485 nm was measured with a FLUOstar OPTIMA (BGM LABTECH) and results were analysed with Excel (Microsoft) and GraphPad Prism 5 (GraphPad) softwares.

2.10 CTL EFFECTOR FUNCTION ASSAYS

2.10.1 Peptide titration assay

CTLs were washed twice in RPMI-PSG and rested in R2 overnight. In the wells of a 96-well round bottomed plate (Greiner Bio-One), 6×10^4 CIR cells (in 45 μ l volume) expressing wild type HLA-A*0201 were pulsed in duplicate with 5 μ L peptide at the stated concentrations (from 10^{-12} to 10^{-3} M) at 37°C / 5% CO₂ for 2 hours. Rested CD8⁺ T-cells were then washed once in PSG and resuspended in R2. 3×10^4 CD8⁺ T-cells (in 50 μ l) were then added per well of pulsed targets and plates were incubated overnight at 37°C / 5% CO₂. Cell supernatant was collected and assayed for MIP-1 β by ELISA using a CCL4 DuoSet ELISA kit (R&D Systems) as described in section 2.10.3.

2.10.2 Peptide library screen

2.10.2.1 A description of positional scanning combinatorial peptide libraries (PS-CPLs)

In PS-CPLs (Pepscan Presto), equimolar peptide mixtures are arranged into sub-libraries that allow for systematic scans on each position of a ligand. Mixtures within each sub-library contain a fixed amino acid drawn from the natural 20 proteogenic L-amino acids in a single position whilst the other positions have all the 19 amino acids (excluding cysteine) residues combined in every possible way. This positional scan is serially repeated across all the positions of the library (Hemmer et al., 1998). Each collection of sub-libraries contains all possible peptide sequences of a given length representing trillions of peptides (Nino-Vasquez et al., 2004). Sequences containing multiple cysteine residues were barred by the exclusion of cysteine from the variable positions in order to reduce the chance of disulphide bond formation

between cysteine residues. The PS-CPLs are extremely diverse in their peptide composition. The decamer combinatorial peptide library screen used in this study contained 9.36×10^{12} ($(10+19) \times 19^9$) different decamer peptides (Ekeruche-Makinde et al., 2012). Cell activation with PS-CPL mixtures is described in section 2.10.2.2.

2.10.2.2 Peptide library screen assay

CD8⁺ T-cells were washed twice in RPMI-PSG and rested in R2 overnight. In the wells of a 96-well round bottomed plate (Greiner Bio-One), 6×10^4 HLA-A2 CIR cells (in 45 μ l volume) were pulsed in duplicate with 5 μ l of peptide mixture from the decapeptide PS-CPL at a final concentration of 100 μ M at 37°C for 2 hours. Rested CD8⁺ T-cells were washed once in RPMI-PSG and resuspended in R2. 3×10^4 CD8⁺ cells (in 50 μ l) were then added per well of pulsed targets. Plates were incubated overnight at 37°C / 5 % CO₂. Cell supernatant was then collected and assayed for MIP-1 β by ELISA using a CCL4 DuoSet ELISA kit (R&D Systems) as described in section 2.10.3.

2.10.3 ELISA (Enzyme-linked immunosorbent assay) for MIP1 β

ELISAs for the detection of MIP1 β production were performed with a CCL4 DuoSet ELISA kit (R&D Systems) and the recommended accessory reagents (Wash buffer, Reagent diluent, Streptavidin-HRP, Chromogen, Peroxide, and Stop solution). All wash steps were performed on an AquaMax 2000 microplate washer (MDS analytical technologies). Briefly, 96-well ELISA microplates (R&D Systems) were coated with 100 μ l of capture antibody diluted according to the manufacturer's recommendation. Plates were incubated overnight at RT after which they were

washed three times with wash buffer and blocked with reagent diluent. After another wash step, 100 µl of cell supernatant collected from an activation assay or 100 µl of standard solution was then placed in each well. Plates were incubated according to the manufacturers' recommendation and washed again. 100 µl of detection antibody diluted in reagent diluent was then added per well. Plates were then incubated as recommended and washed before adding streptavidin-horseradish peroxidase diluted in reagent diluent. After a further incubation, plates were washed and carefully blotted. 100 µl of a 1:1 solution of stabilised chromogen and peroxide was then added per well. Plates were incubated in the dark for up to twenty minutes after which 50 µl of stop solution (2N sulphuric acid) was added per well. OD readings of plates were taken at 450 nm (Bio-rad iMark microplate reader) with correction set to 570 nm. Results were analysed with Excel (Microsoft) and GraphPad Prism 5 (GraphPad) softwares.

2.10.4 Chromium release assay

Target cells (C1R cells expressing wild type HLA-A*0201, Mel526 and Mel624) were resuspended in R10 and labelled with ^{51}Cr (30 µCi per 10^6 cells) (Perkin Elmer) for 1 hour at 37°C then washed once and left for a further hour in fresh media to allow leaching. Labelled HLA-A2 C1R cells were then washed again and pulsed at 2×10^3 cells/well in a 96-well round bottom plate (Greiner Bio-One) with ELAGIGILTV peptide at a final concentration of 100 µM. CD8⁺ T-cells were then added at the indicated E:T ratios (from 25:1 to 0.20:1) and plates were incubated for 4 hours at 37°C / 5% CO₂. Following incubation, 15 µl of cell supernatant was collected and mixed with 150 µl of scintillation cocktail (Optiphase supermix, Perkin Elmer) then analysed for radioactivity using a MicroBeta² plate counter (Perkin

Elmer). Percentage cytotoxicity (or percentage specific lysis) was then calculated using the following equation: Specific lysis = [(Experimental lysis - Spontaneous Lysis) / (Maximum Lysis - Spontaneous Lysis)] x 100%. Values used for calculations were obtained as the average of three replicates. Results were analysed with Excel (Microsoft) and GraphPad Prism 5 (GraphPad) softwares.

CHAPTER 3
DEVELOPMENT OF A TCR/pMHC OPTIMIZED
PROTEIN CRYSTALLIZATION SCREEN

Chapter background.....	106
3.1 Introduction.....	106
3.1.1 Methods for producing recombinant TCRs.....	107
3.1.2 Methods for improving TCR stability.....	108
3.1.3 Generating crystals for high resolution X-ray diffraction.....	109
3.1.4 Aim.....	111
3.2 Results.....	111
3.2.1 Design of a TCR/pMHC Optimized Protein crystallization Screen	111
3.2.2 Comparison of TOPS efficiency with commercially available screens...	115
3.2.3 Optimal conditions for the generation of TCR/pMHC complex crystals	120
3.2.4 TOPS efficiency correlated to the datasets obtained in this screen	123
3.3 Discussion.....	126

Chapter background

A key aim of my PhD was to analyse and further characterize the TCR/pMHCI interaction by SPR and by crystallography. My laboratory possessed the equipment required for efficient protein production and purification as well as a crystallography facility. Due to the wide array of commercial screens available in my laboratory for crystallography, the development of a specific TCR/pMHC screen was not initially planned. However, as my attempts at crystallizing my TCR/pMHCI complexes were unsuccessful with these screens, I decided to develop my own screen (TOPS) based on the crystallization conditions of previously published TCR/pMHC complexes. My colleagues and I crystallized and solved several structures using TOPS. Due to the efficiency of TOPS, we decided to write a scientific paper about TOPS (Bulek et al., 2012b) in order for other scientists to benefit from this screen. The development of TOPS is described herein.

3.1 INTRODUCTION

T-cells play an important role in the protection against pathogens and cancer and have been shown to cause/contribute towards many autoimmune diseases (Bulek et al., 2012a; Rudolph et al., 2006; Wong and Pamer, 2003). The T-cell receptor (TCR) recognizes foreign and self protein fragments bound to the self-major histocompatibility complex (pMHC) (Garboczi et al., 1996). The first structure of a murine TCR (2C) with MHC class I H2-K^b in association with dEV8 peptide was published in 1996 (Garcia et al., 1996). This was shortly followed by the structure of a human TCR (A6) in complex with HLA-A*0201-Tax (peptide derived from human T-cell lymphotropic virus type 1₁₁₋₁₉) (Garboczi et al., 1996). These structures provided the first insight into T-cell antigen recognition and revealed a number of

important features of the interface between the TCR and pMHC. Ten years later, only 10 unique human TCR/pMHC complexes had been solved, reviewed by Rudolph and co-workers (Rudolph et al., 2006). In recent years, this number has increased to <25 unique human TCR/pMHC complexes, but progress has still been relatively slow compared with the number of antibody structures, or unligated pMHC structures that have been reported. This lack of structural information regarding human TCR/pMHC complexes has compromised the determination of a comprehensive and accepted set of rules that govern T-cell antigen recognition and a number of conflicting theories still dominate the field (Bridgeman et al., 2012). In this Chapter I present the methods for producing recombinant TCRs and improving soluble TCR stability. I also briefly describe the requirements for the production of high-quality protein crystals and I then present the development of a crystallization screen optimized for TCR/pMHC complexes.

3.1.1 Methods for producing recombinant TCRs

Difficulties in generating sufficient quantities of soluble TCR and pMHC protein, and in producing high quality TCR/pMHC complex crystals, may explain the low number of these structures. Additionally, TCRs bind to pMHCs with relatively weak affinity ($K_D = 0.1\text{-}270\ \mu\text{M}$ (Bridgeman et al., 2012; Cole et al., 2007)), which may further impede their ability to form stable complexes for crystallization. A number of approaches have been proposed for the production of stable, soluble recombinant TCRs, including modification of the expression vectors and optimization of culture conditions. To date, soluble TCRs have been generated using various eukaryotic expression systems such as: *Drosophila melanogaster* (Garcia et al., 1996), myeloma cells (Wang et al., 1998), Chinese hamster ovary cells (Reiser et al., 2000) and

Spodoptera frugiperda cells (Hahn et al., 2005). However, prokaryotic expression as inclusion bodies using *E. coli* strains, followed by artificial refolding, remains the most popular and robust system because it produces high yields of homogenous non-glycosylated protein (Cole et al., 2008; Cole et al., 2007; Cole et al., 2009). This last method was used for the generation of recombinant TCRs and MHCs in my laboratory.

3.1.2 Methods for improving TCR stability

Contrary to antibodies, TCRs are not naturally expressed in a soluble form but are anchored to the T-cell membrane and are stabilized by an extracellular, membrane proximal, inter-chain disulphide bond. However, the production of soluble TCRs incorporating this native bond has been very poor (Garboczi et al., 1996; van Boxel et al., 2009). Different TCR cloning methods have been designed to improve soluble TCR stability including: (i) expression of the variable domains only in a form of a single chain Fv fragment (scFv) to form a scTCR (Gregoire et al., 1996; Housset et al., 1997); (ii) expression of TCR α and β chains carrying 30 residue-long BASE-p1 (α) and ACID-p1 (β) leucine-zipper heterodimerization motifs at their carboxyl termini (Chang et al., 1994); (iii) expression of TCR α and β chains carrying c-Jun (α) and c-Fos (β) leucine-zipper heterodimerization motifs at their carboxyl termini (Kalandadze et al., 1996; Willcox et al., 1999b); (iv) introduction of a carboxy-terminal flanking sequence to the full length V and C ectodomains to promote the formation of an interchain disulphide bridge (Stewart-Jones et al., 2003); and, (v) introduction of non-native disulphide bond into the interface between the TCR constant domains by mutating residues threonine 48 (α chain) and serine 57 (β chain)

into cysteines (Boulter et al., 2003) to form “dsTCRs” (**Figure 3.1**). The ‘Boulter-disulphide’ method has been the preferred choice in my laboratory.

3.1.3 Generating crystals for high resolution X-ray diffraction

Once expressed and purified, the last challenge is to generate TCR/pMHC complex protein crystals capable of high resolution X-ray diffraction. Even when pure soluble protein is available, producing high-quality crystals remains a major bottleneck in structure determination (Chayen and Saridakis, 2008). Crystallization requires large quantities of protein, highly concentrated solutions, filtration of the protein solutions and "neutral" pHs (4-9) that did not cause proteins to break down (McCoy, 2009). There are, of course, an infinite number of crystallization conditions. Parameters to vary include the type of precipitant (salts, polymers, and organic solvents), precipitant concentration, buffer type and pH of buffer, temperature, and the presence or absence of divalent cations (Asherie, 2004; Blundell and Johnson, 1976). In order to achieve the crystallisation of TCR/pMHC complexes, a number of commercial screens, not tailored specifically for T-cell-associated proteins, have been used by different laboratories with some success (evidenced by the modest number of TCR/pMHC complexes published). Van Boxel et al. designed a crystal screen for isolated TCRs (van Boxel et al., 2009) but no screen was specifically developed for the TCR/pMHC complexes crystallization.

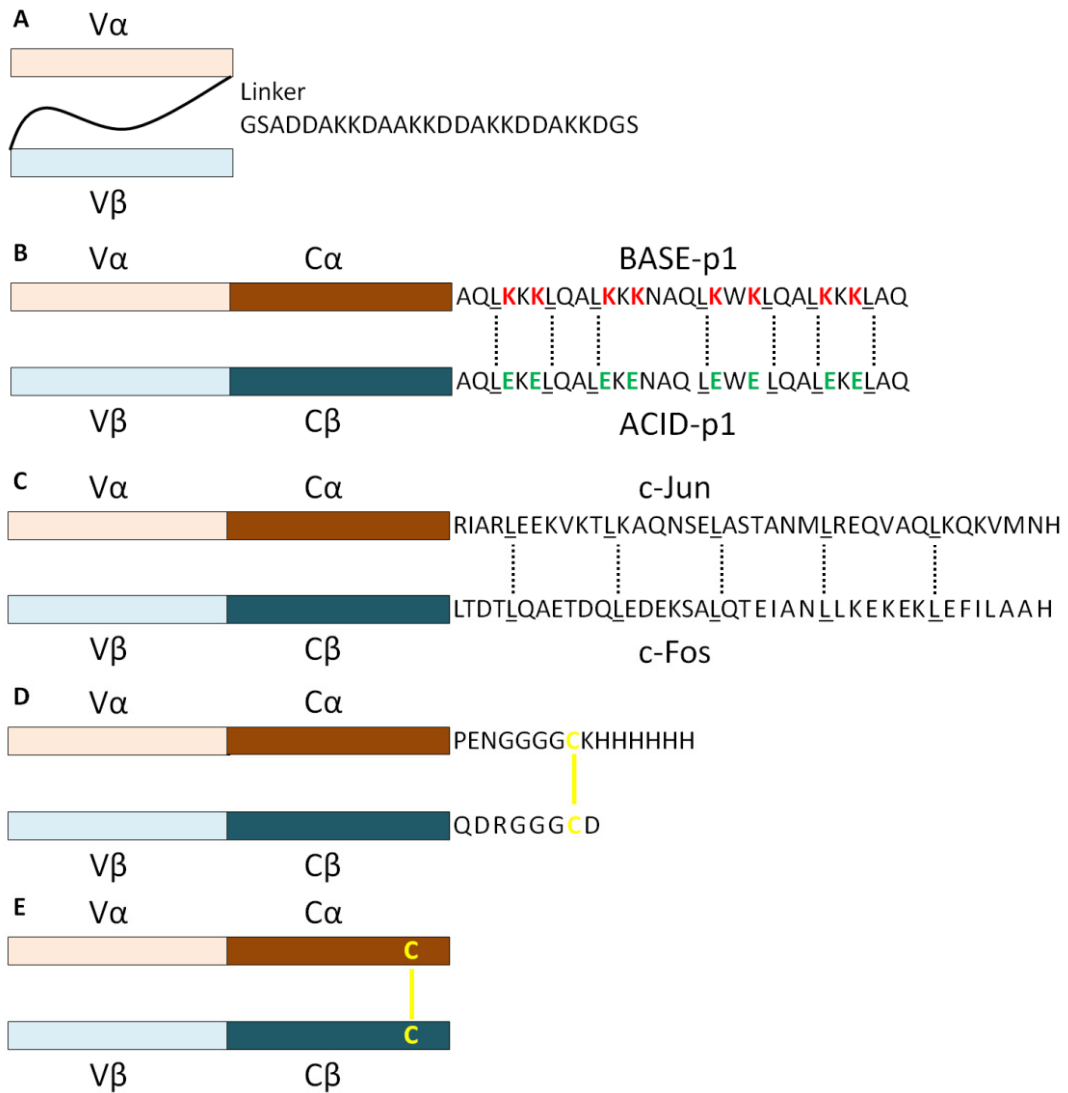


Figure 3.1. Schematic representations of the different methods to increase soluble TCRs stability.

(A) Variable domains of the TCR expressed in the form of a single chain Fv fragment (scFv) to form a scTCR. (B) TCR α and β chains carrying 30 residue-long BASE-p1 (α) and ACID-p1 (β) leucine-zipper heterodimerization motifs at their carboxyl termini. “Leucine-zipper” motifs (dash lines), acidic residues (green) and basic residues (red) are shown. (C) TCR α and β chains carrying c-Jun (α) and c-Fos (β) leucine-zipper heterodimerization motifs at their carboxyl termini. Leucine-zipper” motifs (dash lines) are shown. (D) Introduction of a carboxy-terminal flanking sequence to the full length V and C ectodomains to promote the formation of an interchain disulphide bridge (yellow). (E) Introduction of non-native disulphide bond (yellow) into the interface between the TCR constant domains by mutating residues threonine 48 (α chain) and serine 57 (β chain) into cysteines to form “dsTCRs”.

3.1.4 Aim

My PhD project involved the crystallization of melanoma specific TCRs (MEL5 and $\alpha 24\beta 17$) complexed with HLA-A2 when presenting different melanoma peptides (ELAGIGILTV, EAAGIGILTV and AAGIGILTV). I failed to successfully crystallize these complexes with the commercially available crystal screens after several attempts. I therefore decided to develop my own TCR/pMHC Optimized Protein crystallization Screen (TOPS) by analysing the crystallization conditions of previously published TCR/pMHC complexes. This Chapter will highlight the design of TOPS and will determine the optimal conditions for the generation of TCR/pMHC complex crystals.

3.2 RESULTS

3.2.1 Design of a TCR/pMHC Optimized Protein crystallization Screen

TCR/pMHC complex structures have previously been solved by a number of different groups using individually determined crystallization conditions. In order to combine these data to generate a comprehensive TCR/pMHC Optimized Protein crystallization Screen (TOPS), I investigated the crystallization conditions of 16 previously published TCR/pMHC complexes (Adams et al., 2005; Chen et al., 2005; Cole et al., 2009; Colf et al., 2007; Ding et al., 1998; Garboczi et al., 1996; Hennecke et al., 2000; Hennecke and Wiley, 2002; Kjer-Nielsen et al., 2003; Li et al., 2005a; Maynard et al., 2005; Reiser et al., 2000; Sami et al., 2007; Stewart-Jones et al., 2003; Tynan et al., 2005; Tynan et al., 2007) (**Table 3.1**) (**Figure 3.2**). Although there was substantial variation in the crystallization conditions identified for different TCR/pMHC complexes, certain trends were noticed. The pH lay

between 5.6 and 8.5 in all cases, with the TCR/pMHC complexes tending to crystallize at the higher end of this pH range (**Figure 3.2A**); with 25%, 19% and 19% of complexes crystallizing in the pH range 7.0-7.5, 7.5-8.0 and 8.0-8.5, respectively. Six conditions (38%) contained glycerol as cryoprotectant (**Figure 3.2B**). All conditions contained PEG (polyethylene glycol), although the weight (550-8000 g/mol) and percentage (10-25%) were very variable. The best PEG concentration, representing 31% of the previous structures reported, was between 15% and 17.5%. Molecular weight PEG 3350, 4000 and 8000 were most successful (**Figure 3.2C&D**) evidenced by 31%, 13% and 44% of all structures being obtained with each additive, respectively. Another common component of successful conditions were various salts, with concentrations ranging from 0 to 1 M, the absence of salt (38%) and 0.2 M (31%) being most popular (**Figure 3.2E**). Based on these findings I developed a crystallization screen for TCR/pMHC complexes (**Table 3.2**). The screen consisted of two 48 well PEG/pH screens. Each PEG/pH screen consisted of four buffer systems (C₂H₆AsO₂Na, MES, HEPES and TRIS) at a concentration of 0.1 M in combination with PEG 4000, or PEG 8000 at 15, 20 and 25%. These buffers allowed scanning the pH range from 6.0 to 8.5. 15% glycerol was added to the first subscreen, whereas 0.2 M ammonium sulphate was added to the second subscreen.

In some cases, TOPS generated several crystal hits that were of lower quality, i.e. the crystals were very small, contained cracks or impurities, or did not diffract to high resolution. In these cases, we extended the conditions that yielded crystals to generate a number of other fine screens that proved useful for specific TCR/pMHC complexes.

Table 3.1. Crystallization conditions of 16 previously published TCR/pMHC complexes.

TCR/pMHC complex	Buffer	pH	PEG (%)	PEG (g/mol)	Glycerol (%)	Salt	Reference
ha1G4/A2-NY-ESO-1	85mM HEPES	8.5	17	4000	15		(Sami et al., 2007)
1G4/A2-NY-ESO-1	0.1M Na Nitrate	6.8	20	3350	10		(Chen et al., 2005)
G8/T22	0.1M Na Citrate	5.6	15	4000		2mM Zinc Acetate	(Adams et al., 2005)
HA1.7/DR1-HA	0.1M HEPES	7	14	8000		1M NaCl	(Hennecke et al., 2000)
HA1.7/DR4-HA	0.1M HEPES	7	13	8000		1M NaCl	(Hennecke and Wiley, 2002)
3A6/DR2A-MBP	0.1M Na Citrate	6	10	8000		0.2M Ammonium Sulphate	(Li et al., 2005a)
ELS4/B35	0.1M Na Cacodylate	6.4	16	3350		0.2M CaCl ₂	(Tynan et al., 2007)
A6/A2-tax	50mM TRIS	8.5	14	8000	20	0.1M Mg Acetate	(Garboczi et al., 1996)
JM22/A2-MP(58-66)	50mM MES	6.5	14	8000	10		(Stewart-Jones et al., 2003)
B7/A2-tax	0.1M Mg Acetate	7.1	12	8000			(Ding et al., 1998)
LC13/B8-EBV	0.2M Ammonium Acetate	7.5	25	8000			(Kjer-Nielsen et al., 2003)
MEL5/A2-ELA	0.1M TRIS	7.4	23	550	15		(Cole et al., 2009)
SB27/B3508-LPEP	0.1M Na Cacodylate	6.7	16	3350		0.2M K Iodide	(Tynan et al., 2005)
BM3.3/H-2Kb-pBM1	0.1M HEPES	7.5	15	6000		0.1M Na Acetate	(Reiser et al., 2000)
ha2C/H-2L ^d -QL9	0.1M TRIS	8.5	20	3350	25	0.2M Ammonium Phosphate	(Colf et al., 2007)
172.1/I-A ^u -MBP	0.1M HEPES	7.5	21	3350		0.2M Lithium Sulphate	(Maynard et al., 2005)

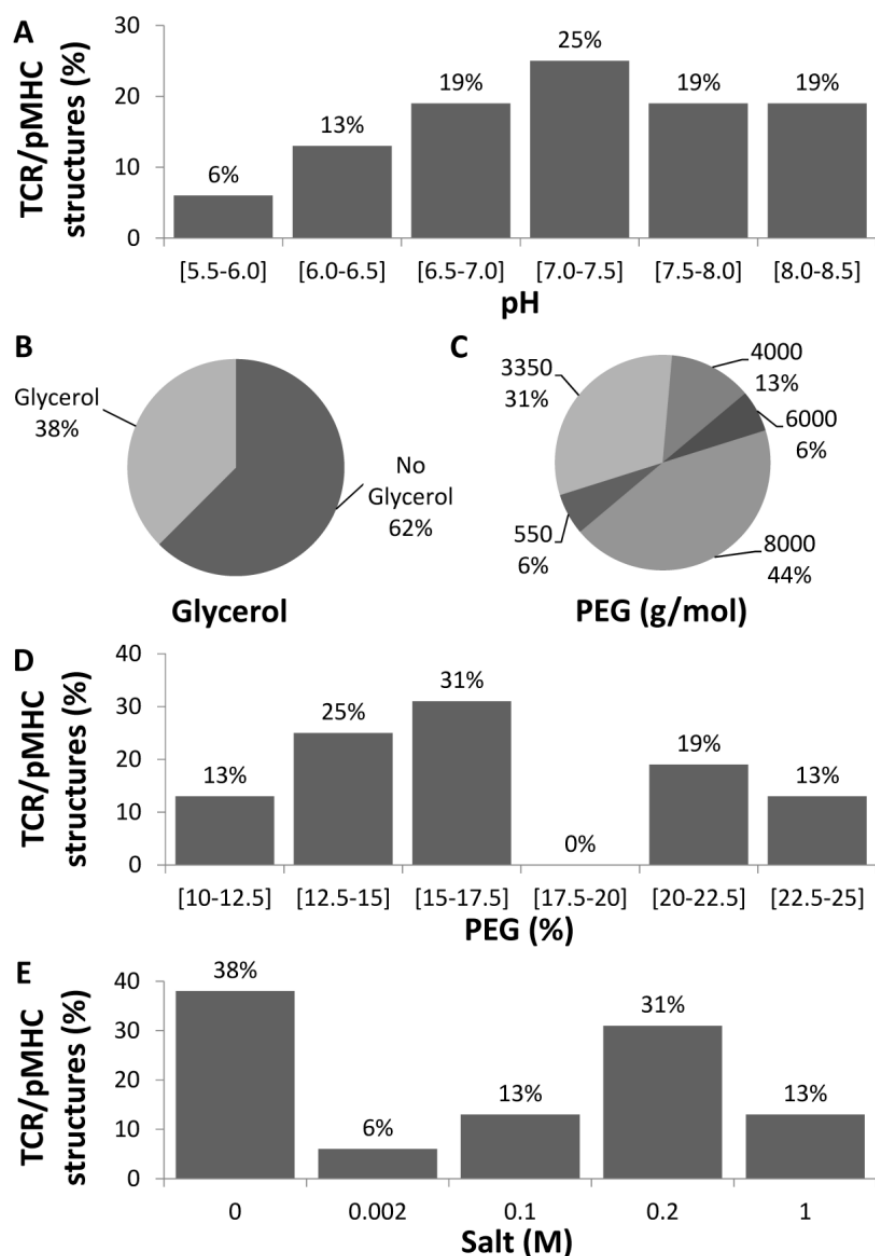


Figure 3.2. Analysis of the crystallization conditions of 16 previously published TCR/pMHC complexes.

(A) The pH of the conditions lay between pH 5.6 to pH 8.5, with a preference for the higher end of this pH range. (B) Glycerol was used as a cryoprotectant in 38% of cases. (C) The molecular weight of the PEG varied from 550 g/mol to 8000 g/mol (PEG 3350, 4000 and 8000 being the most successful). (D) The best PEG concentration was between 15% and 17.5%, with a PEG concentration range from 10% to 25%. (E) Various salts, with concentrations from 0 to 1 M, were used, with a preference for 0.2 M.

TOPS1 (**Table 3.3**) was designed by extending the lower range of pH with $\text{C}_2\text{H}_6\text{AsO}_2\text{Na}$ pH 5.0 and 5.5 of the A07 condition of the TOPS screen. In addition, PEG 3350 was compared versus PEG 4000 in this screen. TOPS2 (**Table 3.4**) was designed by extending the lower range of PEG concentration (10, 12.5, 15, 17.5, 20 and 22.5%) of the second subscreen of the TOPS screen. In addition, one of the buffer systems ($\text{C}_2\text{H}_6\text{AsO}_2\text{Na}$ pH 6.0) was replaced by a non-buffered condition and supplemented by another precipitant (0.2 M sodium sulphate) as some good hits were obtained using a commercially available screen (PACT Premier, condition E08; 0.2 M sodium sulphate and 20% PEG 4000). TOPS3 (**Table 3.5**) was designed by reducing the range of pH (from 6.5 to 7.5) and increasing the number of buffer system (MES pH 6.5, BIS TRIS propane pH 7.0 and TRIS pH 7.0) as well as the range of glycerol concentrations (0, 4.4, 8.7 and 17.4%). PEG 4000 was the PEG of choice in this screen. The only difference between TOPS3 and TOPS4 (**Table 3.6**) was that TOPS4 contained 0.2 M ammonium sulphate. These screens generated 5 TCR/pMHC complexes as detailed in **Table 3.7**.

3.2.2 Comparison of TOPS efficiency with commercially available screens

High-throughput crystallization trials were performed using 3 commercially available screens (PACT Premier, JBScreen and JCSG-plus (Molecular Dimensions Ltd)) and/or 5 different “homemade” screens (TOPS, TOPS1, TOPS2, TOPS3 and TOPS4), the last four screens being derivatives of the TOPS screen. Crystallization conditions were successfully identified for 25 TCR/pMHC complexes, 14 of which were derivatives from a common parent complex.

Table 3.2. TOPS conditions.

Buffer (pH) 0.1 M	15% glycerol						0.2 M ammonium sulphate					
	PEG 4000 (%)			PEG 8000 (%)			PEG 4000 (%)			PEG 8000 (%)		
	15	20	25	15	20	25	15	20	25	15	20	25
C ₂ H ₆ AsO ₂ Na (pH 6)	A1	A2	A3	A4	A5	A6	A7	A8	A9	A10	A11	A12
C ₂ H ₆ AsO ₂ Na (pH 6.5)	B1	B2	B3	B4	B5	B6	B7	B8	B9	B10	B11	B12
MES (pH 7)	C1	C2	C3	C4	C5	C6	C7	C8	C9	C10	C11	C12
HEPES (pH 7)	D1	D2	D3	D4	D5	D6	D7	D8	D9	D10	D11	D12
HEPES (pH 7.5)	E1	E2	E3	E4	E5	E6	E7	E8	E9	E10	E11	E12
TRIS (pH 7.5)	F1	F2	F3	F4	F5	F6	F7	F8	F9	F10	F11	F12
TRIS (pH 8)	G1	G2	G3	G4	G5	G6	G7	G8	G9	G10	G11	G12
TRIS (pH 8.5)	H1	H2	H3	H4	H5	H6	H7	H8	H9	H10	H11	H12

Table 3.3. TOPS1 conditions.

Buffer (pH) 0.1 M	0.2 M ammonium sulphate						
C ₂ H ₆ AsO ₂ Na (pH 5.5)	A1	A2	A3	A4	A5	A6	15% PEG 3350
C ₂ H ₆ AsO ₂ Na (pH 6)	B1	B2	B3	B4	B5	B6	
C ₂ H ₆ AsO ₂ Na (pH 5)	C1	C2	C3	C4	C5	C6	15% PEG 4000
C ₂ H ₆ AsO ₂ Na (pH 5.5)	D1	D2	D3	D4	D5	D6	
C ₂ H ₆ AsO ₂ Na (pH 6)	E1	E2	E3	E4	E5	E6	

Table 3.4. TOPS2 conditions.

Buffer (0.1 M) or non buffered component (0.2 M)	0.2 M ammonium sulphate											
	PEG 4000 (%)						PEG 8000 (%)					
	10	12.5	15	17.5	20	22.5	10	12.5	15	17.5	20	22.5
Na ₂ SO ₄	A1	A2	A3	A4	A5	A6	A7	A8	A9	A10	A11	A12
C ₂ H ₆ AsO ₂ Na (pH 6.5)	B1	B2	B3	B4	B5	B6	B7	B8	B9	B10	B11	B12
MES (pH 7)	C1	C2	C3	C4	C5	C6	C7	C8	C9	C10	C11	C12
HEPES (pH 7)	D1	D2	D3	D4	D5	D6	D7	D8	D9	D10	D11	D12
HEPES (pH 7.5)	E1	E2	E3	E4	E5	E6	E7	E8	E9	E10	E11	E12
TRIS (pH 7.5)	F1	F2	F3	F4	F5	F6	F7	F8	F9	F10	F11	F12
TRIS (pH 8)	G1	G2	G3	G4	G5	G6	G7	G8	G9	G10	G11	G12
TRIS (pH 8.5)	H1	H2	H3	H4	H5	H6	H7	H8	H9	H10	H11	H12

Table 3.5. TOPS3 conditions.

Buffer (pH) 0.1 M	No ammonium sulphate											
	PEG 4000 (%)											
	15	20	25	15	20	25	15	20	25	15	20	25
C ₂ H ₆ AsO ₂ Na (pH 6.5)	A1	A2	A3	A4	A5	A6	A7	A8	A9	A10	A11	A12
MES (pH 6.5)	B1	B2	B3	B4	B5	B6	B7	B8	B9	B10	B11	B12
MES (pH 7)	C1	C2	C3	C4	C5	C6	C7	C8	C9	C10	C11	C12
HEPES (pH 7)	D1	D2	D3	D4	D5	D6	D7	D8	D9	D10	D11	D12
TRIS propane (pH 7)	E1	E2	E3	E4	E5	E6	E7	E8	E9	E10	E11	E12
TRIS (pH 7)	F1	F2	F3	F4	F5	F6	F7	F8	F9	F10	F11	F12
TRIS (pH 7.5)	G1	G2	G3	G4	G5	G6	G7	G8	G9	G10	G11	G12
HEPES (pH 7.5)	H1	H2	H3	H4	H5	H6	H7	H8	H9	H10	H11	H12
	0			4.4			8.7			17.4		
	Glycerol (%)											

Table 3.6. TOPS4 conditions.

Buffer (pH) 0.1 M	0.2 M ammonium sulphate											
	PEG 4000 (%)											
	15	20	25	15	20	25	15	20	25	15	20	25
C ₂ H ₆ AsO ₂ Na (pH 6.5)	A1	A2	A3	A4	A5	A6	A7	A8	A9	A10	A11	A12
MES (pH 6.5)	B1	B2	B3	B4	B5	B6	B7	B8	B9	B10	B11	B12
MES (pH 7)	C1	C2	C3	C4	C5	C6	C7	C8	C9	C10	C11	C12
HEPES (pH 7)	D1	D2	D3	D4	D5	D6	D7	D8	D9	D10	D11	D12
TRIS propane (pH 7)	E1	E2	E3	E4	E5	E6	E7	E8	E9	E10	E11	E12
TRIS (pH 7)	F1	F2	F3	F4	F5	F6	F7	F8	F9	F10	F11	F12
TRIS (pH 7.5)	G1	G2	G3	G4	G5	G6	G7	G8	G9	G10	G11	G12
HEPES (pH 7.5)	H1	H2	H3	H4	H5	H6	H7	H8	H9	H10	H11	H12
	0			4.4			8.7			17.4		
	Glycerol (%)											

Table 3.7. Successfully crystallized TCR/pMHC complexes, TCRs and pMHCs in my laboratory.

TCR/pMHC complex	Screen	Resolution (Å)	pH	PEG (%)	PEG	Glycerol (%)	Salt (M)
<u>α24β17/A2-ELA</u>	<u>TOPS4</u>	<u>2.4</u>	<u>7.0</u>	<u>20</u>	<u>4000</u>	<u>0</u>	<u>0.2</u>
<u>α24β17/A2-AAG</u>	<u>TOPS</u>	<u>2.8</u>	<u>7.0</u>	<u>20</u>	<u>4000</u>	<u>15</u>	<u>0</u>
<u>α24β17/A2-ELA-4A</u>	<u>TOPS3</u>	<u>2.7</u>	<u>7.0</u>	<u>15</u>	<u>4000</u>	<u>17.4</u>	<u>0</u>
<u>α24β17/A2-ELA-7A</u>	<u>TOPS4</u>	<u>2.6</u>	<u>7.0</u>	<u>20</u>	<u>4000</u>	<u>17.4</u>	<u>0.2</u>
<u>α24β17/A2-EAA</u>	<u>TOPS4</u>	<u>2.1</u>	<u>7.5</u>	<u>15</u>	<u>4000</u>	<u>8.7</u>	<u>0.2</u>
<u>MEL5/A2-EAA</u>	<u>TOPS</u>	<u>3.0</u>	<u>6.5</u>	<u>15</u>	<u>4000</u>	<u>15</u>	<u>0</u>
<u>MEL5/A2-AAG</u>	<u>TOPS</u>	<u>3.2</u>	<u>7.5</u>	<u>25</u>	<u>4000</u>	<u>15</u>	<u>0</u>
P1/A2-CLG	TOPS	2.6	6.0	15	4000	15	0
SB7/A2-FLY	TOPS	2.6	6.5	15	4000	0	0.2
868/A2-SLY	TOPS	2.9	6.0	15	4000	0	0.2
868/A2-6I	TOPS	2.9	6.0	15	4000	0	0.2
868/A2-3F6I8V	TOPS1	2.8	5.5	15	4000	0	0.2
1E6/A2-ALW	TOPS	2.6	6.0	15	4000	15	0
1E6/A2-AQW	PACT	3.0	6.5	20	4000	0	0.2
1E6/A2-RQW	PACT	2.3	6.0	20	6000	0	0.2
1E6/A2-YQF	PACT	2.1	7.0	20	6000	0	0.2
1E6/A2-WQY	TOPS	1.9	7.0	25	8000	0	0.2
1E6/A2-KLP	TOPS	2.9	6.5	15	8000	0	0.2
1E6/A2-YLG	TOPS	2.5	6.5	15	4000	0	0.2
1E6/A2-MVW	TOPS	2.0	7.5	15	4000	0	0.2
1E6/A2-RQF(I)	TOPS	1.9	7.5	15	4000	0	0.2

1E6/A2-RQF(A)	TOPS	1.9	7.0	15	4000	0	0.2
GP100/A2-YLE	JBS	2.0	7.0	20	4000	0	0.2
ILA/A2-ILA	TOPS	2.6	7.0	20	8000	0	0.2
AS01/A2-GLC	TOPS	2.6	6.0	20	4000	0	0.2
TCR	Screen	Resolution (Å)	pH	PEG (%)	PEG	Glycerol (%)	Salt (M)
<u>α24β17</u>	<u>TOPS</u>	<u>2.4</u>	<u>6.5</u>	<u>20</u>	<u>8000</u>	<u>0</u>	<u>0.2</u>
P1	TOPS	1.5	6	20	4000	0	0.2
HA1.7	TOPS	2.7	7.5	25	8000	0	0.2
F11	PACT	1.5	7.5	20	3350	0	0.2
1E6	PACT	2.6	7.5	20	3350	0	0.2
pMHC	Screen	Resolution (Å)	pH	PEG (%)	PEG	Glycerol (%)	Salt (M)
<u>A2-ELA-4A</u>	<u>TOPS</u>	<u>2.0</u>	<u>6</u>	<u>20</u>	<u>8000</u>	<u>0</u>	<u>0.2</u>
A2-RQW	TOPS	1.5	8	20	8000	15	0
A2-YQF	TOPS	1.5	8	25	4000	15	0
A2-FLY	TOPS	1.8	7	25	4000	0	0.2
A2-6I	TOPS	1.7	7	20	4000	15	0
A2-3F6I8V	TOPS	1.8	6	25	4000	0	0.2
A2-FAT	TOPS	2.8	6.5	25	8000	0	0.2
A2-CLG	TOPS	2.4	7.0	25	4000	0	0.2
A2-ALW	PACT	1.7	6.5	20	3350	0	0.2
A2-AQW	PACT	1.7	6.5	20	3350	0	0.2
A2-KLP	PACT	1.8	7.5	20	3350	0	0.2
A2-YLG	PACT	1.4	6.5	20	3350	0	0.2

TCR, pMHC and TCR/pMHC complexes I obtained are in bold and underlined

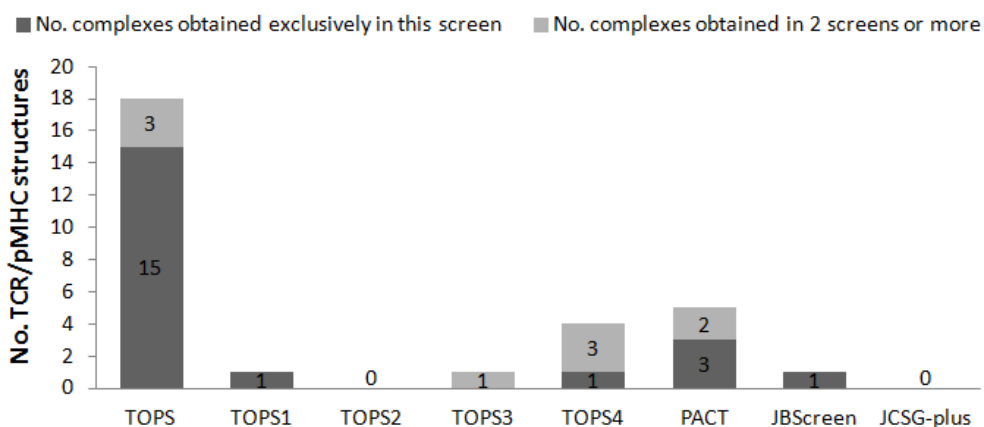


Figure 3.3. Comparison of TCR/pMHC structures obtained in my laboratory in TOPS and TOPS screen-derived versus commercially available screens.

15 structures out of 25 were exclusively obtained in TOPS, 21 being obtained in total in TOPS or TOPS screen-derived. 3 TCR/pMHC structures were exclusively obtained in PACT Premier, 1 in JBScreen and no structures were obtained with the JCSG-plus screen.

Among these 25 unique complexes, 21 were obtained from the TOPS screen or TOPS screen-derived conditions while only 3 were obtained exclusively from the PACT Premier screen and 1 from the JBScreen. No complexes were obtained from the JCSG-plus screen. Thus, TCR/pMHC structures that crystallized in TOPS screen represented more than 80% of the total number of complexes solved (**Table 3.7 and Figure 3.3**). Although the TOPS screen was designed for TCR/pMHC complexes, a selection of uncomplexed TCR and pMHC proteins were generated in the laboratory based on our ongoing research interests, to test the efficacy of TOPS. This approach directly resulted in structures of 3 uncomplexed TCRs and 8 pMHCs proteins (**Table 3.7**).

3.2.3 Optimal conditions for the generation of TCR/pMHC complex crystals

The total number of 25 complexes and 53 datasets (we collected datasets from different conditions for a particular complex) (**Appendix 2**) allowed us to perform an analysis in order to define the most optimal conditions for growing crystals of TCR/pMHC complexes. One dataset represents a full diffraction dataset obtained from one particular crystal growing condition for a given complex and usable to solve, analyze and publish the structure. We often collected several datasets from the same condition for a particular complex but only one is included in the **Appendix 2** in order to avoid any redundancy in the analysis. The results of the analysis are presented in **Figure 3.4**. In all cases, the pH was within a range of 5.0 to 8.5. However, a great majority of crystals (90%) were obtained around a neutral pH of 6.0 to 7.5, and more than a third (35%) at pH 7.0 (**Figure 3.4A**). The presence of salt, a precipitating agent, at 0.2 M was required as 79% of crystals successfully grew in such conditions (**Figure 3.4B**). The best PEG concentrations, another

precipitating agent, were 15% and 20%, resulting in 51% and 40% of the datasets, respectively. In contrast, higher precipitant concentrations produced only 9% of the datasets (**Figure 3.4C**). The most popular PEG size was around 4000 g/mol with 79% of datasets obtained in this condition (13% PEG 3350 and 66% PEG 4000). PEG at smaller molecular weight only generated 2% of the datasets, whereas PEG at higher molecular weight generated 19% of the datasets (6% and 13% of PEG 6000 and 8000 respectively) (**Figure 3.4D**). Although glycerol was a good cryoprotecting agent, the absence of this component was essential in 72% of the cases. However, when the presence of glycerol was required, 15% appeared to be the best concentration (**Figure 3.4E**).

Although this analysis suggested the optimal conditions for obtaining TCR/pMHC complexes, it was performed by taking each variable independently. In order to verify if a given condition was more representative than the others, the frequency of appearance of each particular condition was calculated (**Figure 3.5 and Appendix 3**). The conditions producing less than 5% of the datasets were combined together. This combined fraction of 23 different conditions correlated to 51% of all datasets. The remaining 6 conditions (pH 6.5 20% PEG 3350 0.2 M salt, pH 6.0 15% PEG 4000 0.2 M salt, pH 6.5 15% PEG 4000 0.2 M salt, pH 7.0 15% PEG 4000 0.2 M salt, pH 7.5 15% PEG 4000 0.2 M salt and pH 7.0 20% PEG 4000 0.2 M salt), surprisingly, produced nearly half of all datasets (**Figure 3.5**).

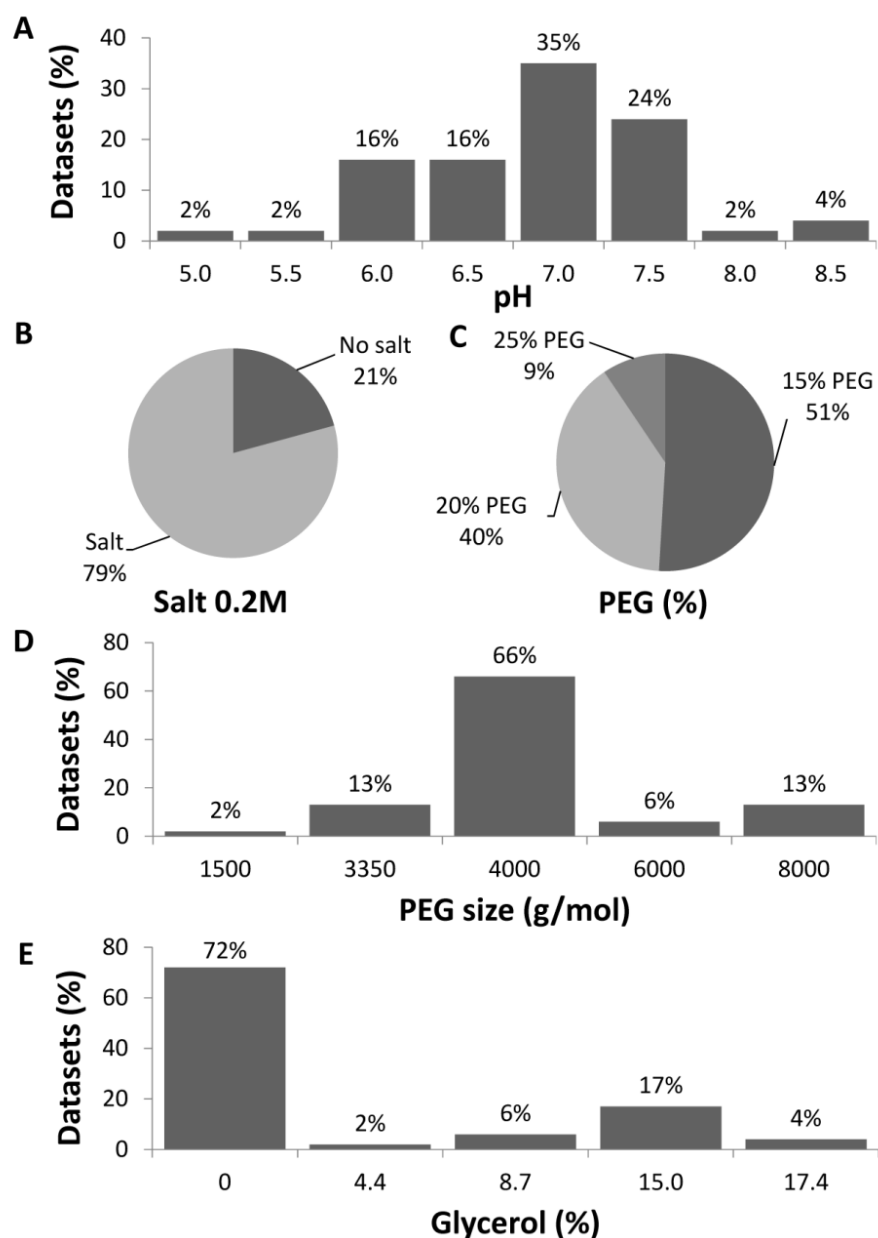


Figure 3.4. Analysis of crystallization conditions obtained from 25 TCR/pMHC complexes.

(A) The pH was within a range of 5.0 to 8.5, with 91% of the datasets obtained around a neutral pH from 6.0 to 7.5. (B) The presence of 0.2 M salt was required in 79% of the conditions. (C) The best PEG concentrations were 15% and 20%, representing 91% of the datasets. (D) The most popular PEG molecular weight was around 4000 g/mol, representing 79% of the datasets (13% PEG 3350 and 66% PEG 4000). (E) The absence of glycerol was dominant (72%), but the best concentration of glycerol when this component was required was 15%.

This analysis completely correlated with the previous independent analysis with a pH range from 6.0 to 7.5, a required presence of 0.2 M salt, a preferred PEG size around 4000 g/mol and PEG concentrations of 15% and 20%. Based on these analyses, it could be possible to significantly restrain the crystallization conditions of TCR/pMHC complexes.

3.2.4 TOPS efficiency correlated to the datasets obtained in this screen

Based on the analysis presented in **Figure 3.4**, a scoring system associated to the percentage of datasets obtained per condition of pH, PEG concentration, PEG size and presence of salt or glycerol was designed (**Table 3.8**). This scoring system allows the generation of a score for each condition of TOPS based on the number of TCR/pMHC complexes crystallized in each condition (**Table 3.9**). For example, condition A1 of TOPS was attributed the score 9 ([score pH 6 = 3] + [score 15% PEG 4000 = 5] + [score glycerol = 1]). Scores were transposed into a colour system (scores <2.5 in dark blue, 2.5-5 in light blue, 5-7.5 in green, 7.5-10 in yellow, 10-12.5 in orange and >12.5 in red) and each datasets obtained in TOPS-like conditions were plotted (**Figure 3.6**). The vast majority of TCR/pMHC complexes crystallized in the conditions with a high score, but a number of complexes crystallized in the low range of this scoring system. Thus, although it is tempting to limit the number of conditions in a protein crystal screen to improve efficiency and reduce protein consumption, broader screens are required to ensure that crystallization conditions are not missed for important proteins.

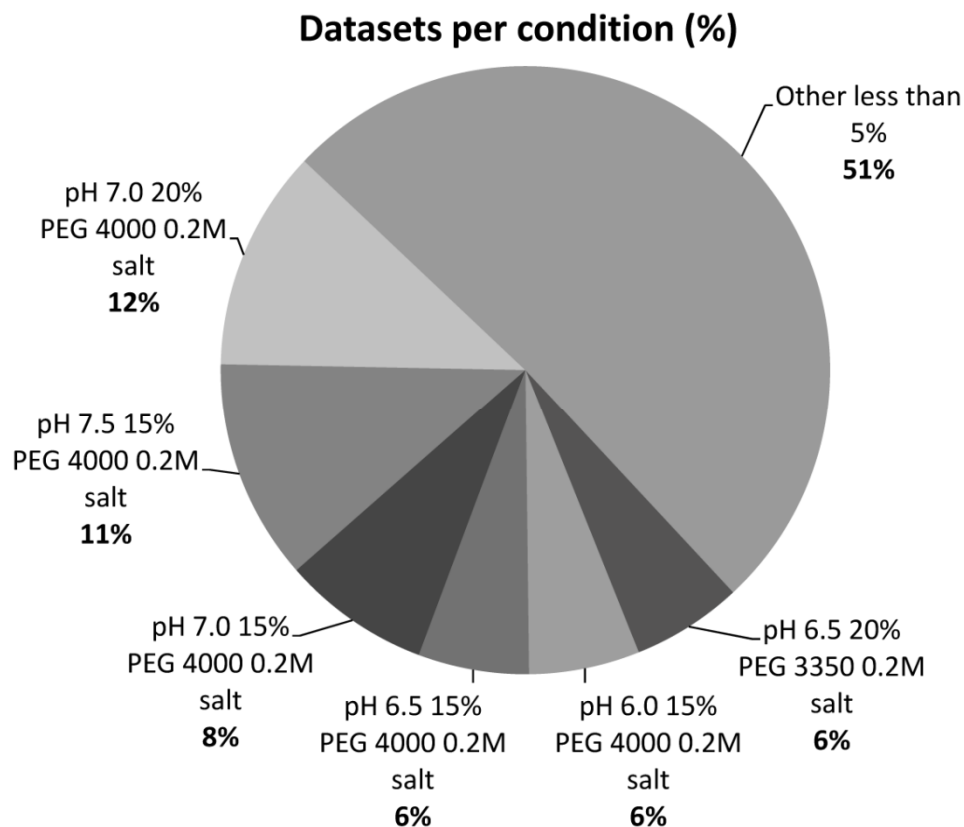


Figure 3.5. Analysis of the frequency of appearance of a particular condition. The conditions producing less than 5% of the datasets were combined together. The 53 datasets were obtained in a total of 29 different conditions. Among these 29 conditions, 6 conditions (pH 6.5 20% PEG 3350 0.2 M salt, pH 6.0 15% PEG 4000 0.2 M salt, pH 6.5 15% PEG 4000 0.2 M salt, pH 7.0 15% PEG 4000 0.2 M salt, pH 7.5 15% PEG 4000 0.2 M salt and pH 7.0 20% PEG 4000 0.2 M salt) produced nearly half of all datasets.

Table 3.8. Scoring system.

pH	Score	PEG concentration and type	Score	Salt or glycerol	Score
6.0	3.0	15% PEG 4000	5.0	Presence salt	4.0
6.5	3.0	20% PEG 4000	3.0	Presence glycerol	1.0
7.0	6.0	25% PEG 4000	1.0		
7.5	6.0	15% PEG 8000	2.0		
8.0	0.5	20% PEG 8000	0.5		
8.5	0.5	25% PEG 8000	0		

Based on **Figure 3.4**, a scoring system related to the percentage of datasets obtained per condition of pH, PEG concentration and size and presence of salt or glycerol was implemented.

Table 3.9. TOPS conditions correlated to the scoring system.

Buffer (pH) 0.1 M	15% glycerol						0.2 M ammonium sulphate					
	PEG 4000 (%)			PEG 8000 (%)			PEG 4000 (%)			PEG 8000 (%)		
	15	20	25	15	20	25	15	20	25	15	20	25
C ₂ H ₆ AsO ₂ Na (pH 6)	9.0	7.0	5.0	6.0	4.5	4.0	12.0	10.0	8.0	9.0	7.5	7.0
C ₂ H ₆ AsO ₂ Na (pH 6.5)	9.0	7.0	5.0	6.0	4.5	4.0	12.0	10.0	8.0	9.0	7.5	7.0
MES (pH 7)	12.0	11.0	8.0	9.0	7.5	7.5	15.0	13.0	11.0	11.0	10.0	10.0
HEPES (pH 7)	12.0	11.0	8.0	9.0	7.5	7.5	15.0	13.0	11.0	11.0	10.0	10.0
HEPES (pH 7.5)	6.5	10.0	8.0	9.0	7.5	7.5	15.0	13.0	11.0	12.0	10.5	10.0
TRIS (pH 7.5)	6.5	10.0	8.0	9.0	7.5	7.5	15.0	13.0	11.0	12.0	10.5	10.0
TRIS (pH 8)	6.5	4.5	2.5	3.5	2.0	1.5	9.5	7.5	5.5	6.5	5.0	4.5
TRIS (pH 8.5)	6.5	4.5	2.5	3.5	2.0	1.5	9.5	7.5	5.5	6.5	5.0	4.5

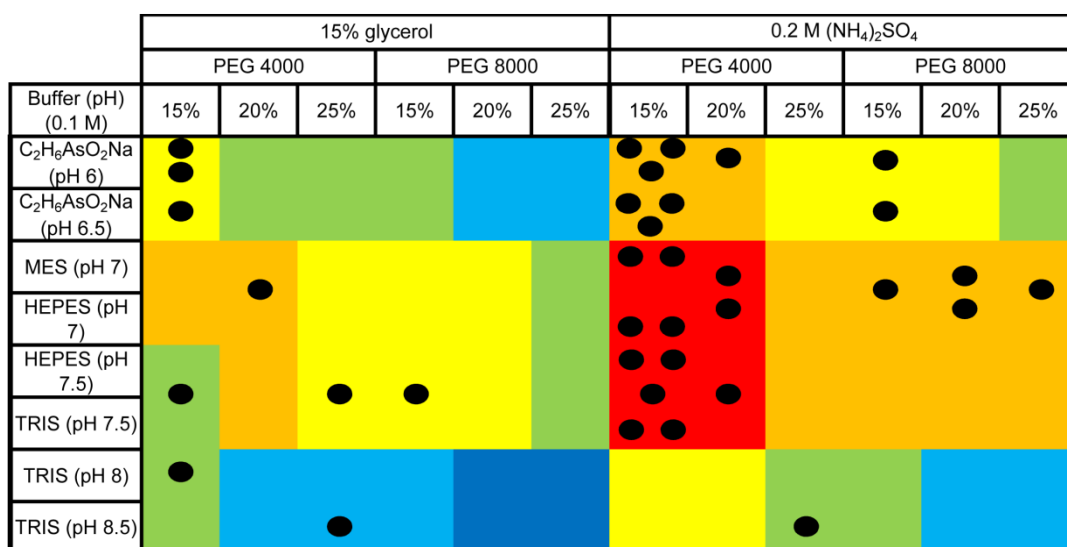


Figure 3.6. Representation of the expected TOPS efficiency correlated to the datasets obtained with that screen based on the implemented scoring system.

Scores <2.5, 2.5-5, 5-7.5, 7.5-10, 10-12.5 and >12.5 were represented in dark blue, light blue, green, yellow, orange and red, respectively. Each dark circle represents a successful dataset. The vast majority of TCR/pMHC complexes crystallized in the conditions with a high score, but a number of complexes crystallized in the low range of this scoring system.

3.3 DISCUSSION

The ability of T-cells to respond to antigen depends on the productive interaction between the TCR and pMHC. The crystal structures of a number of TCR/pMHC complexes have been solved and show that the TCR has a relatively conserved mode of binding to pMHC in which the TCR lines up approximately diagonally to the MHC peptide binding groove, with the TCR α chain contacting the MHC $\alpha 2$ domain and the TCR β chain contacting the MHC $\alpha 1$ domain. The antigen specific portion of the TCR/pMHC interaction occurs between the pMHC surface and the TCR complementarity determining region loops (CDR-loops) (Rudolph et al., 2006). These CDR-loops serve different roles during TCR binding to pMHC; the variable (V)-gene encoded CDR2-loops contact mainly the conserved helical region of the MHC surface, the V-gene encoded CDR1-loops can contact both the MHC and the peptide and the more variable somatically rearranged CDR3-loops contact mainly the antigenic peptide. Although the general features of TCR/pMHC binding have been defined, there are a number of conflicting models that describe the structural basis of T-cell MHC-restriction, cross-reactivity, autoimmunity and alloreactivity. Furthermore, each previous TCR/pMHC complex has been governed by a unique set of contacts that enable T-cell antigen recognition. Thus, there is still a pressing need to increase the number of TCR/pMHC complex structures in the literature in order to: (i) determine an accepted set of rules that describe the generalities of T-cell specificity, and (ii) understand the unique features of individual TCR/pMHC interactions that allow T-cells to target different disease epitopes.

The study of TCR/pMHC complexes has been limited by the challenges in expression, purification and successful crystallization of these soluble proteins. Here,

a new systematic and directed approach for the design of a TCR/pMHC Optimized Protein crystallization Screen (TOPS) that has proved to be useful for the crystallization of this family of immuno-proteins is reported. With this novel crystallization screen, my laboratory and I have successfully generated the majority of the current portfolio of structures that includes 21 TCR/pMHC complexes (13 derived from a common parent complex), 3 TCRs and 8 pMHCs. These structures have already enabled a better understanding of T-cell antigen recognition of viral (Miles et al., 2010), autoimmune (Bulek et al., 2012a) and cancer (Cole et al., 2009) epitopes, as well as a number of so far unpublished observations. I found that TCR/pMHC complex crystals most commonly formed at neutral pH, with 15% to 20% of PEG 4000 and 0.2 M ammonium sulphate. In addition, results from the crystallization trials indicated that it might be possible to significantly restrain the crystallization conditions of TCR/pMHC complexes to around 6 different conditions (rather than 96) thereby saving valuable protein.

In conclusion, TOPS will greatly contribute to a better understanding of molecular basis for T-cell recognition of self, foreign (microbial/viral/parasitic) and autoimmune antigens by providing an improved method for generating TCR/pMHC complex protein crystals capable of high quality X-ray diffraction. Furthermore, TOPS may be useful for the determination of TCR structures in complex with classical and non-classical MHC ligands that are less well characterized, including: pMHC class II, MR1, CD1c and HLA-E. Structural information, detailing the precise atomic contacts that mediate T-cell immunity, can provide clear insights into various immune dysfunctions and could accelerate the rational design of T-cell based therapies and vaccines.

CHAPTER 4

T-CELL RECEPTOR HIGH AFFINITY AND SPECIFICITY BASED ON FAVOURABLE ENTROPY

Chapter background.....	130
4.1 Introduction.....	130
4.1.1 Therapeutic application of monoclonal antibodies	132
4.1.1.1 “Naked” or unconjugated monoclonal antibody therapy.....	132
4.1.1.2 Conjugated monoclonal antibody therapy	133
4.1.1.3 Bispecific antibody therapy.....	134
4.1.2 Monoclonal TCRs	135
4.1.3 Aim.....	138
4.2 Results	138
4.2.1 Production and purification of soluble TCRs and pMHCs for this study	138
4.2.2 $\alpha 24\beta 17$ TCR binds to A2-ELA with high affinity due to an extended off- rate	143
4.2.3 MEL5 and $\alpha 24\beta 17$ TCRs use a similar binding mode to engage A2-ELA	143
4.2.4 Enhanced TCR-MHC interactions govern the high affinity binding of the $\alpha 24\beta 17$ TCR.....	151
4.2.5 The $\alpha 24\beta 17$ TCR is highly sensitive to peptide substitutions.....	154
4.2.6 Peptide substitutions do not alter the overall conformation of the $\alpha 24\beta 17$ /A2-ELA complex.....	157
4.2.7 Peptide substitutions do not directly alter the contact interface between the $\alpha 24\beta 17$ TCR and A2-ELA	158

4.2.8 Peptide substitutions do not alter the overall conformation of unligated A2- ELA molecules.....	161
4.2.9 Peptide specificity is governed by a distinct thermodynamic signature and a reduction in water bridges	164
4.3 Discussion.....	171

Chapter background

The work presented in this Chapter mainly results from the generation of TOPS as well as collaborations with Professor Brian Baker laboratory (University of Notre Dame, Indiana, USA) and with a biotechnology company (Immunocore, Ltd). Immunocore generated the high-affinity variant sequences of MEL5 TCR used in this study from a TCR that was originally described by my primary supervisor, Professor Sewell. Professor Baker's laboratory provided the datasets for solving two unligated pMHC structures and TOPS allowed the generation of the other structures reported here. This study is a continuation of the work started in my laboratory on MEL5 TCR and follows the publication of the in-depth crystallographic and thermodynamic analyses of the MEL5 TCR interaction with the heteroclitic melanoma-derived HLA-A2-restricted MART-1_{26/35} peptide (Cole et al., 2009) published shortly before I started my PhD. The high-affinity TCR variant was produced by Immunocore using a phage display technique originally described by our late Cardiff University colleague Jonathan Boulter (Li et al., 2005b). Such high-affinity TCRs are in development for soluble TCR therapy (Liddy et al., 2012). Detailed analysis of a high-affinity MEL5 variant TCR and its peptide specificity was deemed to be an important step in understanding these molecules. The data presented here were subsequently submitted for publication shortly before the submission of this thesis.

4.1 INTRODUCTION

Monoclonal antibodies (mAbs) are being used as therapeutic agents for a wide range of pathologies and more than 30 mAbs and mAbs-derived molecules are currently registered as approved drugs with hundreds more in clinical trial (Adler and

Dimitrov, 2012; Brekke and Sandlie, 2003). Generally, mAbs are unable to target internal cellular infections or aberrations. In contrast, TCRs can exploit the MHC I presentation pathway to scan the internal proteome for such anomalies and thereby gain access to a much wider range of targets, including tumour associated antigens (TAAs), that are not readily available for antibody-mediated therapies. Unlike antibodies which bind to their cognate antigens with high affinity ($K_D = \text{nM-pM}$), TCRs bind to their cognate pMHC with relatively low affinity ($K_D = 0.1\text{-}270 \mu\text{M}$) (Bridgeman et al., 2012; van der Merwe and Davis, 2003). This weak binding affinity correlates to a half-life of binding of 0.1-12 seconds ruling out efficient cell targeting with soluble TCRs. The weak binding affinity and short half-life of TCR/pMHC interactions can be circumvented using several different methods (e.g. phage display) as described in **Chapter 1**. Previous structural studies revealed that TCR affinity-enhancements were due to contacts made between the TCR and both the peptide and MHC surface, but primary resulted from contact associations with peptide antigen rather than MHC (Dunn et al., 2006; Sami et al., 2007). It is currently unknown how improving the interaction between TCR and MHC (self-interaction) could affect TCR specificity for the peptide component of the bipartite antigen. Loss of TCR specificity could result in recognition of self-derived peptides and precipitate autoimmunity. It is critically important that we gain an understanding of the binding specificity of enhanced affinity TCRs before these molecules are put to widespread use in clinical applications. I will begin by describing the therapeutic use of monoclonal antibodies.

4.1.1 Therapeutic application of monoclonal antibodies

Therapeutic monoclonal antibodies (mAbs) (Kohler and Milstein, 1975) are currently being used in hundreds of clinical trials for conditions ranging from cancer and autoimmunity to cardiovascular disease and transplant rejection (Gura, 2002; Waldmann, 2003). These molecules represent the next wave of medicines and are likely to form the basis of a number of therapies over the coming years. The huge success of these molecules can be partly attributed to their high level of specificity and strong binding affinity (nM–pM). In combination, these attributes allow the specific targeting of important disease epitopes using soluble proteins to deliver therapeutic benefit. There are three categories of antibodies generated for use in therapeutics: (i) “naked” mAbs; (ii) conjugated mAbs; and, (iii) bispecific mAbs.

4.1.1.1 “Naked” or unconjugated monoclonal antibody therapy

“Naked” or unconjugated monoclonal antibodies such as the clinically effective therapeutic agents Trastuzumab (Herceptin®), Rituximab (Rituxan®) or the more recently approved anti-melanoma Ipilimumab (Yervoy®) elicit an antibody-dependent cell-mediated cytotoxicity (ADCC) (Sapoznik et al., 2012). Fc portions of mAbs specifically bound to target cells are engaged by the Fc receptors of the effector cells (most commonly CD16/FcγRIII). These receptors then activate NK cells or macrophages, leading to the lysis and/or phagocytosis of the target cells (Clynes et al., 2000).

4.1.1.2 Conjugated monoclonal antibody therapy

Various conjugated antibodies have been designed to enhance the ADCC process by inducing toxicity via agents such as radioisotopes, cytotoxic drugs and as prodrugs. These conjugated antibodies are constituted by a recombinant antibody covalently bound by a synthetic linker to a given cytotoxic chemical (Chari, 2008). The main objective is to combine the pharmacological potency of cytotoxic drugs and the high specificity of monoclonal antibodies (Beck et al., 2010a). However, the clinical success of these “immuno-conjugates” has been limited compared to the unconjugated mAbs (Haeuw et al., 2009). To date, only one conjugated mAb has been approved by the FDA, namely gemtuzumab ozogamicin (GO) (Mylotarg®) in 2000 (Jurcic, 2012). This anti-CD33 mAb conjugated to calicheamycin was approved for the treatment of patients with acute myeloid leukaemia (AML) but was never approved in Europe and was withdrawn from the US market in June 2010. The reasons for the withdrawal included high level of off-target toxicity and failure to demonstrate improved survival during required post-approval studies combining chemotherapy and Mylotarg. In addition, protease-mediated degradation of the linker joining the mAb to the cytotoxic drug was identified as a further issue (Beck et al., 2010a; Jurcic, 2012). However, there are currently discussions for the reversal of the decision to withdraw GO. It has been shown that AML is not a homogeneous disease but rather a group of diseases, some of which are particularly sensitive to the drug, and the compelling data available from the more recently reported trials strongly suggested that the reversal of the decision might be the correct way forward (Ravandi et al., 2012).

4.1.1.3 *Bispecific antibody therapy*

Bispecific antibodies (or bifunctional antibodies) are mAbs that bind to two different epitopes. These epitopes can be on the same antigen or two different antigens, thereby triggering two different functions (Beck et al., 2010b). As for most diseases several mediators contribute to pathogenesis, the simultaneous blockade of several targets might yield to better therapeutic efficacy than the inhibition of a single target. After years of unsuccessful trials, catumaxomab (Removab®) was the first, and to date the only, approved bispecific antibody (Seimetz, 2011). This bifunctional mAb binds to both epithelial cell adhesion molecule (EpCAM) on tumour cells and CD3 on effector T-cells and was approved in Europe in 2009 for the treatment of malignant ascites (Linke et al., 2010). Another promising example of this class of mAbs is the Bispecific T-cell Engaging (BiTE) antibody (Wolf et al., 2005). The BiTE construct blinatumomab (MT103) has a dual specificity for the tumour-associated CD19 and the T-cell expressed CD3. It has shown promising results in Phase I (non-Hodgkin's lymphoma) and Phase II (acute lymphoblastic leukaemia) clinical trials by instigating the lysis of CD19⁺ lymphoma and leukaemia cells by CD3⁺ T-cells (Beck et al., 2010b).

Although antibodies are able to target disease particles or pathogens, they are not able to detect internal cellular infections or aberrations. Like antibodies, T-cells have the potential to be used to target specific disease markers (Liddy et al., 2012; Morgan et al., 2006; Varela-Rohena et al., 2008). Additionally, because of their ability to detect deleterious proteins that are only expressed inside of cells, T-cells can access disease targets that are hidden from antibody detection. This “X-ray vision”, that T-cells utilize through cell surface antigen recognition via the TCR-pMHC interaction,

offers exciting new possibilities for developing disease specific therapies. A number of strategies have been used to overcome the weak binding affinity of TCRs (see **Chapter 1**). The resultant soluble high affinity T-cell receptors have been called “monoclonal TCRs”.

4.1.2 Monoclonal TCRs

Antibodies undergo affinity maturation *in vivo* via a somatic hypermutation and a selection process where the progeny with highest affinity for antigen win out to receive a survival signal. This process ensures that antibodies bind with high affinity. In contrast, TCRs are fixed at the protein sequence level and do not change in affinity for antigen. TCRs are required to bind to self-antigens during thymic selection so any process that allowed TCRs to “home in” on antigens would rapidly result in autoimmunity.

TCRs are selected in the thymus to bind with a weak affinity ($K_D = 0.1\text{-}270 \mu\text{M}$) (Bridgeman et al., 2012; Cole et al., 2007). However, the combination of advances in soluble TCR technology (described in **Chapter 3**) and molecular affinity evolution systems (described in **Chapter 1**) have enabled the production of soluble high affinity “monoclonal TCRs” that can be coupled to a variety of payloads in a same way that therapeutic mAbs are being used. Despite showing great promise in certain situations, the success of therapeutic mAbs is limited by the nature of antigens that antibody are designed to recognize. Whereas antibodies can only bind to secreted or surface bound antigens (typically in the form of whole proteins), TCRs have access to all antigens when presented by the MHC, regardless of cellular localisation. Since the majority of TAAs and other pathogenic antigens are intracellular, soluble TCRs

(when armed with immune stimulators or cytotoxic agents) are ideal candidates for immunotherapy (**Figure 4.1**) (Molloy et al., 2005). One of the earliest successful soluble TCR immunotherapy studies was reported by Card et al. (Card et al., 2004). This group produced a single-chain TCR-interleukin-2 (IL-2) fusion protein, namely 264scTCR/IL-2, specific for an epitope of the p53 tumour suppressor protein (Card et al., 2004). This TCR-like fusion protein reduced lung metastases in an experimental HLA-A2⁺ mouse tumour model and inhibited the growth of primary tumours derived from the A375 human melanoma cell line (HLA-A2⁺ and p53⁺) in these humanized mice (Belmont et al., 2006). It would be also possible to fuse other immunomodulatory molecules that have been used with conjugated mAbs, including the cytokines tumour necrosis factor (TNF- α) and interleukin-12 (IL-12) (Halin et al., 2003) or an anti-CD3 antibody (Wolf et al., 2005), to TCRs. Recently, high-affinity variants of several anti-tumour TCRs were used in monoclonal TCR therapy models to induce regression of established tumours. These TCRs were fused to an anti-CD3 antibody Fab fragment and have been called ImmTACs (immunomobilizing monoclonal TCRs against cancer) (Liddy et al., 2012). This development represents exciting milestones in both TCR-mediated therapy and the range of potential treatments available for cancer.

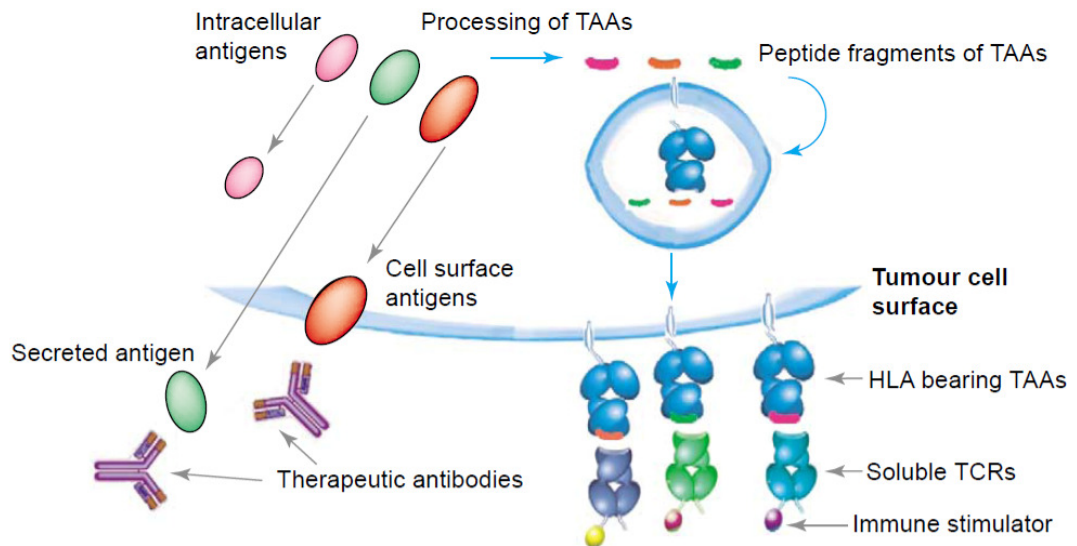


Figure 4.1. Differences in antigen recognition between mAbs and TCRs.

Cytoplasmic proteins, in this case tumour-associated antigens (TAAs) comprise intracellular antigens (shown in pink), cell-surface-bound antigens (shown in red) and secreted antigens (shown in green). These proteins are degraded into short peptides by the proteasome and the peptide fragments are transported to the lumen of the endoplasmic reticulum where they can bind MHC I. The pMHC complex is then displayed on the cell surface with their intracellularly derived peptide fragments (pink, red and green). Whereas antibodies can only bind to secreted or surface bound antigens (typically in the form of whole proteins), TCRs have access to all antigens when presented by the MHC, regardless of cellular localisation. Since the majority of TAAs and other pathogenic antigens are intracellular, soluble TCRs (when armed with immune stimulators or cytotoxic agents) are ideal candidates for immunotherapy (Figure taken from (Molloy et al., 2005)).

4.1.3 Aim

Using phage display (Li et al., 2005b), several high affinity TCRs derived from the MEL5 TCR that is specific for the heteroclitic version of the primary melanoma antigen recognized by T-cells 1 (MART-1₂₆₋₃₅) peptide presented by HLA-A*0201 (A2-ELA) were generated. This Chapter focuses on one of the high-affinity TCRs specific for melanoma, namely $\alpha 24\beta 17$. The aims of this Chapter were to provide a molecular explanation for the high affinity TCR binding observed by solving the structure of $\alpha 24\beta 17$ in complex with A2-ELA and comparing this structure with the previously published MEL5/A2-ELA complex (Cole et al., 2009) and to analyse and understand the peptide specificity of this high-affinity TCR by using biophysical analysis and structural data. These results have importance for the therapeutic use of soluble high-affinity TCRs.

4.2 RESULTS

4.2.1 Production and purification of soluble TCRs and pMHCs for this study

In this Chapter, I solved the structures of the high-affinity TCR $\alpha 24\beta 17$ unbound to a pMHC and in complex with the heteroclitic version of MART-1₂₆₋₃₅ presented by HLA-A*0201 (A2-ELAGIGILTV, A2-ELA), with ELA mutants ELAAIGILTV (A2-ELA4A) and ELAGIGALTV (A2-ELA7A) as well as the structures of A2-ALAGIGILTV (A2-ELA1A), A2-ELA4A and A2-ELAGIGIATV (A2-ELA8A) unbound to a TCR (unligated). I also performed biophysical analyses of the interaction between Melan A-specific TCRs and various antigens. These experiments required the manufacture of considerable amounts of soluble, refolded pMHC and TCR. Protein was produced by expression as inclusion bodies in *E. coli*, purification

of inclusion bodies and then refolding by the dilution of denaturing conditions as described in **Chapter 2** (section 2.3). An example of the process of manufacture of the $\alpha 24\beta 17$ TCR is shown in **Figure 4.2A**. Briefly, the process involved: (i) expression of protein chains as inclusion bodies in *E. coli*; (ii) purification of inclusion bodies; (iii) refolding by dilution of denaturing conditions; (iv) an anion exchange purification step (e.g. **Figure 4.2B&C**); and, (v) several gel filtration purification steps (e.g. **Figure 4.3**) in order to obtain enough pure proteins to perform the different experiments (**Figure 4.3**). For the biophysical analysis by Surface Plasmon Resonance (SPR) using BIAcore® machinery, biotin-tagged pMHC were biotinylated and purified by gel filtration (**Figure 4.3**) before analysis. The biotin group allowed coupling of pMHC to a streptavidin-coated sensor chip (BIAcore®). Conveniently, the antibody-like affinity of $\alpha 24\beta 17$ binding to A2-ELA made it possible to co-purify the $\alpha 24\beta 17$ /A2-ELA complex by gel filtration before setting up crystallization plates (**Figure 4.4**). Conventionally, TCRs and pMHCs, or antibodies and recombinant antigens, are mixed in an equimolar ratio prior to crystallization trials (Bossi et al., 2010) as described in **Chapter 2**. The co-purification step of the $\alpha 24\beta 17$ /A2-ELA complex coupled to the optimization of the crystallization conditions detailed in the previous Chapter (Bulek et al., 2012b) could explain the generation of high-quality crystals $> 200 \mu\text{m}$ long (**Figure 4.4**) for this particular complex. The size of the protein crystal is important for the generation of high resolution X-ray diffraction as the strength of the scattering (or Bragg spot) depends on several factors such as X-ray exposure time or crystal volume (Holton and Frankel, 2010). Bigger crystals will produce stronger patterns and suffer less damage (Garman, 1999).

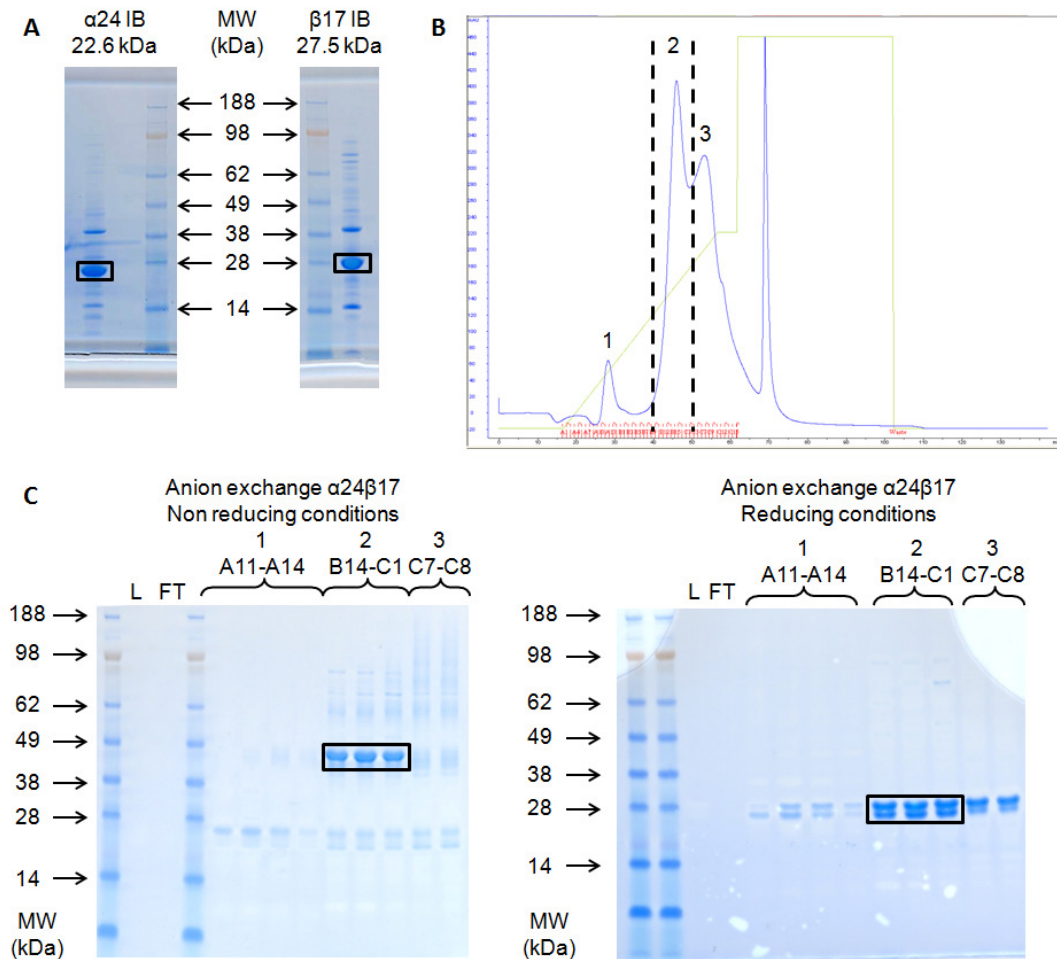


Figure 4.2. Example of inclusion bodies purity and anion exchange purification step.

(A) $\alpha 24$ (left panel) and $\beta 17$ (right panel) chains were produced as inclusion bodies (IB) in *E. coli*. Although the protein of interest was over-expressed (black rectangle), several contaminants remained in the IB preparation. (B) An anion exchange purification step (7.9 mL POROS® 10/100 HQ 50 μ m column) after refolding of $\alpha 24\beta 17$ TCR shows three different peaks (1, 2 and 3). TCR, TCR $\alpha 24$ and $\beta 17$ chains aggregation as well as contaminants from the IB preparation are eluted by gradually increasing the NaCl gradient (green line) from 0 mM to 500 mM and all the proteins bound on the column are eventually eluted with 1 M NaCl to regenerate the column (waste fraction). The analysis of several fractions of each peak by SDS-PAGE and Coomassie staining was required to discriminate the peak containing the protein of interest. (C-D) SDS-PAGE under non reducing (C) and reducing (D) conditions followed by Coomassie staining reveals that the $\alpha 24\beta 17$ TCR was located in the second peak, namely fractions B9-C4. The refold before anion exchange (load fraction, L) and the flow through (FT) were also analysed. Non-refolded $\alpha 24$ or $\beta 17$ chains were eluted in the first peak, TCR aggregation was eluted in the third peak and most of the contaminants from the IB preparation were eluted with 1 M NaCl in the waste fraction. No proteins were detected in the L and FT fractions because of the low protein concentration.

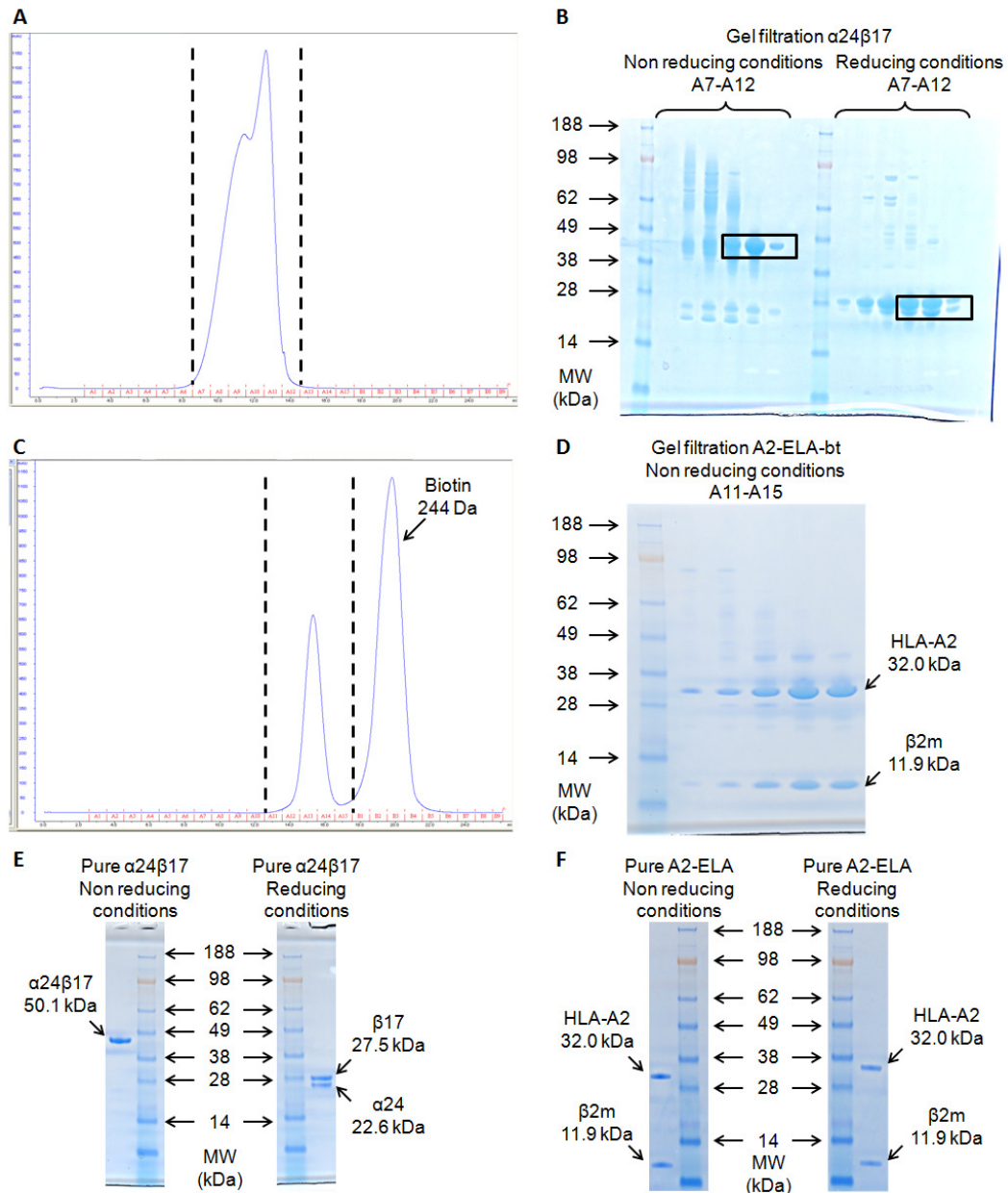


Figure 4.3. Gel filtration examples and purity of proteins for crystallography and biophysical analysis.

(A) After anion exchange, fractions containing the protein of interest were pooled, concentrated and purified by gel filtration (24 mL Superdex 200 10/300 GL column). For $\alpha 24\beta 17$ TCR, two peaks were obtained and fractions A7-A12 were analysed by (B) SDS-PAGE and Coomassie staining under non reducing and reducing conditions. The first peak contains TCR aggregation and the second peak contains relatively pure TCR. (C) After pMHC biotinylation, pMHC-bt were purified by gel filtration to remove the excess biotin (second peak). (D) Analysis by SDS-PAGE and Coomassie staining under non reducing conditions showed that relatively pure pMHC-bt (here A2-ELA-bt) was located in the first peak, namely fractions A11-A15. After several rounds of gel filtration, the purity of (E) $\alpha 24\beta 17$ and (F) pMHCs (here A2-ELA for crystallography) was analysed SDS-PAGE and Coomassie staining under non reducing and reducing conditions and no contaminants were detectable.

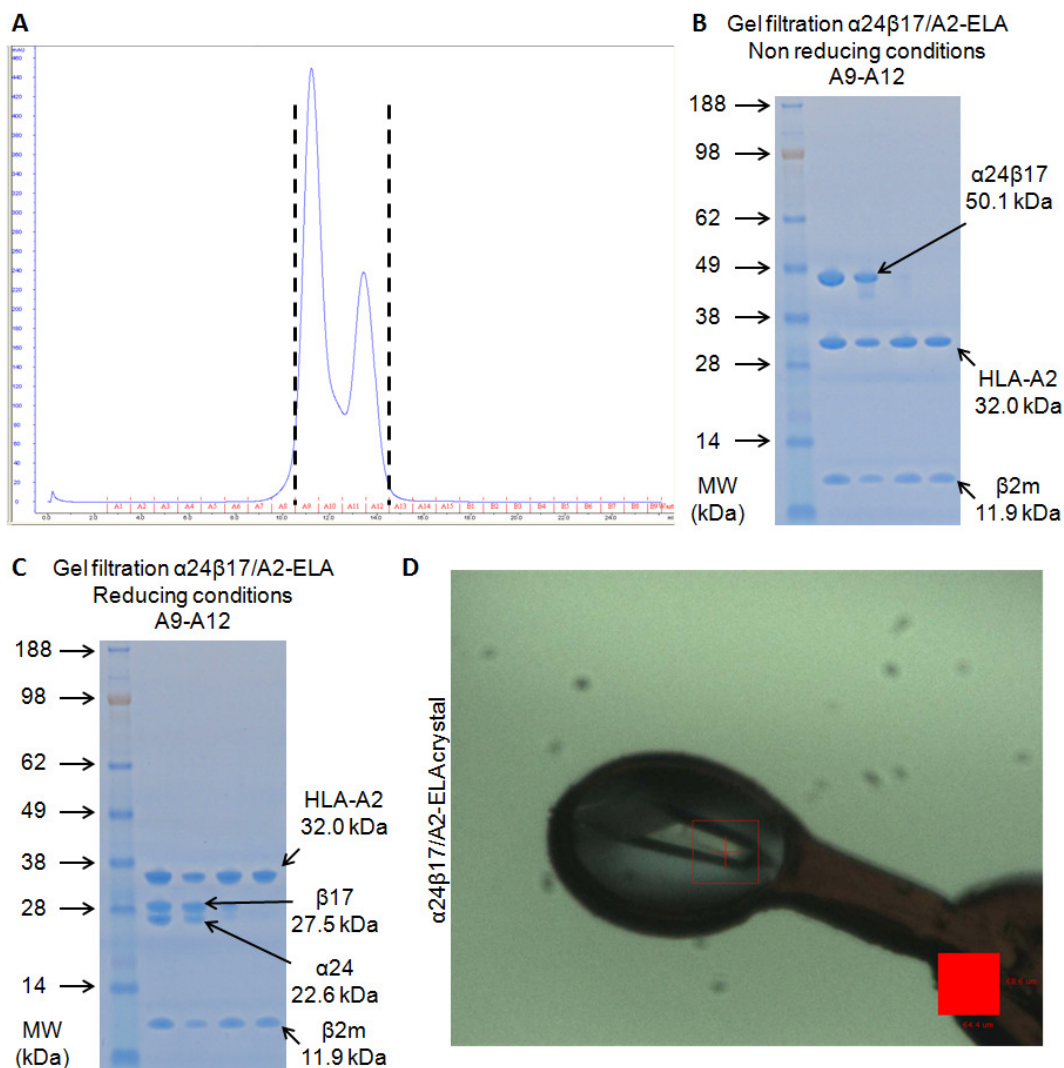


Figure 4.4. Gel filtration, protein crystal and high-resolution diffraction pattern of the $\alpha 24\beta 17/A2$ -ELA complex.

(A) Due to the high-affinity of $\alpha 24\beta 17$ for A2-ELA, the complex was co-purified by gel filtration for crystallography and two peaks were obtained between fractions A9 and A12. Analysis by SDS-PAGE and Coomassie staining under (B) non reducing and (C) reducing conditions showed that the first peak (A9-A10) contains pure $\alpha 24\beta 17/A2$ -ELA complex whereas the second peak (A11-A12) contained the excess A2-ELA. (D) Pure gel filtrated $\alpha 24\beta 17/A2$ -ELA complex was used to generate high quality crystals, here $\sim 210 \mu m$ long, leading to a high resolution X-ray diffraction pattern with $\sim 2.43 \text{ \AA}$ maximum resolution.

Finally, crystals of A2-ELA1A and A2-ELA8A were grown in MES 25 mM pH 6.5, 24% PEG 3350 and 10 mM NaCl by our collaborator Professor Brian Baker and diffraction datasets were obtained at the Advanced Photon Source at Argonne National Labs, USA.

4.2.2 α 24 β 17 TCR binds to A2-ELA with high affinity due to an extended off-rate

The high-affinity α 24 β 17 TCR varied from the MEL5 TCR parental sequence at 19 amino acids located within the CDR1 α , CDR2 α , FW α , CDR3 α , CDR2 β and CDR3 β loops as well as in the β chain between residues 41 and 45 (**Table 4.1**). My group has previously demonstrated that the MEL5 TCR has a binding constant (K_D) of 16-20 μ M (Cole et al., 2010; Cole et al., 2007; Cole et al., 2009) for A2-ELA (**Figure 4.5A**). The high-affinity α 24 β 17 TCR bound to A2-ELA \sim 30,000-fold stronger affinity than the wildtype MEL5 parent receptor ($K_D = 600$ pM) (**Figure 4.5B**). Similar to previously reported high-affinity engineered TCRs (Dunn et al., 2006; Li et al., 2005b; Sami et al., 2007; Varela-Rohena et al., 2008), the enhancement in affinity was due primarily to an extended off-rate of $1.09 \times 10^{-4} \text{ sec}^{-1}$. The off-rate for the MEL5 TCR was too fast to measure ($>0.1 \text{ sec}^{-1}$) (**Figure 4.5**).

4.2.3 MEL5 and α 24 β 17 TCRs use a similar binding mode to engage A2-ELA

Previous structures of high-affinity TCRs have shown that, although these mutated TCRs can bind with many orders of magnitude stronger affinity than their wildtype progenitors, they bind in the same overall conformation (Dunn et al., 2006; Sami et al., 2007).

Table 4.1. Sequence alignment of the $\alpha 24\beta 17$ TCR and the wildtype MEL5 progenitor.

TCR	CDR1 α_{27-32}	CDR2 α_{50-54}	FW α_{67-71}	CDR3 α_{89-100}
MEL5	DRGSQS	IYSNG	KASQY	CAVNVAGKSTFG
$\alpha 24\beta 17$	<u>FL</u> GSQS	<u>TYRE</u> G	KASQ <u>H</u>	CAVND <u>DGGRL</u> TFG
TCR	CDR1 β_{27-32}	β chain $_{41-45}$	CDR2 β_{50-54}	CDR3 β_{91-106}
MEL5	GTSNPN	GRGLQ	SVGIG	CAWSETGLGTGELFFG
$\alpha 24\beta 17$	GTSNPN	GRG <u>P</u> Q	<u>WGPF</u> G	CAWSETGLG <u>MGGWQ</u> FG

Mutations from wildtype sequence are bold and underlined.

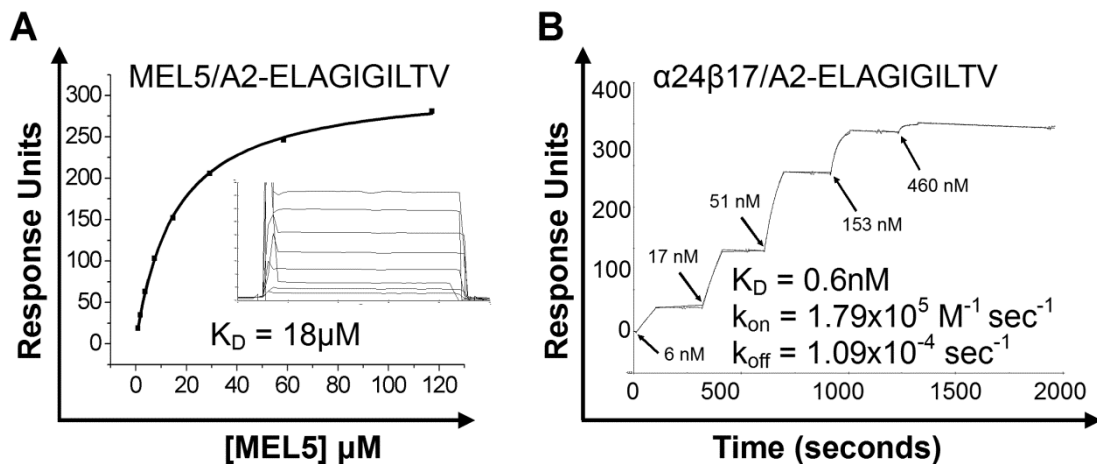


Figure 4.5. Binding affinity and kinetic analysis of the HLA A2-ELAGIGILTV specific wildtype MEL5 TCR and the high-affinity TCR, $\alpha 24\beta 17$.

These data were produced on a BIAcore T100TM using surface plasmon resonance and were then analyzed using (A) equilibrium analysis and (B) single cycle kinetic analysis. The raw data and the fits are shown in each panel. These data illustrate the binding capabilities of (A) the HLA A2-ELAGIGILTV specific wildtype MEL5 TCR (data from the previously published work (Cole et al., 2007)) and (B) the HLA A2-ELAGIGILTV specific high-affinity mutant TCR, $\alpha 24\beta 17$. The $\alpha 24\beta 17$ TCR binds to HLA A2-ELAGIGILTV with 30,000-times stronger affinity than MEL5.

This observation is important because this conserved binding mode increases the likelihood that high-affinity modified TCRs can maintain the rules that govern T-cell antigen recognition (self-tolerance). In order to determine the structural basis of the high-affinity binding for the $\alpha 24\beta 17$ TCR, I solved the $\alpha 24\beta 17/A2$ -ELA complex structure to 2.43 Å. Molecular replacement was successful only in space group $P4_1$ and the resolution was sufficiently high to show that the interface between the two molecules was well ordered and contained well defined electron density (**Figure 4.6**). The crystallographic R/Rfree factors were 21% and 26.3%. The ratio was within the accepted limits shown in the theoretically expected distribution (Tickle et al., 2000) (**Table 4.2**). The overall buried surface area (BSA) of 2705 Å² (TCR/pMHC) for $\alpha 24\beta 17/A2$ -ELA was slightly higher than for the previously published structure of MEL5/A2-ELA (Cole et al., 2009) (BSA = 2327.8 Å²) (**Table 4.3**) but was within the observed range (Rudolph et al., 2006). The high affinity $\alpha 24\beta 17$ TCR bound with a diagonal docking geometry to A2-ELA and showed one-to-one stoichiometry as previously reported of other TCR/pMHC complexes (**Figure 4.7A**) (Rudolph et al., 2006). As with previously reported high-affinity TCR structures (Dunn et al., 2006; Sami et al., 2007), a high level of similarity between the MEL5/A2-ELA and $\alpha 24\beta 17/A2$ -ELA complexes was observed, suggesting that the overall conformation was not substantially affected by the mutations in $\alpha 24\beta 17$. The crossing angles of both TCRs (**Figure 4.8A**) and the positioning of the complementarity determining region (CDR) loops (**Figure 4.8B**) were similar (47.6° for MEL5 and 42.2° for $\alpha 24\beta 17$) and fell within the previously observed range (Rudolph et al., 2006). Importantly, the ELA peptide conformation was virtually identical in both complexes, discounting the possibility that changes in the peptide contributed to the high affinity observed (**Figure 4.8C&D**).

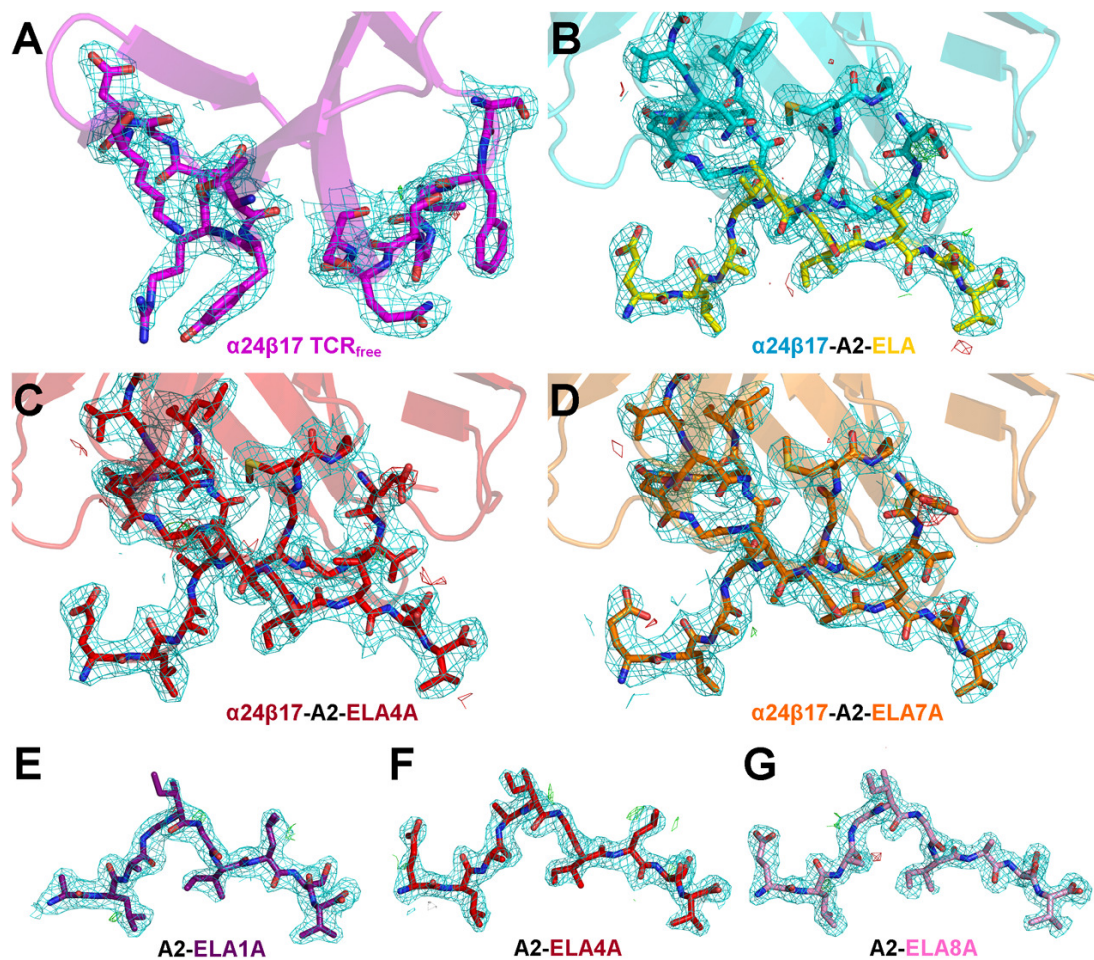


Figure 4.6. 2Fo-Fc electron density maps for all structures reported in this Chapter.

2Fo-Fc electron density maps (shown in cyan) for (A) $\alpha 24\beta 17$ free, (B) $\alpha 24\beta 17$ /A2-ELA complex, (C) $\alpha 24\beta 17$ /A2-ELA4A complex, (D) $\alpha 24\beta 17$ /A2-ELA7A complex, (E) A2-ELA1A, (F) A2-ELA4A and (G) A2-ELA8A. All maps shown are within 2 Å from the atoms to which they relate. Positive density is shown in green and negative density is shown in red.

Table 4.2. Data collection and refinement statistics for unligated $\alpha 24\beta 17$ TCR and complex structures (molecular replacement).

Data set statistics	$\alpha 24\beta 17$	$\alpha 24\beta 17/A2$ -ELA	$\alpha 24\beta 17/A2$ -ELA4A	$\alpha 24\beta 17/A2$ -ELA7A
Space Group	P3 ₂ 21	P4 ₁	P4 ₁	P4 ₁
Unit Cell parameters (Å)	a=97.14, b=97.14, c=123.08, γ =120	a=121.44, b=121.44, c=82.3	a=121.49, b=121.49, c=82.96	a=121.52, b=121.52, c=82.15
Radiation Source	DIAMOND I24	DIAMOND IO3	DIAMOND IO3	DIAMOND IO3
Wavelength (Å)	0.9778	0.9763	0.9763	0.9763
Resolution (Å)	2.4	2.43	2.46	2.7
Unique reflections	26783	45232	44185	35640
Completeness (%)	100	100	100	99.9
Multiplicity	10.9	8.3	8.2	8.1
I/Sigma(I)	16.6	14.8	17.1	13.5
Rmerge (%)	0.192	0.091	0.073	0.103
Refinement statistics (highest resolution shell in parenthesis)				
No reflections used	25403	42931	41936	31318
No reflections in Rfree set	1346	2278	2225	1674
Rcryst (no cutoff) (%)	20.1	21	20.2	20.2
Rfree (%)	24.6	26.3	24.8	25
RMSD from ideal geometry (target values in parenthesis)				
Bond lengths (Å)	0.022 (0.022)	0.021 (0.021)	0.021 (0.021)	0.019 (0.021)
Bond Angles (°)	1.206 (1.956)	1.246 (1.94)	1.174 (1.94)	1.134 (1.934)
Wilson B-factor (Å ²)	37.4	47	58.9	54.4
Overall ESU based on Maximum Likelihood (Å)	13	14.5	14.4	22.4

One crystal was used for data collection.

Table 4.3. Summary of co-complex structures of MEL5/A2-ELA (Cole et al., 2009), α 24 β 17/A2-ELA, α 24 β 17/A2-ELA4A and α 24 β 17/A2-ELA7A.

	MEL5/ A2-ELA	α 24 β 17/ A2-ELA	α 24 β 17/ A2-ELA4A	α 24 β 17/ A2-ELA7A
H-bonds ^a ($\leq 3.2\text{\AA}$)	6	16	15	16
H-bonds ^a ($\leq 3.4\text{\AA}$)	1	6	6	1
vdW ^a ($\leq 3.5\text{\AA}$)	23	21	11	15
vdW ^a ($\leq 4\text{\AA}$)	65	95	109	105
Total contacts	95	138	141	136
Number of α chain CDR1/CDR2/CDR3 contacts ($\leq 4\text{\AA}$)	26/11/13	37/12/21	38/16/18	31/8/20
Number of β chain CDR1/CDR2/CDR3 contacts ($\leq 4\text{\AA}$)	3/6/36	1/38/30	1/41/27	1/46/30
TCR/Peptide contacts	39	42	39	41
TCR/MHC contacts	56	97	102	95
BSA ^b (\AA^2)	2327.8	2705	2650.4	2781.6
SC ^c (TCR/MHC)	0.55	0.71	0.65	0.66
SC ^c (TCR/peptide)	0.71	0.59	0.58	0.62
SC ^c (TCR/pMHC)	0.6	0.66	0.62	0.63
Crossing angle ($^\circ$)	47.6	42.2	41.9	42

^a Number of hydrogen bonds (H-bond) / van der Waals (vdW) contacts calculated with CONTACT program from the CCP4 package (Collaborative Computational Project, 1994)

^b Buried surface area (BSA) (\AA^2) of TCR/pMHC calculated with PISA program from the CCP4 package (Collaborative Computational Project, 1994)

^c Shape complementarity (SC) of TCR/MHC / TCR/peptide / TCR/pMHC calculated with SC program from the CCP4 package (Collaborative Computational Project, 1994)

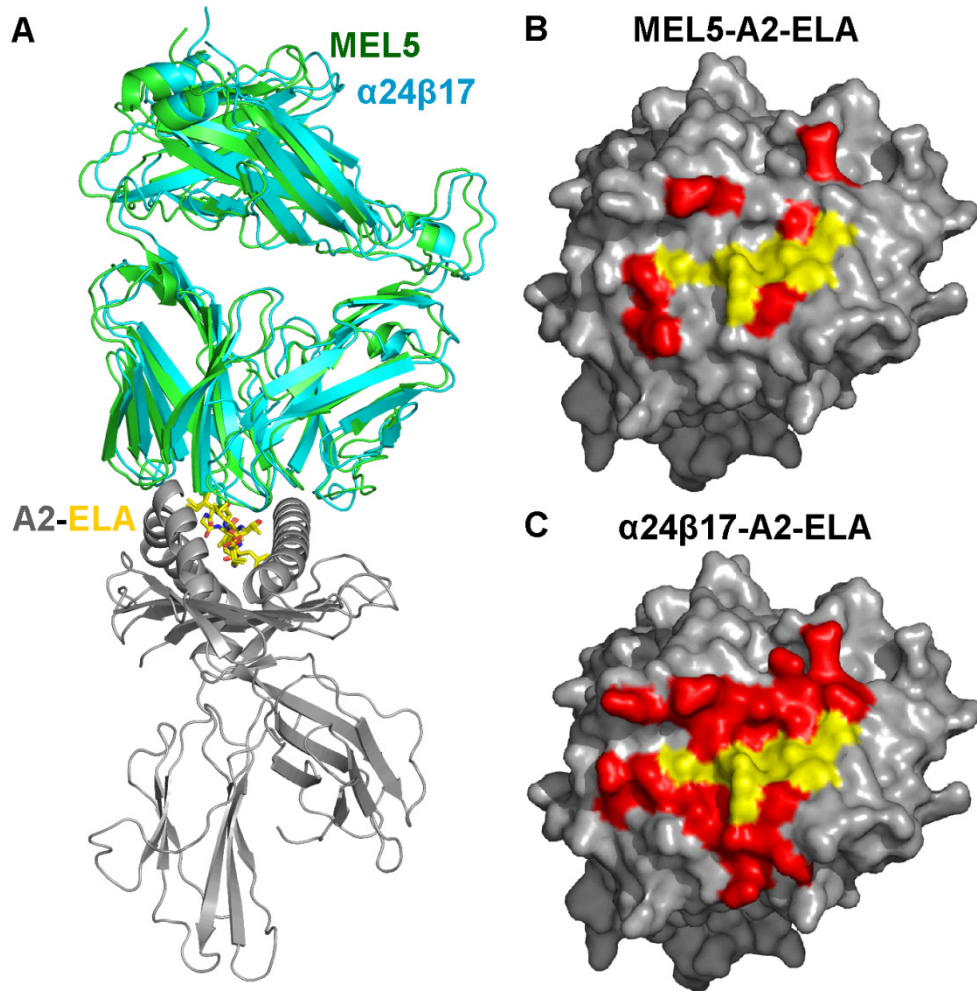


Figure 4.7. Structural analysis of the binding mode implemented by MEL5 versus $\alpha 24\beta 17$ when interacting with A2-ELA.

(A) Overall binding mode of MEL5 (data from the previously published work (Cole et al., 2009)) (green cartoon) and $\alpha 24\beta 17$ (cyan cartoon) interaction with HLA A*0201 (grey cartoon) and the ELA peptide (yellow sticks). Generally, the two TCRs bind in a very similar orientation, with some differences in the CDR loops and more flexible regions of the TCR variable and constant domains. (B&C) Surface representation of the A2-ELA complex looking down at the peptide. MHC residues that are contacted by the TCR are colored in red. Peptide residues that are contacted by the TCR are colored yellow. From this analysis, it is clear that although (B) MEL5 and (C) $\alpha 24\beta 17$ make a similar contact footprint with the peptide (yellow), $\alpha 24\beta 17$ make substantially more interactions with the MHC surface (red).

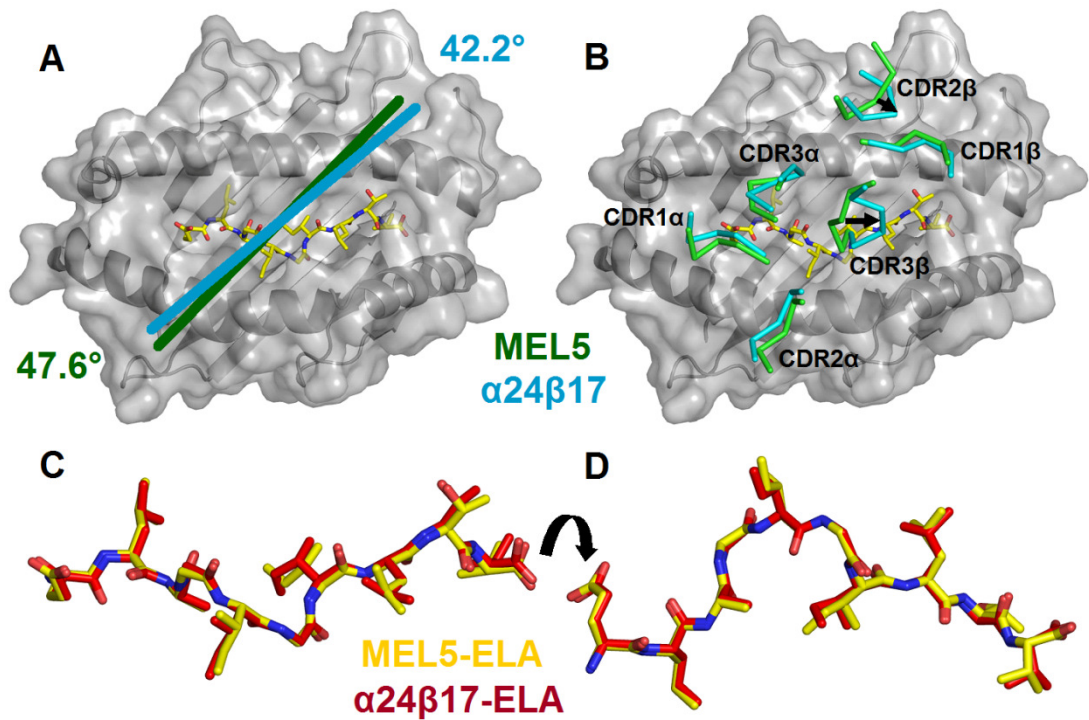


Figure 4.8. Structural differences between the MEL5 TCR versus $\alpha 24\beta 17$ TCR when interacting with A2-ELA.

(A) The $\alpha 24\beta 17$ (cyan) and MEL5 (green) crossing angles when interacting with A2-ELA (grey surface and cartoon, peptide shown as yellow sticks), A2-ELA4A (red cartoon) and A2-ELA7A (orange cartoon) are very similar. (B) Positions of the $\alpha 24\beta 17$ TCR CDR loops when interacting with A2-ELA (cyan cartoon) are similar, but not identical to the positions of the MEL5 TCR CDR loops (green cartoon) when binding to A2-ELA. (C&D) The ELAGIGILTV peptide does not undergo any substantial structural changes when in complex with MEL5 (yellow) compared to $\alpha 24\beta 17$ (red).

Thus, differences in binding affinity between the MEL5 and $\alpha 24\beta 17$ TCRs could not be explained by a large conformational change in geometry, in agreement with our previously published observations (Dunn et al., 2006; Sami et al., 2007).

4.2.4 Enhanced TCR-MHC interactions govern the high affinity binding of the $\alpha 24\beta 17$ TCR

Previous structures of high-affinity TCRs have shown that just a small number of additional contacts at the binding interface can mediate the high affinity binding interaction observed (Dunn et al., 2006; Sami et al., 2007). In order to delineate the mechanism behind the high affinity binding of the $\alpha 24\beta 17$ TCR, I investigated the binding interface in atomic detail. Although the overall conformations of the MEL5 and $\alpha 24\beta 17$ TCRs were similar, there were a number of important differences at the binding interface that probably contributed to the divergent binding affinities between the two TCRs. The interactions with the ELAGIGILTV peptide were very similar for MEL5 and $\alpha 24\beta 17$, with the TCRs making 39 and 42 contacts respectively (**Table 4.3**). However, the $\alpha 24\beta 17$ TCR made a substantial number of new contacts with the MHC surface, making 97 MHC contacts compared to only 56 for MEL5 (**Table 4.3, Figure 4.7B&C**). This increase in interactions with the MHC was consistent with the increased BSA for $\alpha 24\beta 17$ (**Table 4.3**) and was probably the main mechanism enabling $\alpha 24\beta 17$ to bind with an affinity 30,000-fold stronger than MEL5. The majority of the new contacts were directly attributable to the mutated residues in the $\alpha 24\beta 17$ TCR. For instance, MEL5 TCR α chain residue Asp27 made no contacts with the MHC surface. However, when mutated in the $\alpha 24\beta 17$ TCR α chain, the longer aromatic side chain of residue Phe27 was able to make 4 vdW contacts with MHC residue Glu58 (**Table 4.4, Figure 4.9A**).

Table 4.4. Direct contacts made by the wild-type or mutant TCR residues.

	TCR residue	vdW ($\leq 4 \text{ \AA}$)	H-bonds ($\leq 3.4 \text{ \AA}$)
Wild-type MEL5 TCR	α Asp27	0	0
	α Arg28	2 MHC	1 MHC
	α Ser52	0	0
	α Val93	0	0
	α Ala94	6 MHC	1 MHC
	α Lys96	2 MHC	0
	β Val51	4 MHC	0
	β Gly52	0	0
	β Ile53	0	0
	β Thr100	7 MHC	1 MHC
Total		21	3
Mutant $\alpha 24\beta 17$ TCR	α Phe27	4 MHC	0
	α Leu28	5 MHC	0
	α Arg52	3 MHC	0
	α Asp93	4 MHC	2 MHC
	α Gly94	6 MHC	1 MHC
	α Arg96	7 MHC	0
	β Gly51	3 MHC	0
	β Pro52	4 MHC	1 MHC
	β Phe53	18 MHC	1 MHC
	β Met100	2 MHC 1 ELA	1 MHC
Total		68	6

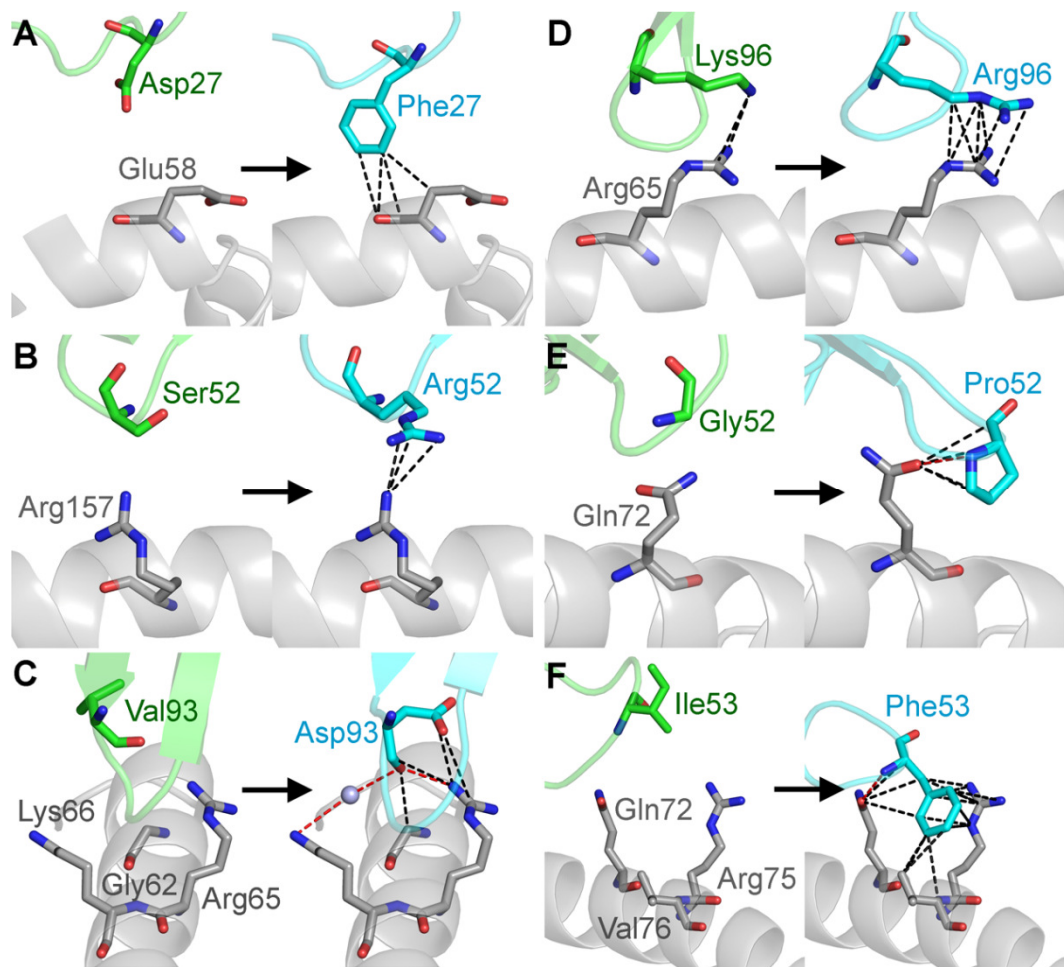


Figure 4.9. The $\alpha 24\beta 17$ mutated residues make an increased number of contacts with the MHC surface compared to MEL5 wildtype residues.

MEL5 residues are shown on the left hand side of each panel in green. The equivalent $\alpha 24\beta 17$ residues are shown on the right hand side of each panel in cyan. Hydrogen bonds ($< 3.4 \text{ \AA}$) are shown as red dotted lines and van der Waals interactions ($< 4.0 \text{ \AA}$) are shown as black dotted lines. In all cases, an increased number of interactions was observed between $\alpha 24\beta 17$ and the MHC surface compared to MEL5. (A) Position 27 in the TCR CDR1 α loop. (B) Position 52 in the TCR CDR2 α loop. (C) Position 93 in the TCR CDR3 α loop. (D) Position 96 in the TCR CDR3 α loop. (E) Position 52 in the TCR CDR2 β loop. (F) Position 53 in the TCR CDR2 β loop.

Similarly, the mutation from MEL5 TCR α chain residue Val93 to Asp93 in the $\alpha 24\beta 17$ TCR α chain resulted in 4 new vdW contacts and 2 new hydrogen bonds, and the mutation from MEL5 TCR β chain residue Ile53 to Phe53 in the $\alpha 24\beta 17$ TCR β chain resulted in 18 new vdW contacts and 1 new hydrogen bond (**Table 4.4, Figure 4.9**). Overall, mutated residues in the $\alpha 24\beta 17$ TCR accounted for 36 new vdW contacts and 3 new hydrogen bonds with the MHC surface (**Table 4.4**). Thus, the vast majority of the 44 new contacts formed by the $\alpha 24\beta 17$ TCR, compared to the MEL5/A2-ELA complex, were made directly by mutated residues with only a small number of new contacts made through indirect effects of the high affinity mutations on non-mutated residues (**Table 4.3, Appendix 4**). This observation, that the $\alpha 24\beta 17$ TCR mediated enhanced affinity through an increase in MHC contacts, substantially altered the ratio of TCR:peptide contacts vs. TCR:MHC contacts compared to MEL5. For instance, the MEL5 TCR made 41% of the total contacts with the peptide, compared to just 30% for the $\alpha 24\beta 17$ TCR. These new contacts contributed to a 30,000-fold increase in affinity (**Figure 4.5**). This change in focus, from peptide interactions to MHC interactions, raised the possibility that the $\alpha 24\beta 17$ TCR could bind in a peptide independent manner. In order to investigate this possibility further, the ability of $\alpha 24\beta 17$ to tolerate changes in the ELAIGIGILTV peptide was probed.

4.2.5 The $\alpha 24\beta 17$ TCR is highly sensitive to peptide substitutions

The $\alpha 24\beta 17$ /A2-ELA structure demonstrated that new MHC contacts were central to the 30,000-fold stronger affinity observed, compared to the MEL5/A2-ELA complex. Thus, in order to investigate the ability of $\alpha 24\beta 17$ to tolerate changes in the peptide, I performed an alanine (Ala) mutagenesis scan across the peptide backbone

and evaluated the capacity of the A2-ELA mutants to bind $\alpha 24\beta 17$ using surface plasmon resonance (SPR) (**Table 4.5, Figure 4.10**). As peptide positions P2 and P10 were buried and are known to be important for MHC binding (Borbulevych et al., 2007), I focused on assessing the solvent exposed positions P1, P4, P5, P6, P7, P8 and P9. I did not assess P3, as this residue is Ala in the native sequence. I observed a striking and unexpected result. Modification of any peptide residue to Ala reduced the binding of $\alpha 24\beta 17$ to wildtype-like affinities, or lower (**Table 4.5**). For example, $\alpha 24\beta 17$ bound A2-ELA with Gly substituted for Ala at position 4 (A2-ELA4A) with 36 μM , 60,000-fold weaker affinity than for A2-ELA ($\Delta\Delta\text{G}$ -6 kcal/mol) (**Table 4.5**). In the $\alpha 24\beta 17/\text{A2-ELA}$ structure, 4 hydrogen bonds and 8 vdW were made between the TCR and peptide residue Gly4 (**Appendix 4**). Thus, although Ala and Gly are similar in terms of size, this mutation could result in the disruption of an important network of TCR-peptide contacts that would explain the reduction in binding affinity. Similarly, $\alpha 24\beta 17$ bound A2-ELA with Ile substituted for Ala at position 7 (A2-ELA7A) with 31 μM , 51,667-fold weaker affinity than for A2-ELA ($\Delta\Delta\text{G}$ -6.1 kcal/mol) (**Table 4.5**). The $\alpha 24\beta 17/\text{A2-ELA}$ structure showed that 3 hydrogen bonds and 8 vdW were made between the TCR and peptide residue Ile7 (**Appendix 4**). Thus, the reduction in binding affinity observed for $\alpha 24\beta 17$ binding to the Ala7 mutant again could be accounted for because of the potential disruption to TCR-peptide contacts. However, substitution of Ala for Ile at position 5 in the peptide completely abrogated binding (**Table 4.5**). The $\alpha 24\beta 17/\text{A2-ELA}$ structure demonstrated that only 4 vdW contacts were made between $\alpha 24\beta 17$ and the peptide residue Ile5. Thus, the observed effect on binding affinity was surprising and was likely due to indirect effects on TCR binding.

Table 4.5. Kinetic binding analysis of $\alpha 24\beta 17$ to alanine substituted peptides.

TCR	Peptide	Peptide sequence	Affinity (K_D)	ΔG° (kcal/mol)	$\Delta\Delta G^\circ$ (kcal/mol)
MEL5	ELA	ELAGIGILTV	18 μ M	-6.5	Nm
$\alpha 24\beta 17$	ELA	ELAGIGILTV	0.6nM	-12.1	Nm
	ELA1A	A LAGIGILTV	140 μ M	-5.3	-4.2
	ELA4A	EL A IGILTV	36 μ M	-6.1	-6
	ELA5A	ELAG A GILTV	No binding	Nm	Nm
	ELA6A	ELAGI A ILTV	41 μ M	-6	-6.1
	ELA7A	ELAGIG A LTV	31 μ M	-6.1	-6
	ELA8A	ELAGIGI A TV	21 μ M	-6.4	-5.7
	ELA9A	ELAGIGIL A V	37 μ M	-6	-6.1

Nm = not measured

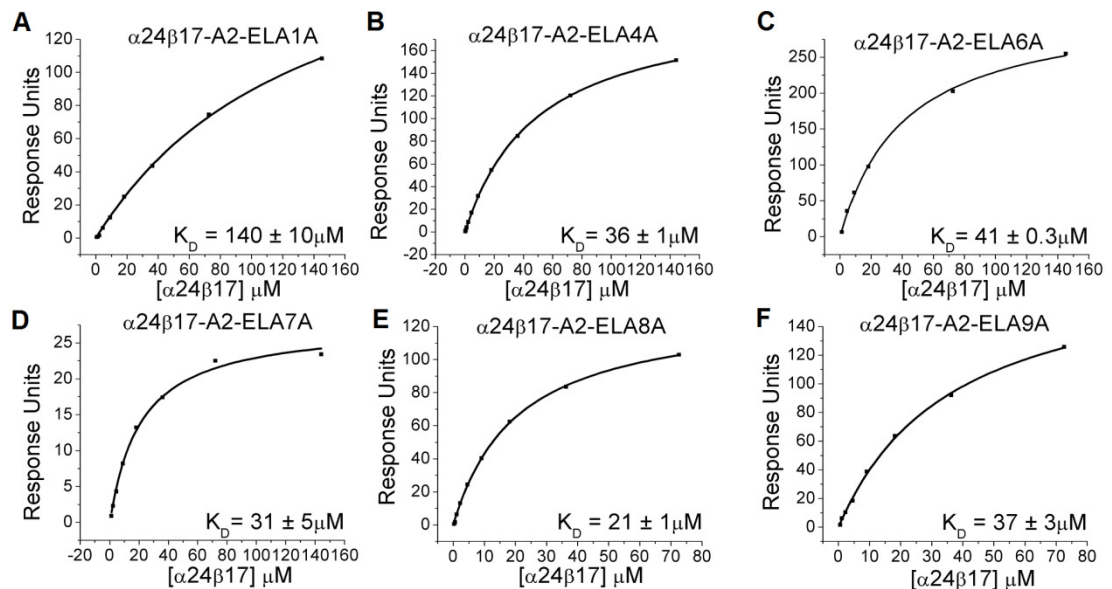


Figure 4.10. $\alpha 24\beta 17$ is extremely sensitive to alanine substitutions within the ELAGIGILTV peptide.

Ten serial dilutions of $\alpha 24\beta 17$ were measured in three separate experiments (with different protein preparations) for each alanine-substituted peptide; representative data from these experiments are plotted. Alanine substitutions in any position within the peptide reduced binding from 600 pM down to wildtype like affinities (μ M). The equilibrium binding constant (K_D) values were calculated using a nonlinear curve fit ($y = (P_1x)/(P_2 + x)$); mean plus SD values are shown. In order to calculate each response, $\alpha 24\beta 17$ was also injected over a control sample (HLA-A*0201 in complex with ILAKFLHWL peptide) that was deducted from the experimental data. (A) $\alpha 24\beta 17$ binding to A2-ALAGIGILTV (B) $\alpha 24\beta 17$ binding to A2-ELAAIGILTV (C) $\alpha 24\beta 17$ binding to A2-ELAGIAILTV (D) $\alpha 24\beta 17$ binding to A2-ELAGIGALTV (E) $\alpha 24\beta 17$ binding to A2-ELAGIGIATV (F) $\alpha 24\beta 17$ binding to A2-ELAGIGILAV. I observed no signal for $\alpha 24\beta 17$ binding to A2-ELAGAGILTV (data not shown).

Importantly, the MEL5 TCR was also very sensitive to Ala substitutions and no binding to the MEL5 TCR with Ala substituted across the ELAGIGILTV peptide was observed (data not shown, experiments performed by Dr David Cole). These data demonstrate that, even though the $\alpha 24\beta 17$ TCR bound with 600 pM, primarily through new contacts made with the MHC, the TCR was still very sensitive to changes in the antigenic peptide. These data have important implications for high affinity TCR antigen recognition and show that TCR-peptide contacts play a dominant role in governing high affinity TCR/pMHC binding.

4.2.6 Peptide substitutions do not alter the overall conformation of the $\alpha 24\beta 17$ /A2-ELA complex

My discovery, that the high affinity $\alpha 24\beta 17$ TCR was sensitive to small changes in the peptide, was highly unanticipated based on the observation that: (i) additional contacts between $\alpha 24\beta 17$ and A2-ELA were mainly with the MHC surface, not the peptide; and, (ii) single peptide mutations, with the potential to directly disrupt only a small number of TCR/pMHC contacts, could have such a dramatic impact on binding affinity. Thus, in order to gain an atomic perspective on how such small changes at the interface could impact binding, I solved the co-complex structures of $\alpha 24\beta 17$ with two of the A2-ELA Ala mutants: A2-ELAAIGILTV (A2-ELA4A) and A2-ELAGIGALTV (A2-ELA7A). I attempted to crystallize a number of other co-complexes with the other Ala mutants, but these attempts were unsuccessful. The $\alpha 24\beta 17$ /A2-ELA4A and $\alpha 24\beta 17$ /A2-ELA7A complex structures were solved to a resolution of 2.46 Å and 2.70 Å respectively, enabling a detailed view of the atomic structure. Molecular replacement was successful only in space group P4₁ for both complexes and the resolution was sufficiently high to show that the interface

between the two molecules was well ordered and contained well-defined electron density (**Figure 4.6**). The crystallographic R/Rfree factors were 20.2% and 24.8% for $\alpha 24\beta 17/A2-ELA4A$ and 20.2% and 25% for $\alpha 24\beta 17/A2-ELA7A$ (**Table 4.2**). Compared to $\alpha 24\beta 17/A2-ELA$, the overall BSA was virtually identical across the three co-complex structures ($\alpha 24\beta 17/A2-ELA$ BSA = 2705 Å², $\alpha 24\beta 17/A2-ELA4A$ BSA = 2650.4 Å², $\alpha 24\beta 17/A2-ELA7A$ BSA = 2781.6 Å²) (**Table 4.3**). Furthermore, the docking geometry and the positions of the TCR CDR loops were indistinguishable between the three complexes (**Table 4.3, Figure 4.11**). Thus, large conformational changes could not explain the difference in binding affinity between $\alpha 24\beta 17/A2-ELA$ and the Ala mutants.

4.2.7 Peptide substitutions do not directly alter the contact interface between the $\alpha 24\beta 17$ TCR and A2-ELA

In order to further probe the effects of the Ala substitutions on $\alpha 24\beta 17$ binding, I investigated the direct effects of these mutations on binding. The structure of $\alpha 24\beta 17$ bound to A2-ELA demonstrated that peptide residue Gly4 made 4 hydrogen bonds and 8 vdW and Ile7 made 3 hydrogen bonds and 8 vdW with the TCR (**Figure 4.12A&B, Appendix 4**). The $\alpha 24\beta 17/A2-ELA4A$ structure revealed that the number of contacts was very similar between peptide residue Ala4 and $\alpha 24\beta 17$ (3 hydrogen bonds and 10 vdW contacts) and the $\alpha 24\beta 17/A2-ELA7A$ structure revealed that the number of contacts was very similar between peptide residue Ala7 and $\alpha 24\beta 17$ (2 hydrogen bonds and 8 vdW contacts) (**Figure 4.12C&D, Appendices 5&6**). Thus, it was unlikely that the Ala peptide substitutions could directly explain the large difference in binding affinity between $\alpha 24\beta 17$ binding to A2-ELA compared to A2-ELA4A and A2-ELA7A.

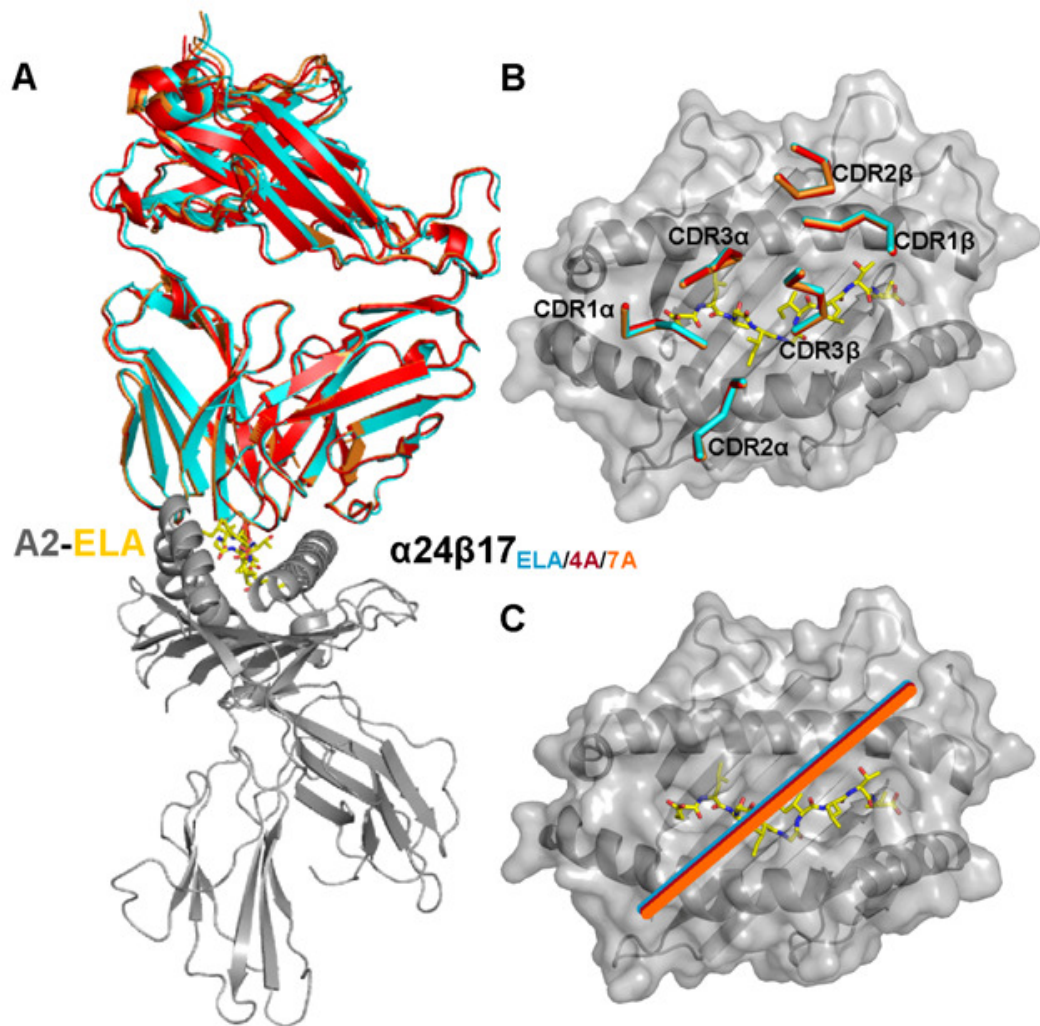


Figure 4.11. Structural comparison of the binding mode implemented by $\alpha 24\beta 17$ when interacting with A2-ELA, A2-ELA4A and A2-ELA7A. A2-ELA is shown in grey cartoon, peptide as yellow sticks. (A) Overall binding mode of $\alpha 24\beta 17$ when interacting with A2-ELA (cyan cartoon), A2-ELA4A (red cartoon) and A2-ELA7A (orange cartoon). $\alpha 24\beta 17$ binds in a virtually identical mode to all three epitopes. (B&C) Surface representation of the A2-ELA complex (colored as in (A)) looking down at the peptide. (B) Positions of the $\alpha 24\beta 17$ TCR CDR loops when interacting with A2-ELA (cyan cartoon), A2-ELA4A (red cartoon) and A2-ELA7A (orange cartoon). (C) $\alpha 24\beta 17$ TCR crossing angle when interacting with A2-ELA (cyan cartoon), A2-ELA4A (red cartoon) and A2-ELA7A (orange cartoon). The positions of the CDR loops and the TCR crossing angles are virtually identical across all three complexes.

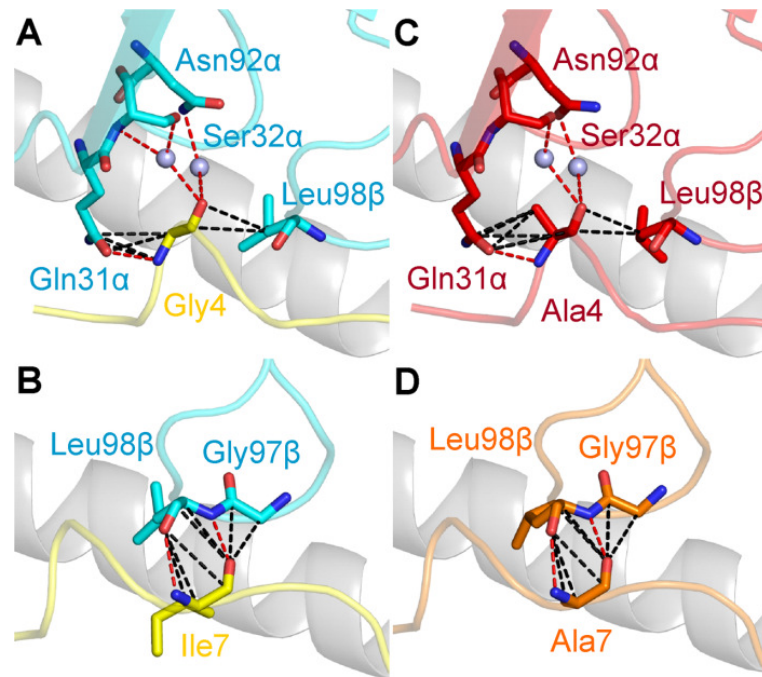


Figure 4.12. Interactions between $\alpha 24\beta 17$ and modified residues in the ELAGIGILTV peptide at positions 4 and 7.

Hydrogen bonds ($<3.4\text{\AA}$) are shown as red dotted lines and van der Waals interactions ($<4.0\text{\AA}$) are shown as black dotted lines and water molecules are shown as grey spheres. $\alpha 24\beta 17$ (cyan sticks) interactions with (A) peptide residues (yellow sticks) Gly4 and (B) Ile7. (C) $\alpha 24\beta 17$ (red sticks) interacting with A2-ELA4A, residue Ala4 (red sticks). (D) $\alpha 24\beta 17$ (orange sticks) interacting with A2-ELA7A, residue Ala7 (orange sticks). Contacts between $\alpha 24\beta 17$ and the three epitopes (A2-ELA, A2-ELA4A and A2-ELA7A) are virtually identical and cannot explain the reduced affinity between $\alpha 24\beta 17$ and the modified peptides.

4.2.8 Peptide substitutions do not alter the overall conformation of unligated A2-ELA molecules

Although the overall conformation of the $\alpha 24\beta 17$ /A2-ELA complex was similar with the Ala substituted peptides, the possibility that Ala substitution could alter the structure of the unligated A2-ELA molecules had to be explored. If $\alpha 24\beta 17$ TCR binding required a conformational shift in the peptide more energy would be required to reach the same final bound state and this could explain the loss of binding affinity. To this end, our collaborator Professor Brian Baker, obtained crystals and diffraction datasets for A2-ELA1A and A2-ELA8A at 2.11 Å and 1.9 Å resolution, respectively, while I obtained crystals and a diffraction dataset for A2-ELA4A at 1.91 Å resolution (**Table 4.6**). I solved the three structures by molecular replacement in space groups P1, C121 and P12₁1 for A2-ELA1A, A2-ELA4A and A2-ELA8A, respectively, and the resolution was sufficiently high to show that the interface between the two molecules was well ordered and contained well-defined electron density (**Figure 4.6**). A comparison of these Ala mutant structures with the unligated structure A2-ELA (Sliz et al., 2001), that does not substantially alter its structure when in complex with different TCRs (Borbulevych et al., 2011; Cole et al., 2009), showed that there was no difference in the overall conformation of the different peptides (**Figure 4.13**). These data discounted the possibility that alterations in the unligated conformation of the Ala substituted A2-ELA peptides could explain the sensitivity of the $\alpha 24\beta 17$ TCR to these single peptide mutations.

Table 4.6. Data collection and refinement statistics for A2-ELA peptide alanine substitution structures (molecular replacement).

Data set statistics	A2-ELA1A	A2-ELA4A	A2-ELA8A
Space Group	P1	C121	P12 ₁ 1
Unit Cell parameters	a=50.283Å, b=63.255Å, c=75.098Å, α=81.96°, β=76.09°, γ=77.98°	a=202.59Å, b=49.11Å, c=117.6, γ=123°	a=84.096Å, b=58.359Å, c=89.432Å, β=109.82°
Radiation Source	ADSC Quantum 210r CCD	DIAMOND IO3	ADSC Quantum 210r CCD
Wavelength (Å)	0.98	0.9763	0.98
Resolution (Å)	2.11	1.91	1.9
Unique reflections	42338	73975	64858
Completeness (%)	78.8	98	97
Multiplicity	2.1	3.5	3.4
I/Sigma(I)	18.9	10.7	16.5
Rmerge (%)	0.10	0.052	0.07
Refinement statistics (highest resolution shell in parenthesis)			
No reflections used	40179	70233	61271
No reflections in Rfree set	2159	3730	3275
Rcryst (no cutoff) (%)	21.8	20.5	21.9
Rfree (%)	29.6	23.9	29.6
RMSD from ideal geometry (target values in parenthesis)			
Bond lengths (Å)	0.021 (0.021)	0.026 (0.021)	0.20 (0.21)
Bond Angles (°)	1.497 (1.930)	1.688 (1.937)	1.845 (1.938)
Wilson B-factor (Å ²)	25.336	37.759	18.057
Overall coordinate ESU based on ML (Å)	0.169	0.101	0.157

One crystal was used for data collection.

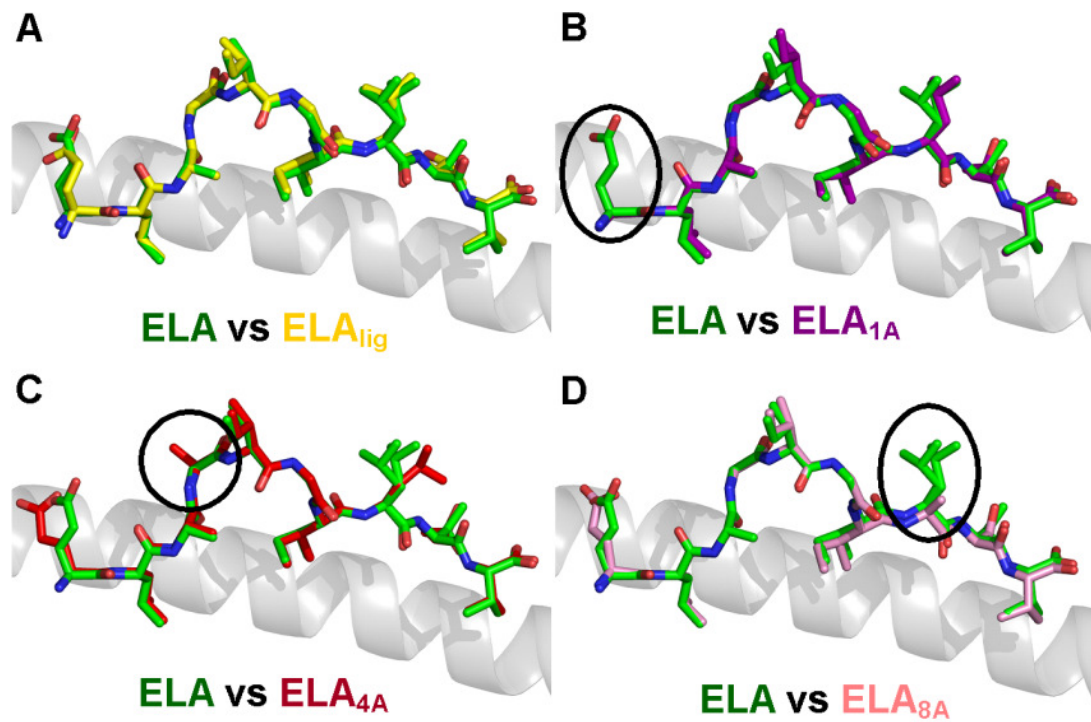


Figure 4.13. Alanine substitutions do not alter the overall conformation of the unligated A2-ELA related pMHCs.

Structural comparison of the A2-ELA unligated crystal structure (1JF1) (Sliz et al., 2001) with: (A) A2-ELA from the $\alpha 24\beta 17$ /A2-ELA complex structure, (B) A2-ELA1A, (C) A2-ELA4A and (D) A2-ELA8A. These structures show that the conformation of the peptide backbone is not altered by TCR binding, or by alanine substitutions. Furthermore, the positions of the solvent exposed side chains is virtually identical in all of the structures, showing that large alterations in peptide conformation in unligated state cannot account for the difference in binding affinity observed between $\alpha 24\beta 17$ binding to A2-ELA compared to the alanine substituted peptides.

4.2.9 Peptide specificity is governed by a distinct thermodynamic signature and a reduction in water bridges

From the previous in-depth structural analysis, the underlying mechanism for the dramatic reduction in binding affinity for $\alpha 24\beta 17$ binding to the alanine substituted peptides was unclear. Thus, I investigated the changes in enthalpy (ΔH°) and entropy ($T\Delta S^\circ$) in order to examine the energetic differences between the binding interaction between $\alpha 24\beta 17$ binding to A2-ELA (**Figure 4.14, Figure 4.17A**) compared to A2-ELA4A (**Figure 4.15, Figure 4.17B**) and A2-ELA7A (**Figure 4.16, Figure 4.17C**).

The $\alpha 24\beta 17$ /A2-ELA interaction (**Figure 4.17A**) was entropically driven ($T\Delta S^\circ \sim 18.1 \text{ kcal.mol}^{-1}$) and enthalpically unfavourable ($\Delta H^\circ \sim 6 \text{ kcal.mol}^{-1}$). While ΔH° was within the range of enthalpy described for a TCR/pMHC interaction, $T\Delta S^\circ$ was one of the highest entropy reported so far in the literature (from -30 to 18 kcal.mol^{-1} for ΔH° and from -23.8 to $23.8 \text{ kcal.mol}^{-1}$ for $T\Delta S^\circ$) (Armstrong et al., 2008a; Holland et al., 2012). I also crystallized and solved the structure of the unligated $\alpha 24\beta 17$ TCR (**Table 4.2**). This structure solved in space group $P3_221$ at 2.4 \AA resolution demonstrated that the change in energy was accompanied by a relatively large conformational shift in the TCR CDR loops upon ligand engagement (**Figure 4.18**). The TCR CDR3 β loop underwent a hinge movement of 8.06 \AA in order to accommodate residues towards the C-terminus of the peptide. These observations suggest that, similarly to the MEL5/A2-ELA complex ($T\Delta S^\circ \sim 8.3 \text{ kcal.mol}^{-1}$) (Cole et al., 2009), an entropically favourable transition from order to disorder was key for driving the high affinity interaction, probably through the expulsion of ordered solvent during binding rather than a loss of order at the TCR/pMHC interface.

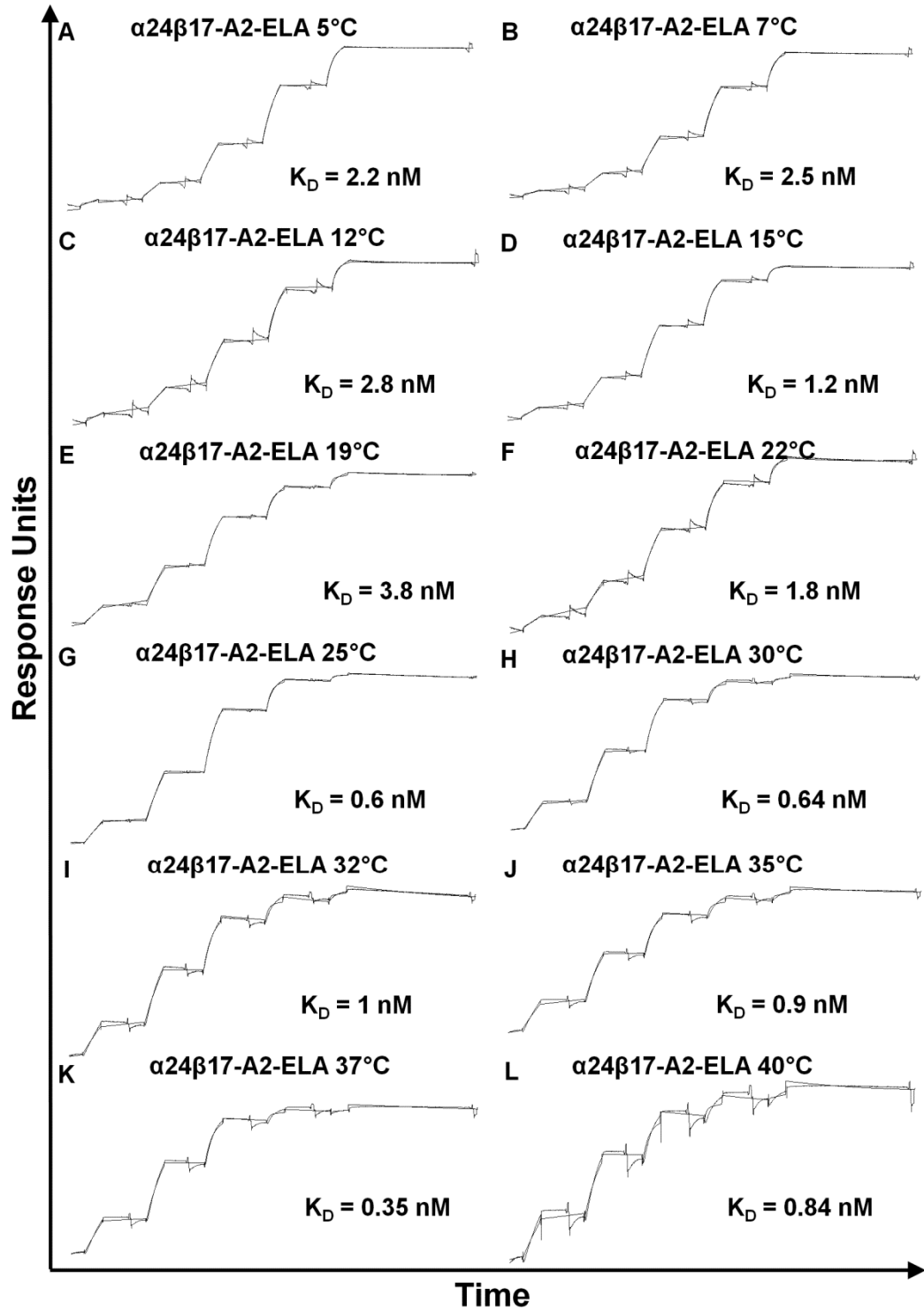


Figure 4.14. Thermodynamic analysis of the $\alpha 24\beta 17/A2-ELA$ interaction. Kinetic titration analysis was used to determine the affinity of the $\alpha 24\beta 17-A2-ELA$ interaction at: (A) 5°C, (B) 7°C, (C) 12°C, (D) 15°C, (E) 19°C, (F) 22°C, (G) 25°C, (H) 30°C, (I) 32°C, (J) 35°C, (K) 37°C and (L) 40°C. The raw data and the fits are shown in each panel. These data were used to fit thermodynamic parameters shown in Figure 4.17A.

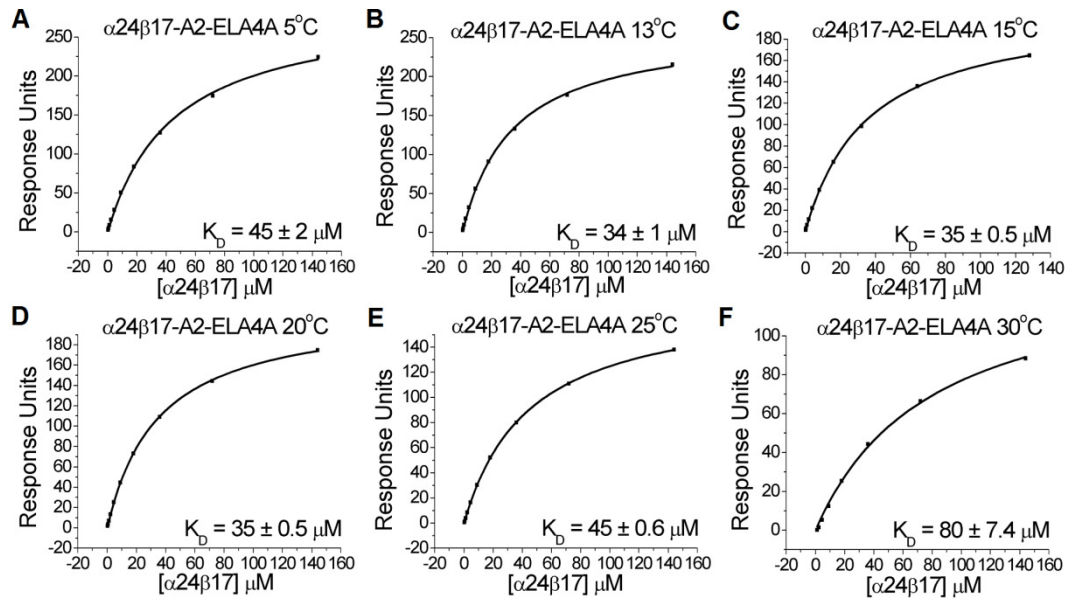


Figure 4.15. Thermodynamic analysis of the $\alpha 24\beta 17$ /A2-ELA4A interaction. Ten serial dilutions of $\alpha 24\beta 17$ were measured in triplicate at each temperature; representative data from these experiments are plotted. The equilibrium binding constant (K_D) values were calculated using a nonlinear curve fit ($y = (P_1x)/P_2 + x$); mean plus SD values are shown. (A) 5°C, (B) 13°C, (C) 15°C, (D) 20°C, (E) 25°C and (F) 30°C. These data were used to fit thermodynamic parameters shown in **Figure 4.17B**.

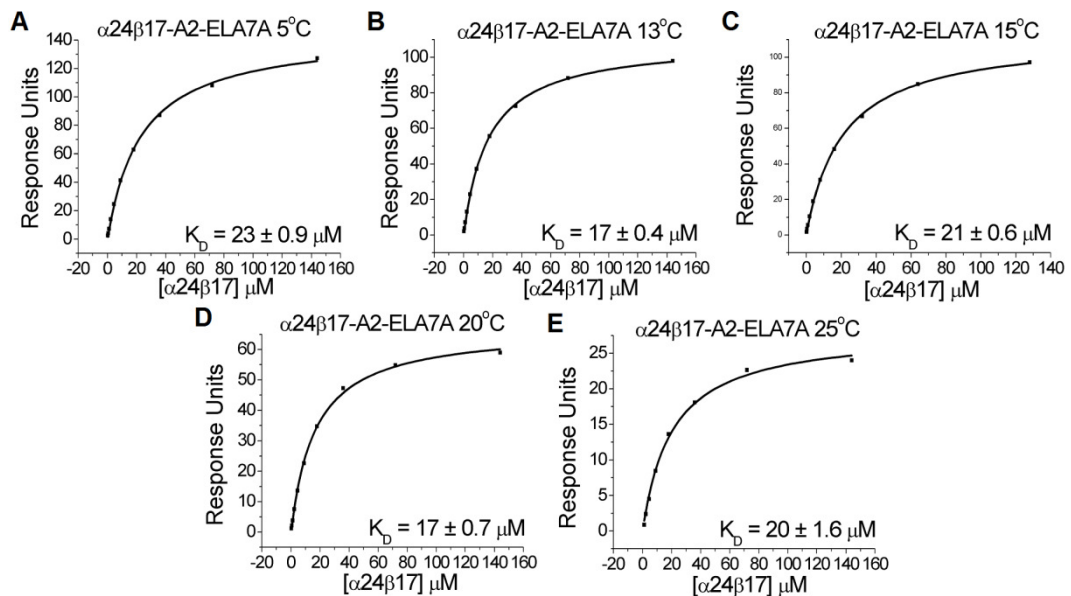


Figure 4.16. Thermodynamic analysis of the $\alpha 24\beta 17$ /A2-ELA7A interaction. Ten serial dilutions of $\alpha 24\beta 17$ were measured in triplicate at each temperature; representative data from these experiments are plotted. The equilibrium binding constant (K_D) values were calculated using a nonlinear curve fit ($y = (P_1x)/P_2 + x$); mean plus SD values are shown. (A) 5°C, (B) 13°C, (C) 15°C, (D) 20°C and (E) 25°C. These data were used to fit thermodynamic parameters shown in **Figure 4.17C**.

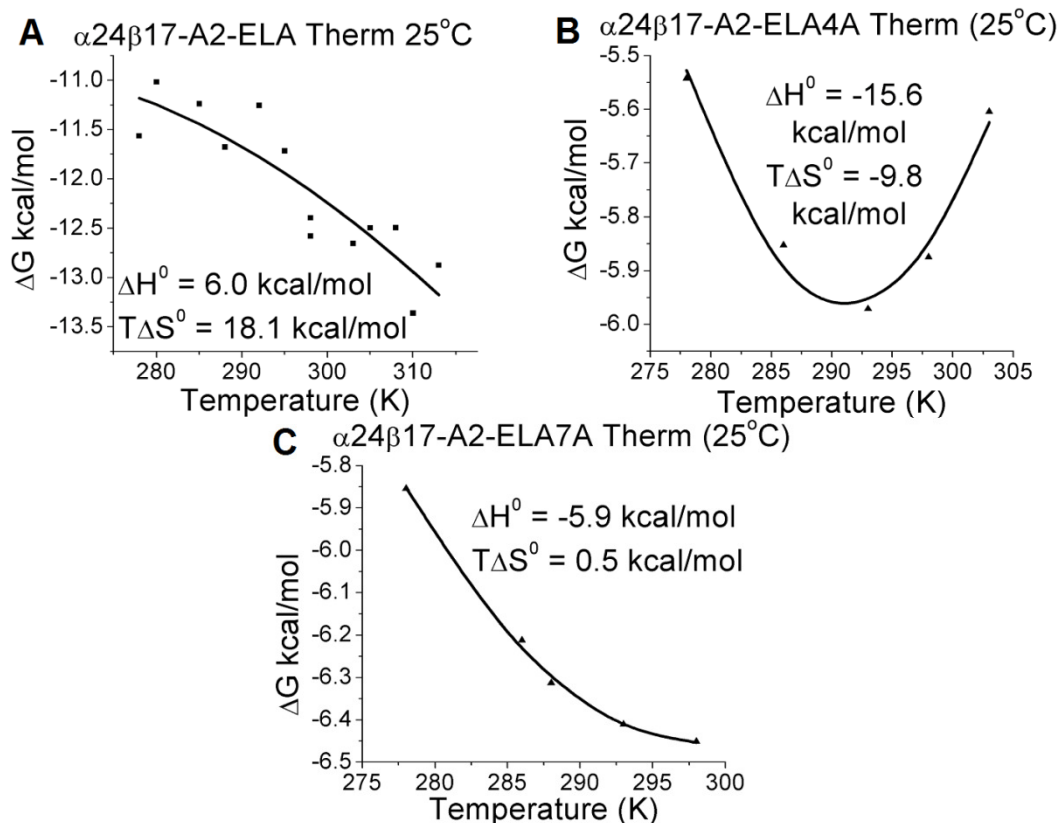


Figure 4.17. Thermodynamic analysis of $\alpha 24\beta 17$ binding to A2-ELA, A2-ELA4A and A2-ELA7A.

The thermodynamic parameters were calculated according to the Gibbs-Helmholtz equation ($\Delta G^\circ = \Delta H - T\Delta S^\circ$). The binding free energies, ΔG° ($\Delta G^\circ = RT \ln K_D$), were plotted against temperature (K) using non-linear regression to fit the three-parameters Van't Hoff equation, ($RT \ln K_D = \Delta H^\circ - T\Delta S^\circ + \Delta C_p^\circ(T-T_0) - T\Delta C_p^\circ \ln(T/T_0)$) with $T_0=298$ K), as previously reported (Cole et al., 2009). Thermodynamic measurements of (A) $\alpha 24\beta 17$ binding to A2-ELA, (B) $\alpha 24\beta 17$ binding to A2-ELA4A and (C) $\alpha 24\beta 17$ binding to A2-ELA7A. $\alpha 24\beta 17$ uses a distinct thermodynamic strategy when binding to each of the three different epitopes.

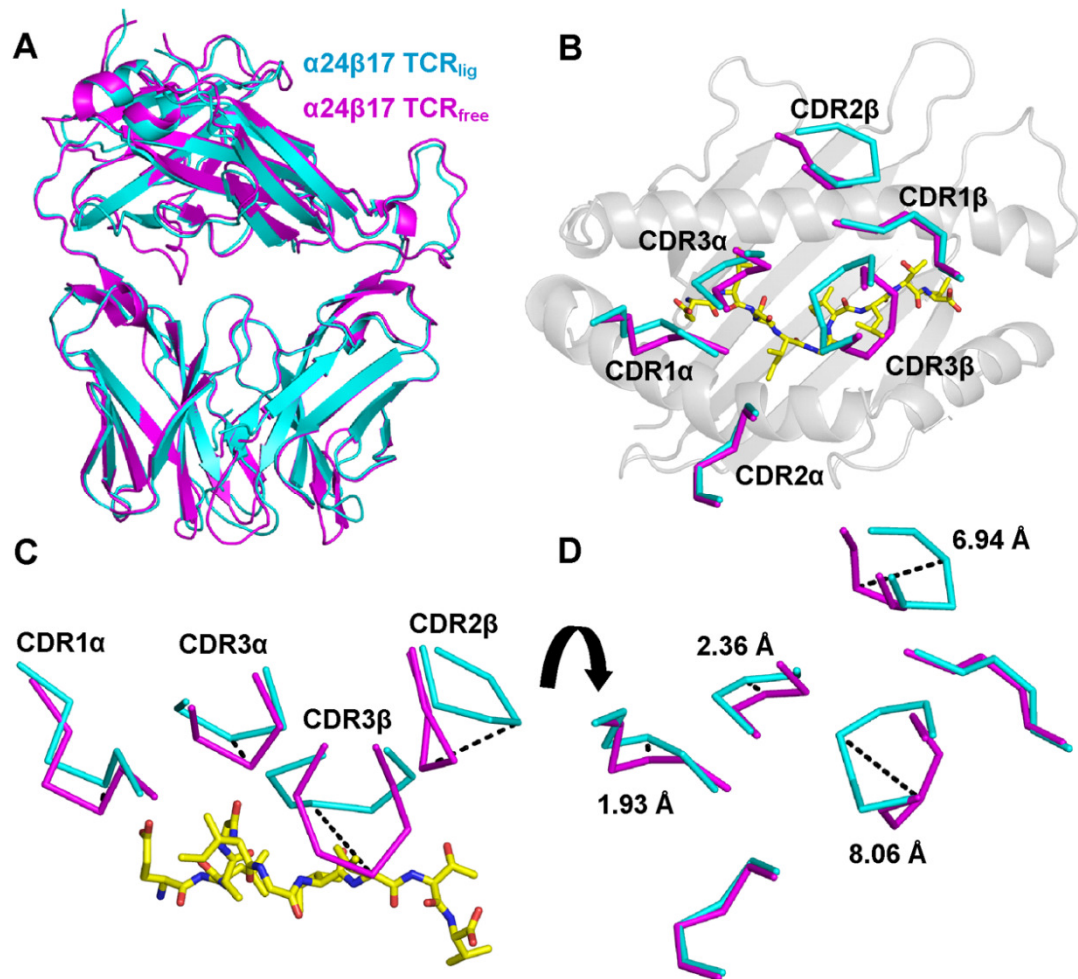


Figure 4.18. $\alpha 24\beta 17$ undergoes large TCR CDR movement during ligand engagement.

Comparison of the conformation of the $\alpha 24\beta 17$ TCR CDR1, CDR2 and CDR3 loops in the $\alpha 24\beta 17/A2$ -ELA complex ($\alpha 24\beta 17_{\text{lig}}$) versus $\alpha 24\beta 17$ unligated ($\alpha 24\beta 17_{\text{free}}$). (A) Superposition of the free (purple cartoon) and complexed (cyan cartoon) TCRs. (B) Superposition of the free (purple lines) and complexed (cyan lines) $\alpha 24\beta 17$ TCR looking down on the peptide (yellow sticks). (C) Superposition of the free (purple lines) and complexed (cyan cartoon) $\alpha 24\beta 17$ CDR1 α , CDR3 α , CDR2 β and CDR3 β loops from the side. The CDR3 β loop has to move in order to avoid a clash with the peptide (yellow sticks) during binding. (D) Superposition of the free (purple lines) and complexed (cyan lines) $\alpha 24\beta 17$ TCR CDR loops during binding showing backbone shifts in Å (orientation as in (B)). The CDR2 β and CDR3 β loops undergo the largest conformational change upon binding.

In contrast, this energetic mechanism was reversed for the $\alpha 24\beta 17/A2\text{-ELA4A}$ and $\alpha 24\beta 17/A2\text{-ELA7A}$ interactions ($\Delta H^\circ \sim -15.6$ and ~ -5.9 kcal.mol⁻¹, respectively) (**Figure 4.17B&C**) with favourable enthalpy driving the interaction. Thus, the loss of binding affinity observed for the interaction between the $\alpha 24\beta 17$ TCR and the alanine modified peptides seemed to be governed by a change in the order-disorder balance during binding, possibly due to differences in the interaction between the unligated molecules and solvent (Holland et al., 2012). To further explore this possibility, the role of water molecules during antigen recognition was examined and some changes in the number of water bridges between the different complexes were noticed. For instance, in the $\alpha 24\beta 17/A2\text{-ELA}$ complex, 9 water bridges were formed between the TCR and pMHC compared to only 7 for $\alpha 24\beta 17/A2\text{-ELA4A}$ and 5 for $\alpha 24\beta 17/A2\text{-ELA7A}$ (**Figure 4.19**). Although this reduction in water bridges, hence a reduction in hydrogen bonds, could partly explain the reduction in binding affinity to the alanine substituted peptide mutants, the difference in water bridges also suggested that the interaction between the TCR, pMHC and solvent was different in the three complexes. For instance, the less favourable entropic values, that were the main driving force governing the weaker binding affinity observed for the $\alpha 24\beta 17/A2\text{-ELA4A}$ and $\alpha 24\beta 17/A2\text{-ELA7A}$ interactions, were most likely due a reduction in the expulsion of ordered solvent during binding. This notion is the best explanation for the sensitivity of the TCR to alanine substitutions, considering the similar binding modes and the distinct thermodynamic signatures observed for the $\alpha 24\beta 17$ TCR interacting with A2-ELA compared to A2-ELA4A and A2-ELA7A. Overall, these data support the idea that TCR specificity can be mediated by changes in solvent interactions between the TCR and pMHC that can occur through a knock-on effect in modifications to the peptide sequence.

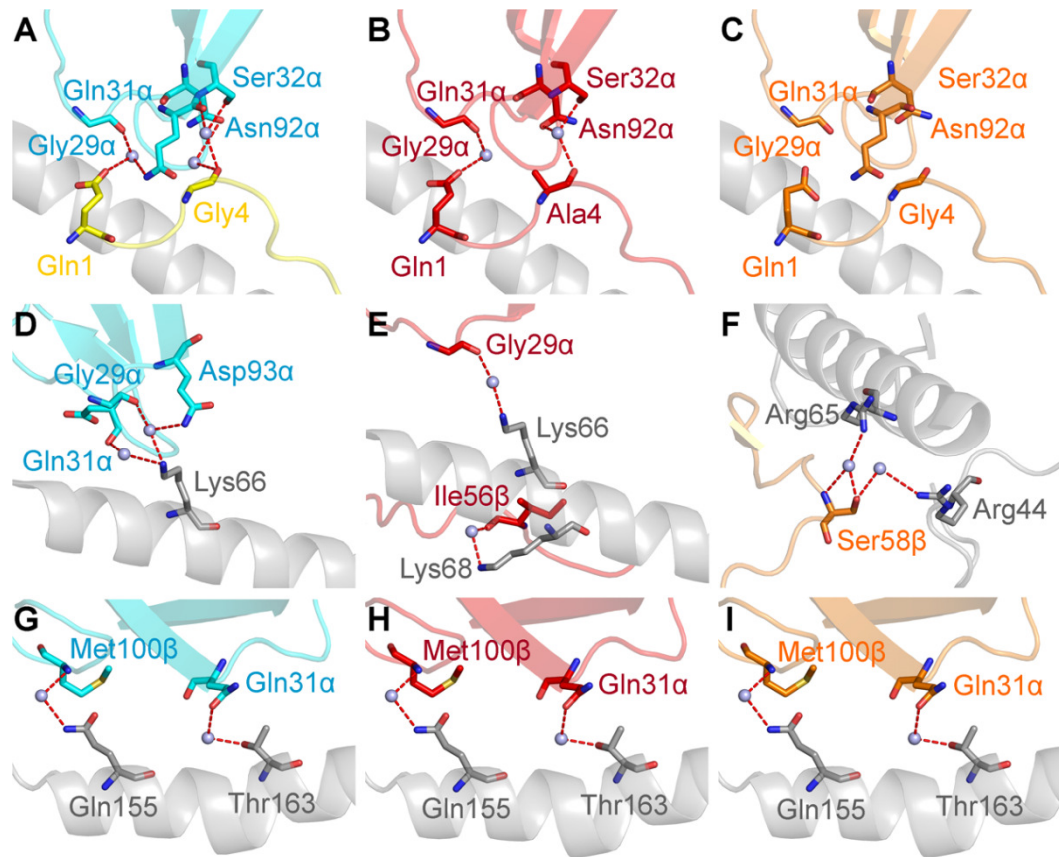


Figure 4.19. $\alpha 24\beta 17$ makes more water bridges with A2-ELA than with A2-ELA4A and A2-ELA7A.

$\alpha 24\beta 17$ binding to A2-ELA is shown in cyan sticks, peptide in yellow sticks. $\alpha 24\beta 17$ binding to A2-ELA4A is shown in red sticks, peptide in red sticks. $\alpha 24\beta 17$ binding to A2-ELA7A is shown in orange sticks, peptide in orange sticks. The MHC is shown in grey sticks and water molecules are shown as grey spheres. Hydrogen bonds ($<3.4\text{\AA}$) are shown as red dotted lines and van der Waals interactions ($<4.0\text{\AA}$) are shown as black dotted lines. Water bridges between the TCR and peptide in (A) the $\alpha 24\beta 17$ /A2-ELA complex, (B) the $\alpha 24\beta 17$ /A2-ELA4A complex and (C) the $\alpha 24\beta 17$ /A2-ELA7A complex. Water bridges between the TCR and MHC $\alpha 1$ helix in (D) the $\alpha 24\beta 17$ /A2-ELA complex, (E) the $\alpha 24\beta 17$ /A2-ELA4A complex and (F) the $\alpha 24\beta 17$ /A2-ELA7A complex. Water bridges between the TCR and MHC $\alpha 2$ helix in (G) the $\alpha 24\beta 17$ /A2-ELA complex, (H) the $\alpha 24\beta 17$ /A2-ELA4A complex and (I) the $\alpha 24\beta 17$ /A2-ELA7A complex.

4.3 DISCUSSION

CD8⁺ T-cells have the ability to detect intracellular deleterious proteins and deliver a cytotoxic payload that can destroy cells that pose a threat to host health. T-cell “X-ray vision” is controlled via the TCR/pMHC interaction. The capacity of TCRs to see internal anomalies from the cell surface offers exciting new possibilities for developing disease-specific therapies. However, unlike antibodies that undergo somatic hypermutation and bind with a relatively strong affinity, TCRs are selected in the thymus to bind with a weak affinity ($K_D = 0.1\text{-}270 \mu\text{M}$) (Bridgeman et al., 2012; Cole et al., 2007). This effect is magnified during cancer-specific T-cell responses because cancer-specific TCRs bind at the weaker end of this scale. The weak affinity of natural TCR/pMHC interactions imposes limitations on the use of TCRs for targeting cell surface expressed pMHCs.

Using phage display, several high affinity TCRs directed against a range of antigens were generated (Li et al., 2005b; Liddy et al., 2012; Varela-Rohena et al., 2008). Herein, I investigated the interaction between a high-affinity TCR, $\alpha 24\beta 17$, derived from the MEL5 TCR that is specific for the HLA-A*0201 restricted MART-1₂₆₋₃₅ antigen. The $\alpha 24\beta 17$ TCR bound to A2-ELA with an enhanced affinity 30,000 times stronger than the MEL5 TCR that could be primarily attributed to a longer off-rate. In order to better understand the consequences of high-affinity TCR binding, I solved the atomic structure of $\alpha 24\beta 17$ in complex with A2-ELA. Although $\alpha 24\beta 17$ used a similar overall binding mode to MEL5 during engagement of A2-ELA, finer examination of the structure demonstrated that 3 new contacts were made between $\alpha 24\beta 17$ and the ELA peptide, compared to 41 new MHC contacts. Thus, the enhanced affinity was mediated primarily through additional interactions with the

surface of the MHC molecule. This observation raised the possibility that the $\alpha 24\beta 17$ TCR might be capable of recognizing HLA-A*0201 independently of the bound peptide and such peptide-independent recognition would be deleterious for a potential use in soluble TCR therapy. In order to investigate the ability of $\alpha 24\beta 17$ to tolerate changes in the peptide, I performed a biophysical investigation of the effect of alanine mutations scan across the peptide backbone. Surprisingly, the $\alpha 24\beta 17$ TCR was highly sensitive to changes in the peptide with some single mutations capable of completely abrogating binding, supporting the notion the TCR-peptide contacts are required to enable TCR-MHC binding. The finding that $\alpha 24\beta 17$ was highly sensitive to alanine peptide mutations was unexpected and warranted further investigations to uncover the molecular mechanism behind this observation. Thus, I solved the structure of $\alpha 24\beta 17$ in complex with two alanine mutants; A2-ELA4A and A2-ELA7A. Additionally, I solved the structure of the unligated $\alpha 24\beta 17$ TCR and unligated A2-ELA1A, A2-ELA4A and A2-ELA8A molecules. These structures demonstrated that $\alpha 24\beta 17$ used a virtually identical structural strategy to engage the alanine mutants compared to A2-ELA and that the alanine mutations did not alter the peptide conformation of the unligated pMHCs. The total number of contacts made in the $\alpha 24\beta 17$ /A2-ELA complex compared to the $\alpha 24\beta 17$ /A2-ELA4A and $\alpha 24\beta 17$ /A2-ELA7A complexes was also very similar (138, 141 and 136 respectively) and could not explain the weaker binding affinity. Next, I conducted a thermodynamic investigation of $\alpha 24\beta 17$ binding to A2-ELA and the alanine substituted variants. I found that $\alpha 24\beta 17$ used a distinct thermodynamic signature to engage A2-ELA compared to A2-ELA4A and A2-ELA7A involving a marked decrease in favourable entropy. This observation suggested that differences in ordered solvent molecules involved during $\alpha 24\beta 17$ binding could have an important role in governing antigen

sensitivity. In support to this notion, I observed a reduction in the number of water bridges for $\alpha 24\beta 17$ binding to A2-ELA4A and A2-ELA7A compared to A2-ELA. Overall, these data support the idea that TCR specificity can be mediated by changes in solvent interactions between the TCR and pMHC that can occur through a knock-on effect in modifications to the peptide sequence.

One interesting characteristic of the TCR that is not fully understood is its natural weak binding affinity for pMHC, especially considering the similarity in TCR structure to antibodies. If generated, T-cells bearing TCRs that bind to pMHC with antibody-like affinity must be removed during thymic selection as they have never been detected in peripheral responses. How and why these T-cells are removed is unclear. There are, at least, three obvious possibilities. First, high affinity TCRs are self-reactive and are removed during negative selection (Palmer and Naeher, 2009). Second, the thymic auditioning may require that TCRs exhibit specific biophysical properties that are consistent with serial triggering by pMHC in the periphery (Irving et al., 2012; Valitutti et al., 1995). Third, it has recently been shown that T-cells must, and do, confer a high level of cross-reactivity in order to fully protect the host against all potential pathogens (Mason, 1998; Wooldridge et al., 2012). Thus, it is possible that T-cells with high-affinity TCRs are culled in the thymus because they are too “focused” on a limited number of potential foreign peptides. In other words, T-cells with TCRs that bind too strongly could be focused on a small number of antigens rendering them unable to provide adequate cross-protection. However, despite my data supporting this notion, more work (particularly on cellular experiments and on testing the high-affinity TCR specificity toward different peptides) is required to add support to this idea. Whilst this characteristic would be

deleterious in the context of a natural immune response where a high level of T-cell cross-reactivity may be essential for effective immunity, a high level of specificity is desirable for epitope targeting during drug delivery. Although more work, particularly cellular experiments, are required to add support to these ideas, these findings here suggest that high-affinity TCRs may be more “focused” on their cognate target antigens, which is a promising discovery in context of the development of specific tools and therapies for targeting human diseases.

In summary, my data show that TCR affinity can be enhanced by increasing interactions between the TCR and the MHC surface without obvious concomitant loss of peptide specificity. Although this strategy of affinity enhancement has potential to lead to peptide-independent TCR/pMHC binding, I showed that the high-affinity $\alpha 24\beta 17$ TCR was highly sensitive to single alanine mutations in the peptide backbone at every position. My data supports the notion that the TCR must contact the peptide to enable optimal TCR docking with MHC. The mechanism for this sensitivity to peptide modifications was unclear based on the structural evidence, which showed that TCR binding was virtually identical for the alanine modified and natural peptide variants. However, the in depth biophysical and thermodynamic analysis revealed an unexpected and novel mechanism for TCR specificity in which different interactions with solvent molecules seemed to govern the reduction in affinity for the high-affinity TCR when single alanine mutations were introduced into the peptide. Overall, these data highlight the complex and unpredictable nature of T-cell antigen recognition and have important implications for the development of high-affinity TCRs as therapeutic agents.

CHAPTER 5
STRUCTURAL AND BIOPHYSICAL COMPARISON
OF TCR BINDING TO NATURAL VARIANT HLA-
A2-RESTRICTED MELANOMA PEPTIDES

Chapter background	177
5.1 Introduction	177
5.1.1 Conformational changes observed upon TCR recognition	178
5.1.1.1 TCR flexibility on pMHC engagement.....	179
5.1.1.2 MHC flexibility on pMHC engagement	179
5.1.1.3 Peptide flexibility on pMHC engagement.....	180
5.1.2 Structural observations of the common HLA-A2-restricted melanoma antigens	180
5.1.3 Aim.....	183
5.2 Results	183
5.2.1 Production and purification of soluble TCRs and pMHCs	183
5.2.2 MEL5 and $\alpha 24\beta 17$ TCR binding to natural MART-1 antigens	185
5.2.3 Protein crystallization.....	188
5.2.4 Structures of MEL5 and $\alpha 24\beta 17$ complexed to A2-EAA and A2-AAG .	190
5.2.5 The high affinity of $\alpha 24\beta 17$ toward MART-1 _{26/27-35} is due to an increase in the interaction between the TCR and the MHC	190
5.2.6 Binding mechanisms of two melanoma-specific TCRs to the HLA-A2- restricted EAAGIGILTV MART-1 antigen.....	193
5.2.7 The MEL5 TCR distinguishes EAA with ELA due to an enhanced flexibility of the natural decamer	195

5.2.8	TCR binding to A2-AAGIGILTV induces a peptide anchor switch	197
5.2.9	Different binding mechanisms of recognition for MEL5/AAG _{bulged} and MEL5/AAG _{stretched}	203
5.2.10	Reduction in interactions between MEL5 TCR and A2-AAG results in weaker binding affinity	205
5.2.11	The binding of MEL5 and $\alpha 24\beta 17$ to A2-AAG leads to a gain of enthalpy and entropy compared to the binding to A2-EAA	207
5.3	Discussion.....	213

Chapter background

The results in this Chapter follow on from **Chapter 3** and **Chapter 4**. The HLA-A2-restricted MART-1_{26/35} system is the best-studied human cancer antigen to date and has been used in thousands of published studies. These efforts and at least 4 peptide vaccine trials have largely focussed on an MHC anchor-modified “heteroclitic” version of the natural peptide. Recent work from my laboratory has questioned this approach by showing that TCRs can distinguish between the heteroclitic and the natural sequence (Cole et al., 2010). Thus, T-cells primed with the heteroclitic sequence often do not recognise melanoma cells well (Cole et al., 2010). The MEL5 TCR exhibits a strong preference for the natural sequence over the anchor-modified sequence. In this Chapter, I aimed to solve the structure of MEL5 complexed with this natural decameric peptide in order to understand the reason why a TCR could distinguish between these two peptides that differ only at a buried MHC anchor residue. Studies of MART-1-derived peptides presented at the melanoma cell surface suggest that a nonamer version of the peptide is more common than the natural decamer (Skipper et al., 1999; Valmori et al., 1998). Thus, the nonameric antigen might be the best peptide to target. I therefore also set out to solve the structure of MEL5 complexed with the natural nonameric peptide and found some unanticipated and novel findings.

5.1 INTRODUCTION

The clonotypic $\alpha\beta$ T-cell receptor (TCR), expressed on the surface of T-cells, can bind to peptide-Major Histocompatibility Complex (pMHC) molecules on the surface of target cells (Jenkins et al., 2010). Thymic TCR affinity editing produces a population of peripheral T-cells with TCRs that bind to their cognate pMHC ligands

relatively weakly ($K_D = 0.1\text{-}270\ \mu\text{M}$), with self-reactive T-cells towards the weaker end of this range (Bridgeman et al., 2011). Because the majority of cancer epitopes are derived from self-proteins, robust immune responses to cancer epitopes have not been commonly observed. In support of this notion, my laboratory has recently shown that TCRs bind to cancer epitopes with around ten times weaker affinity than to viral epitopes (Cole et al., 2007). I described the MEL5 TCR and its high-affinity variant $\alpha 24\beta 17$ in **Chapter 4**. MEL5 TCR binding to the heteroclitic version of the melanoma antigen MART1 (A2-ELA) is relatively weak ($K_D \sim 18\ \mu\text{M}$) (Cole et al., 2007). However, the MEL5 TCR can recognise the natural decamer epitope EAAGIGILTV (A2-EAA) with a substantially stronger affinity ($\sim 6\text{-}8\ \mu\text{M}$). Thus, I decided to investigate the molecular rules governing this relatively strong affinity anti-cancer TCR recognition. I extended the study to determine the ability of MEL5 to recognise the native nonamer epitope, AAGIGILTV. This nonamer peptide is thought to represent the dominant species on the surface of melanoma cells (Skipper et al., 1999). I also investigated the recognition of these two natural epitopes by the high-affinity variant $\alpha 24\beta 17$.

5.1.1 Conformational changes observed upon TCR recognition

The crystal structures of several TCR/pMHC complexes have been solved and reviewed (Rudolph et al., 2006). In some cases there is also a corresponding structure of the uncomplexed TCR allowing observation of the molecular movements that take place upon ligand engagement. While some TCRs bind in a rigid ‘lock-and-key’ mechanism (Bulek et al., 2012a), most exhibit a degree of plasticity at the TCR/pMHC interface. So far, three main types of conformational changes have been observed when TCRs bind to pMHCs: (i) Changes in the TCR;

(ii) Changes in the MHC; and (iii) Changes in the central ‘bulge’ region of the peptide.

5.1.1.1 TCR flexibility on pMHC engagement

TCR complementarity determining region (CDR) loops can exhibit considerable plasticity upon binding pMHC (Armstrong et al., 2008b). The types of loop shift can be placed into three major classes: (i) Loop remodelling facilitated by multiple ϕ/ψ bond angle changes; (ii) Hinge-bending motions; and, (iii) Rigid-body shifts (Armstrong et al., 2008b). Kjer-Nielsen et al. have also shown that pMHC ligation can lead to a conformational change within the TCR constant domain, an observation that was recently confirmed by Beddoe et al. (Beddoe et al., 2009; Kjer-Nielsen et al., 2002). Overall, the plasticity of the TCR allows engagement of a wide range of different pMHC “landscapes”.

5.1.1.2 MHC flexibility on pMHC engagement

The MHC α -helices flanking the peptide-binding groove can shift upon TCR binding. Such movements have been observed in the recognition of pBM8/H-2K^{bm8} (MHCI) by the BM3.3 TCR (Auphan-Anezin et al., 2006) and MBP/HLA-DR2a (MHCII) by the 3A6 TCR (Li et al., 2005a). In both cases, rigid-body shifts of approximately 1 Å were distributed across both the $\alpha 1$ and $\alpha 2$ helices (Armstrong et al., 2008b). More unusual HLA-A2 $\alpha 2$ -helix conformational changes have also been observed. Upon the recognition of Tel1p/HLA-A2 by the A6 TCR, a conformational “switch” occurred at the hinge of the short and long helical elements that shortened the short arm and extended the long arm of the $\alpha 2$ -helix (Borbulevych et al., 2009).

5.1.1.3 Peptide flexibility on pMHC engagement

There have been several reports that TCR binding can induce conformational changes in the solvent exposed central peptide residues, mediating TCR docking and T-cell recognition (Rudolph et al., 2006; Ruppert et al., 1993). Small backbone shifts have been observed upon recognition of the Tax and NY-ESO peptides presented by HLA-A2 (Chen et al., 2005; Garboczi et al., 1996; Khan et al., 2000; Webb et al., 2004), whereas binding of the ELS4 TCR dramatically “squashed” the EPLP backbone (peptide from the BZLF1 antigen of Epstein-Barr virus) presented by HLA-B35, with a large shift of 5 Å occurring in the centre of the peptide (Tynan et al., 2007). Another large shift occurred upon recognition of the malignant melanoma MART-1₂₇₋₃₅ nonamer peptide by the DMF4 TCR, with the amide nitrogen of Gly5 moving 2.7Å toward the HLA-A2 α 2-helix (Borbulevych et al., 2011). My work has focussed on TCR binding of two HLA-A2-restricted peptides from Melan-A/MART-1. Observations in this system are detailed below.

5.1.2 Structural observations of the common HLA-A2-restricted melanoma antigens

Melan-A (for melanoma antigen A)/MART-1 (for melanoma antigen recognised by T-cells 1) is a tumor differentiation antigen which is expressed by melanocytes and malignant melanoma cells from tumours in >95% of patients (Derre et al., 2007). There are two natural peptide variants derived from Melan-A presented by HLA*0201 and recognized by Melan-A specific T-cells. Initial studies identified the MART-1₂₇₋₃₅ nonamer AAGIGILTV (referred to herein as AAG) as the numerically dominant epitope at the melanoma cell surface from the MART-1 protein (Skipper et al., 1999), although the MART-1₂₆₋₃₅ decamer EAAGIGILTV (referred to herein as

EAA) has also been reported at the surface of melanoma cells (Held et al., 2007; Valmori et al., 1998). Several studies suggest that the majority of Melan-A-specific T-cells preferentially recognise the minority decamer rather than the nonamer (Cole et al., 2010; Romero et al., 1997). The atomic structures of both peptides complexed to HLA*0201 have been solved previously (Borbulevych et al., 2007) and showed a bulged conformation and an extended conformation for EAA and AAG, respectively, which could explain the difference in recognition by Melan-A specific T-cells (**Figure 5.1A**). In both cases the peptide position 2 (P2) anchored in the B pocket of the MHC groove and the C-terminus (P10 for EAA and P9 for AAG) anchored in the F pocket (**Figure 5.1B**). The crystallographic structures of DMF4 and DMF5, the first TCRs used in cancer gene therapy (Morgan et al., 2006), in complex with both the nonamer AAG and a heteroclitic form of the decamer (ELAGIGILTV, referred to as ELA) have been solved recently (Borbulevych et al., 2011), but there remains no atomic structure of the natural decamer EAA in complex with a TCR. This is an important omission because work from my host laboratory recently showed that TCRs can distinguish between A2-EAA and A2-ELA peptides (Cole et al., 2010). This difference offers a potential molecular reason for why all the clinical trials with the ELAGIGILTV peptide have been a universal failure (Bins et al., 2007; Cole et al., 2010; Rosenberg et al., 2004). Borbulevych et al. showed that there were no major changes in either peptide or MHC conformation upon TCR recognition of the A2-ELA (Borbulevych et al., 2011).

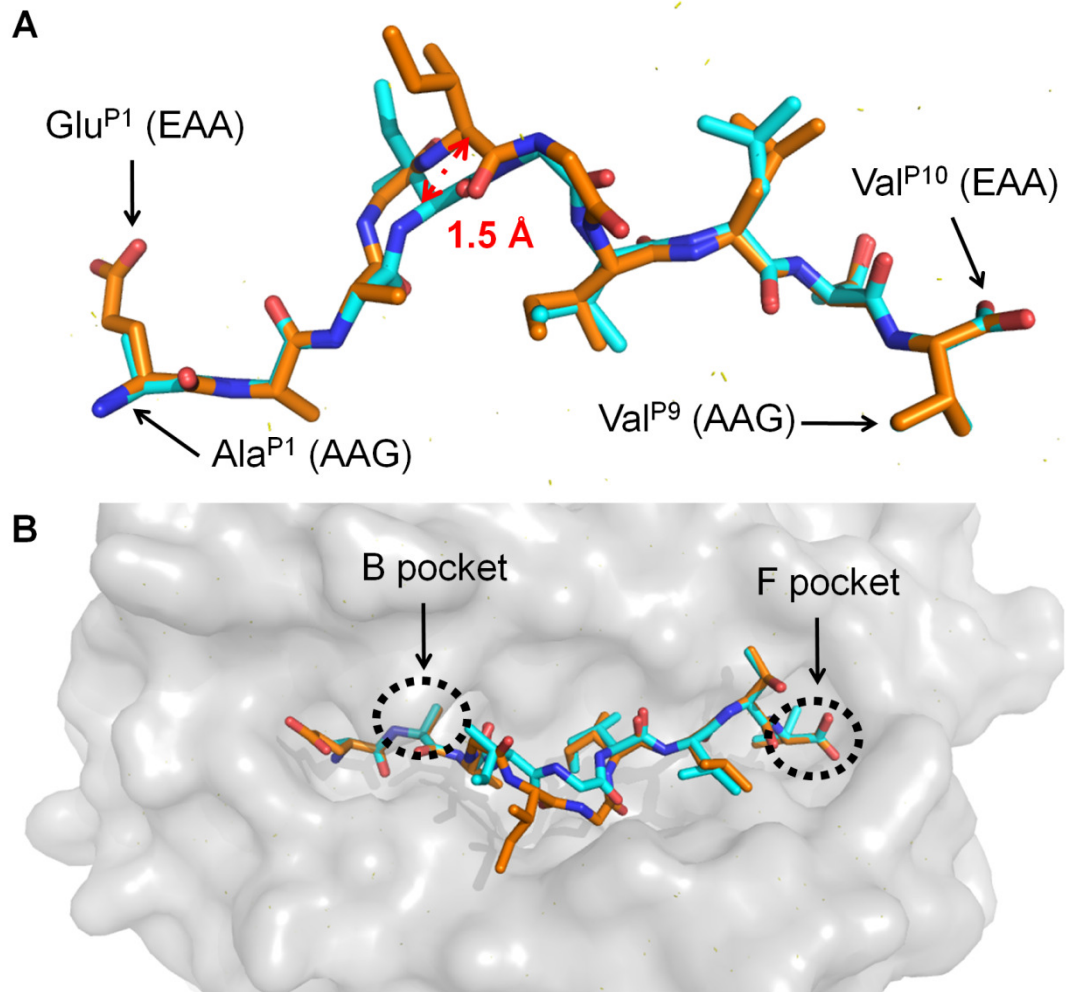


Figure 5.1. Atomic structures of AAGIGILTV and EAAGIGILTV complexed to HLA-A2.

(A) When complexed to HLA-A2, EAAGIGILTV (orange stick) displays a “bulged” and “zig-zagged” conformation whereas AAGIGILTV (blue stick) displays a “stretched” (also referred as “extended”) conformation. The dissimilar conformations result, for example, in a significant 2.6 Å distance between Ile^{P4} (AAG) and Ile^{P5} (EAA). (B) For both peptides, the peptide position 2 (P2) anchors in the B pocket of the MHC groove (grey) and the C-terminus (P10 for EAA and P9 for AAG) anchors in the F pocket.

However binding of TCRs to the nonamer A2-AAG induced a shift in the peptide conformation, bringing the centre of AAG closer to that seen with A2-ELA. Nevertheless, due to the presence of the additional amino acid in the decamer, there were still conformational differences between A2-AAG and A2-ELA, with the peptides out of alignment at Ile4 (AAG) and Ile5 (ELA).

5.1.3 Aim

The MEL5 affinity for A2-EAA and A2-AAG has been described previously (Cole et al., 2010; Ekeruche-Makinde et al., 2012). This particular melanoma-specific TCR binds to both natural MART-1 peptides with a stronger affinity compared to previous published MART-1-specific TCRs and within the affinity range normally associated with TCR response to non-self peptides (Cole et al., 2007). The MEL5 TCR is thus the best natural TCR for the natural HLA-A2-restricted MART-1 antigens described to date. The aims of this Chapter were to provide a molecular explanation for MEL5 ability to interact with a greater affinity with MART-1, particularly the physiologically relevant MART-1₂₇₋₃₅ nonamer, and to investigate the interaction between the high-affinity variant $\alpha 24\beta 17$ and the two clinically relevant natural MART-1 peptides.

5.2 RESULTS

5.2.1 Production and purification of soluble TCRs and pMHCs

This work required the production of substantial amounts of the proteins listed in **Table 5.1**. Protein production and purification are described in **Chapter 2** (section 2.3) and **Chapter 4** (section 4.2.1) of this thesis.

Table 5.1. List of the proteins produced for the work reported in this Chapter.

	Protein produced for SPR and crystallography analyses
Inclusion bodies	HLA-A2 HLA-A2-bt β 2m MEL5 α chain MEL5 β chain α 24 chain β 17 chain
TCRs	MEL5 α 24 β 17
pMHCs	HLA-A2-EAA HLA-A2-EAA-bt HLA-A2-AAG HLA-A2-AAG-bt

5.2.2 MEL5 and $\alpha 24\beta 17$ TCR binding to natural MART-1 antigens

The affinities of MEL5 for A2-EAA (Cole et al., 2010) and A2-AAG (Ekeruche-Makinde et al., 2012) have been described previously and were confirmed here (**Figure 5.2A&B**). With a $K_D \sim 8.4 \pm 0.2 \mu\text{M}$ and $\sim 18.4 \pm 2.2 \mu\text{M}$ toward A2-EAA and A2-AAG, respectively, the affinity was within the range described previously for TCR interactions with a tumor antigen (Cole et al., 2007). Interestingly, MEL5 bound to both natural MART-1 peptides with a stronger affinity than other MART-1 specific TCRs (**Table 5.2**). I also analyzed here the interaction of $\alpha 24\beta 17$ with A2-EAA and A2-AAG by surface plasmon resonance (SPR) using the single-cycle kinetics method (Karlsson et al., 2006) (**Figure 5.2C&D**). $\alpha 24\beta 17$ TCR bound to A2-EAA and A2-AAG with K_{DS} of $\sim 750 \text{ pM}$ and $\sim 19.7 \text{ nM}$, respectively. This represented a 11,200-fold enhancement in binding to A2-EAA and a 934-fold enhancement in A2-AAG binding compared to MEL5. As with previously published high-affinity TCRs (Jones et al., 2008; Li et al., 2005b; Sami et al., 2007), the enhanced binding of $\alpha 24\beta 17$ TCR was attributed to a substantially slower off-rate compared to the wild-type progenitor (**Figure 5.2A-D**). In order to further understand the mechanism underlying the difference in the recognition of the two natural MART-1 peptides, I solved the crystal structure of MEL5 and $\alpha 24\beta 17$ complexed to A2-EAA and A2-AAG.

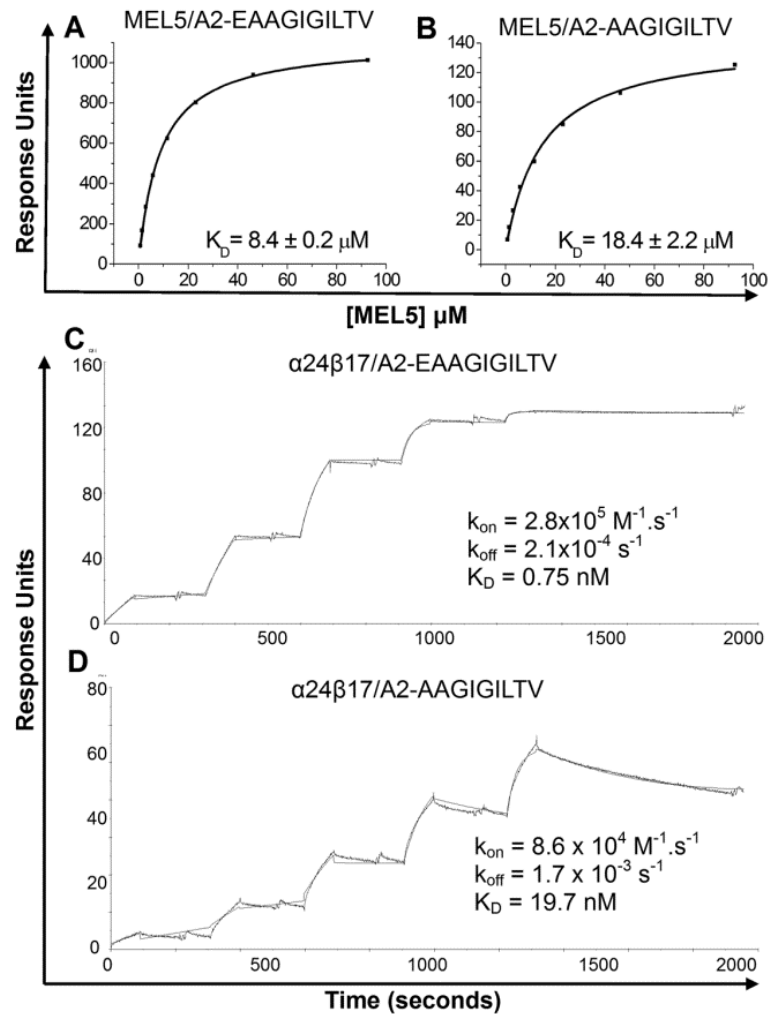


Figure 5.2. Binding affinities of the MEL5 and $\alpha 24\beta 17$ TCRs with A2-EAA and A2-AAG.

(A&B) Ten serial dilutions of MEL5 were measured in triplicate at 25°C. Representative data from these experiments are plotted. The equilibrium binding constant (K_D) values were calculated using a nonlinear curve fit (Langmuir binding equation $AB = (B \times AB_{max}) / (K_D + B)$); mean plus SD values are shown. The MEL5/A2-EAA K_D (A) was $\sim 8.4 \mu\text{M}$ and the MEL5/A2-AAG K_D (B) was $\sim 18.4 \mu\text{M}$. (C&D) Five serial dilutions of $\alpha 24\beta 17$ were measured in triplicate at 25°C. Representative data from these experiments are plotted. Association constant (k_{on}), dissociation constant (k_{off}) and affinity constant (K_D) were estimated by global fitting of the data using the single-cycle kinetics method (Karlsson et al., 2006). The raw data and the fits are shown in each panel. The $\alpha 24\beta 17$ /A2-EAA K_D (C) was $\sim 750 \text{ pM}$ and the $\alpha 24\beta 17$ /A2-AAG K_D (D) was $\sim 19.7 \text{ nM}$.

Table 5.2. MEL187.c, DMF4, DMF5, MEL5 and α 24 β 17 binding analysis and thermodynamics toward A2-EAA and A2-AAG.

TCR/ pMHC	k_{on}^a	k_{off}^a	K_D^a	ΔG^{ob}	ΔG^{oc}	ΔH^{oc}	$T\Delta S^{oc}$	Reference
MEL187. c5/A2- EAA	nd	nd	42 \pm 0.3 μ M	-5.97	nd	nd	nd	(Cole et al., 2010)
MEL187. c5/A2- AAG	nd	nd	94 \pm 22 μ M	-5.49	nd	nd	nd	(Ekeruche- Makinde et al., 2012)
DMF4 /A2-AAG	nd	>0.5	170 \pm 11 μ M	-5.14	nd	nd	nd	(Borbulevych et al., 2011)
DMF5 /A2-EAA	nd	nd	11.3 \pm 0.3 μ M	-6.75	nd	nd	nd	(Insaidoo et al., 2011)
DMF5 /A2-AAG	nd	nd	68 \pm 4 μ M	-5.65	nd	nd	nd	(Borbulevych et al., 2011; Insaidoo et al., 2011)
MEL5/ A2-EAA	nd	nd	8.4 \pm 0.2 μ M	-6.92	-6.75	-14.0	-7.2	
MEL5/ A2-AAG	nd	nd	18.4 \pm 2.2 μ M	-6.46	-6.62	-6.1	0.49	
α 24 β 17/ A2-EAA	2.8x10 ⁵	2.1x10 ⁻⁴	0.75 nM	-12.44	-12.0	11.1	23.1	
α 24 β 17/ A2-AAG	8.6x10 ⁴	1.7x10 ⁻³	19.7 nM	-10.51	-10.72	33.6	44.1	

^a k_{on} ($M^{-1}.s^{-1}$), k_{off} (s^{-1}) and K_D were measured at 25°C.

^b ΔG° ($kcal.mol^{-1}$) calculated from $\Delta G^\circ = RT_0 \ln(K_D)$ with $R = 1.987 cal.K^{-1}.mol^{-1}$ and $T_0 = 298 K$.

^c ΔG° ($kcal.mol^{-1}$), ΔH° ($kcal.mol^{-1}$) and $T\Delta S^\circ$ ($kcal.mol^{-1}$) calculated from the non-linear van't Hoff equation with T the reference temperature (T=298 K)

5.2.3 Protein crystallization

As for the purification of $\alpha 24\beta 17/A2-ELA$ (**Chapter 4**, section 4.2.1), it was also possible to co-purify $\alpha 24\beta 17/A2-EAA$ for crystallography because of the TCR antibody-like affinity (**Figure 5.2**). However, the $\alpha 24\beta 17$ affinity toward A2-AAG was not high enough and the complex dissociated during the gel filtration (**Figure 5.3**) probably because of a shorter half-life compared to A2-EAA binding (**Figure 5.2**). The $\alpha 24\beta 17/A2-AAG$ complex was therefore crystallized using the “classical method” where TCR and pMHC are mixed in equimolar ratio before setting up crystallization trials (**Chapter 2**, section 2.5.1). Crystallization of MEL5/A2-AAG and MEL5/A2-EAA was not straightforward. After unsuccessful attempts at growing crystals with the classical method for both complexes, I tried the “seeding” method where crystals of the same lattice and symmetry as the crystals one wants to grow are used to initiate crystal formation (McCoy, 2009). I attempted to seed MEL5 crystals using the relevant $\alpha 24\beta 17/pMHC$ complex crystals ($\alpha 24\beta 17/A2-AAG$ and $\alpha 24\beta 17/A2-EAA$ to seed MEL5/A2-AAG and MEL5/A2-EAA, respectively). These attempts were unsuccessful. I eventually crystallized MEL5/A2-AAG with a method never described before but related to seeding (**Chapter 2**, section 2.5.2.1). Seeding is used to initiate crystal formation in conditions where critical nuclei do not spontaneously form, or only form slowly (McCoy, 2009). In order to allow the formation of critical nuclei and to avoid the generation of high-affinity TCR/pMHC complex crystals, a very low quantity of equimolar $\alpha 24\beta 17/A2-AAG$ was added to a large excess of equimolar MEL5/A2-AAG (**Chapter 2**, section 2.5.2.1). This approach successfully facilitated the generation of MEL5/A2-AAG crystals. These MEL5/A2-AAG crystals were then used to successfully seed MEL5/A2-EAA crystallisation.

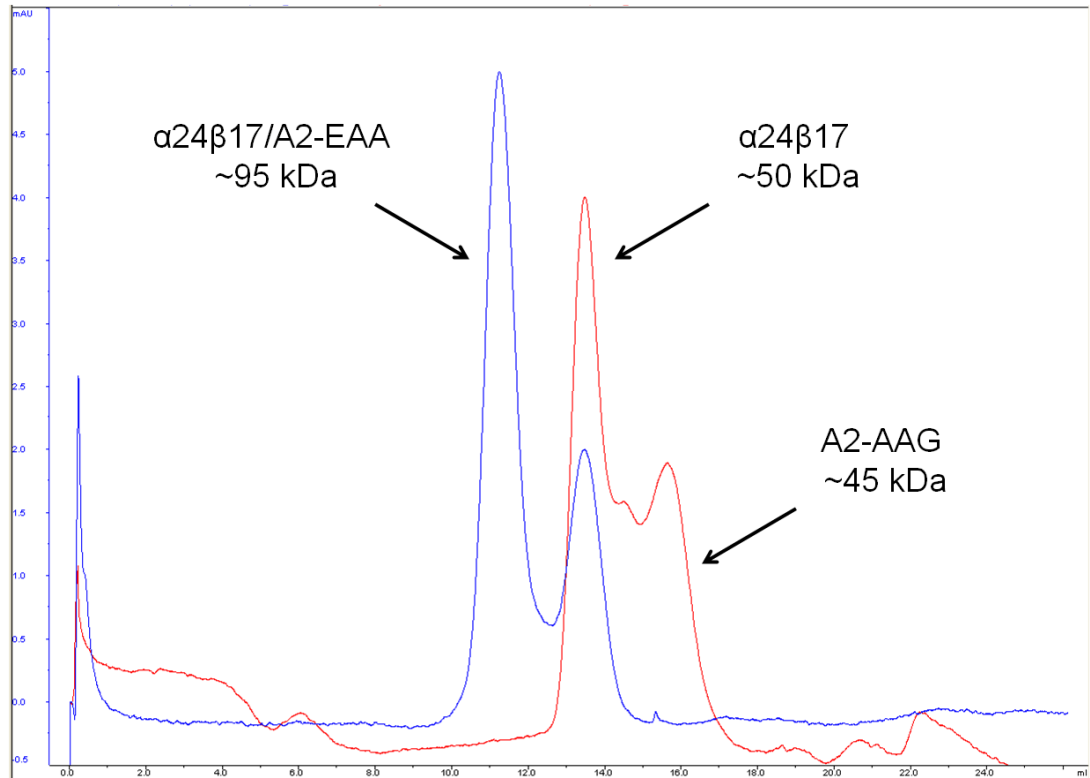


Figure 5.3. Co-purification by gel filtration of $\alpha 24\beta 17/A2-EAA$ and $\alpha 24\beta 17/A2-AAG$ complexes for crystallography.

$\alpha 24\beta 17/A2-EAA$ complex (blue line) was successfully co-purified before setting up crystallization trials, the first peak being the complex (~95 kDa) and the second peak being the excess of TCR (~50 kDa). $\alpha 24\beta 17/A2-AAG$ complex (red line) could not be co-purified by gel filtration with the first peak being the TCR (~50 kDa) and the second peak being the pMHC (~45 kDa).

5.2.4 Structures of MEL5 and $\alpha 24\beta 17$ complexed to A2-EAA and A2-AAG

The structures of MEL5 bound to MART-1₂₇₋₃₅ natural nonamer (AAGIGILTV) and MART-1₂₆₋₃₅ natural decamer (EAAGIGILTV) were determined at resolutions of 3.16 Å and 3.00 Å, respectively (**Table 5.3**). I also solved the structures of $\alpha 24\beta 17$ bound to A2-AAG and A2-EAA at a better resolution: 2.81 Å and 2.10 Å, respectively (**Table 5.3**). These higher resolution structures with the $\alpha 24\beta 17$ TCR were useful for confirming results with the wildtype TCR. In all four complex structures, the TCR bound in a canonical diagonal docking mode to the pMHCI. MEL5 bound at a crossing angle of $\sim 47^\circ$ for both complexes and the $\alpha 24\beta 17$ bound with a crossing angle of $\sim 42^\circ$. The crossing angles, as well as other structural factors such as shape complementarity (SC) or buried surface area (BSA) (summarized in **Table 5.4**), were within the range described for other TCR/pMHC interactions (Miles et al., 2010; Rudolph et al., 2006). I first analysed the reasons for the affinity enhancement of $\alpha 24\beta 17$ toward the natural MART-1 antigens.

5.2.5 The high affinity of $\alpha 24\beta 17$ toward MART-1_{26/27-35} is due to an increase in the interaction between the TCR and the MHC

As I observed before (**Chapter 4**), the increased affinity compared to MEL5 was mainly due to an increase in interactions between the $\alpha 24\beta 17$ TCR and the MHC. Indeed, there was a gain of 2 H-bonds, 1 salt bridge and 59 vdW contacts with the MHC when presenting AAG and a gain of 2 H-bonds and 39 vdW with the MHC when presenting EAA (**Table 5.4**).

Table 5.3 Data collection and refinement statistics (molecular replacement).

Data set statistics	MEL5/A2-AAG	MEL5/A2-EAA	α 24 β 17/A2-AAG	α 24 β 17/A2-EAA
Space Group	P4 ₁	P4 ₁	P4 ₁	P4 ₁
Unit Cell parameters (Å)	a=121.40, b=121.40, c=82.32	a=121.44, b=121.44, c=82.3	a=120.77, b=120.77, c=82.25	a=121.49, b=121.49, c=82.68
Radiation Source	DIAMOND I04-1	DIAMOND I24	DIAMOND I03	DIAMOND I02
Wavelength (Å)	0.9173	0.9778	0.9363	0.9795
Resolution (Å)	3.16	3.00	2.81	2.10
Unique reflections	20733	23795	29094	69920
Completeness (%)	100	99.9	100	99.4
Multiplicity	6.6	7.5	8.0	8.3
I/Sigma(I)	13.4	12.8	9.9	16.0
Rmerge	0.119	0.122	0.146	0.084
Refinement statistics				
No reflections used	19653	22556	27589	66386
No reflections in Rfree set	1062	1588	1478	3532
Rcryst (no cutoff) (%)	18.6	20.3	20.0	17.3
Rfree (%)	26.3	26.2	25.7	20.9
RMSD from ideal geometry (target values in parenthesis)				
Bond lengths (Å)	0.013 (0.021)	0.013 (0.020)	0.016 (0.021)	0.016 (0.021)
Bond Angles (°)	1.431 (1.936)	1.452 (1.933)	1.597 (1.937)	1.556 (1.941)
Wilson B-factor (Å ²)	58.1	56.3	61.0	40.3
Overall ESU based on Maximum Likelihood (Å ²)	46.2	16.3	29.72	6.78

One crystal was used for data collection.

Table 5.4 Summary of co-complex structures of Mel5/A2-AAG, Mel5/A2-EAA, α 24 β 17/A2-AAG and α 24 β 17/A2-EAA.

	MEL5/ A2-EAA	MEL5/A2- AAG _{bulged}	MEL5/A2- AAG _{stretched}	α 24 β 17/ A2-EAA	α 24 β 17/A2 -AAG _{bulged}	α 24 β 17/A2 -AAG _{stretched}
Total No. TCR/pMHC contact ^a	9/3/116	8/1/84	8/1/84	11/1/143	12/2/156	11/2/146
No. V $_{\alpha}$ contacts ^a	5/2/57	3/1/35	3/1/38	5/1/68	6/2/67	5/2/64
No. V $_{\beta}$ contacts ^a	4/1/59	5/0/49	5/0/46	6/0/75	6/0/89	6/0/82
No. TCR/peptide contacts ^a	6/1/43	4/0/29	4/0/29	6/1/31	6/0/42	5/0/32
No. TCR/MHC contacts ^a	3/2/73	4/1/55	4/1/55	5/0/112	6/2/114	6/2/114
No. peptide/MHC contacts $\leq 4\text{\AA}$ ^b	147	107	122	154	97	113
BSA ^c (\AA^2)	1684/682/ 2366	1620/655/ 2275	1625/545/ 2170	1833/695/ 2528	1944/682/ 2626	1951/662/ 2613
SC ^d (%)	59.9/74.5/ 64	53.8/63.4/ 56.8	53.8/57.9/ 53.5	73.1/56/ 66.6	73.2/61.1/ 70.9	73.2/42/ 62
Crossing angle ($^{\circ}$)	46.9	48.0	48.0	42.6	42.3	42.3

The structures involving A2-AAG have been divided into a bulged and a stretched model.

^a Number of hydrogen bonds (H-bond) ($\leq 4\text{\AA}$) / salt bridges ($\leq 4\text{\AA}$) / van der Waals (vdW) (3.2-4 \AA) contacts calculated with CONTACT program from the CCP4 package (Collaborative Computational Project, 1994)

^b Peptide/MHC contacts $\leq 4\text{\AA}$ calculated with CONTACT program from the CCP4 package (Collaborative Computational Project, 1994)

^c Buried surface area (BSA) (\AA^2) of TCR-MHC / TCR-peptide / TCR-pMHC calculated with PISA program from the CCP4 package (Collaborative Computational Project, 1994)

^d Shape complementarity (SC) (%) of TCR-MHC / TCR-peptide / TCR-pMHC calculated with SC program from the CCP4 package (Collaborative Computational Project, 1994)

The mutations and the different binding angle between MEL5 and $\alpha 24\beta 17$ induced a shift between the TCR V α domains (**Figure 5.4**). These shifts brought the $\alpha 24\beta 17$ CDR loops closer to the MHC, increasing the binding network and allowing some mutated residues to greatly interact with the MHC helices compared to MEL5 (**Table 5.4 and Appendices 7-10**).

5.2.6 Binding mechanisms of two melanoma-specific TCRs to the HLA-A2-restricted EAAGIGILTV MART-1 antigen

The structure of several TCRs with the heteroclitic ELA peptide have been solved (Borbulevych et al., 2011; Cole et al., 2009) but to date there are no TCR structures with the natural EAA peptide, an omission that has hampered the understanding of TCR recognition to this relevant MART-1 antigen. The newly solved MEL5/A2-EAA showed similarities with the previously solved MEL5/A2-ELA structure (Cole et al., 2009) in that the V α domain of MEL5 made predominant contacts with peptide residues P1 to P5 via the CDR1 α . The use of a germline-encoded CDR loop for peptide discrimination is in opposition with the long-held belief that contacts with peptide are dominated by the hypervariable CDR3 loops. The MEL5 V β domain contacted residues P5 to P9 with CDR3 β aligning alongside the C-terminal half of the peptide as seen with the DMF4 TCR (Borbulevych et al., 2011). A comparison of the previously solved structure of EAAGIGILTV complexed to HLA-A2 (Borbulevych et al., 2007) with the newly solved ternary complex MEL5/A2-EAA showed that the peptide conserved its overall “bulged” conformation upon the recognition by the TCR (**Figure 5.5A**).

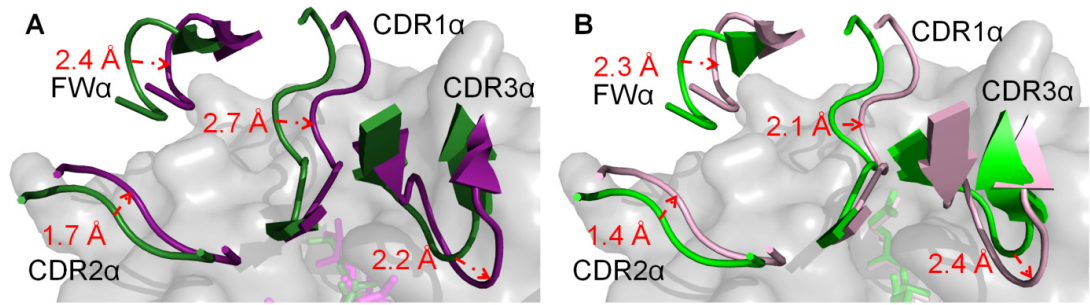


Figure 5.4. Structural differences in the TCR Va domain between MEL5 and $\alpha 24\beta 17$ bound to A2-AAG and A2-EAA.

The mutations and the different binding angle to the pMHC I (shown in grey) between MEL5 and $\alpha 24\beta 17$ induced a shift between the TCR Va domains. (A) The comparison of $\alpha 24\beta 17$ /A2-AAG (deep purple) with MEL5/A2-AAG (forest green) showed an average shift of ~ 2.3 Å with the CDR1 α , CDR2 α , FW α and CDR3 α shifting of 2.7 Å, 1.7 Å, 2.4 Å and 2.2 Å. (B) The comparison of $\alpha 24\beta 17$ /A2-EAA (light pink) with MEL5/A2-EAA (green) showed an average shift of ~ 2.1 Å, with the CDR1 α , CDR2 α , FW α and CDR3 α shifting of 2.1 Å, 1.4 Å, 2.3 Å and 2.4 Å, respectively.

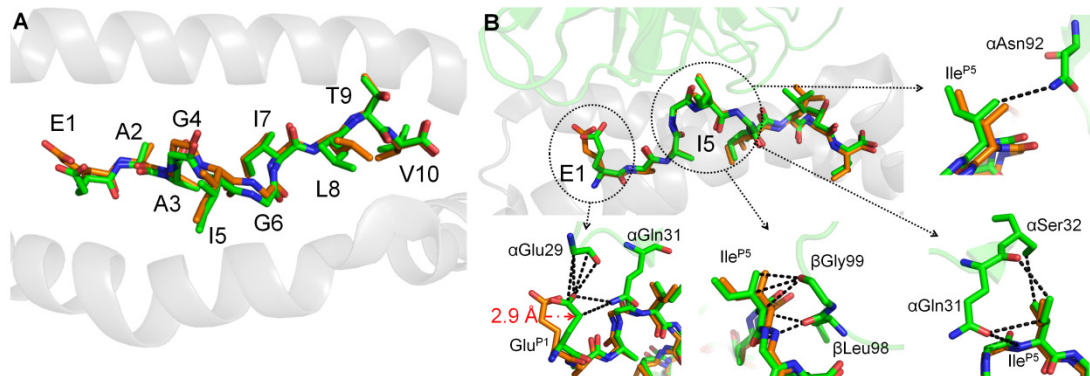


Figure 5.5. Peptide contacts between the MEL5 TCR and A2-EAA.

(A) Upon MEL5 TCR binding, EAA (green) conserved the bulged and “zig-zagged” conformation observed with the unligated EAA (orange) in the peptide binding groove of the MHC (grey cartoon). (B) MEL5 (green cartoon, upper left panel) bound to EAA (green) in the MHC peptide binding groove (grey cartoon). Compared with EAA unligated (orange), there was a 2.9 Å shift of the Glu^{P1} side chain when ligated with MEL5 allowing more contacts with α Gly29 and α Gln31 (green, lower left panel). Ile^{P5} (green) was contacted by TCR residues α Gln31, α Ser32, α Asn92, β Leu98 and β Gly99 (green) making a total of 10 vdW (upper right panel, lower middle panel and lower right panel).

The mechanism of recognition of the EAAGIGILTV peptide involved a 2.9 Å shift in the side chain of the peptide residue Glu^{P1} enabling contacts between residues Gly29 and Gln31 of the TCR CDR1 α , including: 1 H-bond, 1 salt bridge and 4 vdW contacts (**Figure 5.5B**). One of the key peptide residues was Ile^{P5}, contacted by 5 different TCR residues (α Gln31, α Ser32, α Asn92, β Leu98 and β Gly99) of 3 CDRs (CDR1 α , CDR3 α and CDR3 β), and a total of 10 vdW contacts (**Figure 5.5B**). Two other important peptide residues were Gly^{P4} and Ile^{P7}, contacting the TCR with 1 H-bond and 8 vdW and 2 H-bonds and 12 vdW respectively.

The structure of α 24 β 17 complexed to A2-EAA confirmed the MEL5/A2-EAA results. When complexed with α 24 β 17, EAA conserved its bulged conformation (**Figure 5.6**). The P1 shift was also observed upon TCR recognition, the glutamic acid side chain shifting by 2.4 Å. However, the shift in the α 24 β 17 V α led to a slightly different binding mechanism (**Figure 5.6**). Gly29 and Gln31 of the α 24 β 17 CDR1 α loops still contacted Glu^{P1}, but Ile^{P5} was contacted by α Gln31, α Ser32, α Tyr51 and β Leu98.

5.2.7 The MEL5 TCR distinguishes EAA with ELA due to an enhanced flexibility of the natural decamer

My laboratory recently showed that T-cells can distinguish between A2-ELA and A2-EAA (Cole et al., 2010) so that T-cells primed with ELA might not cross-recognize tumours (Bins et al., 2007; Rosenberg et al., 2004).

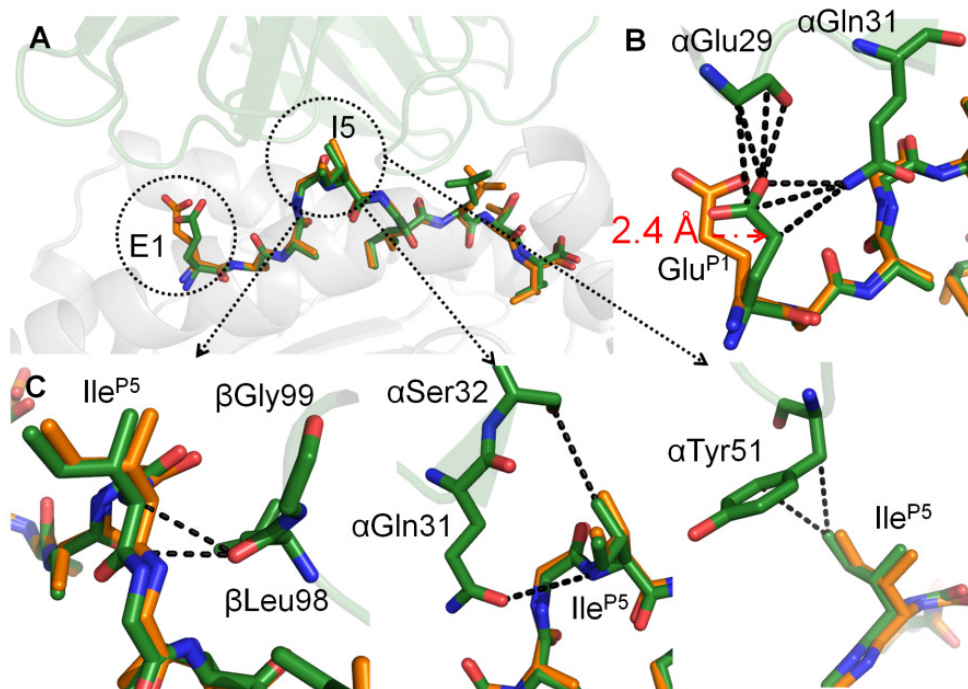


Figure 5.6. Binding mechanism of $\alpha 24\beta 17/A2$ -EAA.

(A) The structure of $\alpha 24\beta 17$ (forest green cartoon) complexed to EAA (forest green) in the binding groove of HLA-A2 (grey cartoon) displayed a bulged conformation similar to the EAA unligated conformation (orange) (Borbulevych et al., 2007). (B) The P1 glutamic acid side chain shifted by 2.4 Å upon $\alpha 24\beta 17$ binding, allowing residues α Gly29 and α Gln31 to contact Glu^{P1}. (C). Ile^{P5} was contacted by β Leu98 (left panel), α Gln31 and α Ser32 (middle panel) and α Tyr51 (right panel).

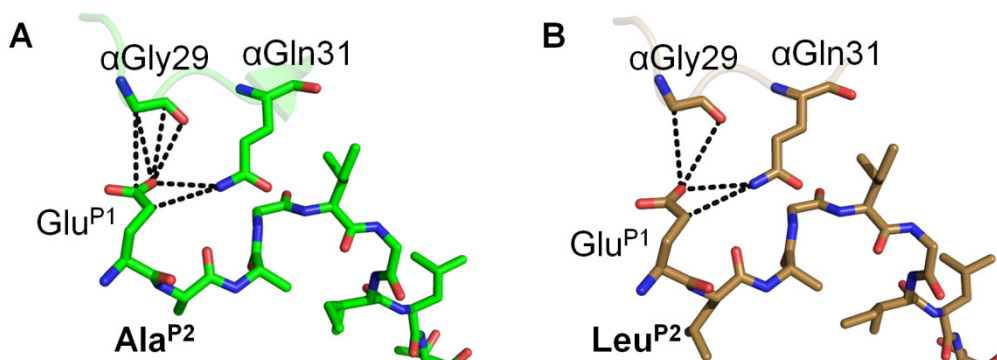


Figure 5.7. Structural differences between MEL5/A2-EAA and MEL5/A2-ELA.

(A) MEL5/EAA and (B) MEL5/ELA are shown in green and brown, respectively. (A) α Gly29 and α Gln31 contacted Glu^{P1} with 4 vdW, 1 H-bond and 1 salt bridge. (B) α Gly29 and α Gln31 contacted Glu^{P1} with only 4 vdW. As there were no modifications in the CDR1 α loop between the two structures, the difference in the bonding network was due to the peptide flexibility. The improved anchor position Leu^{P2} reduced the ELA peptide flexibility compared to the natural decamer EAA, hence inducing the loss of 1 H-bond and 1 salt bridge.

The comparison of the MEL5/A2-ELA structure my laboratory previously solved (Cole et al., 2009) with the newly solved MEL5/A2-EAA structure showed that, despite MEL5 TCR binding to EAA and ELA displaying similarities, a major difference was observed regarding the anchor position P2. MEL5 TCR residues α Gly29 and α Gln31 contacted Glu^{P1} with only 4 vdW contacts in MEL5/A2-ELA, hence losing 1 H-bond and 1 salt bridge compared to EAA with no structural modifications in the CDR1 α loop (**Figure 5.7**). The improved anchored position Leu^{P2} reduced the ELA peptide flexibility leading to a reduction in the bonding network. This loss of flexibility possibly contributes to the T-cells ability to distinguish between the two peptides and explains the MEL5 TCR lower affinity for A2-ELA ($K_D = 18 \mu\text{M}$) compared to A2-EAA ($K_D = 8.4 \mu\text{M}$).

5.2.8 TCR binding to A2-AAGIGILTV induces a peptide anchor switch

The numerically dominant HLA-A2-restricted MART-1-derived peptide at the melanoma surface is believed to be the nonamer AAG, but most MART-1-specific TCRs bind this peptide poorly and it is an extremely poor antigen (Ekeruche-Makinde et al., 2012). As MEL5 TCR interacts with a greater affinity with this peptide compared to other published TCRs, I aimed to understand the better affinity by solving MEL5/A2-AAG complex structure.

The results were highly unexpected as they showed that the TCR recognized two different conformations of AAG (bulged and stretched), both conformations being present in the crystal (**Figure 5.8**). It is likely that this observation indicates that the N-terminus of the AAG peptide was quite mobile during binding to MEL5.

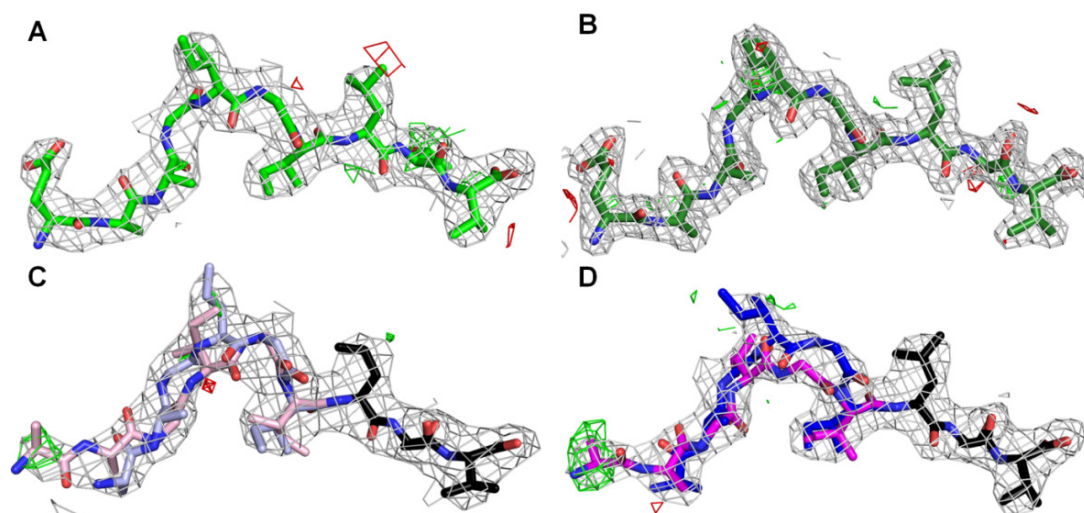


Figure 5.8. 2Fo-Fc peptide electron density maps for all structures reported in this Chapter.

2Fo-Fc peptide electron density maps (shown in grey) in (A) MEL5/A2-EAA, (B) $\alpha 24\beta 17/A2$ -EAA, (C) MEL5/A2-AAG with AAG_{bulged} shown in light blue, AAG_{stretched} shown in light pink and the identical conformation of the last three residues at the C-terminal end of the peptide shown in black and (D) $\alpha 24\beta 17/A2$ -AAG with AAG_{bulged} shown in blue, AAG_{stretched} shown in magenta and the identical conformation of the last three residues at the C-terminal end of the peptide shown in black. All maps shown are within 2Å from the atoms to which they relate. Positive density is shown in green and negative density is shown in red.

In order to understand the effect of each peptide conformation on TCR binding, I separated the structures into two different models: MEL5/A2-AAG_{stretched} (anchor position P2) and MEL5/A2-AAG_{bulged} (anchor position P1). In both conformations the C-terminal end of the peptide possessed an identical conformation. However, the region from Ala^{P1} to Ile^{P6} was different (**Figure 5.9A**).

The MEL5/A2-AAG_{stretched} model presented the extended conformation of AAG (AAG_{stretched}), the same conformation observed in all previously known A2-AAG structures, complexed or uncomplexed with a TCR (Borbulevych et al., 2007; Borbulevych et al., 2011; Insaïdoo et al., 2011) (**Figure 5.9B**). Notably, the C-alpha of Gly^{P5} (Gly5^{C α}) shifted by 1.7 Å between AAG_{stretched} and AAG_{uncomplexed}. Without this shift, steric clashes would occur between this peptide residue and the carbonyl oxygen of β Leu98 (**Figure 5.9B**). In the bulged conformation model, the C α of Ala^{P1} executed a large translation of 4.7 Å to become the anchor position Ala^{P1}_{bulged}, thus leaving the A pocket empty during recognition by MEL5 (**Figure 5.10**). An empty A pocket has not been seen before during TCR binding to a MHC I-restricted natural nonamer. The C α of the anchor residue Ala^{P2} of the A2-AAG structure shifted 3.8 Å in this model, hence losing its role as anchor in the B pocket of the MHC groove (**Figure 5.10**). The analysis of the peptide/MHC interaction (**Table 5.4**) showed that there were more contacts within A2-AAG_{stretched} (122 contacts) than A2-AAG_{bulged} (107 contacts). This was mainly due to the empty A pocket and thus the loss of contact between the MHC helices and Ala^{P1}_{stretched}.

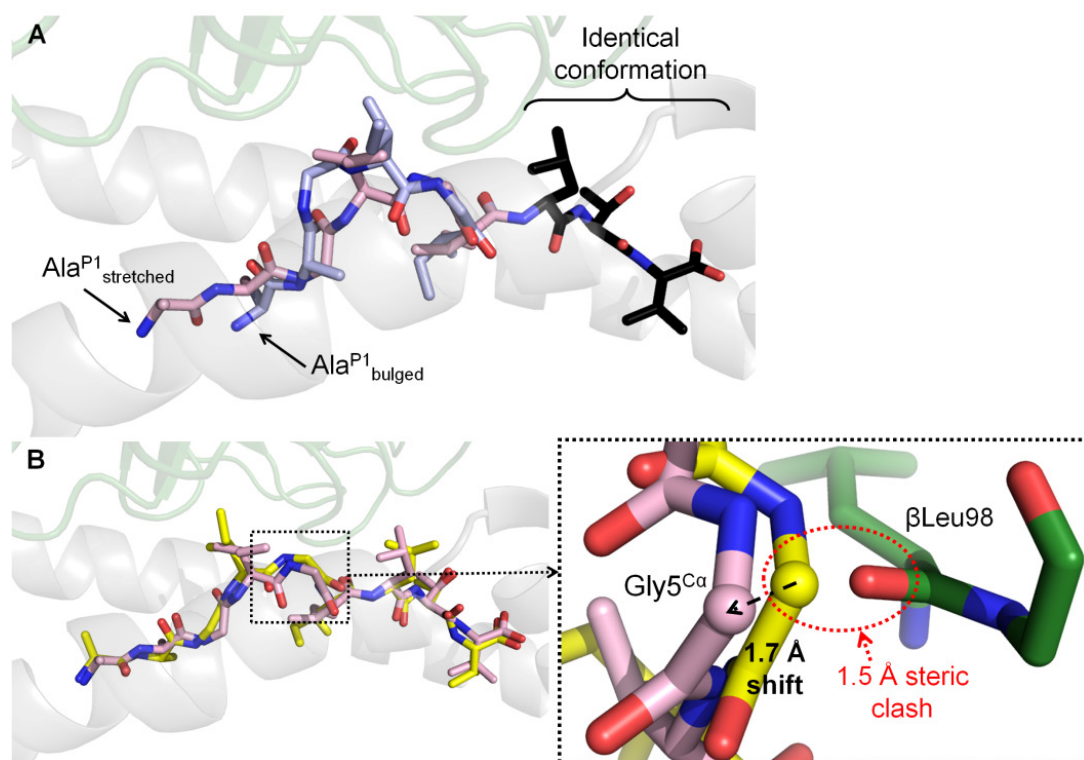


Figure 5.9. Stretched and bulged conformations of AAG during MEL5 binding. (A) When bound to MEL5 (forest green cartoon), AAG displayed two different conformations: AAG_{stretched} (light pink) with the anchor position Ala^{P2} and AAG_{bulged} (light blue) with the anchor position Ala^{P1}. The last 3 residues at the C-terminal end of the peptide possessed an identical conformation (black). (B) The comparison of the unligated AAG (yellow) with AAG_{stretched} (light pink) when bound to MEL5 (forest green cartoon) revealed that the peptides conformations are similar. However, in order to avoid steric clashes with MEL5 residue βLeu98 (forest green) upon MEL5 binding (right panel), Cα of Gly^{P5} (Gly^{5Ca}) shifted of 1.7 Å between AAG_{stretched} and the unligated AAG.

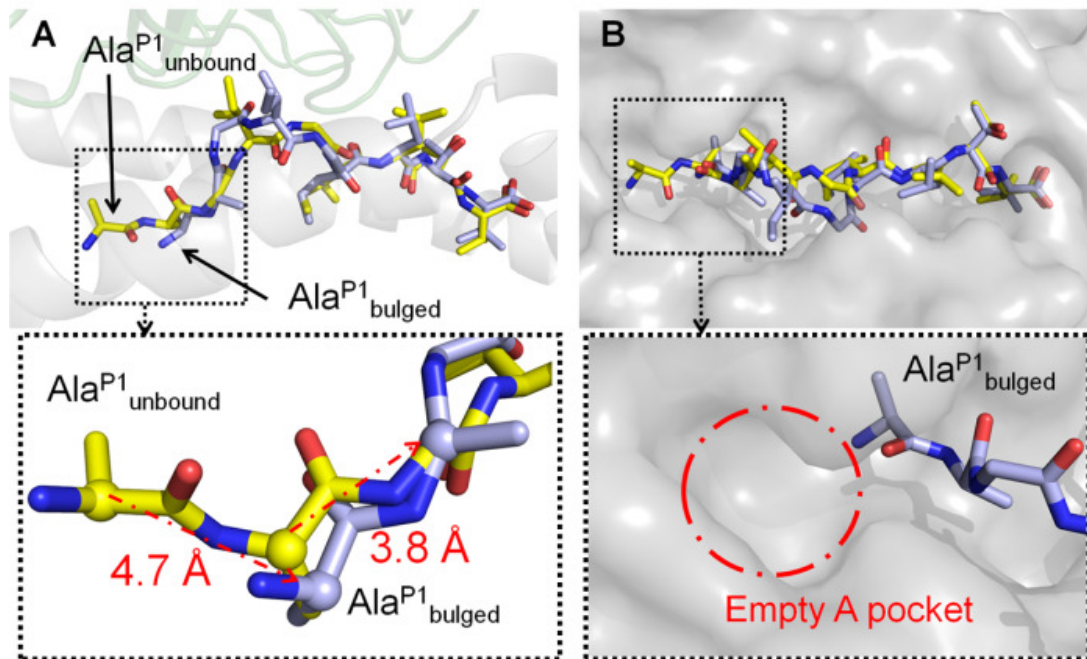


Figure 5.10. AAG peptide anchor residue switch during MEL5 binding. (A) The comparison of the unligated AAG (yellow) with AAG_{bulged} (light blue) when bound to MEL5 (forest green cartoon) revealed a peptide anchor position switch. The C α of Ala^{P1} executed a large translation of 4.7 Å to become the anchor position Ala^{P1}_{bulged} and the C α of the anchor residue Ala^{P2} shifted 3.80 Å in the Ala^{P2}_{bulged} structure, hence losing its role as anchor in the MHC groove (lower panel). (B) The peptide anchor residue switch between the unligated AAG (yellow) and AAG_{bulged} (light blue) left an empty A pocket, a binding mode that has not been observed with natural nonameric peptides (Borbulevych et al., 2007).

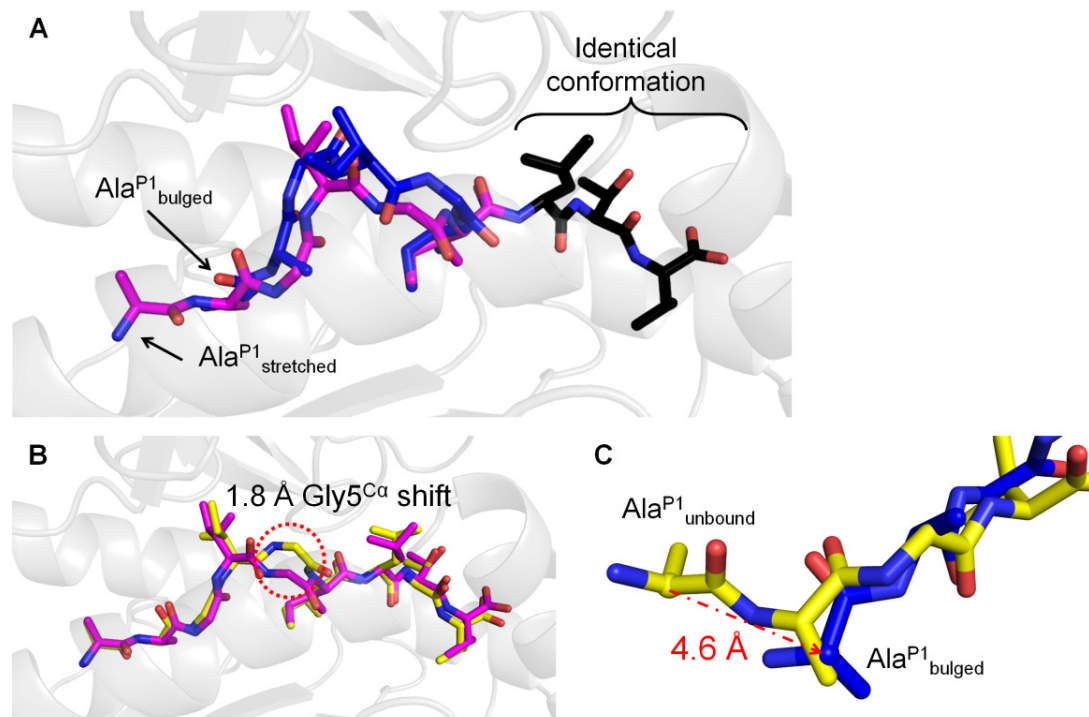


Figure 5.11. Structural differences in the peptide conformation between the unligated A2-AAG and $\alpha 24\beta 17$ /A2-AAG structures.

(A) When bound to $\alpha 24\beta 17$ (grey cartoon), AAG displayed two different conformations: AAG_{stretched} (magenta) with the anchor position Ala^{P2} and AAG_{bulged} (blue) with the anchor position Ala^{P1}. The last 3 residues at the C-terminal end of the peptide possessed an identical conformation (black). (B) The comparison of the unligated AAG (yellow) (Borbulevych et al., 2007) with AAG_{stretched} (magenta) when bound to $\alpha 24\beta 17$ (grey cartoon) revealed that the peptides conformations were similar. However, in order to avoid steric clashes with β Leu98, C-alpha of Gly^{P5} (Gly5^{C α}) shifted of 1.8 Å between AAG_{stretched} and the unligated AAG. (C) The comparison of the unligated AAG (yellow) with AAG_{bulged} (blue) when bound to $\alpha 24\beta 17$ confirmed a peptide anchor position switch. The C- α of Ala^{P1} executed a large translation of 4.6 Å to become the anchor position Ala^{P1}_{bulged}.

The presence of the two AAG conformations was confirmed by solving $\alpha 24\beta 17$ complexed to A2-AAG (**Figure 5.11A**). In this structure, the peptide displayed the same features: a stretched conformation close to the unbound conformation but with a 1.8 Å shift at Gly^{C α} level to avoid a steric clash (**Figure 5.11B**) and a bulged conformation leading to the anchor position switch due to a 4.6 Å shift of Ala^{P1} and resulting in an empty P1 pocket upon $\alpha 24\beta 17$ binding (**Figure 5.11C**).

5.2.9 Different binding mechanisms of recognition for MEL5/AAG_{bulged} and MEL5/AAG_{stretched}

MEL5 made an identical number of contacts with the peptide in bulged and stretched conformations (4 H-bonds and 29 vdW contacts). These contacts were, however, distributed differently due to the switch in anchor position (**Appendix 10**), the most striking evidence being Gly^{P3} which made more contacts in the bulged conformation (1 H-bond and 9 vdW contacts) than in the stretched conformation (1 vdW contacts), whereas Ile^{P4} made more contacts with the TCR in the stretched conformer (12 vdW contacts) than the bulged conformer (5 vdW contacts) (**Figure 5.12**). MEL5 stabilized the bulged peptide conformation using hydrophobic TCR residues β Leu98 and β Gly99 to contact hydrophobic peptide residues Ala^{P2}_{bulged}, Gly^{P3}_{bulged}, Ile^{P4}_{bulged} and Gly^{P5}_{bulged} (**Figure 5.12A**). Compared to the interaction between MEL5 and AAG_{bulged}, the binding interface between MEL5 and AAG_{stretched} was distinct. TCR residue β Leu98 contacted Gly^{P3}_{stretched}, Ile^{P4}_{stretched} and Gly^{P5}_{stretched} with longer vdWs and did not contact Ala^{P2}_{stretched}. TCR residue α Gln31 interacted with Ile^{P4}_{stretched} making 8 contacts compared to no contacts with Ile^{P4}_{bulged} and there was an additional H-bond between TCR residue α Gln31 and Ala^{P2}_{stretched} (**Figure 5.12B**).

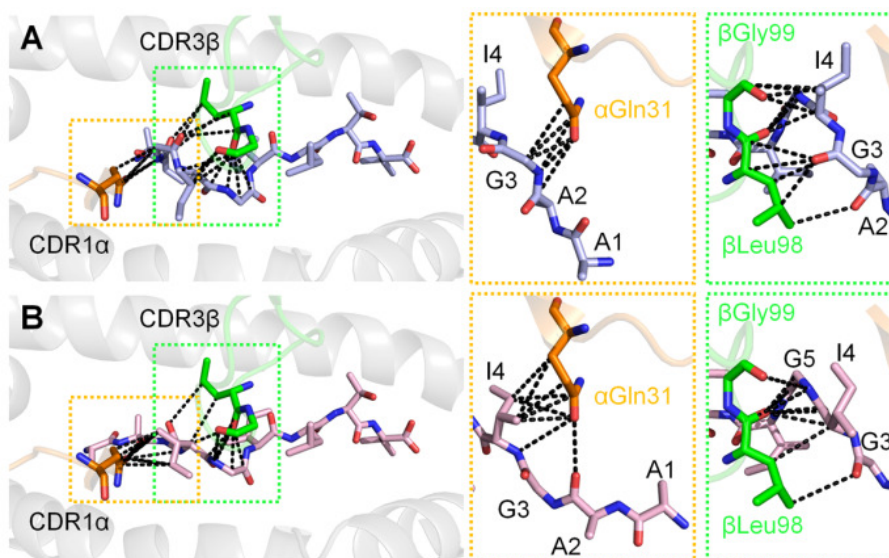


Figure 5.12. Different mechanisms of recognition for MEL5/AAG_{bulged} and MEL5/AAG_{stretched}.

(A) The mechanism of recognition for MEL5 binding to AAG_{bulged} (light blue) involved α Gln31 (orange) contacting Gly^{P3} (orange panel) while β Leu98 and β Gly99 (green) were contacting peptide residues Ala^{P2}, Gly^{P3}, Ile^{P4} and Gly^{P5} (green panel). (B) The mechanism of recognition for MEL5 binding to AAG_{stretched} (light pink) involved α Gln31 (orange) contacting Ala^{P2}_{stretched} with an additional H-bond compared to Ala^{P2}_{bulged} and contacting Ile^{P4}_{stretched} with 8 contacts compared to no contacts with Ile^{P4}_{bulged} (orange panel). β Leu98 (green) contacted Gly^{P3}, Ile^{P4} and Gly^{P5} with longer vdWs compared to MEL5/AAG_{bulged} and did not contact Ala^{P2} (green panel).

Despite the same overall number of contacts for the TCR/peptide interaction, the two conformations exhibited different BSA and shape complementarity (SC) features (**Table 5.4 and Appendix 11**). Interestingly, both BSA and SC were higher for the bulged conformation (655 Å² and 63.4%) compared to the stretched conformation (545 Å² and 57.9%).

5.2.10 Reduction in interactions between MEL5 TCR and A2-AAG results in weaker binding affinity

I described above the binding mechanisms of MEL5 TCR toward A2-EAA and A2-AAG. In accordance with the other melanoma-specific TCRs described in the literature, MEL5 TCR has a preference for the natural decamer. I thus examined the reasons for the difference in affinity by further investigating the MEL5/A2-EAA and MEL5/A2-AAG structures.

The overall number of MEL5 contacts with the MHC surface was greater when the natural decamer EAA was presented (3 H-bonds, 2 salt bridges and 73 vdW) than during the presentation of the natural nonamer AAG (4 H-bonds, 1 salt bridge and 55 vdW) (**Table 5.4**). This increase in interactions likely explained the superior affinity of MEL5/A2-EAA ($K_D \sim 8.4 \mu\text{M}$) compared to MEL5/A2-AAG ($K_D \sim 18.4 \mu\text{M}$).

The comparison of the TCR/peptide interactions for MEL5/A2-AAG and MEL5/A2-EAA structures revealed that, independent of the AAG conformation, there was an increase of the vdW contacts, H-bonds and an added salt bridge when MEL5 bound to the decamer. This was mainly due to the additional glutamic acid at the N terminus.

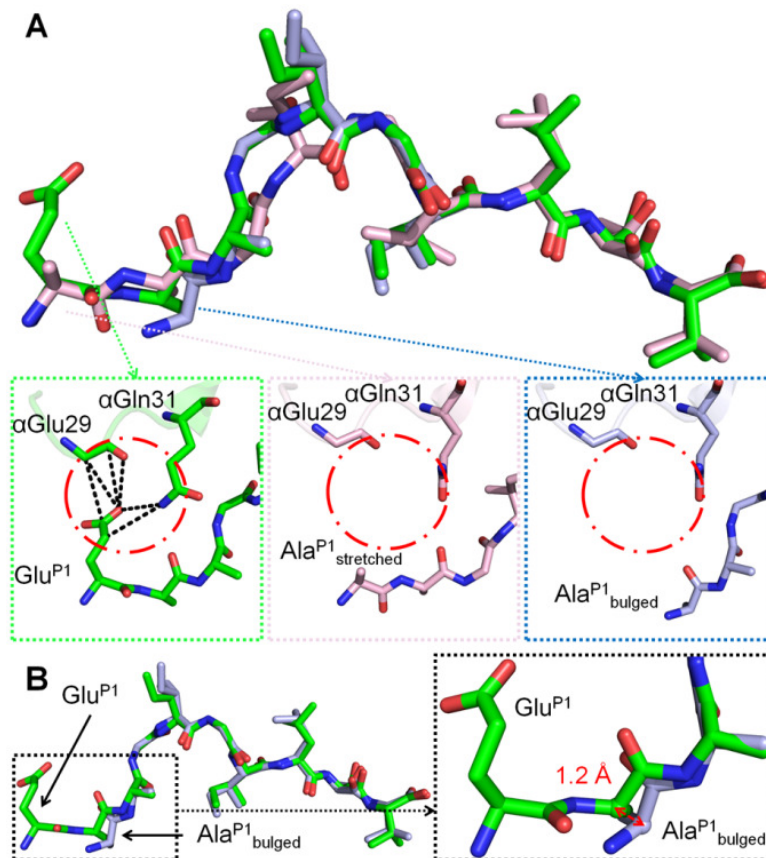


Figure 5.13. Structural differences in the MEL5 interaction with the first peptide residue of EAA, AAG_{stretched} and AAG_{bulged}.

(A) Overlay of EAA (green), AAG_{stretched} (light pink) and AAG_{bulged} (light blue) upon MEL5 recognition. The additional glutamic acid at the N terminus of EAA (Glu^{P1}) made 4 vdW, 1 H-bond and 1 salt bridge with MEL5 α Glu29 and α Gln31 (green panel) whereas Ala^{P1}_{stretched} (light pink panel) and Ala^{P1}_{bulged} (light blue panel) did not contact these MEL5 residues which contributed to the better affinity of MEL5/A2-EAA. (B) The anchor residue Ala^{P1}_{bulged} (light blue) was buried 1.2 Å deeper into the MHC groove than the anchor residue Glu^{P1} (green), this shift possibly helping the stabilisation of AAG_{bulged} into the MHC binding groove.

Indeed, Glu^{P1} contacted the TCR with 4 vdW, 1 H-bond and 1 salt bridge (**Figure 5.13A**). This salt bridge did not appear in the MEL/A2-AAG (**Figure 5.13A**) interaction and could contribute to the better affinity of MEL5/A2-EAA.

The comparison of AAG_{bulged} and EAA showed that the anchor position Ala^{P1} of the nonamer was buried 1.2 Å deeper into the MHC groove compared to the anchor position Ala^{P2} of the decamer (**Figure 5.13B**), this shift possibly helping to stabilize AAG_{bulged} in the binding groove. However, MEL5 bound to AAG_{bulged} and EAA with the same mechanism: αGln31 and βLeu98 were contacting Gly^{P3}_{bulged}/Gly^{P4}_{EAA} while βLeu98 and βGly99 were contacting residues Ile^{P4}_{bulged}/Ile^{P5}_{EAA} and Gly^{P5}_{bulged}/Gly^{P6}_{EAA}.

5.2.11 The binding of MEL5 and α24β17 to A2-AAG leads to a gain of enthalpy and entropy compared to the binding to A2-EAA

As TCR conformational changes upon pMHC recognition have been found to correlate with changes in thermodynamic parameters (Armstrong et al., 2008a; Armstrong et al., 2008b), I then analyzed the changes in standard free energy (ΔG°), enthalpy (ΔH°) and entropy ($T\Delta S^\circ$) for the binding of MEL5 and α24β17 to A2-EAA and A2-AAG. I used the K_D determined by SPR at different temperatures with the thermodynamic equation $\Delta G = RT \ln K_D$ and the standard non-linear van't Hoff equation ($\Delta G^\circ = \Delta H^\circ - T\Delta S^\circ + \Delta C_p^\circ(T-T_0) - T\Delta C_p^\circ \ln(T/T_0)$) with $T_0=298$ K (**Table 5.1 and Figures 5.14 - 5.16**).

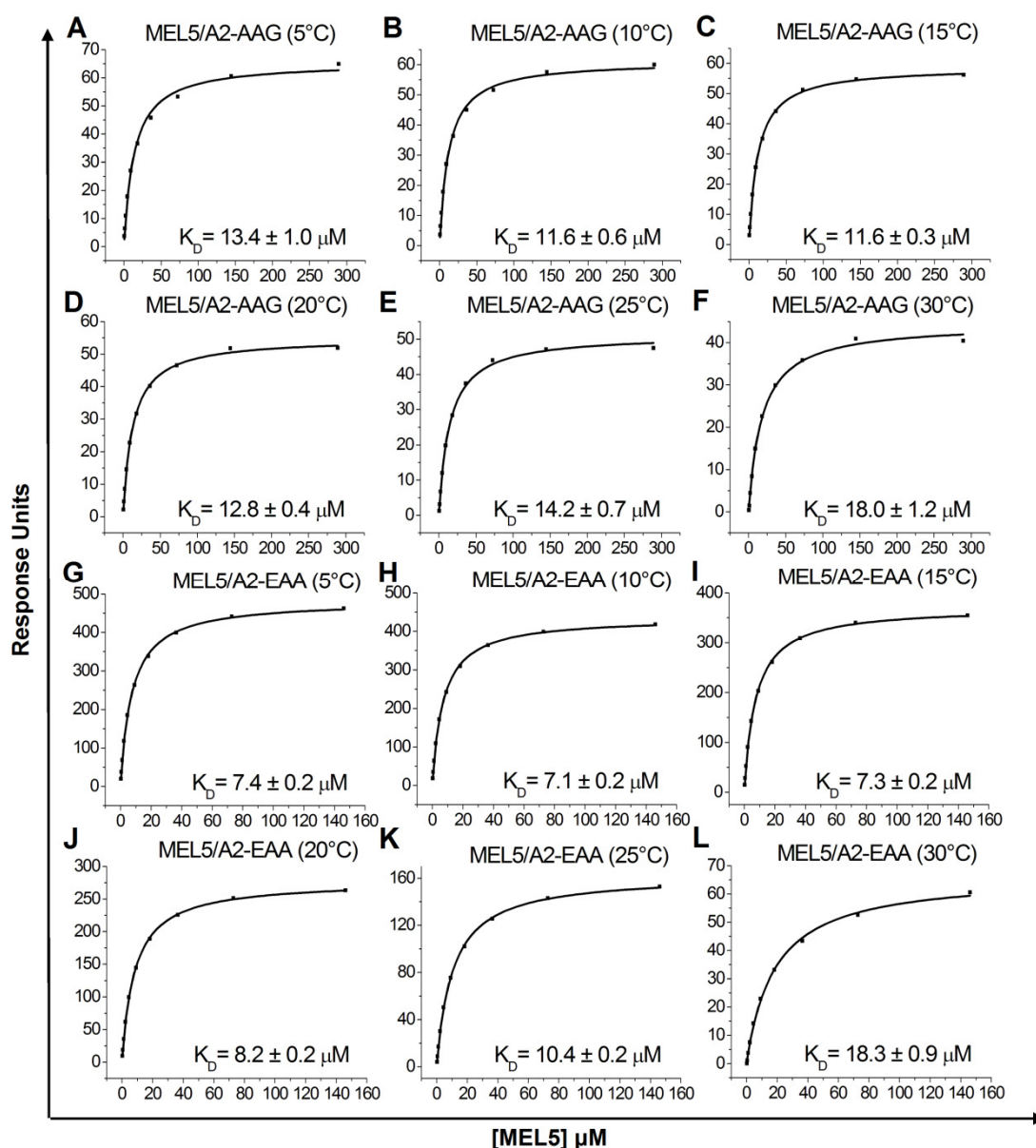


Figure 5.14. Thermodynamic analysis of the MEL5 interaction with A2-AAG and A2-EAA.

(A-L) Ten serial dilutions of MEL5 were measured in triplicate at 5°C, 10°C, 15°C, 20°C, 25°C and 30°C; Representative data from these experiments are plotted. The equilibrium binding constant (K_D) values were calculated using a nonlinear curve fit (Langmuir binding equation $AB = (B \times AB_{\max}) / (K_D + B)$); mean plus SD values are shown. (A-F) MEL5/A2-AAG interaction at (A) 5°C, (B) 10°C, (C) 15°C, (D) 20°C, (E) 25°C and (F) 30°C. (G-L) MEL5/A2-EAA interaction at (G) 5°C, (H) 10°C, (I) 15°C, (J) 20°C, (K) 25°C and (L) 30°C.

These data were used to fit thermodynamic parameters shown in **Figure 5.17**.

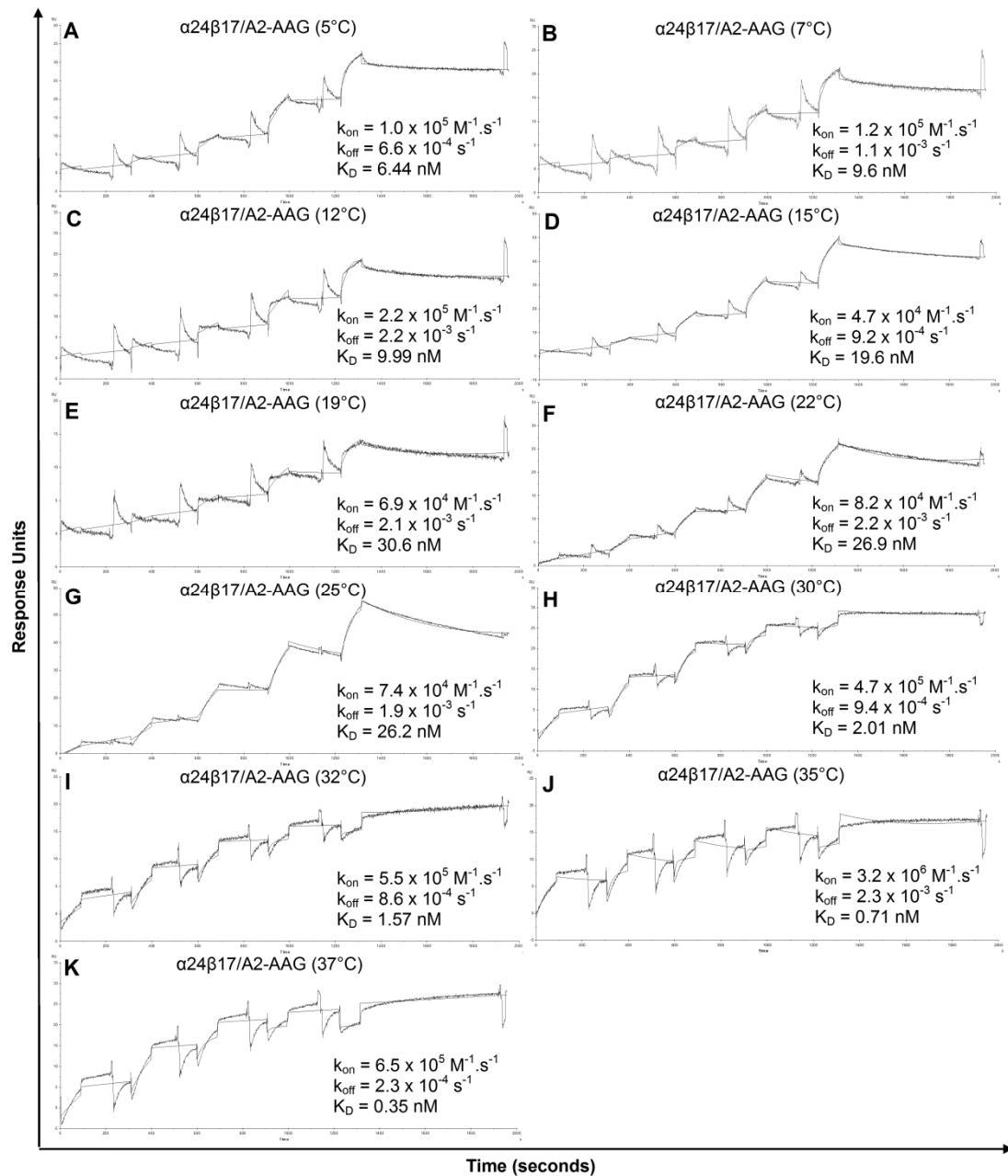


Figure 5.15. Thermodynamic analysis of the $\alpha 24\beta 17$ interaction with A2-AAG. (A-K) Five serial dilutions of $\alpha 24\beta 17$ were measured in triplicate at (A) 5°C, (B) 7°C, (C) 12°C, (D) 15°C, (E) 19°C, (F) 22°C, (G) 25°C, (H) 30°C, (I) 32°C, (J) 35°C and (K) 37°C for the $\alpha 24\beta 17$ /A2-AAG interaction; Representative data from these experiments are plotted. Association constant (k_{on}), dissociation constant (k_{off}) and affinity constant (K_D) were estimated by global fitting of the data using the single-cycle kinetics method (Karlsson et al., 2006).

These data were used to fit thermodynamic parameters shown in **Figure 5.17**.

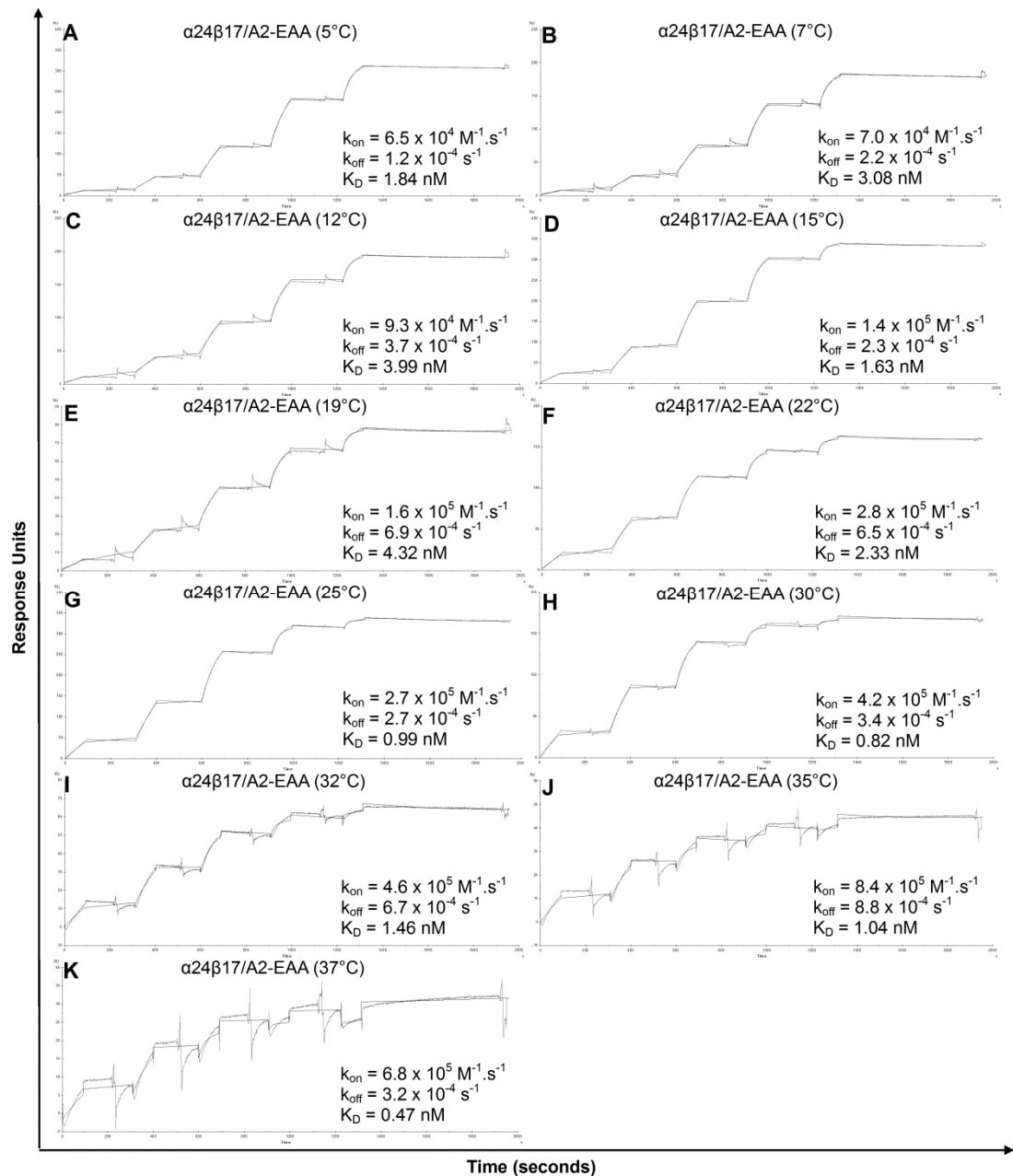


Figure 5.16. Thermodynamic analysis of the $\alpha 24\beta 17$ interaction with A2-EAA. (A-K) Five serial dilutions of $\alpha 24\beta 17$ were measured in triplicate at (A) 5°C, (B) 7°C, (C) 12°C, (D) 15°C, (E) 19°C, (F) 22°C, (G) 25°C, (H) 30°C, (I) 32°C, (J) 35°C and (K) 37°C for the $\alpha 24\beta 17$ /A2-EAA interaction; Representative data from these experiments are plotted. Association constant (k_{on}), dissociation constant (k_{off}) and affinity constant (K_D) were estimated by global fitting of the data using the single-cycle kinetics method (Karlsson et al., 2006).

These data were used to fit thermodynamic parameters shown in **Figure 5.17**.

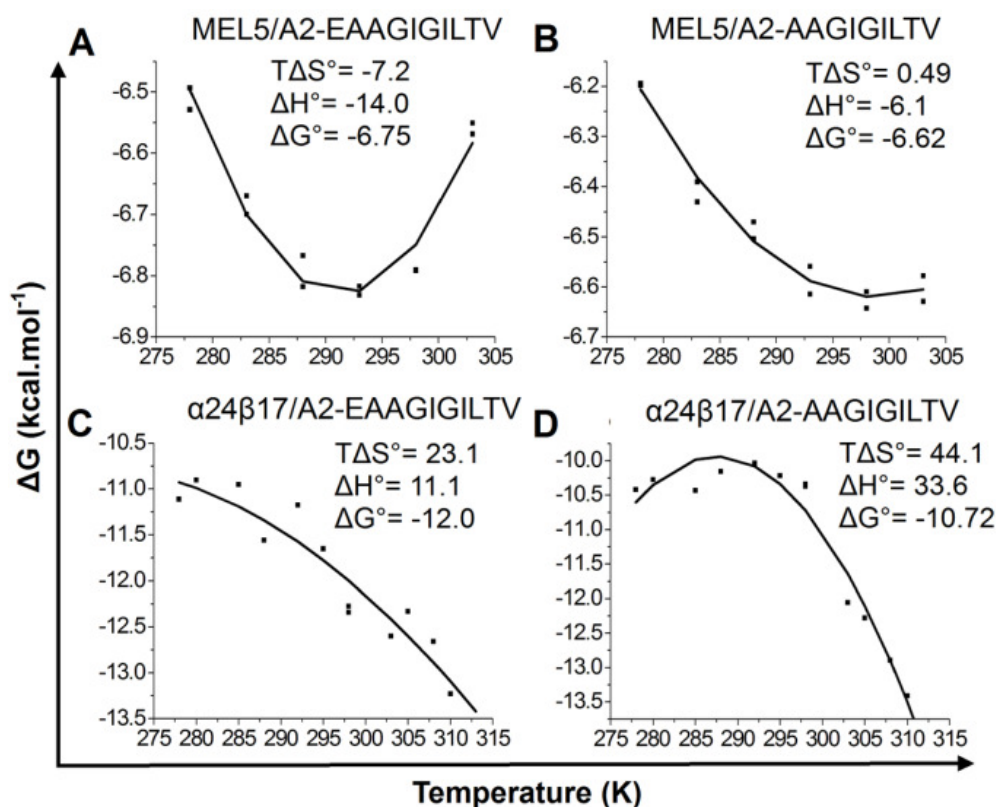


Figure 5.17. Thermodynamic analysis of the MEL5 and $\alpha 24\beta 17$ interactions with A2-EAA and A2-AAG.

(A-B) K_D s were measured in triplicate at 5°C, 10°C, 15°C, 20°C, 25°C and 30°C with ten serial dilutions of MEL5; representative data from these experiments are plotted. (C-D) K_D s were measured in triplicate at 5°C, 7°C, 12°C, 15°C, 19°C, 22°C, 25°C, 30°C, 32°C, 35°C and 37°C with five serial dilutions of $\alpha 24\beta 17$; representative data from these experiments are plotted. The binding free energies ($\Delta G = RT \ln K_D$) were plotted against temperature and the thermodynamic parameters (ΔH° and $T\Delta S^\circ$) were calculated according to the non-linear van't Hoff equation ($RT \ln K_D = \Delta H^\circ - T\Delta S^\circ + \Delta C_p^\circ(T-T_0) - T\Delta C_p^\circ \ln(T/T_0)$) for (A) MEL5/A2-EAA, (B) MEL5/A2-AAG, (C) $\alpha 24\beta 17$ /A2-EAA and (D) $\alpha 24\beta 17$ /A2-AAG.

The MEL5/A2-EAA interaction (**Figure 5.17A**) was enthalpically driven ($\Delta H^\circ \sim -14$ kcal.mol⁻¹) and entropically unfavourable ($T\Delta S^\circ \sim -7.2$ kcal.mol⁻¹), similar to that observed for other TCR/pMHC interactions (from -30 to 18 kcal.mol⁻¹ for ΔH° and from -23.8 to 23.8 kcal.mol⁻¹ for $T\Delta S^\circ$) (Armstrong et al., 2008a; Holland et al., 2012). Although the standard free energies were similar for MEL5/A2-EAA ($\Delta G^\circ \sim -6.75$ kcal.mol⁻¹) and MEL5/A2-AAG ($\Delta G^\circ \sim -6.62$ kcal.mol⁻¹) interactions, ΔG° being related to the K_D at 25°C, MEL5 TCR used different energetic strategies to bind to EAA and to AAG (**Figure 5.17B**). Whereas the binding to A2-EAA was entropically unfavored, the binding to A2-AAG was slightly entropically favoured ($T\Delta S^\circ \sim 0.49$ kcal.mol⁻¹). Moreover, the binding enthalpy changes differed by ~ 8 kcal.mol⁻¹ (MEL5/A2-AAG $\Delta H^\circ \sim -6.1$ kcal.mol⁻¹) at 25°C, the reaction being less enthalpically favorable (**Table 5.1**). These two different energetic strategies are in line with the newly solved structures, the mechanism of recognition of the two peptides by MEL5 being markedly different.

The analysis of $\alpha 24\beta 17/A2-EAA$ and $\alpha 24\beta 17/A2-AAG$ thermodynamics (**Figure 5.17C&D and Table 5.1**) followed the trend observed for MEL5 and showed that the binding to A2-AAG led to a gain of enthalpy and was more entropically favourable. However, with the high affinity TCR, the binding to both peptides was entropically driven, with the highest positive ΔH° and $T\Delta S^\circ$ measured to date for a TCR/pMHC interaction ($\Delta H^\circ \sim 11.1$ kcal.mol⁻¹ and $T\Delta S^\circ \sim 23.1$ kcal.mol⁻¹ for $\alpha 24\beta 17/A2-EAA$ and $\Delta H^\circ \sim 33.6$ kcal.mol⁻¹ and $T\Delta S^\circ \sim 44.1$ kcal.mol⁻¹ for $\alpha 24\beta 17/A2-AAG$).

Finally, the fact that the binding to A2-AAG compared to the binding to A2-EAA with both TCRs led to a higher enthalpy and entropy was consistent with the dynamic movement of AAG and supported the structural differences observed between the peptides when bound to MEL5 and α 24 β 17. Indeed, the higher enthalpy was probably due to the energy required to break and create bonds when the peptide switched from one conformation to the other and the higher entropy was representative of the energetically favourable order-disorder transition generated by the conformational switch in the AAG peptide.

5.3 DISCUSSION

The HLA A*0201 MART-1 system has been extensively studied for T-cell-related therapies directed against melanoma (Johnson et al., 2009; Liddy et al., 2012; Morgan et al., 2006; Rosenberg et al., 2004). This tumour-associated antigen is expressed by malignant melanoma cells from tumours in >95% of patients (Derre et al., 2007). Two HLA-A2-restricted, MART-1-derived peptides have been found at the melanoma surface presented by HLA-A2; EAAGIGILTV (EAA) and AAGIGILTV (AAG) (Held et al., 2007; Skipper et al., 1999; Valmori et al., 1998). The nonamer AAG peptide has been reported to be the dominant species (Skipper et al., 1999). Several studies suggested that the majority of MART-1-specific T-cells preferentially recognize the minority-expressed decamer (EAA) rather than the nonamer (Cole et al., 2010; Romero et al., 1997). Indeed, the nonamer peptide is a very poor antigen (Ekeruche-Makinde et al., 2012). The weak immunogenicity of the EAA and AAG peptides (Valmori et al., 1998) has resulted in a preference for using the MHC anchor-modified “heteroclitic” form of the decamer ELAIGIGILTV (ELA) in this system (Valmori et al., 1998). The ELA peptide elicits huge T-cell responses

and has been used in all peptide vaccine trials to date (Bins et al., 2007; Panelli et al., 2000). It was assumed that changes in this buried MHC-anchor residue would not result in substantial changes to the TCR docking platform of this antigen. Contrary to this assumption, my group recently showed that TCRs bind to A2-EAA and A2-ELA differently (Cole et al., 2010). The fact that TCR distinguish between these two antigens might explain why all vaccine trials with ELA peptide have been a universal failure (Bins et al., 2007; Rosenberg et al., 2004). The absence of a TCR/A2-EAA structure in this system has not allowed visualization of the molecular reason for why TCRs recognise A2-EAA and A2-ELA differently.

My newly solved structures of MEL5 and $\alpha 24\beta 17$ TCRs complexed with A2-EAA showed no major peptide conformational change upon TCR binding. EAA displayed the bulged conformation observed in the unligated A2-EAA structure (Borbulevych et al., 2007). However, MEL5/A2-EAA and $\alpha 24\beta 17$ /A2-EAA structures supported the findings of our binding biophysics data in this system (Cole et al., 2010) showing that peptides with suboptimal anchor residues may be more flexible within the MHC binding groove, thereby enabling them to form subtly different conformational motifs that T-cells can distinguish between. In the case of MEL5 TCR, my group hypothesized that increased flexibility in the P1-P2 region of the peptide could allow for stronger, or even new, TCR-peptide contacts that could explain the enhanced TCR affinity and preferential antigen sensitivity of MEL5 for A2-EAA (8.4 μM) compared with A2-ELA (18 μM) (Cole et al., 2010). My MEL5/A2-EAA structure confirmed that increased flexibility in the N-terminus of A2-EAA compared to A2-ELA could affect TCR binding. Indeed the MEL5/A2-EAA structure shows how the P2 alanine residue allows $\alpha\text{Gly}29$ and $\alpha\text{Gln}31$ to contact Glu^{P1} with an additional H-

bond and salt-bridge compared to A2-ELA. These new contacts led to the better interaction with the natural decamer compared to the heteroclitic decamer that has been favoured in this system.

The best published binding affinity of a TCR to A2-AAG is 68 μ M (Borbulevych et al., 2011; Insaidoo et al., 2011). This weak affinity possibly explains the relatively low response rate in adoptive cell therapy trials (Johnson et al., 2009; Morgan et al., 2006) as it has been shown that weak TCR affinity correlates with poor T-cell responses (Irving et al., 2012; Stone et al., 2009). I showed that the MEL5 TCR bound with the best affinity to A2-AAG. Thus, I also solved the structure of MEL5 TCR complexed with the HLA-A2-restricted natural nonamer peptide AAG in order to understand the substantially stronger affinity of MEL5 for this natural antigen compared to previous published MART-1-specific TCRs (**Table 5.2**). Unexpectedly, the MEL5/A2-AAG structure showed a novel mechanism of TCR/pMHC recognition mediated by a peptide conformational change upon TCR ligation and described herein as a “peptide anchor residue switch”. The peptide residue Ala^{P1} was in the A pocket of the MHC groove before TCR recognition with the peptide anchored at position Ala^{P2}. Upon TCR engagement, the peptide Ala^{P1} residue executed a large translation of 4.7 Å to become anchored in the B pocket of the MHC groove thus leaving an empty A pocket, a feature never observed before during TCR binding to a MHCI-restricted natural nonamer. The peptide anchor residue switch changed the original AAG “extended” conformation into an AAG “bulged” conformation, almost perfectly mimicking that of EAA and ELA. These results may explain why the MEL5 TCR binds to A2-AAG with stronger affinity compared to MEL187.c5 (Ekeruche-Makinde et al., 2012), DMF4 (Borbulevych et

al., 2011) and DMF5 (Borbulevych et al., 2011; Insaidoo et al., 2011) MART-1-specific TCRs. This “molecular switch” during peptide binding was also observed in the structure of the high-affinity $\alpha 24\beta 17$ TCR complexed with A2-AAG adding further confidence in the finding. The flexibility in N-terminal anchoring when MEL5 TCR engages A2-AAG was also consistent with the in-depth thermodynamic analysis of this interaction. The thermodynamic parameters obtained for the MEL5 and $\alpha 24\beta 17$ interactions with A2-AAG and A2-EAA revealed a higher enthalpy and entropy when both TCRs bind to the nonamer. The more favourable entropy could represent an energetically favourable increase in disorder generated by the conformational switch. The less favourable enthalpy when the TCRs bind to A2-AAG was more likely due to the energy required to disrupt and generate bonds when AAG peptide switched conformations.

Sliz et al. solved the structures of the two closely MART-1-related HLA-A2-restricted peptides, ELAGIGILTV and ALGIGILTV (referred here as ALG) (Sliz et al., 2001). This study hypothesized that the native AAG nonamer complexed to HLA-A2 would adopt a bulged and “zig-zagged” conformation similar to that of the ELA decamer in order to be recognized by T-cells (Sliz et al., 2001). The hypothesis was based on the fact that the extended conformation displayed by ALG was not recognized by T-cells (Valmori et al., 1998). However, the different structures of the unligated A2-AAG (Borbulevych et al., 2007; Insaidoo et al., 2011) showed that the peptide always adopted a stretched conformation. Based on the unligated A2-EAA, A2-AAG and A2-ALG structures, Insaidoo et al. raised the question of how multiple T-cells clones could, on one hand, be highly sensitive to a very small structural perturbation (A2-AAG vs A2-ALG) while, on the other, be tolerant of a much more

dramatic structural difference (A2-AAG vs A2-EAA) (Insaiddo et al., 2011). Borbulevych et al. hypothesized that a possible mechanism for achieving both cross-reactivity and selectivity in T-cell recognition of MART-1_{26/27-35} antigens is that MART-1_{26/27-35}-reactive T-cells induce a structural shift in the AAG nonamer upon TCR binding, forcing the peptide to adopt a conformation resembling that of the EAA and ELA peptides (Borbulevych et al., 2007). A structural shift was recently observed in the recognition of AAG by the two melanoma-specific DMF4 and DMF5 TCRs (Borbulevych et al., 2011), the nonamer mimicking the heteroclitic decamer in a mechanism first described as “peptide induced-fit molecular mimicry” (Macdonald et al., 2009). However, the molecular shift was imperfect (peptides out of alignment at Ile4 (AAG) and Ile5 (ELA)) because AAG retained its original anchor positions (Borbulevych et al., 2011). My findings show that the TCR that binds best to the natural A2-AAG antigen of those described to date, MEL5, perfects the molecular fit by altering the way the peptide is anchored in the MHC groove. This novel observation extends the possibilities of changes that are known to occur in the peptide upon TCR engagement (section 5.1.1.3 above). If such a peptide anchor residue switch or “induced fit” is obligatory for good TCR binding in this system then it might also explain why the AAG peptide is such a poor antigen even when there are rare TCRs like MEL5 that appear to be capable of engaging it efficiently.

6.2.5	Jurkat TCR negative GLuc cells transduced with enhanced affinity melanoma-specific TCRs reveal an unexpected glycosylation site	248
6.2.6	An affinity optimum for T-cell activation in the MEL5 system	250
6.3	Discussion.....	250

Chapter background

Work from my laboratory has established that anti-self (anti-tumour) TCRs bind with ~5-fold weaker affinity than pathogen-specific TCRs (Cole et al., 2007). Numerous studies, including several from my own group, have shown that TCR affinity and/or half-life is critical to the sensitivity of T-cells to antigen. Thus, tumour-specific T-cells are at a distinct disadvantage when compared to their pathogen-specific counterparts. As part of these studies I had access to a range of well-characterised MART-1-specific TCRs that bound to the cognate antigen with a range of affinities and half-lives. My aim in this Chapter was to determine the optimal TCR affinity for the most efficient TCR gene therapy approach against melanoma. At the outset, I had hoped that these experiments would be straightforward but I encountered numerous issues not reported herein regarding plasmid constructs or cloning steps. As a result of these difficulties and the 3-year time limit to my work, I present here a preliminary study in a Jurkat cell model. Unfortunately, I did not have the opportunity to duplicate the experiments in a CD8⁺ T-cell model as I had hoped.

6.1 INTRODUCTION

Although CD8⁺ T-cells play an important role during viral infections that typically elicit strong CD8⁺ T-cell responses, cancer specific T-cell mediated immune responses are often less effective. As reported in earlier Chapters, because cancer cells normally express only self proteins (Voskens et al., 2009), cancer-specific T-cell clones with strong affinity TCRs are likely to be deleted during negative selection in the thymus. In support of this notion, it has been demonstrated that cancer specific T-cells express TCRs that generally have a lower binding affinity

compared to anti-pathogen specific TCRs (Cole et al., 2007). The low natural affinity of cancer-specific TCRs may be a barrier to effective anti-cancer CD8⁺ T-cell immunity. Tolerance to self-antigens can be broken by using alloreactive T-cells as such cells have undergone thymic selection in the absence of the restricting HLA molecule (Kronig et al., 2009; Sadovnikova and Stauss, 1996). Alternatively, it is now possible to engineer TCRs by phage display, yeast display or computational design as described in the earlier Chapters of this thesis. Such TCRs can then be expressed in autologous T-cells *in vitro* prior to transfer back to patient blood in an approach termed “adoptive cell therapy” (ACT) as described below.

6.1.1 TCR gene transfer

Adoptive cell therapy (ACT) consists of transferring autologous tumour-reactive T-cells to a patient. **Figure 6.1** summarises the main steps involved when using either tumour-infiltrating lymphocytes (TILs) or TCR gene transfer (TCR gene therapy). I concentrate on TCR gene therapy here as this approach is relevant to my work.

TCR gene transfer consists of reprogramming CD8⁺ T-cells to effectively bypass T-cell tolerance to tumour cells (Rosenberg et al., 2004). TCR gene transfer provides an effective mechanism for the rapid generation of large numbers of T-cells endowed with the desired specificity and affinity (Bobisse et al., 2009). Original proof of principle was first demonstrated in 1986 when transfer of TCR α and β genes using a cosmid vector transferred T-cell specificity from one T-cell clone to another (Dembic et al., 1986).

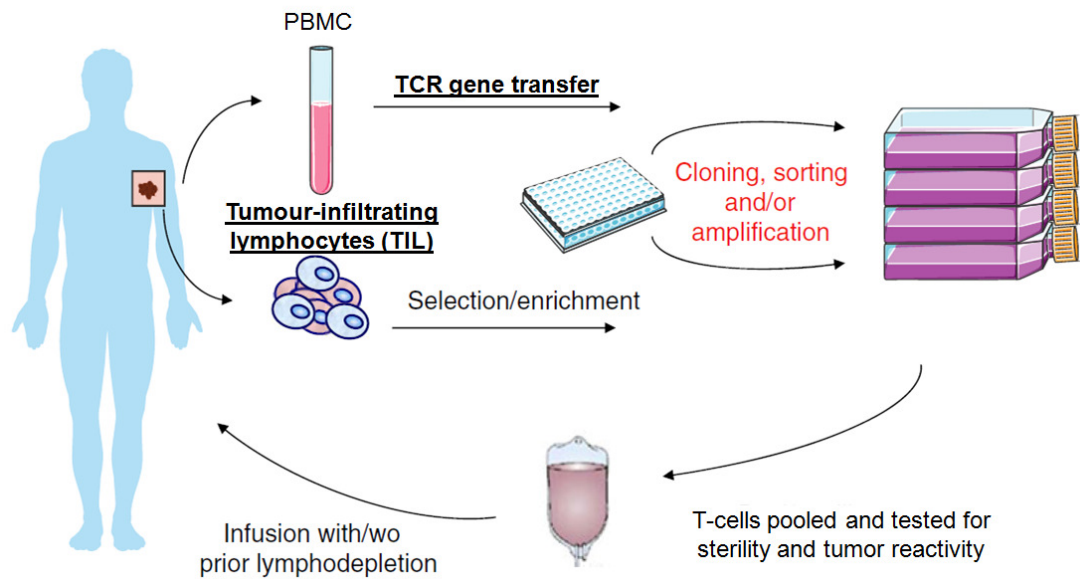


Figure 6.1. Schematic representation of adoptive cell therapy process.

The generation of autologous cancer-specific T-cells for ACT can be obtained either from TIL or PBMC. PBMC can be enriched in cancer-specific T-cells by TCR gene transfer whereas TIL population can be enriched in cancer-specific T-cells by different steps of selection based on antigen specificity or tumour reactivity. Then, cancer-specific T-cells can be sorted, cloned and in vitro expanded. After expansion, T-cells are tested for sterility and tumour reactivity before being transferred to the patient. Figure adapted from (Jotereau et al., 2012).

More than 20 years later, the first clinical studies in melanoma patients have recently shown promise (Johnson et al., 2009; Morgan et al., 2006). In spite of the low response rates after the adoptive transfer of genetically modified autologous peripheral blood lymphocytes (PBLs) expressing a melanoma specific TCR (e.g. DMF4 or DMF5), these trials have established that TCR gene therapy is achievable in a clinical setting.

6.1.2 Vectors for transfer of TCR genes

TCR gene therapy relies on the transfer of TCR genes to autologous T-cells. TCR genes can be transiently transferred using mRNA (Schaft et al., 2006; Zhao et al., 2007). Such transfer is short-term and often of low efficiency. Most clinical trials of the TCR gene transfer have utilized viral transduction technologies. γ -retroviral vectors (RVs) have been the preferred transfer vector due to high transduction efficiency and stable expression of the transferred gene (Engels and Uckert, 2007). This type of vector was used in the two melanoma clinical trials (Johnson et al., 2009; Morgan et al., 2006). Recently, lentiviral vectors (LVs, a subfamily of RVs) have also been used to redirect human T-cell antigen specificity (Joseph et al., 2008; Tsuji et al., 2005). As LVs are self-inactivating, they reduce the risk of side effects due to insertional mutagenesis (Kieback and Uckert, 2010). LVs can also carry a larger transgene cassette compared to RVs, thus enabling expression of TCR α and β chains genes and a third gene (e.g. a reporter gene) (Kieback and Uckert, 2010). My studies utilized a LV construct.

6.1.3 Optimised transfer of an $\alpha\beta$ TCR

6.1.3.1 *Choosing a transgene cassette*

Various mechanisms have been used for expression of $\alpha\beta$ TCR at the T-cell surface. These include the use of single chain TCRs (scTCRs) (Alajez et al., 2006) or chimeric antigen receptors (CARs) (Mitsuyasu et al., 2000). I expressed TCRs as separate TCR α and β chains. It is preferable to have both chains expressed from the same vector to ensure optimal transfer of the required TCR. The two TCR chains can be expressed from separate promoters (Emerman and Temin, 1984), or expressed from the same promoter and the latter situation is most common. In the transgene cassette, genes are either separated by an inter-ribosomal entry site (IRES) or a “self-cleavage” peptide (Uckert and Schumacher, 2009).

My laboratory’s experience with TCR chains expressed and separated by an IRES sequence was that TCR expression was low due to suboptimal expression of the gene downstream of the IRES sequence. We have found separation of TCR chains by “self-cleavage” peptides (such as 2A peptides) to give the best results. Additionally, it has been shown that the efficiency of the 2A-mediated cleavage is close to 100% and leads to an equimolar ratio of the gene products (Szymczak et al., 2004). The 2A-like peptides utilized in this study, T2A (EGRGSLTTCGDVEENPGP) and P2A (ATNFSLKQAGDVEENPGP), are used by members of the picornavirus family (Palmenberg, 1990). Such peptides function by a ribosome “skipping mechanism”. The transcription of a cassette containing a 2A-like sequence leads to a single mRNA encoding both TCR genes (de Felipe et al., 1999; Yang et al., 2008). During translation, the ribosome “skips” a peptide bond between the last (here a proline) and the second last (here a glycine) amino acid of the 2A peptide sequence (de Felipe et

al., 1999; Yang et al., 2008) and this cotranslational cleavage event leads to the release of each individual protein product in mammalian cells (Osborn et al., 2005). The skipping mechanism generates a 17 (T2A) or 18 (P2A) residue-long tail on the upstream gene while the downstream protein starts with a proline instead of a methionine. This tail can be cleaved off by including a furin cleavage site (Johnson et al., 2009; Yang et al., 2008). However, TCRs expressed without the furin cleavage site are fully functional (Holst et al., 2006; Yang et al., 2008), indicating that these modifications do not impair TCR function.

6.1.3.2 *Choosing a transfer vector*

In this study, I used a “third generation” LV construct derived from the human immunodeficiency virus type 1 (HIV-1) (Dull et al., 1998) which is one the safest and most efficient vector for gene transfer (He and Falo, 2007). HIV-1 contains nine genes that are involved in the life cycle and pathogenicity of the virus. Six accessory genes (*vif*, *vpr*, *vpu*, *nef*, *env* and *tat*), that are either related to pathogenesis or not necessary for vector production and functionality, are either replaced with another gene (for *env*) or deleted from the vector system (Demaison et al., 2002; Dull et al., 1998). Three genes (*rev*, *pol* and *gag*) involved in viral packaging are retained in the vector system (Demaison et al., 2002; Dull et al., 1998). I describe herein the components of the “third generation” LV system that consists of one lentivirus-based vector (here pELNSxv, **Figure 6.2A**) and three packaging plasmids: pRSV.REV (**Figure 6.2B**), pMDLg/p.RRE (**Figure 6.2C**) and pVSV-G (**Figure 6.2D**).

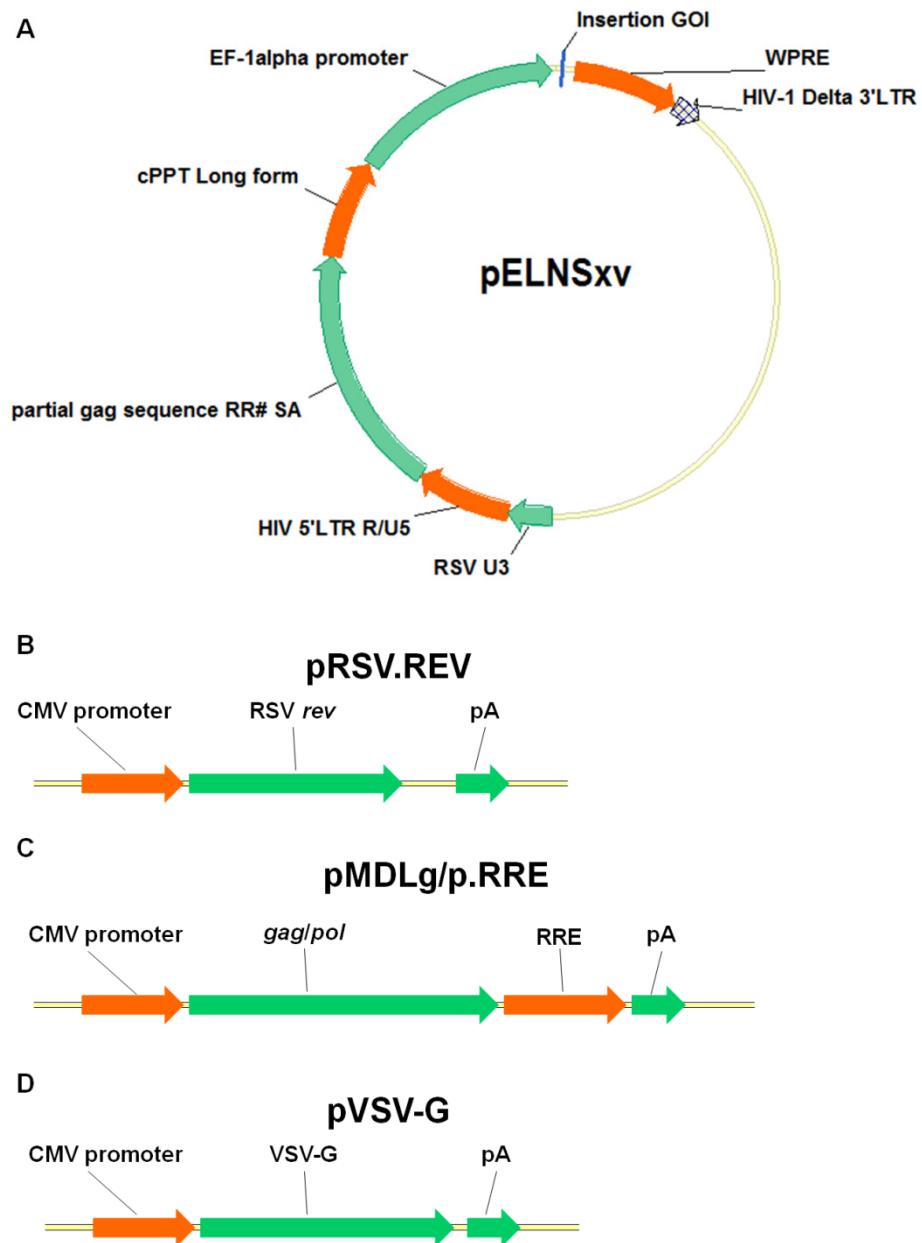


Figure 6.2. Schematic representation of the “third generation” lentivirus system used in this study.

The “third generation” lentivirus system used in this study is composed of 4 vectors. (A) Lentivirus-based pELNSxV contains a partial *gag* sequence and the *env*, *rev* and *pol* genes have been deleted. The plasmid contains the central polypurine tract (cPPT) of HIV-1. The gene of interest (GOI) is inserted between the EF-1 alpha promoter and the Woodchuck Hepatitis Post-transcriptional Regulatory Element (WPRE). HIV-1 delta3' LTR has been partially deleted to render the lentivirus “self-inactivating”. Chimeric 5' LTRs have been constructed by replacing the U3 region of the 5'LTR with the Rous sarcoma virus (RSV) U3 sequence. (B) pRSV.REV contains RSV *rev* gene under the CMV promoter and a polyadenylation (pA) sequence. (C) pMDLg/p.RRE contains *gag* and *pol* genes under the CMV promoter, Rev response element (RRE) and pA sequences. (D) pVSV-G contains a pA sequence and a gene encoding the vesicular stomatitis virus glycoprotein (VSV-G) under the CMV promoter.

The backbone of the lentivirus-based vector (**Figure 6.2A**) is constructed by removing the viral genes *env*, *rev*, *gag* (partially removed) and *pol* from the viral genome into packaging plasmids, freeing up space for the insertion of the gene of interest (GOI) and a number of elements which function to increase or regulate the expression of that gene. For instance, the viral long terminal repeat (LTR) flanking the GOI are often unsuitable for efficient expression and are replaced by a stronger promoter (here human elongation factor-1 alpha, EF-1 alpha **Figure 6.2A**) (Teschendorf et al., 2002). The U3 region 3' LTR is dispensable for a replication-defective vector and has been partially deleted (HIV-1 delta3' LTR, **Figure 6.2A**) to remove all transcriptionally active sequences, generating “self-inactivating” (SIN) LTR (Zufferey et al., 1998). Chimeric 5' LTRs have been constructed to make the LV promoter Tat-independent by replacing the U3 region of the 5'LTR with the Rous sarcoma virus (RSV) U3 sequence (Dull et al., 1998) (**Figure 6.2A**). Finally, the central polypurine tract (cPPT) sequence of HIV-1 (Follenzi et al., 2000) and the Woodchuck Hepatitis Post-transcriptional Regulatory Element (WPRE) (Zufferey et al., 1999) have been added to increase transgene expression (**Figure 6.2A**).

Genes from the three packaging constructs are expressed under the cytomegalovirus (CMV) promoter and contain a polyadenylation site of the human β -globin gene (**Figure 6.2B-D**) (Dull et al., 1998). pRSV.REV contains RSV *rev* gene encoding a protein (Rev) that binds *env* gene HIV RNA (Rev response element, RRE) and that is essential for the export of the viral RNA out of the nucleus (Tang et al., 1999) (**Figure 6.2B**). pMDLg/p.RRE contains *gag* and *pol* genes as well as RRE (Dull et al., 1998). The *gag* gene encodes structural proteins that make up the viral core: matrix, capsid and nucleocapsid (Tang et al., 1999) (**Figure 6.2C**). The *pol* gene

encodes viral replication enzymes (protease, reverse transcriptase and integrase) that have been engineered for safety reasons so the virus has the ability to complete only a single round of the retroviral replication cycle (Demaison et al., 2002; Dull et al., 1998). Finally, pVSV-G contains a gene replacing *env* gene and encoding the vesicular stomatitis virus glycoprotein (VSV-G) (Dull et al., 1998) (**Figure 6.2D**). *env* gene from HIV-1 provides host cell specificity such that HIV-1 only infects CD4⁺ T-cells but VSV-G broadens the tropism of the vector and reduces the requirement for HIV-1 accessory proteins for infectivity by directing the vector to an endocytic pathway (Dull et al., 1998; Tang et al., 1999).

6.1.4 Choosing a tumour antigen to target

An important parameter to consider in TCR gene therapy is the desired specificity and affinity of the exogenous TCR. Two classes of tumour antigens have been described: (i) tumour-specific antigens (TSAs) which are uniquely expressed on cancer cells, caused by random mutations or virally-induced (Parmiani et al., 2007) and (ii) tumour-associated antigens (TAAs) which are overexpressed in tumour cells but also expressed, at a lower level, on healthy cells (Novellino et al., 2005). As TSAs are rarely shared between patients, TAAs (such as MART-1 in melanoma) have been studied more thoroughly in TCR gene transfer (Kieback and Uckert, 2010).

6.1.5 Enhanced affinity TCRs

CD8⁺ T-cells elicit a strong immune response during viral infections (Miles et al., 2010; Sigal et al., 1999) but are often less effective against tumours (Delves and Roitt, 2000a; Rosenberg et al., 2008; Rosenberg et al., 2004). As cancer cells

normally express self proteins (Valitutti et al., 1995; Voskens et al., 2009), thymic education probably leads to T-cells presenting a relatively low affinity TCR against these tumour-associated antigens (TAAs) (average $K_D = 90 \mu\text{M}$) (Boon et al., 2006; Bridgeman et al., 2012; Cole et al., 2007). Importantly, weak TCR binding affinity can be associated with a less sensitive/effective T-cell response (Irving et al., 2012; Stone et al., 2009), hence one way to increase tumour sensitivity would be to increase TCR affinity (Bobisse et al., 2009). TCR affinity can be improved by technologies such as phage display (Li et al., 2005b) by increasing TCR/peptide contacts (Colf et al., 2007; Sami et al., 2007) and by increasing TCR/MHC contacts (**Chapter 4** and **Chapter 5**). Affinity-enhanced TCRs can then be used in TCR gene transfer. However, a number of potential problems with enhanced affinity TCR gene transfer have been raised. For the sake of completeness these are described below.

6.1.6 Potential problems with TCR gene transfer of enhanced TCRs

The aim of TCR gene transfer is to produce T-cells that are effective at killing tumour without destroying healthy tissue. This technology is still in its infancy and a number of potential issues have been raised as detailed in turn below.

6.1.6.1 TCR chain mispairing

When TCR chains are transferred to a T-cell the resulting cell can then potentially express 4 different TCRs: (i) Endogenous α chain paired with endogenous β chain; (ii) Transduced α chain paired with transduced β chain; (iii) Endogenous α chain paired with transduced β chain; and (iv) Transduced α chain paired with endogenous β chain as described in **Figure 6.3**.

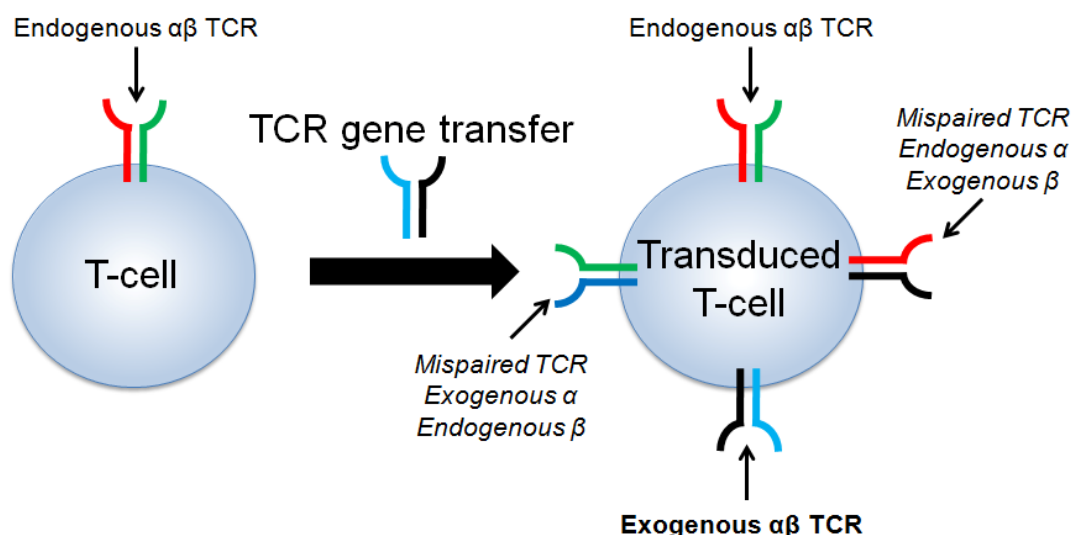


Figure 6.3. Schematic representation of $\alpha\beta$ TCR mispairing after TCR gene transfer.

After TCR gene transfer, transduced T-cell could express the endogenous $\alpha\beta$ TCR (α and β chains in red and green, respectively), the exogenous $\alpha\beta$ TCR (α and β chains in blue and black, respectively) and two types of mispaired $\alpha\beta$ TCRs (exogenous α chain associated to endogenous β chain or endogenous α chain associated to exogenous β chain).

Table 6.1. Strategies to eliminate or limit TCR mispairing.

Strategy	Reference
Transfer of a fully murine TCR or partially “murinized” TCR	(Cohen et al., 2006; Sommermeyer et al., 2006)
Insertion of the additional ‘Boulter-disulphide’ bond between the α and β constant regions as described in Chapter 3	(Boulter et al., 2003; Kuball et al., 2007)
Co-transduction of the TCR α and β chains fused to the extracellular, transmembrane and intracellular domains of CD3 ζ	(Sebestyén et al., 2008)
Exchanging an amino acid pair that normally forms a “knob-into-hole” motif at the interface between the constant regions of the α and β chains to create a “hole-into-knob” motif	(Voss et al., 2008)
Silencing or down-regulating the expression of the endogenous TCR by using small interfering RNA (siRNA)	(Okamoto et al., 2009)
Knocking-out the endogenous TCR expression by using zinc-finger nucleases (ZFNs)	(Provasi et al., 2012)
Transducing $\gamma\delta$ T-cells with an $\alpha\beta$ TCR	(van der Veken et al., 2006).

Combinations (i) and (ii) have known pMHC specificities but the antigen specificity of TCRs produced from combinations (iii) and (iv) above are unknown and thereby have potential to target self antigens. Murine studies have suggested that such mispairing can be highly problematic (Bendle et al., 2009; Bendle et al., 2010). Thankfully, clinical trials to date have not reported off-target toxicity due to mispaired TCRs, but their formation occurred regularly in several models after transduction of polyclonal T-cells (Govers et al., 2010) so this important issue should be taken into consideration. Various strategies can be used to limit or eliminate TCR chain mispairing as detailed in **Table 6.1**. The ‘Boulter-disulphide’ method has been the preferred method in this study.

6.1.6.2 Engineered TCRs bypass thymic editing

Natural TCRs have undergone a thymic selection process that culls T-cells bearing TCRs with a high affinity for self as described in **Chapter 1** (section 1.3.2). Engineered TCRs have not been through this editing process and therefore have the potential to recognise self-antigens. Although enhanced affinity TCRs have been reported to be highly specific in soluble form (Holler et al., 2003; Irving et al., 2012; Li et al., 2005b; Liddy et al., 2012; Purbhoo et al., 2006), these molecules only need to bind to a single self pMHC with a $K_D \sim 100 \mu\text{M}$ in order to cause a problem if they are transduced into autologous T-cells and then adoptively transferred. Several studies have highlighted the potential danger of T-cells expressing the affinity-enhanced TCRs compared to T-cells expressing the wild-type TCR (Holler et al., 2003; Robbins et al., 2008; Udyavar et al., 2009; Zhao et al., 2007). Gene-modified CD8^+ T-cells expressing the wild-type HLA-A2-restricted 1G4 TCR were reported to retain specificity for HLA-A2-expressing target cells presenting the cognate

peptide NY-ESO-1 ($K_D = 32 \mu\text{M}$) but CD8⁺ T-cells expressing the high-affinity variant ($K_D = 26 \text{ pM}$) lost antigen specificity (Zhao et al., 2007). However, CD8⁺ T-cells expressing 1G4 TCR variants with enhanced affinities in the intermediate range ($K_D = 4\mu\text{M}$ and $0.45 \mu\text{M}$) demonstrated antigen-specific recognition (Zhao et al., 2007). Moreover, Robbins et al. defined an upper affinity limit between $K_D = 0.45 \mu\text{M}$ and $K_D = 0.28 \mu\text{M}$ for these 1G4 TCR variants allowing gene-modified CD8⁺ T-cells to retain cognate peptide specificity (Robbins et al., 2008). Collectively, such results suggested that TCRs displaying enhanced affinities within the natural range ($K_D = 0.1\text{-}270 \mu\text{M}$) should be used for TCR gene transfer in order to maintain T-cell antigen specificity. Studies to date also suggest that each system will have its own optimal TCR affinity as described below. The optimal affinity and half-life for TCR binding can only be determined by rigorous testing.

6.1.6.3 TCRs exhibit an affinity/dwell time optimum for T-cell activation

Based on the serial triggering and kinetic proofreading models described in **Chapter 1** (section 1.7), it has been suggested that long TCR/pMHC interaction half-life might impede optimal TCR triggering and T-cell signalling (Coombs et al., 2002; Valitutti et al., 1995). As enhanced affinity TCRs display longer half-life of interaction with the pMHC than their wild-type equivalent (Li et al., 2005b), transferring modified TCRs displaying very long half-lives might be suboptimal for T-cell activation. It has been suggested that a TCR/pMHC interaction might reach an “affinity ceiling” above which there is no improvement, or a decrease, in T-cell activation. Indeed, the existence of a TCR affinity threshold of T-cell activation has recently been demonstrated (Irving et al., 2012; Schmid et al., 2010). In summary optimal TCR gene therapy most likely requires the transfer of a TCR with an optimal

binding affinity and/or half-life. This affinity may differ between different TCR/antigen pairings and can therefore only be determined experimentally.

6.1.7 Aim

I had access to MART-1-specific TCRs with a range of enhanced affinities. My aim was to establish the optimal TCR affinity for targeting melanoma cells by TCR gene transfer in this system.

6.2 RESULTS

6.2.1 Testing of MEL5 TCR transduction in Jurkat cells

Jurkat J.RT3-T3.5 Gluc cells were transduced with a lentiviral vector containing the MEL5 TCR sequence and a rCD2 reporter gene (**Figure 6.4**). After cloning of the MEL5-rCD2 cassette into the lentiviral vector pELNSxv (**Figure 6.4**), I produced the lentivirus and transduced Jurkat TCR negative GLuc cells as described in **Chapter 2** (sections 2.2 and 2.7). Transduced cells were stained with an anti-rCD2-PE antibody and a positive (ELA-APC, melanoma antigen) and control (SLY-APC, HIV antigen) pMHCI tetramer (**Figure 6.5**). Staining of the transduced cells with anti-CD3-FITC antibodies also indicated TCR expression (**Figure 6.5**). After transduction of the cells, ~85% of the cells expressed CD3 and ~58% expressed rCD2, thus showing a high transduction efficiency (**Figure 6.5B&D**). ~76% of the transduced cells stained with the positive ELA-APC tetramer, whereas none were stained with the control tetramer (**Figure 6.5A&B**).

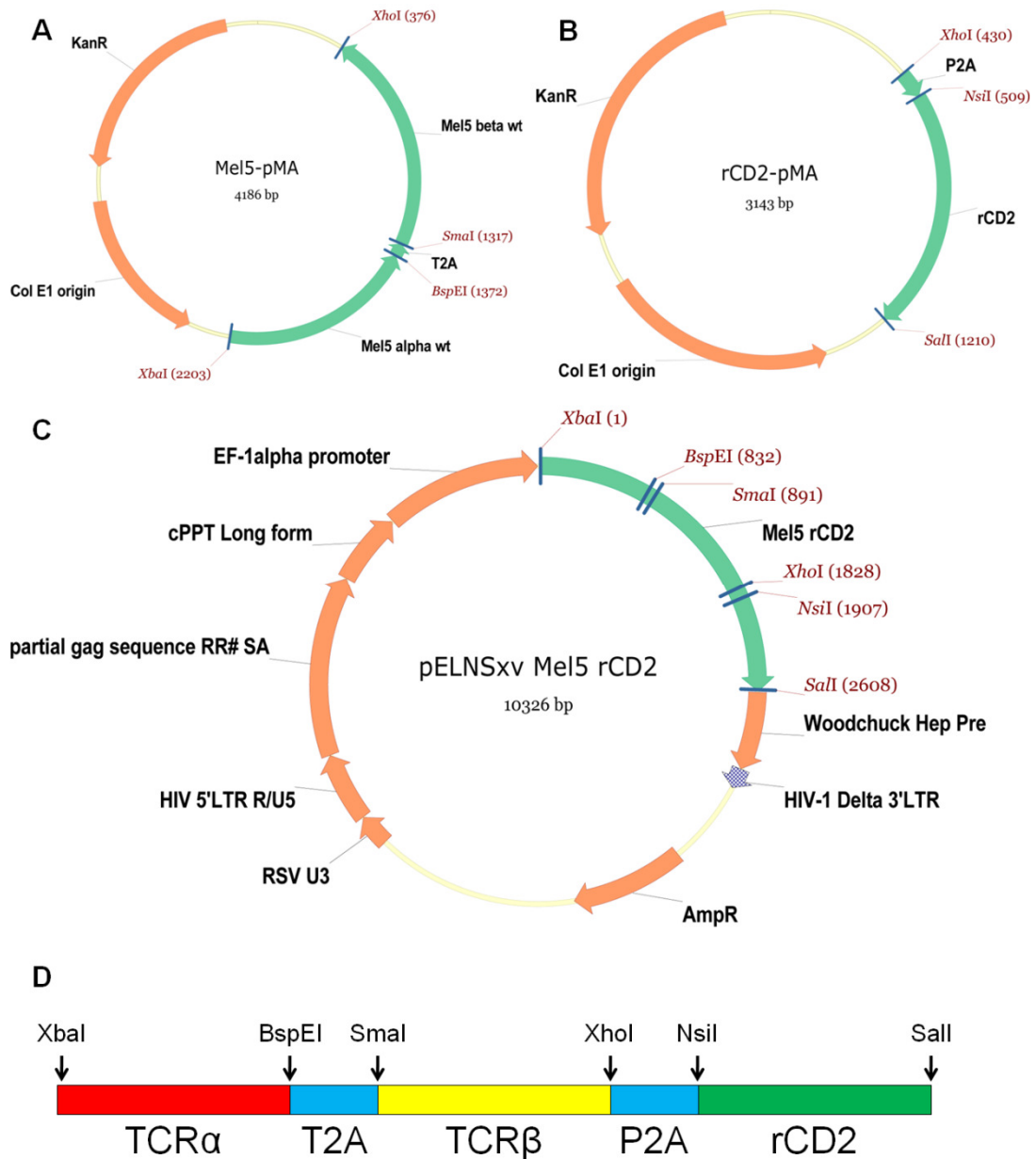


Figure 6.4. Schematic representation of the vectors and transgene cassette for the production of lentivirus.

(A & B) Schematic representation of the pMA plasmids generated by GeneArt and conferring a resistance to kanamycin. (C) Lenti vector pELNSxv with the MEL5-rCD2 cassette. (D) Representation of the cassette cloned into pELNSxv lenti vector. Restriction sites XbaI and BspEI, SmaI and XhoI, and NsiI and Sall, flanked the TCR α chain, TCR β chain and rCD2, respectively. The 2A-like sequences, T2A (amino acid sequence EGRGSLLLTCGDVEENPGP) and P2A (amino acid sequence ATNFSLLKQAGDVEENPGP), mediates the cotranslational cleavage of the TCR α chain, the TCR β chain and the rCD2 reporter gene.

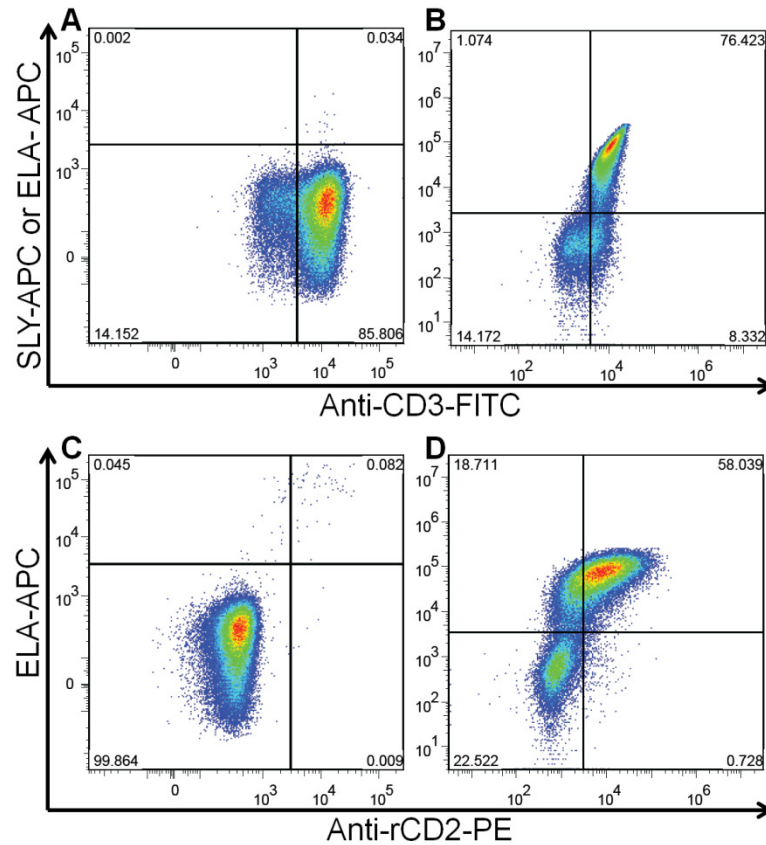


Figure 6.5. Transduction of Jurkat TCR negative GLuc cells with a lentivirus for the expression of rCD2 and MEL5 TCR.

(A-B) Jurkat J.RT3-T3.5 cells were transduced with a lentivirus driving the expression of rCD2 (reporter gene) and MEL5 TCR α and TCR α chains. Transduced cells were stained with anti-CD3-FITC antibodies and either (A) SLY-APC tetramer (control HIV-specific tetramer) or (B) ELA-APC tetramer and analysed by FACS. The shift in CD3 expression and in positive tetramer binding revealed a high transduction efficiency. (C-D) Comparison of (C) untransduced and (D) transduced Jurkat J.RT3-T3.5 cells stained with ELA-APC tetramer and anti-rCD2-PE antibodies confirmed the high transduction efficiency and the expression of both the reporter gene rCD2 and the melanoma specific MEL5 TCR.

Interestingly, there was a 9% difference between the CD3 and the MEL5 TCR expression suggesting the presence of mispaired TCRs not binding to A2-ELA. Indeed, the formation of mispaired TCRs has been observed after transfection of Jurkat J.RT3-T3.5 cells with a TCR β chain despite a low level of endogenous TCR α chain expression (Alajez et al., 2006). The comparison of untransduced and transduced Jurkat stained with HLA-A2-ELA-APC tetramer and anti-rCD2-PE confirmed the specific staining of MEL5 (**Figure 6.5C&D**). Untransduced Jurkat did not stain with anti-rCD2-PE, whereas ~58% of the transduced Jurkat were rCD2⁺ (**Figure 6.5C&D**). The lower percentage of rCD2⁺ staining compared to CD3⁺ and MEL5⁺ was curious but was thought to be a staining artefact. Staining with different anti-rCD2-PE antibody clones from AbD Serotec and BD Biosciences revealed a rCD2⁺ population equivalent to that of CD3⁺.

6.2.2 Transduction of primary HLA A2⁺ CD8⁺ T-cells with MEL5 TCR

In order to verify the expression of a fully functional MEL5 TCR after transduction of primary T-cells with a lentivirus, primary CD8⁺ T-cells were obtained from an HLA A*0201⁺ healthy blood donor as described in **Chapter 2** (section 2.7.3.1). CD8⁺ T-cells were magnetically sorted from PBMCs after incubation with anti-CD8 microbeads. Staining of the sorted population with anti-CD8-FITC antibodies confirmed that cells were 100% CD8⁺ (**Figure 6.6A**). Staining with anti-rCD2-PE showed that only ~32% of the population was rCD2⁺ (**Figure 6.6B**) highlighting a lower transduction efficiency compared with Jurkat J.RT3-T3.5 GLuc cells (~58%) (**Figure 6.5D**).

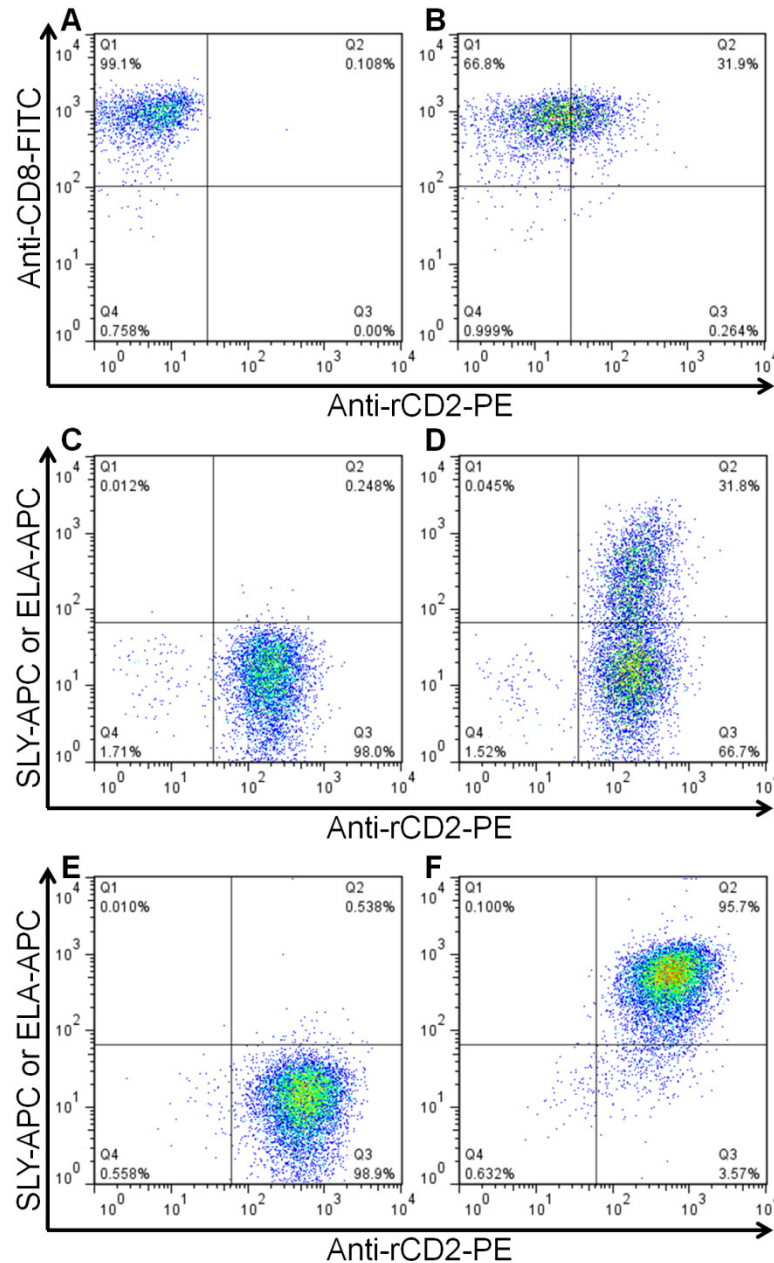


Figure 6.6. Transduction of primary HLA A2⁺ CD8⁺ T-cells with a lentivirus for the expression of rCD2 and MEL5 TCR

(A) Magnetically sorted primary HLA A2⁺ CD8⁺ T-cells are 100% CD8⁺ (B) After transduction, ~32% of CD8⁺ T-cells were rCD2⁺. (C-D) Transduced T-cells were magnetically sorted using anti-rCD2 antibodies and the sorted population was 100% rCD2⁺ with (C) no non-specific binding to the HIV-specific tetramer SLY-APC and (D) ~32% of sorted T-cells expressing MEL5 TCR. (E-F) Transduced T-cells were sorted a second time using ELA tetramers. (E) The sorted population did not bind SLY-APC tetramer. (F) ~96% of the MEL5⁺ CD8⁺ T-cells stained with ELA-APC tetramer confirming that the vast majority of the cells had the required specificity.

In order to test the effector functions of the transduced CD8⁺ T-cells, a pure population expressing MEL5 TCR was required. MEL5 transduced CD8⁺ T-cells were first magnetically sorted with anti-rCD2 antibodies (**Figure 6.6C&D**). Staining with anti-rCD2-PE antibodies showed a population 100% rCD2⁺. Transduced rCD2⁺ cells did not stain with SLY-APC tetramer (**Figure 6.6C**). However, ~32% of the rCD2-sorted cells stained with ELA-APC (**Figure 6.6D**). A second sorting step was required to obtain a pure population of CD8⁺ MEL5⁺ transduced T-cells. This was done with ELA tetramer sorting as described in **Chapter 2** (section 2.7.3.2) and led to ~96% of the transduced T-cells binding to the ELA-APC tetramer (**Figure 6.6E&F**).

To determine if the transduced T-cells retained their effector functions, I performed a MIP1 β activation assay (peptide titration) (**Figure 6.7A-C**) and a cytotoxicity assay (⁵¹Cr release assay) (**Figure 6.7D-F**). MIP1 β activation assay of the MEL13 clone (expressing MEL5 TCR) with the heteroclitic melanoma decameric peptide antigen ELAGIGILTV (ELA) was described previously (Ekeruche-Makinde et al., 2012) and was duplicated here as a positive control (**Figure 6.7A**). First, the untransduced cell line was not activated by ELA as there was no production of MIP1 β (**Figure 6.7B**). ELA activated both MEL13 clone (**Figure 6.7A**) and the transduced cell line with similar sensitivity (**Figure 6.7C**) with MIP1 β production starting when target cells were pulsed with ELA at 10⁻¹¹ M. Maximal MIP1 β production was observed with concentrations of 10⁻⁸ M peptide and higher.

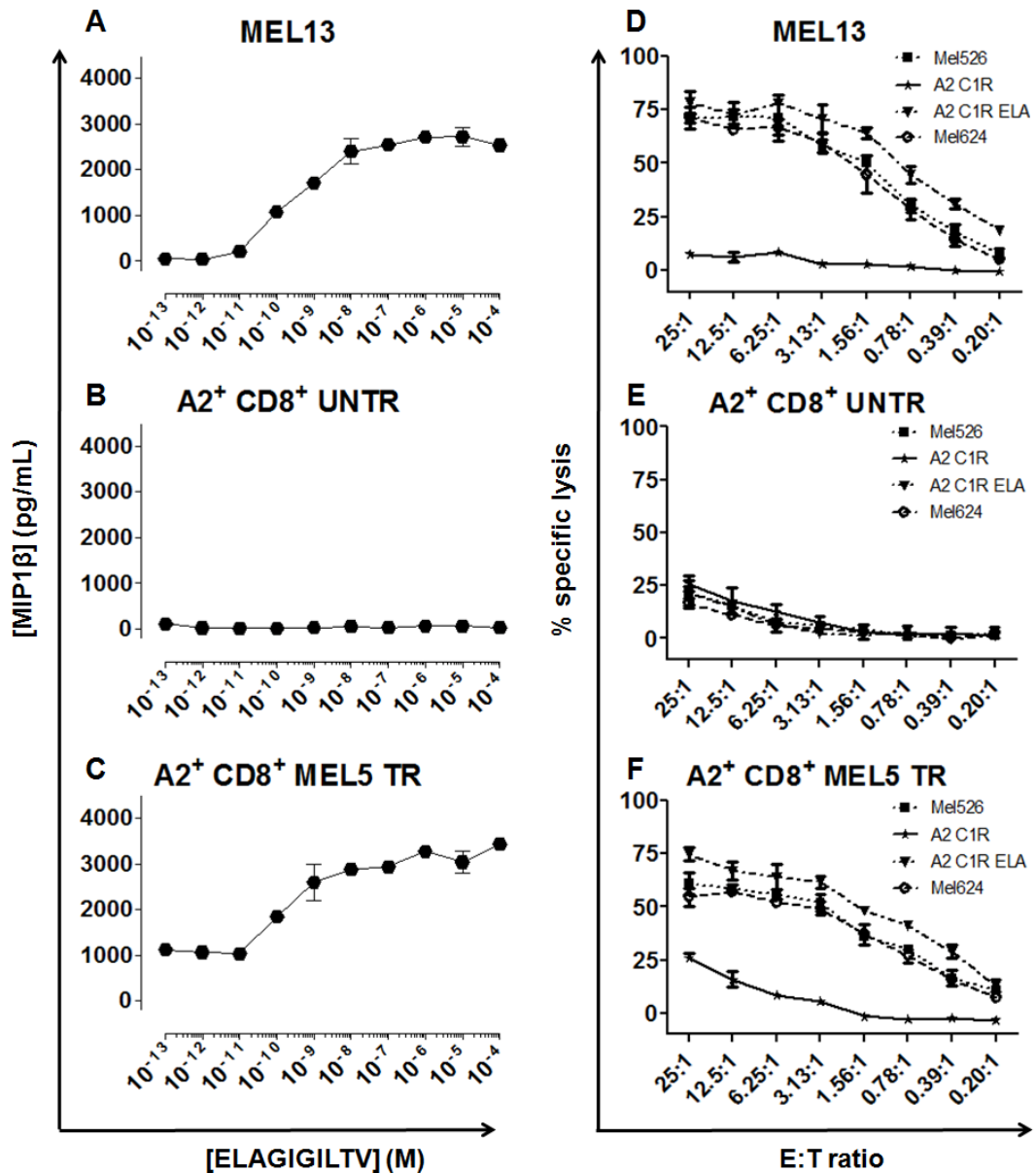


Figure 6.7. MEL5 TCR transduced primary T-cells recognise HLA A2⁺ targets pulsed with cognate peptide and natural levels of antigen presented on the surface of melanoma cells.

(A-C) 3×10^4 (A) MEL13 clone, (B) untransduced A2⁺ CD8⁺ T-cells and (C) MEL5 transduced A2⁺ CD8⁺ T-cells were incubated for 2 hours with 6×10^4 A2 C1R pre-pulsed with various concentrations of ELA. Supernatants were harvested and assayed for MIP1β by ELISA. (D-F) 2×10^3 A2 C1R, A2 C1R pulsed with ELA (100 μM final concentration), Mel526 and Mel624 target cells labelled with ⁵¹Cr were incubated for 4 hours with different concentrations of (D) MEL13 clone, (E) untransduced A2⁺ CD8⁺ T-cells and (F) MEL5 transduced A2⁺ CD8⁺ T-cells (effector to target ratio, E:T). Supernatants were harvested and assayed for ⁵¹Cr release in order to obtain the % of specific lysis.

MEL5 transduced, but not untransduced, T-cell lines recognised two A2⁺ melanoma cell lines (Mel526 and Mel624) (**Figure 6.7D-F**). Importantly, this confirms that these cells are able to recognise natural surface densities of the natural antigen(s).

6.2.3 Peptide specificity of HLA A2⁺ CD8⁺ T-cells transduced with MEL5 TCR

In order to further investigate the specificity of the MEL5 transduced A2⁺ CD8⁺ T-cells, I performed a PS-CPL activation assay. I compared the output with the PS-CPL activation assay previously described for the MEL13 clone that was derived from the same CTL line as MEL5 at the same time and which expresses an identical TCR to MEL5 at the nucleotide level (i.e. this clone is MEL5) (Ekeruche-Makinde et al., 2012) (**Figure 6.8-6.10**).

Briefly, MEL13 PS-CPL activation assay showed that several different residues at each position of the peptide can be recognized and some of these residues displayed markedly different biochemical properties compared to the corresponding residues in the index peptide ELA (**Figure 6.8** and **Figure 6.10**). For example, the Phe^{P1} residue of the decapeptide library screen induced the maximal T-cell activation for position 1 and differs from the native Glu^{P1} residue by possessing an aromatic side chain and by being strongly apolar. The recognition requirements appeared to be stringent at positions 4, 5, 6 and 7 which is the peptide region mainly contacted by MEL5 TCR (Cole et al., 2009) and less stringent at positions 1, 2, 3, 8, 9 and 10 (Ekeruche-Makinde et al., 2012).

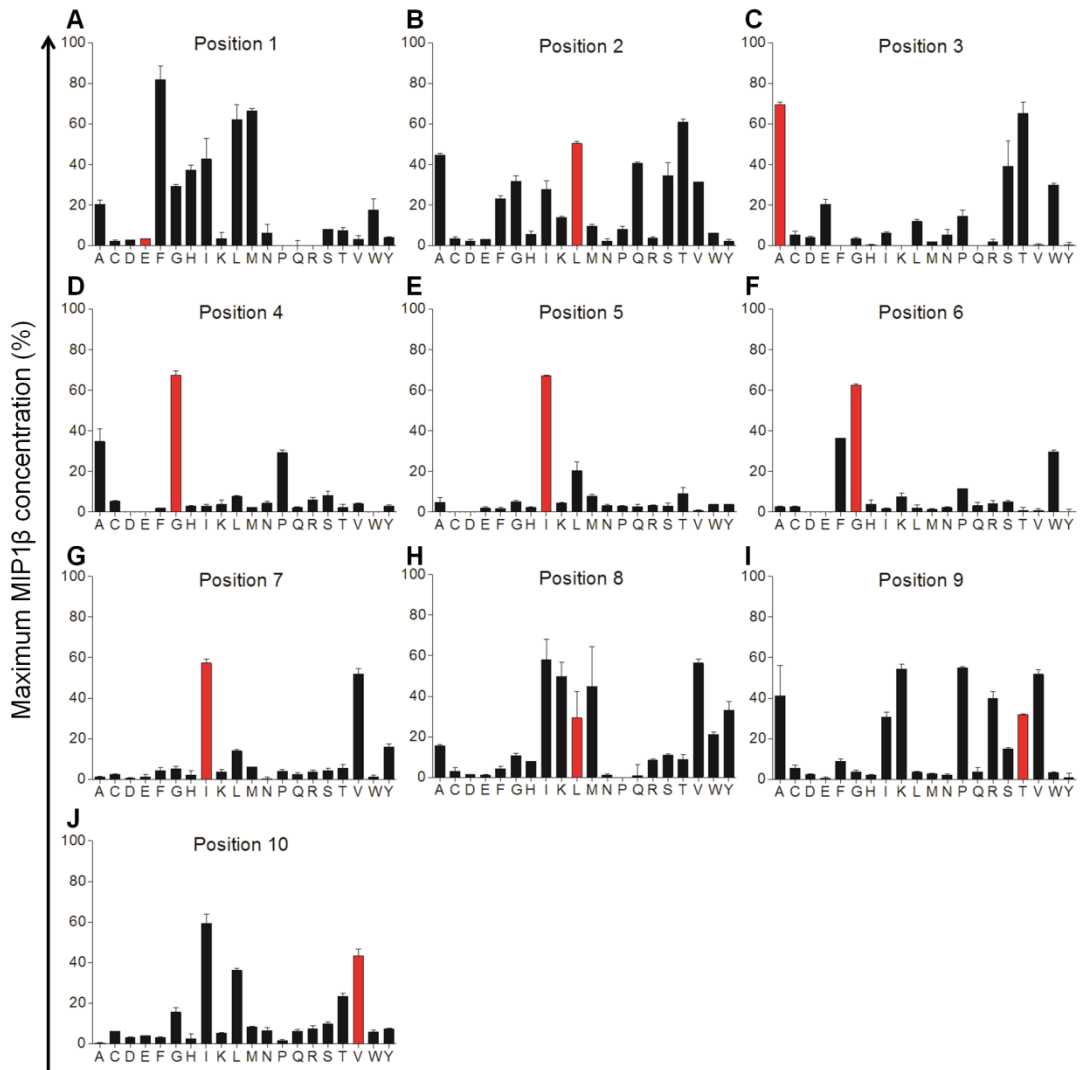


Figure 6.8. Decameric peptide PS-CPL activation assay of the MEL13 clone.

MEL13 cells were stimulated for 2 hours with A2 C1R cells pulsed in duplicate with the index peptide or each of the 200 mixtures from the decameric peptide library as described in **Chapter 2** section 2.10.2. Responses to peptides were quantified in a MIP1 β ELISA using cell supernatant, stimulation with the index peptide representing the maximum MIP1 β concentration. Responses are displayed as a cluster of 10 histograms plots, each plot representing a set of 20 mixtures having the defined residues listed on the x-axis at position (A) P1, (B) P2, (C) P3, (D) P4, (E) P5, (F) P6, (G) P7, (H) P8, (I) P9 and (J) P10. The red bars represent the mixture with a fixed amino acid that corresponds to the MEL13 index peptide (ELAGIGILTV). Adapted from (Ekeruche-Makinde et al., 2012).

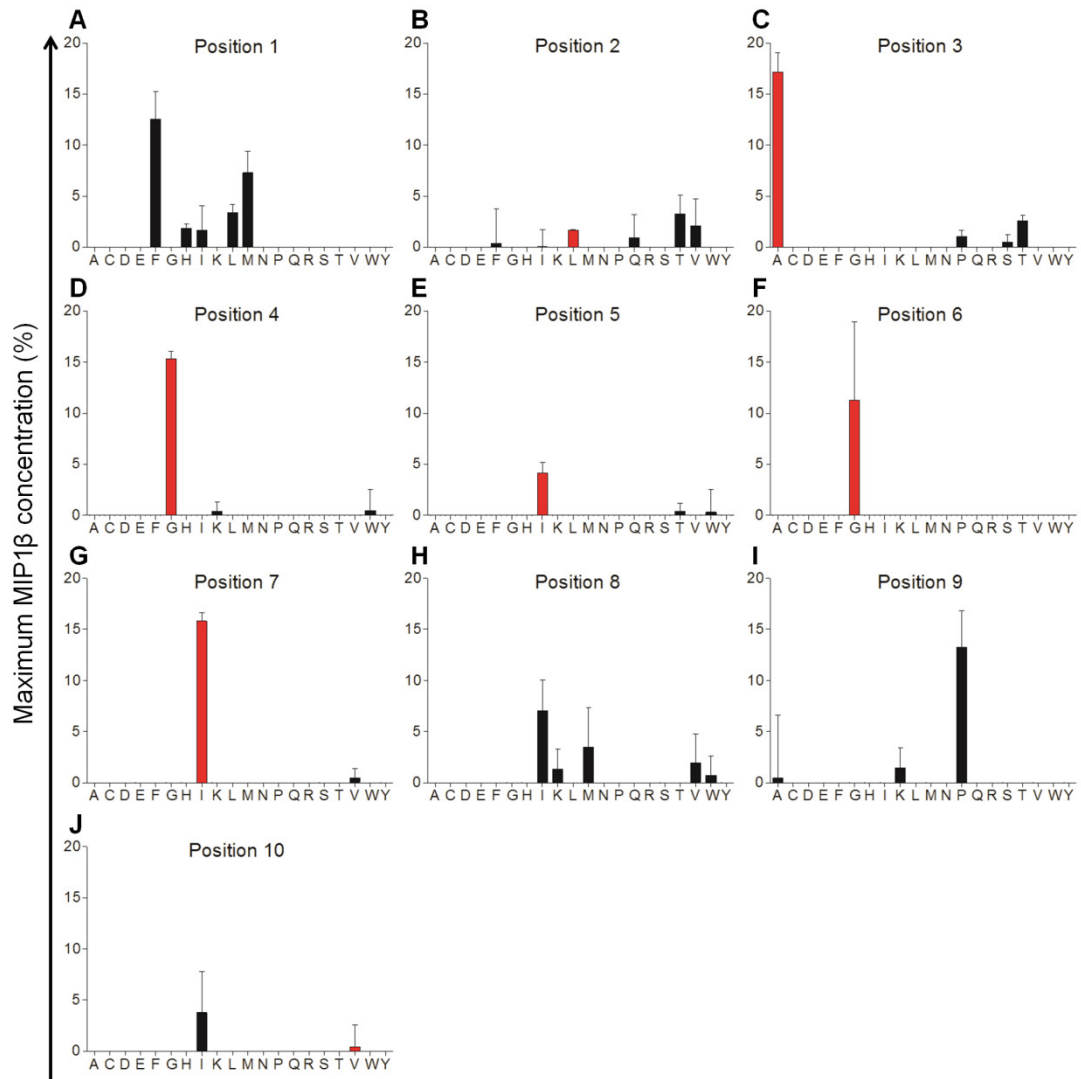


Figure 6.9. Decameric peptide PS-CPL activation assay of the MEL5 transduced A2⁺ CD8⁺ T-cells.

MEL5 transduced A2⁺ CD8⁺ T-cells were stimulated for 2 hours with A2 C1R cells pulsed in duplicate with the index peptide or each of the 200 mixtures from the decameric peptide library as described in **Chapter 2** section 2.10.2. Responses to peptides were quantified in a MIP1 β ELISA using cell supernatant, stimulation with the index peptide representing the maximum MIP1 β concentration. Responses are displayed as a cluster of 10 histograms plots, each plot representing a set of 20 mixtures having the defined residues listed on the x-axis at position (A) P1, (B) P2, (C) P3, (D) P4, (E) P5, (F) P6, (G) P7, (H) P8, (I) P9 and (J) P10. The red bars represent the mixture with a fixed amino acid that corresponds to the MEL5 index peptide (ELAGIGILTV).

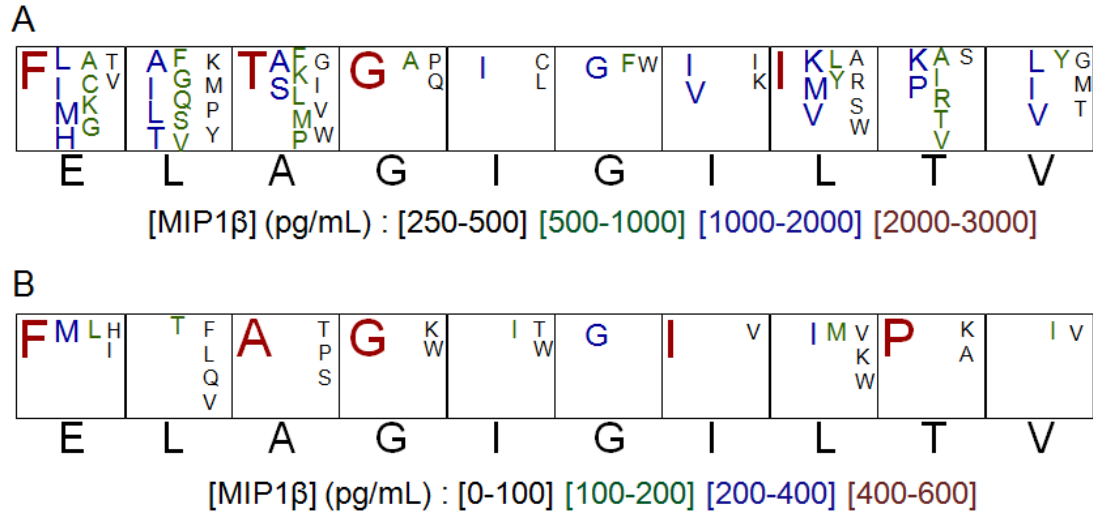


Figure 6.10. Box plot summary of the PS-CPL activation assays for MEL13 clone and MEL5 transduced A2⁺ CD8⁺ T-cells.

Mixture reactivity is represented by the one-letter nomenclature of the fixed residue within the mixture. The colours and size of the letters correspond to the magnitude of responses observed in the screen and range from black to red with red representing the highest response for (A) MEL13 clone and (B) MEL5 transduced A2⁺ CD8⁺ T-cells. (A) adapted from (Ekeruche-Makinde et al., 2012).

The recognition profiles of the MEL13 monoclonal T-cell expressing the MEL5 TCR and MEL5 transduced CD8⁺ T-cells were similar although the transduced cells were a little less responsive (**Figure 6.9** and **Figure 6.10**). These results do not indicate any systemic difference in peptide specificity due to TCR chain mispairing at the population level.

Having established that the MEL5 transduction system worked and that transduced cells acquired the desired peptide specificity and ability to recognise melanoma targets, I next moved to compare different affinity-modified MEL5 TCR variants.

6.2.4 Transduction of Jurkat TCR negative GLuc with a panel of affinity-enhanced TCRs

In order to determine the optimal melanoma-specific TCR affinity for maximum T-cell activation, Jurkat J.RT3-T3.5 GLuc cells were transduced with a lentivirus driving the expression of rCD2 (reporter gene) and one of the six MEL5 TCR mutants obtained by affinity maturation of MEL5 as described in **Chapter 1** (Li et al., 2005b). These variants were composed of the MEL5 α chain and a mutated version of the MEL5 β chain (**Appendix 12** and **Table 6.2**). The six variants (MEL5 β 5, MEL5 β 9, MEL5 β 12, MEL5 β 13, MEL5 β 15 and MEL5 β 17) had mutated CDR3 β loops, MEL5 β 15 and MEL5 β 17 having additional mutations in the CDR2 β loop as well as in the β chain between CDR1 β and CDR2 β (**Appendix 12**). In previous experiments, my laboratory measured the kinetic parameters and the affinity of these TCR mutants for A2-ELA binding by SPR (**Table 6.2**).

Table 6.2. MEL5 and MEL5 variants binding analysis toward A2-ELA.

TCR	K _D (μM)	Enhanced MEL5 affinity	k _{on} (M ⁻¹ s ⁻¹)	k _{off} (s ⁻¹)
MEL5	16-20		n/m	n/m
MEL5 β5	29		1.3 x 10 ⁴	3.9 x 10 ⁻¹
MEL5 β9	11	~2.5	2.4 x 10 ⁴	2.5 x 10 ⁻¹
MEL5 β12	4.4	~6	3.1 x 10 ⁴	1.4 x 10 ⁻¹
MEL5 β13	2.1	~12	8 x 10 ⁴	1.7 x 10 ⁻¹
MEL5 β15	2.1	~12	2.5 x 10 ⁵	5.2 x 10 ⁻¹
MEL5 β17	0.54	~48	4.6 x 10 ⁴	2.5 x 10 ⁻²

n/m: non measurable

These variants displayed a range of affinities toward ELA from no enhancement (MEL5 β 5) compared to the wild-type MEL5 to 48 times enhanced (MEL5 β 17). Even at 48 times enhanced, this affinity was within the physiological range observed for the TCR/pMHC interaction ($K_D = 0.1\text{-}270 \mu\text{M}$) (Bridgeman et al., 2012; van der Merwe and Davis, 2003). The kinetic parameters for MEL5 were too fast to be measured but were obtained for the mutants. The binding enhancements were due to a combination of a slower off-rate and/or a faster on-rate. Interestingly, MEL5 β 13 and MEL5 β 15 displayed the same affinity but possessed different kinetic parameters, MEL β 15 having a faster on-rate than MEL β 13 but the latter having a slower off-rate.

In order to transduce Jurkat J.RT3-T3.5 GLuc cells with these variants, I first cloned the different TCR-rCD2 cassettes into the lentiviral vector and produced the lentiviruses as described in **Chapter 2** (sections 2.2 and 2.7). After transduction, cells were stained with anti-CD3-FITC and anti-rCD2-PE antibodies and analysed by FACS (**Figure 6.11**). Despite a high transduction efficiency, some variability was observed regarding the rCD2 and the CD3 expression between the transduced cell lines. As observed above, in all cell lines CD3 expression was superior to rCD2 expression (section 6.2.1) but CD3 expression varied from ~52% to ~80% and rCD2 expression varied from ~25% to ~48%. Therefore, transduced cells were magnetically sorted with anti-CD3 antibodies in order to obtain a pure population for the activation assay. After sorting, the six transduced cell lines were 100% CD3⁺ rCD2⁺ (**Appendix 13**).

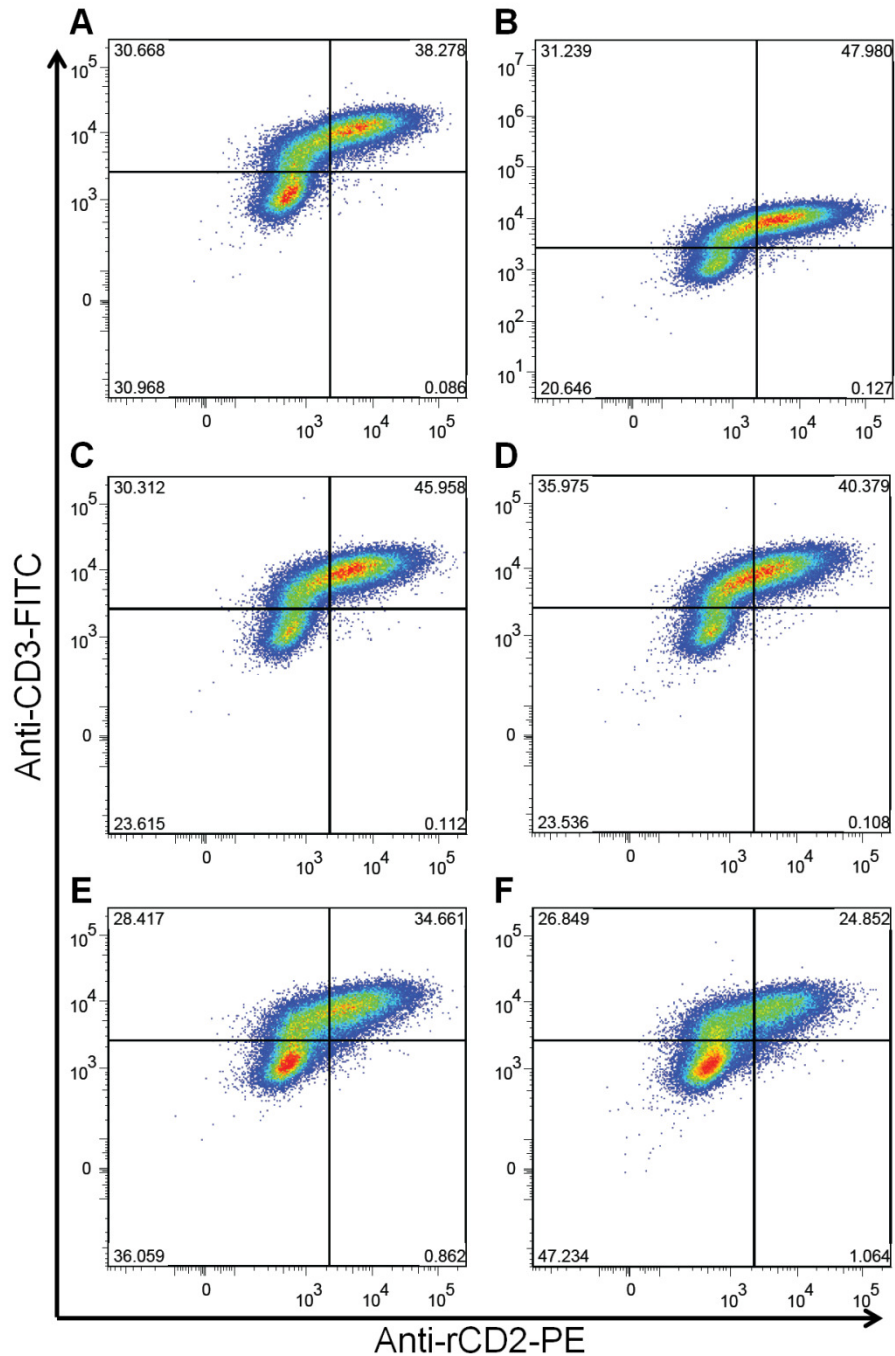


Figure 6.11. Transduction of Jurkat J.RT3-T3.5 GLuc cells with a lentivirus for the expression of six MEL5 TCR mutants.

Jurkat J.RT3-T3.5 GLuc cells were transduced with a lentivirus driving the expression of rCD2 (reporter gene) and MEL5 mutants (A) $\beta 5$, (B) $\beta 9$, (C) $\beta 12$, (D) $\beta 13$, (E) $\beta 15$ and (F) $\beta 17$. Transduced cells were stained with anti-CD3-FITC and anti-rCD2-PE antibodies and analysed by FACS.

6.2.5 Jurkat TCR negative GLuc cells transduced with enhanced affinity melanoma-specific TCRs reveal an unexpected glycosylation site

To determine the optimal melanoma-specific TCR affinity for maximum T-cell activation I used an activation assay based on the ability of the transduced and untransduced Jurkat J.RT3-T3.5 GLuc cells to express *Gaussia* Luciferase when activated. T-cell activation measurements were performed either after addition of phytohaemagglutinin (PHA) or after exposure to target cells (pulsed and unpulsed with ELA) (**Figure 6.12**). MEL5 β 13 transduced cells failed to respond to pulsed A2 C1R. A subsequent analysis of the β 13 sequence (**Appendix 12**) revealed the presence of one N-linked glycosylation site in the mutated CDR3 β sequence (tripeptide sequence Asn-(Val)-Ser). Due to the very rare occurrence of post-translational modifications such as glycosylation in *E. coli* (Benz and Schmidt, 2001; Lindenthal and Elsinghorst, 1999; Sherlock et al., 2006), the glycosylation site was undetected during affinity maturation by phage display. However, TCRs undergo post-translational modifications before expression at the cell surface (Amon et al., 2006). Therefore, MEL5 β 13 was unable to bind to A2-ELA because the glycosylated residue in the CDR3 β loop probably blocked the interaction with the pMHC. I was therefore unable to perform further experiments with MEL5 β 13 transductants.

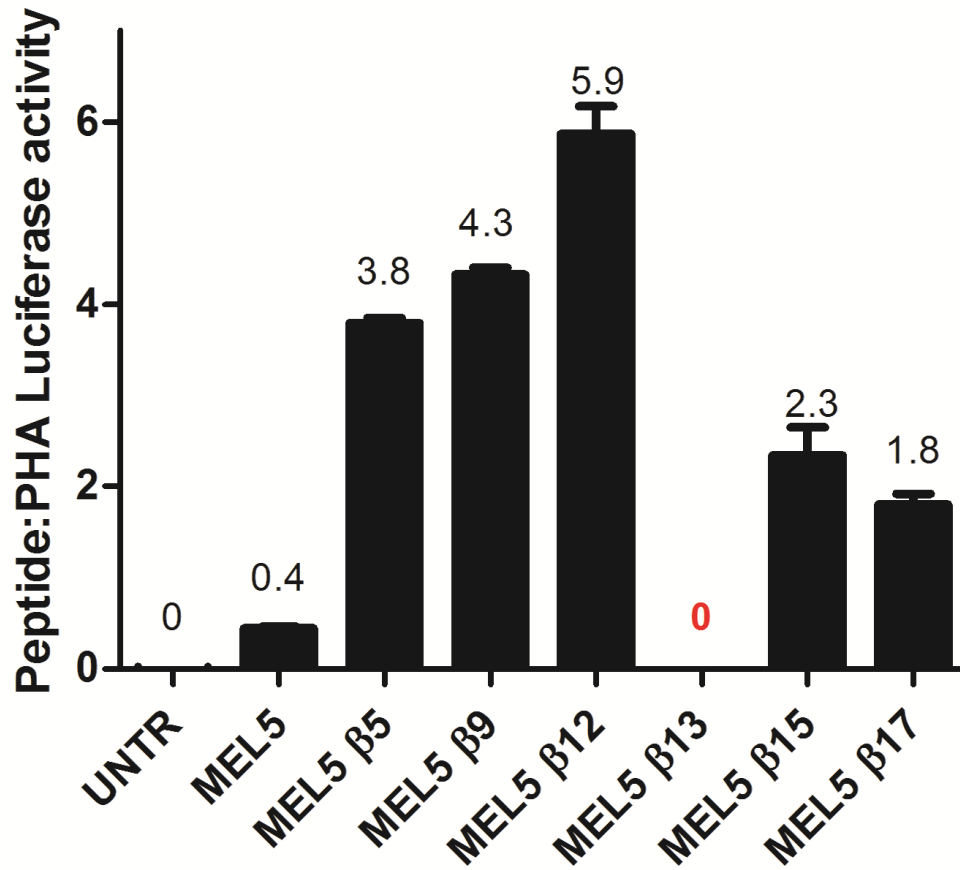


Figure 6.12. Threshold of melanoma-specific TCR affinity for maximum T-cell activation.

1×10^5 untransduced (UNTR), MEL5, MEL5 β 5, MEL5 β 9, MEL5 β 12, MEL5 β 13, MEL5 β 15 and MEL5 β 17 transduced Jurkat J.RT3-T3.5 GLuc cells were activated with PHA or incubated for 5 hours with 1×10^5 A2 C1R cells pre-pulsed with ELA. Supernatants were harvested and assayed for *Gaussia* luciferase expression. Jurkat activation is represented by the ratio between the luciferase activity when incubated with target cells and when activated by PHA. The luciferase activity ratio of each variant is displayed above the bar.

6.2.6 An affinity optimum for T-cell activation in the MEL5 system

Untransduced Jurkat cells failed to recognize A2 C1R cells pulsed with ELA peptide. Recognition of cognate target cells gradually increased until the TCR affinity reached ~6 times the MEL5 TCR affinity (MEL5 β 12 K_D ~4.4 μ M), leading to ~15-fold stronger signal compared with MEL5 transduced cells (**Figure 6.12**). Beyond this threshold T-cell activation decreased (**Figure 6.12**). These results show that there is an optimal TCR affinity for the recognition of target cells by T-cells transduced with the MEL5 TCR. This optimum is ~6-fold higher than the wildtype interaction suggesting that use of enhanced affinity TCRs in the clinic might be beneficial. Enhancing TCR affinity beyond this level was detrimental to T-cell activation. This result is in accordance with other recent data from other laboratories (Irving et al., 2012; Schmid et al., 2010; Stone et al., 2009).

6.3 DISCUSSION

In the study reported here, I aimed to analyze the specificity of T-cells transduced with the melanoma-specific MEL5 TCR and to determine the optimal TCR affinity for TCR gene transfer targeting of melanoma using the MEL5 system. I tested a panel of affinity-enhanced TCRs derived from the melanoma-specific MEL5 TCR.

I first transduced an in-house modified Jurkat J.RT3-T3.5 cell clone (J.RT3-T3.5 GLuc) with a lentiviral vector containing MEL5 TCR sequences in order to verify that transfer of MEL5 TCR genes produced T-cells with desired specificity. Tetramer staining of the transduced cells showed that MEL5 TCR was expressed on the cell surface (staining with ELA-APC) and that the transduced cells were melanoma-specific (no staining with SLY-APC presenting an HIV derived peptide).

Moreover, as observed in other TCR gene transfer studies using Jurkat cells (Provasi et al., 2012; Thomas et al., 2011), transduction was efficient as ~76% of the transduced cells were stained with the ELA-APC tetramer. However, the difference between CD3 and MEL5 TCR expression suggested that either the TCR density on some cells was too low for staining with pMHC tetramer (Wooldridge et al., 2009) or that there might be a small fraction of mixed TCRs on the cell surface that did not bind to the tetramer (Alajez et al., 2006).

I next transduced the HLA-A2-restricted MEL5 TCR into primary A2⁺ CD8⁺ T-cells as this situation is analogous to what is done in TCR gene transfer therapy. This allowed me to analyse the effector functions and antigen specificity of gene-modified T-cells in comparison to the parent CD8⁺ T-cell clone (MEL5 and MEL13 are identical). The transduction efficiency was lower for CD8⁺ T-cells than Jurkat cells J.RT3-T3.5 GLuc, a result consistent with other studies using retroviral and lentiviral vectors (Provasi et al., 2012; Thomas et al., 2011). Moreover, the MEL5 TCR expression level was relatively low after transduction as measured by tetramer staining. This might suggest that some of the MEL5 TCR chains might be mispaired with endogenous TCR chains. Recent studies have introduced the concept of “strong” and “weak” TCRs when it comes to their ability to pair correctly and compete with the endogenous TCR for expression at the T-cell surface (Kieback and Uckert, 2010; Sommermeyer et al., 2006). The terms “strong” and “weak” are ambiguous when it comes to TCRs. My laboratory therefore prefers the terms “competitive” and “uncompetitive” to describe how well individual TCRs express at the T-cell surface. This factor is thought to represent the ability of TCR chains to pair with each other and then compete for a limited quantity of other molecules

required for surface expression of TCR protein. The availability of CD3 (particularly CD3 ζ chain) is thought to be key to the total amount of TCR expressed at the T-cell surface (Koning et al., 1990; Manolios et al., 1994; Minami et al., 1987). Competitive (or strong) TCRs appear to pair well with each other and outcompete most endogenous TCRs for CD3 components so as to be expressed at the cell surface at high density. Conversely, uncompetitive (or weak) TCRs fail to compete well with endogenous TCRs and transduction of cells with such TCRs results in poor expression of the transduced TCR at the T-cell surface and poor responsiveness to the cognate antigen for the transduced TCR. Experiments performed by Dr John Bridgeman in my laboratory suggested that MEL5 TCR can be defined as an “average” TCR for cell surface expression. This factor may therefore explain the low expression of MEL5 TCR in some cells. Also, staining with pMHC multimer requires that a second pMHC within a single pMHC multimer molecule binds to a TCR during the dwell time of the first TCR/pMHC interaction in order for the “avidity effect” to come into play and capture the multimer from solution (Wooldridge et al., 2009). TCR density is a critical factor in whether a second TCR is available for capture of pMHC multimer from solution and T-cells that express low surface density of a cognate natural affinity TCR are unable to stain with pMHC tetramer (Wooldridge et al., 2009).

MEL5 transduced CD8⁺ T-cells were analysed for two effector functions: MIP1 β production and cytotoxicity towards target cells. The MIP1 β activation assay showed that the gene-modified T-cells were as sensitive as the MEL13 clone. Moreover, the cytotoxicity assay showed that, as for MEL13 clone, the transduced cell line was able to lyse HLA-A2⁺ target cells pulsed with ELA as well as two HLA-A2⁺

melanoma cell lines (Mel526 and Mel624) (Topalian et al., 1990; Topalian et al., 1989). Collectively, these assays showed that the MEL5 transduced CD8⁺ T-cell line was fully functional and that the gene-modified T-cells acquired an anti-melanoma specificity. Some background activation was detected. This is believed to be due to the high sensitivity of the MIP1 β assay compared to the cytotoxicity assay sensitivity (Laugel et al., 2007; Price et al., 1998).

The precise specificity of MEL5 transduced CD8⁺ T-cells was probed using positional scanning combinatorial peptide library (PS-CPL) screen. PS-CPLs, coupled to a mathematical analysis, can determine the cross-reactivity profile of a T-cell clone (e.g. 1E6) (Wooldridge et al., 2012). These data can then be used to design optimal peptide sequences that enhance functional activation of a T-cell clone (e.g. MEL13) (Ekeruche-Makinde et al., 2012). Comparison of the MEL13 clone PS-CPL assay (Ekeruche-Makinde et al., 2012) with the MEL5 transduced CD8⁺ T-cells PS-CPL assay revealed an identical specificity profile despite the potential for expression of endogenous TCRs and transduced/endogenous mixed chain paired TCRs. These experiments showed that there was no dominant, systemic change in TCR specificity of MEL5 transduced CD8⁺ T-cells although it remains possible that individual cells in the population expressed different TCRs and exhibited a different peptide-specificity profile. Such events would be in vast numeric minority and would therefore not be visible at the population level.

Having demonstrated that T-cells retained their effector functions and displayed melanoma specificity after transduction with a lentiviral vector containing MEL5 TCR sequences, I then aimed to determine the optimal TCR affinity for maximal T-

cell activation. J.RT3-T3.5 GLuc cells were transduced with different lentiviral vectors expressing a panel of affinity-enhanced, melanoma-specific TCRs. T-cell activation was measured after recognition of HLA-A2 C1R pulsed with ELA peptide. We had failed to anticipate that phage display in *E. coli* might introduce mutations that would interfere with protein folding or post-translational modifications in eukaryotic cells. The MEL5 β 13 TCR failed to recognise antigen. Closer inspection of the modified TCR sequence revealed that the phage display process had introduced an N-linked glycosylation site (tripeptide sequence Asn-(Val)-Ser) in the CDR3 β sequence of this TCR. In future, sequences generated by phage display should be systematically analysed for the occurrence of glycosylation sites and other motifs that might interfere with protein expression or function prior to expression in T-cells. I was unable to examine the MEL5 β 13 TCR in activation assays. Thankfully, the other TCRs expressed well and I was able to analyse how cells expressing these TCRs responded to cognate antigen.

Jurkat activation assays revealed a “bell shape” curve of T-cell activation depending on TCR affinity. Maximal T-cell activation was achieved when T-cells expressed a TCR (MEL5 β 12) with a $K_D \sim 4.4 \mu\text{M}$ (~ 6 -fold enhancement compared to MEL5 TCR affinity). This optimal affinity is close to pathogen-specific TCR affinities (average $K_D \sim 8 \mu\text{M}$) (Bridgeman et al., 2012; Cole et al., 2007), possibly explaining the better T-cell activation. The “bell shape” curve strongly supports the existence of an “affinity ceiling” above which T-cells become less effective (Irving et al., 2012; Schmid et al., 2010; Sewell, 2002). Thus, tumour-specific TCRs may only need modest affinity enhancement for optimal results in for TCR gene therapy.

Collectively, the results of this study suggested that MEL5 TCR gene transfer can lead to a rapid generation of fully functional and highly specific T-cells for targeting melanoma in TCR gene therapy. TCR affinity can be optimized to improve T-cell activation but a TCR “affinity ceiling” exists that seems to be within the range for natural TCR affinities ($K_D = 0.1\text{-}270 \mu\text{M}$) (Bridgeman et al., 2012; Cole et al., 2007; Schmid et al., 2010).

CHAPTER 7

GENERAL DISCUSSION

7.1 Implications of my results	257
7.1.1 New crystallization screening improves study of TCR/pMHC recognition	257
7.1.2 Enhanced MHC contacts mediate TCR high affinity without loss of specificity	260
7.1.3 A novel thermodynamic mechanism mediates high-affinity TCR specificity	261
7.1.4 A new molecular mechanism of TCR/pMHC recognition	261
7.1.5 Heteroclitic peptides can alter T-cell antigen specificity due to changes at the atomic level	263
7.1.6 MEL5 TCR gene transfer generates melanoma-specific T-cells	265
7.1.7 Detrimental motifs can be introduced during TCR affinity maturation...	265
7.1.8 An optimal TCR affinity for TCR gene therapy against melanoma	267
7.2 Perspectives.....	268
7.3 Summary	269

The work outlined in my thesis aimed to investigate the structural and biophysical features of TCR/pMHCI interactions as well as explore the potential use of affinity-matured TCRs for gene therapy. Specifically, I aimed to:

1. Develop an optimized screen for the crystallization of TCR/pMHC complexes (**Chapter 3**)
2. Analyse the specificity of a high-affinity TCR directed against a melanoma antigen (**Chapter 4**)
3. Investigate the structural and biophysical differences between TCRs with different affinities in the recognition of melanoma antigens (**Chapter 5**)
4. Determine the optimal TCR affinity for adoptive cell therapy directed against melanoma (**Chapter 6**)

7.1 IMPLICATIONS OF MY RESULTS

7.1.1 New crystallization screening improves study of TCR/pMHC recognition

X-ray crystallography has revolutionised our understanding of the molecular events that govern TCR/pMHC recognition (Armstrong et al., 2008b; Rudolph et al., 2006). However, the relatively small number of TCR/pMHC structures (<25 unique human TCR/pMHC complexes in total and just 6 unique TCR/pMHCI complexes) (Broughton et al., 2012; Deng et al., 2007; Rudolph et al., 2006), has hampered the determination of an accepted set of rules that describe the generalities of T-cell specificity. Indeed, there are now several TCRs that fail to obey any of the original “rules of engagement” that were based on just the first 6 interactions described (Gras et al., 2012) and there is a pressing need for further structures to advance our understanding of what is possible.

A major obstacle in using X-ray crystallography to study T-cell antigen recognition has been finding an optimal set of crystallization conditions to produce high quality TCR/pMHC crystals that diffract well and the crystallization step is generally considered to be the limiting factor in structural studies of proteins (Segelke, 2001). As a given condition contains multiple parameters (e.g. type of buffer, temperature, pH, salt), there is an almost limitless number of crystallization conditions. Over 1500 conditions are commercially available alone (McCoy, 2009). Testing a wide range of crystallization conditions is time consuming and requires the production of a large amount of protein. Therefore, the generation of a screen containing the optimal conditions for the crystallization TCRs, pMHCs and complexes was important to enable a more directed approach to the crystallization of these proteins. In **Chapter 3**, I report the development of a new 96-well “sparse matrix” crystallization screen designed specifically for the generation of TCR/pMHC complex structures (TOPS). The “sparse matrix” screening method, such as TOPS or most of the commercially available screens (Wooh et al., 2003), involves screening conditions based on previous successful crystallization experiments (Jancarik and Kim, 1991). However, sparse matrix screens have an intentional bias towards combinations of conditions that have worked previously. The wide use of such screens continually further biases the set of conditions used for screening. This focussing can have a deleterious effect on the development of further matrix screens (McCoy, 2009). Indeed, such a bias was observed in the last section of **Chapter 3** where some complexes crystallized in the low range of the scoring system. Thus, although it is tempting to limit the number of conditions in a protein crystal screen to improve efficiency and reduce protein consumption, broader screens are required to ensure that crystallization conditions are not missed. Nonetheless, the screening I perfected used a relatively

low number of conditions and resulted in the generation of a high number of human TCR/pMHC structures. The resultant TOPS screen has already produced 21 TCR/pMHC, 3 TCR and 8 pMHCI structures. Notably, the use of TOPS has furthered our knowledge of TCR cross-reactivity to different pMHCII (Holland et al., 2012). Only 6 TCR/pMHCII structures have been described to date. It is important that this very limited database is expanded and my TOPS screen has already helped in this respect. Analysis of successful crystallisation conditions used by other groups show that the Class II MHC molecule HLA-DR1 presenting the phosphopeptide MART-1₁₀₀₋₁₁₄ was crystallized in 20% PEG 8000 and 0.1 M sodium cacodylate pH 6.5 (Li et al., 2010), corresponding to TOPS conditions B5 or B11. Recently, the non-classical MHC-related molecule 1 (MR1) presenting a vitamin B9 metabolite (6-formylpterin) was crystallized in 25% PEG 3350, 0.2 M salt and 0.1 M HEPES pH 7.5 (Kjer-Nielsen et al., 2012), an equivalent of TOPS condition E9. The KK50.4 TCR complexed to the MHC class Ib molecule HLA-E presenting a UL40 peptide of the human cytomegalovirus (CMV) was crystallized in 18-22% PEG 3350 and 0.2 M potassium iodide pH 6.4-7.4 (Hoare et al., 2006), a condition extremely close to some of the conditions contained in TOPS1. A human NKT TCR (NKT15) complexed to the human CD1d presenting the glycolipid α -galactosylceramide (α -GalCer) was crystallised in 13% PEG 10000, 0.1M bis-tris propane pH 8.5 and 0.2 M tri-sodium citrate (Borg et al., 2007), a condition close to TOPS H10. Hence, TOPS is, by far, the best screen for the crystallization of TCR/pMHCI complexes described to date and it has already saved our laboratory several grams of protein. This screen could also prove to be really useful for other T-cell-associated proteins or non classical T-cell protein targets as indicated by the successes described above. Finally, the use of TOPS and the determination of

immune-protein structures might lead to a better understanding of different pathologies as suggested by our recently published study on the autoimmune type 1 diabetes (Bulek et al., 2012a) or by the studies reported here on melanoma. Relevant TCR/pMHC structures could also be useful for the development of T-cell based therapies, vaccines or soluble TCR therapy. Indeed, our collaborators have now made a high affinity variant of the 1E6 insulin-specific TCR (Immunocore, unpublished data). Initial attempts to obtain such a reagent failed. Our recent crystal structure of this TCR (Bulek et al., 2012a) allowed intelligent design of modifications to help the phage display process that would not have been possible without knowing how, and which, CDR loops engage the peptide component of the bipartite HLA A2-insulin peptide ligand.

7.1.2 Enhanced MHC contacts mediate TCR high affinity without loss of specificity

I used TOPS to crystallize and solve 9 T-cell-associated melanoma-related protein structures (7 TCR/pMHCI complexes, 1 free TCR and 1 free pMHCI) as described in **Chapter 4** and **Chapter 5**. I also performed an in-depth thermodynamic analysis of melanoma antigen recognition by a wild-type and an enhanced affinity melanoma-specific TCR. Altogether, my data revealed that TCR affinity could be enhanced, without losing peptide specificity. Surprisingly, specificity was maintained even when the vast majority of new bonds were made with the restricting MHC molecule rather than with the peptide. These results do not support the suggestion that improved CDR3 loop/peptide contacts is a general structural feature of high-affinity TCRs that retain peptide specificity (Colf et al., 2007; Sami et al., 2007). This unanticipated and interesting observation begged further exploration in order to

understand the mechanism that allowed the unexpected maintenance of peptide specificity.

7.1.3 A novel thermodynamic mechanism mediates high-affinity TCR specificity

The exquisite peptide specificity we observed for $\alpha 24\beta 17$ TCR (**Chapter 4**) could not be explained by the final structure of the complexes or by movements in pMHC required to accommodate TCR binding. We therefore examined the thermodynamics of binding and discovered a surprising result, that specificity can be mediated by changes in solvent interactions between the TCR and the pMHC occurring through a knock-on effect in modifications to the peptide sequence. Unfortunately, it was not possible to witness these altered interactions in real-time as no technique exists for visualising such rearrangements.

My results are consistent with a model for T-cell antigen recognition in which TCR/peptide scanning permits TCR/MHC engagement (Borg et al., 2005; Rudolph et al., 2006; Tynan et al., 2005; Tynan et al., 2007). As such my results fail to support the current “two-step model” postulating that the germline-encoded elements of the TCR and pMHC engage prior to peptide scanning by the hypervariable CDR3-loops (Wu et al., 2002).

7.1.4 A new molecular mechanism of TCR/pMHC recognition

The first clinical studies of genetically modified autologous PBLs expressing MART-1 specific TCRs (DMF4 or DMF5) adoptively transferred into melanoma patients (Johnson et al., 2009; Morgan et al., 2006) have established that TCR gene

therapy is achievable and safe in a clinical setting. However, the low response rates for objective cancer regression of 13% (Morgan et al., 2006) and 30% (Johnson et al., 2009) suggest that there is room for significant improvement of the technique.

Structures of the DMF4 and the DMF5 TCRs complexed with the heteroclitic MART-1 decamer (ELAGIGILTV) and the natural MART-1 nonamer (AAGIGILTV) presented by HLA-A2 have been recently solved (Borbulevych et al., 2011). Borbulevych et al. observed that, upon A2-AAG recognition, both TCRs induced a peptide conformational change so that the nonamer mimicked the heteroclitic decamer, a mechanism first described as “peptide induced-fit molecular mimicry” by Macdonald et al. (Macdonald et al., 2009). However, the molecular mimicry was imperfect due to the additional glutamic acid in the decamer and the difference in the peptide anchor positions ($P2^{\text{Leu}}$ for ELA and $P2^{\text{Ala}}$ for AAG) (Borbulevych et al., 2011). Here, I reported a novel peptide anchor residue switch from $P2^{\text{Ala}}$ to $P1^{\text{Ala}}$ upon MEL5 TCR ligation of A2-AAG. This “molecular switch” led to a nearly identical bulged ELA, EAA and AAG peptide conformation. The anchor position switch explains the ability of MEL5 to bind to A2-AAG with a higher affinity compared to all other published melanoma specific TCRs including Mel187.c5, DMF4 and DMF5 (Borbulevych et al., 2011; Ekeruche-Makinde et al., 2012; Insaïdoo et al., 2011). The AAG nonamer peptide is believed to be the dominant species at the melanoma surface (Skipper et al., 1999). Thus, the low response rates observed in the clinical trials might be due to poor recognition of the AAG nonamer. MEL5 T-cells are effective at recognising the AAG peptide and in lysing melanoma cells. I therefore conclude that use of a MEL5-like TCR would be

likely to result in a higher clinical response rate than observed with either DMF4 or DMF5 TCRs.

7.1.5 Heteroclitic peptides can alter T-cell antigen specificity due to changes at the atomic level

The identification of the tumour-associated antigens (TAAs) (van der Bruggen et al., 1991) suggested that therapeutic vaccination to target these antigens might be an effective treatment for cancer. Unfortunately, the early optimism about this approach has not been realised. The majority of tumour antigens are derived from self-proteins and T-cells with high affinity TCRs against such antigens are likely to be culled during thymic selection.

In order to break tolerance, development of melanoma vaccines in the HLA-A2-restricted MART-1 system has focused on heteroclitic antigens that have been optimized for HLA-A2 binding (Sliz et al., 2001; Valmori et al., 1998). Such peptides are likely to be presented at a substantially higher surface density compared to the natural antigens with a poor N-terminal anchor for HLA-A2. This increased density is likely to have greater potential for T-cell stimulation and the breaking of peripheral tolerance mechanisms. Indeed, the heteroclitic ELA version of the MART-1 antigen primes the biggest population of T-cells seen to date in HLA-A2⁺ humans and this system has become the model of choice for the study of human T-cell priming (Challier et al., 2012; Dutoit et al., 2002; Valmori et al., 1998). However, my laboratory recently described how TCRs can distinguish between the heteroclitic decamer peptide ELA and the natural progenitor EAA (Cole et al., 2010). These results suggest that the HLA-A2-ELA must be viewed as a non-self

structure - in part explaining why T-cell responses against this supposedly ‘self’ antigen can be so strong. To date, the structural difference between HLA-A2-EAA and HLA-A2-ELA has only been inferred from differences in TCR binding to these to molecules. I aimed to see this difference by solving the structure of the MEL5/HLA-A2-EAA structure. Comparison of this structure to the previously solved MEL5/HLA-A2-ELA structure showed the improved anchoring provided by position Leu^{P2} reduced peptide flexibility and altered the bonding with MEL5 TCR compared to the Ala^{P2} natural peptide. Collectively, the results reported here suggest that the failure of the vaccination trials using the heteroclitic ELA was due to the primed T-cells being unable to recognize the flexible EAA and AAG natural MART-1 antigens. The use of anchor-modified heteroclitic peptides for vaccination thus requires further re-evaluation (Cole et al., 2010; Ekeruche-Makinde et al., 2012; Speiser et al., 2008). Nevertheless, a recent study from my laboratory demonstrated that it is possible to design altered peptide antigens for the selection of T-cell clonotypes with enhanced specific antigen recognition by using an approach termed TOPSORT (“TCR-optimized peptide skewing of the repertoire of T-cells”) (Ekeruche-Makinde et al., 2012). This approach uses a TCR-optimized peptide (TOP) for a “good” T-cell clonotype like MEL5 in order to skew the repertoire of T-cells towards more effective T-cell clonotypes. In short, TOPSORT is an approach aimed to sort the top T-cell clonotypes in a given situation (Sewell, 2012).

Interestingly, vaccination with EAA peptide induced T-cells with superior lytic activity against tumour cells compared to those induced by vaccination with ELA peptide (Speiser et al., 2008). To date, there have been no trials with the dominant natural nonamer AAG peptide. I hypothesise that vaccination with this antigen will

produce a better outcome and I hope that such trials are initiated soon. Our collaborators at the Danish Cancer Immunotherapy Centre are currently trying to raise funding for such a trial.

7.1.6 MEL5 TCR gene transfer generates melanoma-specific T-cells

The superior affinity of MEL5 for HLA-A2-AAG compared to other TCRs that have been used in therapeutic approaches against melanoma to date combines with data showing that this peptide is the dominant species at the melanoma surface (Derre et al., 2007; Held et al., 2007; Michaeli et al., 2009; Skipper et al., 1999) to suggest that therapeutic approaches that used MEL5-like TCRs would have better response rates than the trials undertaken to date. I therefore completed my studies by examining how the MEL5 TCR performed in TCR gene transfer experiments. My unique access to MEL5 TCR variants with a range of affinities for cognate antigen also allowed me to establish what the optimal TCR affinity was for recognition of antigen in this system.

MEL5 TCR gene transfer into CD8⁺ T-cells resulted in the generation of cells with the required antigen specificity. Crucially, these cells were also able to kill real melanoma targets suggesting that they recognise natural levels of the natural peptide(s) presented at the melanoma surface.

7.1.7 Detrimental motifs can be introduced during TCR affinity maturation

Phage display has been used extensively to identify and affinity mature antibodies (Richman and Kranz, 2007). TCR affinity maturation was enabled thanks to the “Boulter-disulphide” method of pairing TCR α and β chains using a non-natural,

TCR constant domain-internal disulphide bond. Excitingly, my laboratory has just demonstrated how such affinity-enhanced TCRs can be used to induce tumour regression as soluble molecules (Liddy et al., 2012). My laboratory has also shown how such TCRs could be useful in gene therapy approaches to HIV infection (Varela-Rohena et al., 2008).

In order to examine high-affinity TCRs in the MART-1 system, I obtained a panel of MART-1-specific TCRs that exhibited a range of affinity for cognate antigen. These TCRs were generated by a phage display and directed evolution process originally described by Boulter and colleagues (Li et al., 2005b). One of these TCRs failed to confer specificity for the cognate antigen despite being expressed at the cell surface (as determined by CD3 expression in TCR-negative Jurkat cells). Subsequent close examination of the altered sequence of this TCR revealed that the process of TCR affinity maturation had introduced an N-linked glycosylation site into the TCR β chain CDR3 loop. As protein glycosylation rarely occurs in *E. coli* (Benz and Schmidt, 2001; Lindenthal and Elsinghorst, 1999; Sherlock et al., 2006), addition of this motif did not cause a problem prior to expression in eukaryotic cells and I had not considered such problems prior to building the lentiviral construct to express this TCR in T-cells. TCRs expressed in T-cells undergo post-translational modifications such as glycosylation prior to expression on the T-cell surface (Moremen et al., 2012). The presence of oligosaccharides on the CDR loops is likely to abolish the TCR/pMHC interaction by blocking the TCR access to the pMHC surface as observed with the MEL5 β 13 TCR. Therefore, my results demonstrated that, when enhancing TCR affinity by phage display for a use in TCR gene transfer, particular attention should be paid to the presence of motifs that might add post-translational

modifications to the protein of interest or that introduce other potentially problematic sequences such as protease sites.

7.1.8 An optimal TCR affinity for TCR gene therapy against melanoma

I used a panel of enhanced affinity TCRs derived from MEL5 to determine the optimal TCR affinity for TCR gene transfer directed against melanoma. Because TCR gene transfer of high-affinity TCRs could lead to a loss of specificity (Holler et al., 2003; Robbins et al., 2008; Udyavar et al., 2009; Zhao et al., 2007) and/or a loss of effector functions (Irving et al., 2012; Schmid et al., 2010; Stone et al., 2009), I used a panel of TCRs with a range of affinities ($K_D = 0.54\text{-}29\ \mu\text{M}$) within the natural range ($K_D = 0.1\text{-}270\ \mu\text{M}$). Preliminary results were promising, showing that a 6-fold enhancement over the wild-type affinity produced T-cells that were substantially more responsive to cognate antigen than T-cells transduced with wild-type TCR. As described before (Irving et al., 2012; Schmid et al., 2010), self-specific TCR affinity may not need to be optimized beyond a given affinity threshold as above the optimal affinity transduced T-cells displayed a gradual attenuation in activity. The attenuation in T-cell activity with higher affinity TCRs could be related to the longer off-rates of the high affinity TCRs inhibiting serial triggering during T-cell activation (Palmer and Naeher, 2009). Lower responsiveness might also be the result of T-cell/T-cell recognition; such a situation has recently been shown by my colleague Dr. Mai Ping Tan in several different systems (unpublished). In summary, my results suggest that enhancing the TCR affinity for cognate tumour antigen into the range normally reserved for interactions with non-self, pathogen-derived antigens could considerably improve the effectiveness of TCR gene transfer therapy.

7.2 PERSPECTIVES

The new mechanism for conferring TCR peptide specificity during antigen recognition by a high-affinity TCR was revealed by my in-depth structural and thermodynamic analyses. My results suggest that future TCR/pMHC studies should include these sorts of analyses in order to reveal new important molecular information of the nature of T-cell antigen recognition. It would be especially useful to obtain detailed thermodynamic parameters for all of the TCR/pMHC interactions for which both ligated and unligated TCR and/or pMHC structures are already available (Armstrong et al., 2008a; Rudolph et al., 2006). I think it is likely that the MEL5 example that I discovered will not be the only example of where a TCR maintains specificity through altered thermodynamics of binding and it remains possible that this mechanism of upholding TCR specificity is commonplace. It is well established that binding kinetics provides a wealth of information for rational drug design (De Mol and Fischer, 2008) and that an increase of water molecules at the interaction interface can extend the complementarity of the surfaces and increase the hydrogen bond networks (Ladbury, 1996; Perozzo et al., 2004). Moreover, it is increasingly acknowledged that there is a need for thermodynamic and kinetic studies to fully appreciate the properties of potential drug candidates (De Mol and Fischer, 2008; Henriques and Ladbury, 2001; Holdgate et al., 1997; Murphy and Freire, 1995). My results show that this need clearly extends to examination of TCR/pMHC interactions.

The next step in the development of the optimal TCR for TCR gene transfer will be to use a CD8⁺ T-cell model. One major concern is the effect that TCR affinity enhancements could have on self-tolerance of T-cells that have not undergone

thymic auditioning. Artificial engineering of TCR sequences might lead to altered peptide specificity and the possibility of autoimmunity. The preferred peptide landscape recognised by CD8⁺ T-cells transduced with MEL5 TCR was tested by PS-CPL screening and compared with the MEL13 (equivalent to MEL5) T-cell clone. No macro level differences in TCR specificity were observed. My group has recently established that the CD8 glycoprotein controls TCR cross-reactivity (Wooldridge et al., 2010). Jurkat cells do not express CD8 so it will be interesting to see how introduction of this T-cell co-receptor alters the TCR affinity optima in the MEL5 system.

7.3 SUMMARY

Overall, the work reported in this thesis has improved our knowledge of TCR/pMHC interaction. The design of a specific TCR/pMHC crystallization screen led to the discovery of a new mechanism of TCR binding and TCR specificity. Important implications for melanoma therapy have been uncovered, such as the optimal TCR affinity for anti-melanoma TCR gene therapy and the unexpected maintenance of the exquisite specificity of a high-affinity anti-melanoma TCR via an unanticipated thermodynamic molecular mechanism. In conclusion, both soluble TCR therapy and TCR gene transfer therapy are showing great promise for the future treatment of cancer and careful evaluation in patients at several centres is now needed. Monoclonal antibodies accounted for >45% of all new drugs that came on the market in 2012. It is possible that drugs based around the other type of antigen receptor, the TCR, may come to eclipse even this phenomenal success so that TCR-based therapeutic approaches could become commonplace in a near future.

REFERENCES

- Adams E. J., Chien Y. H. and Garcia K. C. (2005) Structure of a gammadelta T cell receptor in complex with the nonclassical MHC T22. *Science* **308**, 227-31.
- Adler M. J. and Dimitrov D. S. (2012) Therapeutic antibodies against cancer. *Hematol Oncol Clin North Am* **26**, 447-81, vii.
- Agostini C., Trentin L., Zambello R., Bulian P., Siviero F., Masciarelli M., Festi G., Cipriani A. and Semenzato G. (1993) CD8 alveolitis in sarcoidosis: incidence, phenotypic characteristics, and clinical features. *Am J Med* **95**, 466-72.
- Alajez N. M., Eghtesad S. and Finn O. J. (2006) Cloning and expression of human membrane-bound and soluble engineered T cell receptors for immunotherapy. *J Biomed Biotechnol* **2006**, 68091.
- Alam S. M., Davies G. M., Lin C. M., Zal T., Nasholds W., Jameson S. C., Hogquist K. A., Gascoigne N. R. and Travers P. J. (1999) Qualitative and quantitative differences in T cell receptor binding of agonist and antagonist ligands. *Immunity* **10**, 227-37.
- Alam S. M., Travers P. J., Wung J. L., Nasholds W., Redpath S., Jameson S. C. and Gascoigne N. R. (1996) T-cell-receptor affinity and thymocyte positive selection. *Nature* **381**, 616-20.
- Alarcon B., Mestre D. and Martinez-Martin N. (2011) The immunological synapse: a cause or consequence of T-cell receptor triggering? *Immunology* **133**, 420-5.
- Alli R., Nguyen P., Boyd K., Sundberg J. P. and Geiger T. L. (2012) A mouse model of clonal CD8+ T lymphocyte-mediated alopecia areata progressing to alopecia universalis. *J Immunol* **188**, 477-86.
- Alli R., Zhang Z. M., Nguyen P., Zheng J. J. and Geiger T. L. (2011) Rational design of T cell receptors with enhanced sensitivity for antigen. *PLoS One* **6**, e18027.
- Amon M. A., Ali M., Bender V., Chan Y. N., Toth I. and Manolios N. (2006) Lipidation and glycosylation of a T cell antigen receptor (TCR) transmembrane hydrophobic peptide dramatically enhances in vitro and in vivo function. *Biochim Biophys Acta* **1763**, 879-88.
- Armstrong K. M., Insaïdo F. K. and Baker B. M. (2008a) Thermodynamics of T-cell receptor-peptide/MHC interactions: progress and opportunities. *J Mol Recognit* **21**, 275-87.
- Armstrong K. M., Piepenbrink K. H. and Baker B. M. (2008b) Conformational changes and flexibility in T-cell receptor recognition of peptide-MHC complexes. *Biochem J* **415**, 183-96.
- Arstila T. P., Casrouge A., Baron V., Even J., Kanellopoulos J. and Kourilsky P. (1999) A direct estimate of the human alpha beta T cell receptor diversity. *Science* **286**, 958-61.
- Asherie N. (2004) Protein crystallization and phase diagrams. *Methods* **34**, 266-72.
- Auphan-Anezin N., Mazza C., Guimezanes A., Barrett-Wilt G. A., Montero-Julian F., Roussel A., Hunt D. F., Malissen B. and Schmitt-Verhulst A. M. (2006) Distinct orientation of the alloreactive monoclonal CD8 T cell activation program by three different peptide/MHC complexes. *Eur J Immunol* **36**, 1856-66.
- Banham A. H. and Smith G. L. (1993) Characterization of vaccinia virus gene B12R. *J Gen Virol* **74** (Pt 12), 2807-12.

- Barber E. K., Dasgupta J. D., Schlossman S. F., Trevillyan J. M. and Rudd C. E. (1989) The CD4 and CD8 antigens are coupled to a protein-tyrosine kinase (p56lck) that phosphorylates the CD3 complex. *Proc Natl Acad Sci U S A* **86**, 3277-81.
- Beck A., Haeuw J. F., Wurch T., Goetsch L., Bailly C. and Corvaia N. (2010a) The next generation of antibody-drug conjugates comes of age. *Discov Med* **10**, 329-39.
- Beck A., Wurch T., Bailly C. and Corvaia N. (2010b) Strategies and challenges for the next generation of therapeutic antibodies. *Nat Rev Immunol* **10**, 345-52.
- Beddoe T., Chen Z., Clements C. S., Ely L. K., Bushell S. R., Vivian J. P., Kjer-Nielsen L., Pang S. S., Dunstone M. A., Liu Y. C., Macdonald W. A., Perugini M. A., Wilce M. C., Burrows S. R., Purcell A. W., Tiganis T., Bottomley S. P., McCluskey J. and Rossjohn J. (2009) Antigen ligation triggers a conformational change within the constant domain of the alphabeta T cell receptor. *Immunity* **30**, 777-88.
- Belmont H. J., Price-Schiavi S., Liu B., Card K. F., Lee H. I., Han K. P., Wen J., Tang S., Zhu X., Merrill J., Chavillaz P. A., Wong J. L., Rhode P. R. and Wong H. C. (2006) Potent antitumor activity of a tumor-specific soluble TCR/IL-2 fusion protein. *Clin Immunol* **121**, 29-39.
- Bendle G. M., Haanen J. B. and Schumacher T. N. (2009) Preclinical development of T cell receptor gene therapy. *Curr Opin Immunol* **21**, 209-14.
- Bendle G. M., Linnemann C., Hooijkaas A. I., Bies L., de Witte M. A., Jorritsma A., Kaiser A. D., Pouw N., Debets R., Kieback E., Uckert W., Song J. Y., Haanen J. B. and Schumacher T. N. (2010) Lethal graft-versus-host disease in mouse models of T cell receptor gene therapy. *Nat Med* **16**, 565-70, 1p following 570.
- Benz I. and Schmidt M. A. (2001) Glycosylation with heptose residues mediated by the aah gene product is essential for adherence of the AIDA-I adhesin. *Mol Microbiol* **40**, 1403-13.
- Bins A., Mallo H., Sein J., van den Bogaard C., Nooijen W., Vyth-Dreese F., Nuijen B., de Gast G. C. and Haanen J. B. (2007) Phase I clinical study with multiple peptide vaccines in combination with tetanus toxoid and GM-CSF in advanced-stage HLA-A*0201-positive melanoma patients. *J Immunother* **30**, 234-9.
- Bjorkman P. J. (1997) MHC restriction in three dimensions: a view of T cell receptor/ligand interactions. *Cell* **89**, 167-70.
- Bluestone J. A., Mackay C. R., O'Shea J. J. and Stockinger B. (2009) The functional plasticity of T cell subsets. *Nat Rev Immunol* **9**, 811-6.
- Blundell T. L. and Johnson L. N. (1976) *Protein Crystallography*. Academic Press.
- Bobisse S., Rondina M., Merlo A., Tisato V., Mandruzzato S., Amendola M., Naldini L., Willemsen R. A., Debets R., Zanovello P. and Rosato A. (2009) Reprogramming T lymphocytes for melanoma adoptive immunotherapy by T-cell receptor gene transfer with lentiviral vectors. *Cancer Res* **69**, 9385-94.
- Boehm T. (2011) Design principles of adaptive immune systems. *Nat Rev Immunol* **11**, 307-17.
- Boniface J. J., Rabinowitz J. D., Wulfig C., Hampl J., Reich Z., Altman J. D., Kantor R. M., Beeson C., McConnell H. M. and Davis M. M. (1998) Initiation of signal transduction through the T cell receptor requires the multivalent engagement of peptide/MHC ligands [corrected]. *Immunity* **9**, 459-66.

- Bonilla F. A. and Oettgen H. C. (2010) Adaptive immunity. *J Allergy Clin Immunol* **125**, S33-40.
- Boon T., Coulie P. G., Van den Eynde B. J. and van der Bruggen P. (2006) Human T cell responses against melanoma. *Annu Rev Immunol* **24**, 175-208.
- Borbulevych O. Y., Insaïdoo F. K., Baxter T. K., Powell D. J., Jr., Johnson L. A., Restifo N. P. and Baker B. M. (2007) Structures of MART-126/27-35 Peptide/HLA-A2 complexes reveal a remarkable disconnect between antigen structural homology and T cell recognition. *J Mol Biol* **372**, 1123-36.
- Borbulevych O. Y., Piepenbrink K. H., Gloor B. E., Scott D. R., Sommese R. F., Cole D. K., Sewell A. K. and Baker B. M. (2009) T cell receptor cross-reactivity directed by antigen-dependent tuning of peptide-MHC molecular flexibility. *Immunity* **31**, 885-96.
- Borbulevych O. Y., Santhanagopalan S. M., Hossain M. and Baker B. M. (2011) TCRs used in cancer gene therapy cross-react with MART-1/Melan-A tumor antigens via distinct mechanisms. *J Immunol* **187**, 2453-63.
- Borg N. A., Ely L. K., Beddoe T., Macdonald W. A., Reid H. H., Clements C. S., Purcell A. W., Kjer-Nielsen L., Miles J. J., Burrows S. R., McCluskey J. and Rossjohn J. (2005) The CDR3 regions of an immunodominant T cell receptor dictate the 'energetic landscape' of peptide-MHC recognition. *Nat Immunol* **6**, 171-80.
- Borg N. A., Wun K. S., Kjer-Nielsen L., Wilce M. C., Pellicci D. G., Koh R., Besra G. S., Bharadwaj M., Godfrey D. I., McCluskey J. and Rossjohn J. (2007) CD1d-lipid-antigen recognition by the semi-invariant NKT T-cell receptor. *Nature* **448**, 44-9.
- Bosselut R. (2004) CD4/CD8-lineage differentiation in the thymus: from nuclear effectors to membrane signals. *Nat Rev Immunol* **4**, 529-40.
- Bossi S., Ferranti B., Martinelli C., Capasso P. and de Marco A. (2010) Antibody-mediated purification of co-expressed antigen-antibody complexes. *Protein Expr Purif* **72**, 55-8.
- Boulter J. M., Glick M., Todorov P. T., Baston E., Sami M., Rizkallah P. and Jakobsen B. K. (2003) Stable, soluble T-cell receptor molecules for crystallization and therapeutics. *Protein Eng* **16**, 707-11.
- Boulter J. M., Schmitz N., Sewell A. K., Godkin A. J., Bachmann M. F. and Gallimore A. M. (2007) Potent T cell agonism mediated by a very rapid TCR/pMHC interaction. *Eur J Immunol* **37**, 798-806.
- Bowley D. R., Labrijn A. F., Zwick M. B. and Burton D. R. (2007) Antigen selection from an HIV-1 immune antibody library displayed on yeast yields many novel antibodies compared to selection from the same library displayed on phage. *Protein Eng Des Sel* **20**, 81-90.
- Brekke O. H. and Sandlie I. (2003) Therapeutic antibodies for human diseases at the dawn of the twenty-first century. *Nat Rev Drug Discov* **2**, 52-62.
- Brennan P. J., Tatituri R. V., Brigl M., Kim E. Y., Tuli A., Sanderson J. P., Gadola S. D., Hsu F. F., Besra G. S. and Brenner M. B. (2012) Invariant natural killer T cells recognize lipid self antigen induced by microbial danger signals. *Nat Immunol* **12**, 1202-11.
- Bridgeman J. S., Sewell A. K., Miles J. J., Price D. A. and Cole D. K. (2011) Structural and biophysical determinants of alphabeta T-cell antigen recognition. *Immunology* **135**, 9-18.

- Bridgeman J. S., Sewell A. K., Miles J. J., Price D. A. and Cole D. K. (2012) Structural and biophysical determinants of alphabeta T-cell antigen recognition. *Immunology* **135**, 9-18.
- Broughton S. E., Petersen J., Theodossis A., Scally S. W., Loh K. L., Thompson A., van Bergen J., Kooy-Winkelaar Y., Henderson K. N., Beddoe T., Tye-Din J. A., Mannering S. I., Purcell A. W., McCluskey J., Anderson R. P., Koning F., Reid H. H. and Rossjohn J. (2012) Biased T cell receptor usage directed against human leukocyte antigen DQ8-restricted gliadin peptides is associated with celiac disease. *Immunity* **37**, 611-21.
- Brunger A. T. (1992) Free R Value: A Novel Statistical Quantity for Assessing the Accuracy of Crystal Structures. *Nature* **355**, 472-475.
- Bukowski J. F., Morita C. T. and Brenner M. B. (1994) Recognition and destruction of virus-infected cells by human gamma delta CTL. *J Immunol* **153**, 5133-40.
- Bulek A. M., Cole D. K., Skowera A., Dolton G., Gras S., Madura F., Fuller A., Miles J. J., Gostick E., Price D. A., Drijfhout J. W., Knight R. R., Huang G. C., Lissin N., Molloy P. E., Wooldridge L., Jakobsen B. K., Rossjohn J., Peakman M., Rizkallah P. J. and Sewell A. K. (2012a) Structural basis for the killing of human beta cells by CD8(+) T cells in type 1 diabetes. *Nat Immunol* **13**, 283-9.
- Bulek A. M., Madura F., Fuller A., Holland C. J., Schauenburg A. J., Sewell A. K., Rizkallah P. J. and Cole D. K. (2012b) TCR/pMHC Optimized Protein crystallization Screen. *J Immunol Methods* **382**, 203-10.
- Burrows S. R., Chen Z., Archbold J. K., Tynan F. E., Beddoe T., Kjer-Nielsen L., Miles J. J., Khanna R., Moss D. J., Liu Y. C., Gras S., Kostenko L., Brennan R. M., Clements C. S., Brooks A. G., Purcell A. W., McCluskey J. and Rossjohn J. (2009) Hard wiring of T cell receptor specificity for the major histocompatibility complex is underpinned by TCR adaptability. *Proc Natl Acad Sci U S A* **107**, 10608-13.
- Card K. F., Price-Schiavi S. A., Liu B., Thomson E., Nieves E., Belmont H., Builes J., Jiao J. A., Hernandez J., Weidanz J., Sherman L., Francis J. L., Amirhosravi A. and Wong H. C. (2004) A soluble single-chain T-cell receptor IL-2 fusion protein retains MHC-restricted peptide specificity and IL-2 bioactivity. *Cancer Immunol Immunother* **53**, 345-57.
- Cavani A., Pennino D. and Eyerich K. (2012) Th17 and Th22 in skin allergy. *Chem Immunol Allergy* **96**, 39-44.
- Ccp. (1994) The CCP4 suite: programs for protein crystallography. *Acta Crystallogr D Biol Crystallogr* **50**, 760-763.
- Challier J., Bruniquel D., Sewell A. K. and Laugel B. (2012) Adenosine and cAMP signaling skew human dendritic cell differentiation towards a tolerogenic phenotype with defective CD8(+) T-cell priming capacity. *Immunology*.
- Chang H. C., Bao Z., Yao Y., Tse A. G., Goyarts E. C., Madsen M., Kawasaki E., Brauer P. P., Sacchettini J. C., Nathenson S. G. and et al. (1994) A general method for facilitating heterodimeric pairing between two proteins: application to expression of alpha and beta T-cell receptor extracellular segments. *Proc Natl Acad Sci U S A* **91**, 11408-12.
- Chang S. C., Momburg F., Bhutani N. and Goldberg A. L. (2005) The ER aminopeptidase, ERAP1, trims precursors to lengths of MHC class I peptides by a "molecular ruler" mechanism. *Proc Natl Acad Sci U S A* **102**, 17107-12.
- Chaplin D. D. (2010) Overview of the immune response. *J Allergy Clin Immunol* **125**, S3-23.

- Chari R. V. (2008) Targeted cancer therapy: conferring specificity to cytotoxic drugs. *Acc Chem Res* **41**, 98-107.
- Chayen N. E. and Saridakis E. (2008) Protein crystallization: from purified protein to diffraction-quality crystal. *Nat Methods* **5**, 147-53.
- Chen J. L., Stewart-Jones G., Bossi G., Lissin N. M., Wooldridge L., Choi E. M., Held G., Dunbar P. R., Esnouf R. M., Sami M., Boulter J. M., Rizkallah P., Renner C., Sewell A., van der Merwe P. A., Jakobsen B. K., Griffiths G., Jones E. Y. and Cerundolo V. (2005) Structural and kinetic basis for heightened immunogenicity of T cell vaccines. *J Exp Med* **201**, 1243-55.
- Chervin A. S., Aggen D. H., Raseman J. M. and Kranz D. M. (2008) Engineering higher affinity T cell receptors using a T cell display system. *J Immunol Methods* **339**, 175-84.
- Clynes R. A., Towers T. L., Presta L. G. and Ravetch J. V. (2000) Inhibitory Fc receptors modulate in vivo cytotoxicity against tumor targets. *Nat Med* **6**, 443-6.
- Cohen C. J., Zhao Y., Zheng Z., Rosenberg S. A. and Morgan R. A. (2006) Enhanced antitumor activity of murine-human hybrid T-cell receptor (TCR) in human lymphocytes is associated with improved pairing and TCR/CD3 stability. *Cancer Res* **66**, 8878-86.
- Cohen C. J., Zheng Z., Bray R., Zhao Y., Sherman L. A., Rosenberg S. A. and Morgan R. A. (2005) Recognition of fresh human tumor by human peripheral blood lymphocytes transduced with a bicistronic retroviral vector encoding a murine anti-p53 TCR. *J Immunol* **175**, 5799-808.
- Cole D. K., Dunn S. M., Sami M., Boulter J. M., Jakobsen B. K. and Sewell A. K. (2008) T cell receptor engagement of peptide-major histocompatibility complex class I does not modify CD8 binding. *Mol Immunol* **45**, 2700-9.
- Cole D. K., Edwards E. S., Wynn K. K., Clement M., Miles J. J., Ladell K., Ekeruche J., Gostick E., Adams K. J., Skowera A., Peakman M., Wooldridge L., Price D. A. and Sewell A. K. (2010) Modification of MHC anchor residues generates heteroclitic peptides that alter TCR binding and T cell recognition. *J Immunol* **185**, 2600-10.
- Cole D. K., Pumphrey N. J., Boulter J. M., Sami M., Bell J. I., Gostick E., Price D. A., Gao G. F., Sewell A. K. and Jakobsen B. K. (2007) Human TCR-Binding Affinity is Governed by MHC Class Restriction. *J Immunol* **178**, 5727-34.
- Cole D. K., Yuan F., Rizkallah P. J., Miles J. J., Gostick E., Price D. A., Gao G. F., Jakobsen B. K. and Sewell A. K. (2009) Germ line-governed recognition of a cancer epitope by an immunodominant human T-cell receptor. *J Biol Chem* **284**, 27281-9.
- Colf L. A., Bankovich A. J., Hanick N. A., Bowerman N. A., Jones L. L., Kranz D. M. and Garcia K. C. (2007) How a single T cell receptor recognizes both self and foreign MHC. *Cell* **129**, 135-46.
- Collaborative Computational Project N. (1994) The CCP4 suite: programs for protein crystallography. *Acta Crystallogr D Biol Crystallogr* **50**, 760-3.
- Coombs D., Kalergis A. M., Nathenson S. G., Wofsy C. and Goldstein B. (2002) Activated TCRs remain marked for internalization after dissociation from pMHC. *Nat Immunol* **3**, 926-31.
- Cooper A. (2005) Heat capacity effects in protein folding and ligand binding: a re-evaluation of the role of water in biomolecular thermodynamics. *Biophys Chem* **115**, 89-97.

- Croft M., Carter L., Swain S. L. and Dutton R. W. (1994) Generation of polarized antigen-specific CD8 effector populations: reciprocal action of interleukin (IL)-4 and IL-12 in promoting type 2 versus type 1 cytokine profiles. *J Exp Med* **180**, 1715-28.
- Croxford J. L., Miyake S., Huang Y. Y., Shimamura M. and Yamamura T. (2006) Invariant V(alpha)19i T cells regulate autoimmune inflammation. *Nat Immunol* **7**, 987-94.
- Daniel C., Horvath S. and Allen P. M. (1998) A basis for alloreactivity: MHC helical residues broaden peptide recognition by the TCR. *Immunity* **8**, 543-52.
- Davis-Harrison R. L., Armstrong K. M. and Baker B. M. (2005) Two different T cell receptors use different thermodynamic strategies to recognize the same peptide/MHC ligand. *J Mol Biol* **346**, 533-50.
- Davis D. M. and Dustin M. L. (2004) What is the importance of the immunological synapse? *Trends Immunol* **25**, 323-7.
- Davis M. M. and Bjorkman P. J. (1988) T-cell antigen receptor genes and T-cell recognition. *Nature* **334**, 395-402.
- Davis M. M., Boniface J. J., Reich Z., Lyons D., Hampl J., Arden B. and Chien Y. (1998) Ligand recognition by alpha beta T cell receptors. *Annu Rev Immunol* **16**, 523-44.
- Davis S. J. and van der Merwe P. A. (1996) The structure and ligand interactions of CD2: implications for T-cell function. *Immunol Today* **17**, 177-87.
- Davodeau F., Peyrat M. A., Necker A., Dominici R., Blanchard F., Leget C., Gaschet J., Costa P., Jacques Y., Godard A., Vie H., Poggi A., Romagne F. and Bonneville M. (1997) Close phenotypic and functional similarities between human and murine alphabeta T cells expressing invariant TCR alpha-chains. *J Immunol* **158**, 5603-11.
- De Mol N. J. and Fischer M. J. E. (2008) Kinetic and Thermodynamic Analysis of Ligand-Receptor Interactions: SPR Applications in Drug Development. In *Hanbook of Surface Plasmon Resonance* (Edited by Schasfoort R. B. M. and Tudos A. J.), p. 123-172. RSCPublishing.
- Degano M., Garcia K. C., Apostolopoulos V., Rudolph M. G., Teyton L. and Wilson I. A. (2000) A functional hot spot for antigen recognition in a superagonist TCR/MHC complex. *Immunity* **12**, 251-61.
- Delano. (2002) The PyMOL Molecular Graphics System, Version 1.2r3pre, Schrödinger, LLC.
- Delves P. J. and Roitt I. M. (2000a) The immune system. First of two parts. *N Engl J Med* **343**, 37-49.
- Delves P. J. and Roitt I. M. (2000b) The immune system. Second of two parts. *N Engl J Med* **343**, 108-17.
- Demaison C., Parsley K., Brouns G., Scherr M., Battmer K., Kinnon C., Grez M. and Thrasher A. J. (2002) High-level transduction and gene expression in hematopoietic repopulating cells using a human immunodeficiency virus type 1-based lentiviral vector containing an internal spleen focus forming virus promoter. *Hum Gene Ther* **13**, 803-13.
- Dembic Z., Haas W., Weiss S., McCubrey J., Kiefer H., von Boehmer H. and Steinmetz M. (1986) Transfer of specificity by murine alpha and beta T-cell receptor genes. *Nature* **320**, 232-8.
- Deng L., Langley R. J., Brown P. H., Xu G., Teng L., Wang Q., Gonzales M. I., Callender G. G., Nishimura M. I., Topalian S. L. and Mariuzza R. A. (2007)

- Structural basis for the recognition of mutant self by a tumor-specific, MHC class II-restricted T cell receptor. *Nat Immunol* **8**, 398-408.
- Derre L., Ferber M., Touvrey C., Devedre E., Zoete V., Leimgruber A., Romero P., Michielin O., Levy F. and Speiser D. E. (2007) A novel population of human melanoma-specific CD8 T cells recognizes Melan-AMART-1 immunodominant nonapeptide but not the corresponding decapeptide. *J Immunol* **179**, 7635-45.
- Ding Y. H., Baker B. M., Garboczi D. N., Biddison W. E. and Wiley D. C. (1999) Four A6-TCR/peptide/HLA-A2 structures that generate very different T cell signals are nearly identical. *Immunity* **11**, 45-56.
- Ding Y. H., Smith K. J., Garboczi D. N., Utz U., Biddison W. E. and Wiley D. C. (1998) Two human T cell receptors bind in a similar diagonal mode to the HLA-A2/Tax peptide complex using different TCR amino acids. *Immunity* **8**, 403-11.
- Dong C. and Martinez G. J. (2010) T cells: the usual subsets. *Nature*.
- Dull T., Zufferey R., Kelly M., Mandel R. J., Nguyen M., Trono D. and Naldini L. (1998) A third-generation lentivirus vector with a conditional packaging system. *J Virol* **72**, 8463-71.
- Dunn S. M., Rizkallah P. J., Baston E., Mahon T., Cameron B., Moysey R., Gao F., Sami M., Boulter J., Li Y. and Jakobsen B. K. (2006) Directed evolution of human T cell receptor CDR2 residues by phage display dramatically enhances affinity for cognate peptide-MHC without increasing apparent cross-reactivity. *Protein Sci* **15**, 710-21.
- Dushek O., Das R. and Coombs D. (2009) A role for rebinding in rapid and reliable T cell responses to antigen. *PLoS Comput Biol* **5**, e1000578.
- Dutoit V., Rubio-Godoy V., Pittet M. J., Zippelius A., Dietrich P. Y., Legal F. A., Guillaume P., Romero P., Cerottini J. C., Houghten R. A., Pinilla C. and Valmori D. (2002) Degeneracy of antigen recognition as the molecular basis for the high frequency of naive A2/Melan-a peptide multimer(+) CD8(+) T cells in humans. *J Exp Med* **196**, 207-16.
- Ekeruche-Makinde J., Clement M., Cole D. K., Edwards E. S., Ladell K., Miles J. J., Matthews K. K., Fuller A., Lloyd K. A., Madura F., Dolton G. M., Pentier J., Lissina A., Gostick E., Baxter T. K., Baker B. M., Rizkallah P. J., Price D. A., Wooldridge L. and Sewell A. K. (2012) T-Cell Receptor optimized peptide skewing of the T-cell repertoire can enhance antigen targeting. *J Biol Chem*.
- Ely L. K., Beddoe T., Clements C. S., Matthews J. M., Purcell A. W., Kjer-Nielsen L., McCluskey J. and Rossjohn J. (2006) Disparate thermodynamics governing T cell receptor-MHC-I interactions implicate extrinsic factors in guiding MHC restriction. *Proc Natl Acad Sci U S A* **103**, 6641-6.
- Emerman M. and Temin H. M. (1984) Genes with promoters in retrovirus vectors can be independently suppressed by an epigenetic mechanism. *Cell* **39**, 449-67.
- Emsley P. and Cowtan K. (2004) Coot: model-building tools for molecular graphics. *Acta Crystallogr D Biol Crystallogr* **60**, 2126-32.
- Engels B. and Uckert W. (2007) Redirecting T lymphocyte specificity by T cell receptor gene transfer--a new era for immunotherapy. *Mol Aspects Med* **28**, 115-42.
- Evans P. and McCoy A. (2008) An introduction to molecular replacement. *Acta Crystallogr D Biol Crystallogr* **64**, 1-10.

- Feng D., Bond C. J., Ely L. K., Maynard J. and Garcia K. C. (2007) Structural evidence for a germline-encoded T cell receptor-major histocompatibility complex interaction 'codon'. *Nat Immunol* **8**, 975-83.
- Fleischer B. (1984) Acquisition of specific cytotoxic activity by human T4+ T lymphocytes in culture. *Nature* **308**, 365-7.
- Follenzi A., Ailles L. E., Bakovic S., Geuna M. and Naldini L. (2000) Gene transfer by lentiviral vectors is limited by nuclear translocation and rescued by HIV-1 pol sequences. *Nat Genet* **25**, 217-22.
- Gadola S. D., Dulphy N., Salio M. and Cerundolo V. (2002) Valpha24-JalphaQ-independent, CD1d-restricted recognition of alpha-galactosylceramide by human CD4(+) and CD8alphabeta(+) T lymphocytes. *J Immunol* **168**, 5514-20.
- Gadola S. D., Koch M., Marles-Wright J., Lissin N. M., Shepherd D., Matulis G., Harlos K., Villiger P. M., Stuart D. I., Jakobsen B. K., Cerundolo V. and Jones E. Y. (2006) Structure and binding kinetics of three different human CD1d-alpha-galactosylceramide-specific T cell receptors. *J Exp Med* **203**, 699-710.
- Gagnon S. J., Borbulevych O. Y., Davis-Harrison R. L., Turner R. V., Damirjian M., Wojnarowicz A., Biddison W. E. and Baker B. M. (2006) T cell receptor recognition via cooperative conformational plasticity. *J Mol Biol* **363**, 228-43.
- Gapin L. (2009) Where do MAIT cells fit in the family of unconventional T cells? *PLoS Biol* **7**, e70.
- Gapin L. (2010) iNKT cell autoreactivity: what is 'self' and how is it recognized? *Nat Rev Immunol* **10**, 272-7.
- Garbi N., Tanaka S., Momburg F. and Hammerling G. J. (2006) Impaired assembly of the major histocompatibility complex class I peptide-loading complex in mice deficient in the oxidoreductase ERp57. *Nat Immunol* **7**, 93-102.
- Garboczi D. N., Ghosh P., Utz U., Fan Q. R., Biddison W. E. and Wiley D. C. (1996) Structure of the complex between human T-cell receptor, viral peptide and HLA-A2. *Nature* **384**, 134-41.
- Garcia K. C., Adams J. J., Feng D. and Ely L. K. (2009) The molecular basis of TCR germline bias for MHC is surprisingly simple. *Nat Immunol* **10**, 143-7.
- Garcia K. C., Degano M., Pease L. R., Huang M., Peterson P. A., Teyton L. and Wilson I. A. (1998) Structural basis of plasticity in T cell receptor recognition of a self peptide-MHC antigen. *Science* **279**, 1166-72.
- Garcia K. C., Degano M., Stanfield R. L., Brunmark A., Jackson M. R., Peterson P. A., Teyton L. and Wilson I. A. (1996) An alphabeta T cell receptor structure at 2.5 Å and its orientation in the TCR-MHC complex. *Science* **274**, 209-19.
- Garcia K. C., Teyton L. and Wilson I. A. (1999) Structural basis of T cell recognition. *Annu Rev Immunol* **17**, 369-97.
- Garman E. (1999) Cool data: quantity AND quality. *Acta Crystallogr D Biol Crystallogr* **55**, 1641-53.
- Garman E. and Murray J. W. (2003) Heavy-atom derivatization. *Acta Crystallogr D Biol Crystallogr* **59**, 1903-13.
- Govers C., Sebastyen Z., Coccoris M., Willemsen R. A. and Debets R. (2010) T cell receptor gene therapy: strategies for optimizing transgenic TCR pairing. *Trends Mol Med* **16**, 77-87.

- Grakoui A., Bromley S. K., Sumen C., Davis M. M., Shaw A. S., Allen P. M. and Dustin M. L. (1999) The immunological synapse: a molecular machine controlling T cell activation. *Science* **285**, 221-7.
- Gras S., Burrows S. R., Turner S. J., Sewell A. K., McCluskey J. and Rossjohn J. (2012) A structural voyage toward an understanding of the MHC-I-restricted immune response: lessons learned and much to be learned. *Immunol Rev* **250**, 61-81.
- Gregoire C., Malissen B. and Mazza G. (1996) Characterization of T cell receptor single-chain Fv fragments secreted by myeloma cells. *Eur J Immunol* **26**, 2410-6.
- Gura T. (2002) Therapeutic antibodies: magic bullets hit the target. *Nature* **417**, 584-6.
- Haeuw J. F., Caussanel V. and Beck A. (2009) [Immunoconjugates, drug-armed antibodies to fight against cancer]. *Med Sci (Paris)* **25**, 1046-52.
- Hahn M., Nicholson M. J., Pyrdol J. and Wucherpfennig K. W. (2005) Unconventional topology of self peptide-major histocompatibility complex binding by a human autoimmune T cell receptor. *Nat Immunol* **6**, 490-6.
- Halin C., Gafner V., Villani M. E., Borsi L., Berndt A., Kosmehl H., Zardi L. and Neri D. (2003) Synergistic therapeutic effects of a tumor targeting antibody fragment, fused to interleukin 12 and to tumor necrosis factor alpha. *Cancer Res* **63**, 3202-10.
- Hammer G. E., Gonzalez F., Champsaur M., Cado D. and Shastri N. (2006) The aminopeptidase ERAAP shapes the peptide repertoire displayed by major histocompatibility complex class I molecules. *Nat Immunol* **7**, 103-12.
- Hayday A. C. (2009) Gammadelta T cells and the lymphoid stress-surveillance response. *Immunity* **31**, 184-96.
- He Y. and Falto L. D., Jr. (2007) Lentivirus as a potent and mechanistically distinct vector for genetic immunization. *Curr Opin Mol Ther* **9**, 439-46.
- Held G., Wadle A., Dauth N., Stewart-Jones G., Sturm C., Thiel M., Zwick C., Dieckmann D., Schuler G., Hoogenboom H. R., Levy F., Cerundolo V., Pfreundschuh M. and Renner C. (2007) MHC-peptide-specific antibodies reveal inefficient presentation of an HLA-A*0201-restricted, Melan-A-derived peptide after active intracellular processing. *Eur J Immunol* **37**, 2008-17.
- Hemmer B., Vergelli M., Pinilla C., Houghten R. and Martin R. (1998) Probing degeneracy in T-cell recognition using peptide combinatorial libraries. *Immunol Today* **19**, 163-8.
- Hennecke J., Carfi A. and Wiley D. C. (2000) Structure of a covalently stabilized complex of a human alphabeta T-cell receptor, influenza HA peptide and MHC class II molecule, HLA-DR1. *EMBO J* **19**, 5611-24.
- Hennecke J. and Wiley D. C. (2002) Structure of a complex of the human alpha/beta T cell receptor (TCR) HA1.7, influenza hemagglutinin peptide, and major histocompatibility complex class II molecule, HLA-DR4 (DRA*0101 and DRB1*0401): insight into TCR cross-restriction and alloreactivity. *J Exp Med* **195**, 571-81.
- Henriques D. A. and Ladbury J. E. (2001) Inhibitors to the Src SH2 domain: a lesson in structure--thermodynamic correlation in drug design. *Arch Biochem Biophys* **390**, 158-68.
- Henze K. and Martin W. (2003) Evolutionary biology: essence of mitochondria. *Nature* **426**, 127-8.

- Hoare H. L., Sullivan L. C., Pietra G., Clements C. S., Lee E. J., Ely L. K., Beddoe T., Falco M., Kjer-Nielsen L., Reid H. H., McCluskey J., Moretta L., Rossjohn J. and Brooks A. G. (2006) Structural basis for a major histocompatibility complex class Ib-restricted T cell response. *Nat Immunol* **7**, 256-64.
- Holdgate G. A., Tunnicliffe A., Ward W. H., Weston S. A., Rosenbrock G., Barth P. T., Taylor I. W., Pauptit R. A. and Timms D. (1997) The entropic penalty of ordered water accounts for weaker binding of the antibiotic novobiocin to a resistant mutant of DNA gyrase: a thermodynamic and crystallographic study. *Biochemistry* **36**, 9663-73.
- Holland C. J., Rizkallah P. J., Vollers S., Calvo-Calle J. M., Madura F., Fuller A., Sewell A. K., Stern L. J., Godkin A. and Cole D. K. (2012) Minimal conformational plasticity enables TCR cross-reactivity to different MHC class II heterodimers. *Sci Rep* **2**, 629.
- Holler P. D., Chlewicki L. K. and Kranz D. M. (2003) TCRs with high affinity for foreign pMHC show self-reactivity. *Nat Immunol* **4**, 55-62.
- Holler P. D., Lim A. R., Cho B. K., Rund L. A. and Kranz D. M. (2001) CD8(-) T cell transfectants that express a high affinity T cell receptor exhibit enhanced peptide-dependent activation. *J Exp Med* **194**, 1043-52.
- Holton J. M. and Frankel K. A. (2010) The minimum crystal size needed for a complete diffraction data set. *Acta Crystallogr D Biol Crystallogr* **66**, 393-408.
- Homola J. (2003) Present and future of surface plasmon resonance biosensors. *Anal Bioanal Chem* **377**, 528-39.
- Housset D. and Malissen B. (2003) What do TCR-pMHC crystal structures teach us about MHC restriction and alloreactivity? *Trends Immunol* **24**, 429-37.
- Housset D., Mazza G., Gregoire C., Piras C., Malissen B. and Fontecilla-Camps J. C. (1997) The three-dimensional structure of a T-cell antigen receptor V alpha V beta heterodimer reveals a novel arrangement of the V beta domain. *EMBO J* **16**, 4205-16.
- Insaïdoo F. K., Borbulevych O. Y., Hossain M., Santhanagopalan S. M., Baxter T. K. and Baker B. M. (2011) Loss of T cell antigen recognition arising from changes in peptide and major histocompatibility complex protein flexibility: implications for vaccine design. *J Biol Chem* **286**, 40163-73.
- Inui N., Chida K., Suda T. and Nakamura H. (2001) TH1/TH2 and TC1/TC2 profiles in peripheral blood and bronchoalveolar lavage fluid cells in pulmonary sarcoidosis. *J Allergy Clin Immunol* **107**, 337-44.
- Irvine D. J., Purbhoo M. A., Krogsgaard M. and Davis M. M. (2002) Direct observation of ligand recognition by T cells. *Nature* **419**, 845-9.
- Irving M., Zoete V., Hebeisen M., Schmid D., Baumgartner P., Guillaume P., Romero P., Speiser D., Luescher I., Rufer N. and Michielin O. (2012) Interplay between T cell receptor binding kinetics and the level of cognate peptide presented by major histocompatibility complexes governs CD8+ T cell responsiveness. *J Biol Chem* **287**, 23068-78.
- Jancarik J. and Kim S. H. (1991) Sparse matrix sampling: a screening method for crystallization of proteins. *Journal of applied Crystallography* **24**, 409-411.
- Janin J. (1997) The kinetics of protein-protein recognition. *Proteins* **28**, 153-61.
- Jansson A. (2011) Kinetic proofreading and the search for nonself-peptides. *Self Nonself* **2**, 1-3.

- Jason-Moller L., Murphy M. and Bruno J. (2006) Overview of Biacore systems and their applications. *Curr Protoc Protein Sci* **Chapter 19**, Unit 19 13.
- Jenkins M. K., Chu H. H., McLachlan J. B. and Moon J. J. (2010) On the composition of the preimmune repertoire of T cells specific for Peptide-major histocompatibility complex ligands. *Annu Rev Immunol* **28**, 275-94.
- Jerne N. K. (1955) The Natural-Selection Theory of Antibody Formation. *Proc Natl Acad Sci U S A* **41**, 849-57.
- Jerne N. K. (1971) The somatic generation of immune recognition. *Eur J Immunol* **1**, 1-9.
- Johnson L. A., Morgan R. A., Dudley M. E., Cassard L., Yang J. C., Hughes M. S., Kammula U. S., Royal R. E., Sherry R. M., Wunderlich J. R., Lee C. C., Restifo N. P., Schwarz S. L., Cogdill A. P., Bishop R. J., Kim H., Brewer C. C., Rudy S. F., VanWaes C., Davis J. L., Mathur A., Ripley R. T., Nathan D. A., Laurencot C. M. and Rosenberg S. A. (2009) Gene therapy with human and mouse T-cell receptors mediates cancer regression and targets normal tissues expressing cognate antigen. *Blood* **114**, 535-46.
- Johnson R. M., Lancki D. W., Sperling A. I., Dick R. F., Spear P. G., Fitch F. W. and Bluestone J. A. (1992) A murine CD4-, CD8- T cell receptor-gamma delta T lymphocyte clone specific for herpes simplex virus glycoprotein I. *J Immunol* **148**, 983-8.
- Jones L. L., Colf L. A., Bankovich A. J., Stone J. D., Gao Y. G., Chan C. M., Huang R. H., Garcia K. C. and Kranz D. M. (2008) Different thermodynamic binding mechanisms and peptide fine specificities associated with a panel of structurally similar high-affinity T cell receptors. *Biochemistry* **47**, 12398-408.
- Joseph A., Zheng J. H., Follenzi A., Dilorenzo T., Sango K., Hyman J., Chen K., Piechocka-Trocha A., Brander C., Hooijberg E., Vignali D. A., Walker B. D. and Goldstein H. (2008) Lentiviral vectors encoding human immunodeficiency virus type 1 (HIV-1)-specific T-cell receptor genes efficiently convert peripheral blood CD8 T lymphocytes into cytotoxic T lymphocytes with potent in vitro and in vivo HIV-1-specific inhibitory activity. *J Virol* **82**, 3078-89.
- Jotereau F., Gervois N. and Labarriere N. (2012) Adoptive transfer with high-affinity TCR to treat human solid tumors: how to improve the feasibility? *Target Oncol* **7**, 3-14.
- Juno J. A., Keynan Y. and Fowke K. R. (2012) Invariant NKT cells: regulation and function during viral infection. *PLoS Pathog* **8**, e1002838.
- Jurcic J. G. (2012) What happened to anti-CD33 therapy for acute myeloid leukemia? *Curr Hematol Malig Rep* **7**, 65-73.
- Kalandadze A., Galleno M., Foncerrada L., Strominger J. L. and Wucherpfennig K. W. (1996) Expression of recombinant HLA-DR2 molecules. Replacement of the hydrophobic transmembrane region by a leucine zipper dimerization motif allows the assembly and secretion of soluble DR alpha beta heterodimers. *J Biol Chem* **271**, 20156-62.
- Kappler J. W., Roehm N. and Marrack P. (1987) T cell tolerance by clonal elimination in the thymus. *Cell* **49**, 273-80.
- Karlsson R. (2004) SPR for molecular interaction analysis: a review of emerging application areas. *J Mol Recognit* **17**, 151-61.
- Karlsson R., Katsamba P. S., Nordin H., Pol E. and Myszka D. G. (2006) Analyzing a kinetic titration series using affinity biosensors. *Anal Biochem* **349**, 136-47.

- Kersh E. N., Shaw A. S. and Allen P. M. (1998a) Fidelity of T cell activation through multistep T cell receptor zeta phosphorylation. *Science* **281**, 572-5.
- Kersh G. J., Kersh E. N., Fremont D. H. and Allen P. M. (1998b) High- and low-potency ligands with similar affinities for the TCR: the importance of kinetics in TCR signaling. *Immunity* **9**, 817-26.
- Kessels H. W., van Den Boom M. D., Spits H., Hooijberg E. and Schumacher T. N. (2000) Changing T cell specificity by retroviral T cell receptor display. *Proc Natl Acad Sci U S A* **97**, 14578-83.
- Khan A. R., Baker B. M., Ghosh P., Biddison W. E. and Wiley D. C. (2000) The structure and stability of an HLA-A*0201/octameric tax peptide complex with an empty conserved peptide-N-terminal binding site. *J Immunol* **164**, 6398-405.
- Kieback E. and Uckert W. (2010) Enhanced T cell receptor gene therapy for cancer. *Expert Opin Biol Ther* **10**, 749-62.
- King C., Tangye S. G. and Mackay C. R. (2008) T follicular helper (TFH) cells in normal and dysregulated immune responses. *Annu Rev Immunol* **26**, 741-66.
- Kinjo Y., Tupin E., Wu D., Fujio M., Garcia-Navarro R., Benhnia M. R., Zajonc D. M., Ben-Menachem G., Ainge G. D., Painter G. F., Khurana A., Hoebe K., Behar S. M., Beutler B., Wilson I. A., Tsuji M., Sellati T. J., Wong C. H. and Kronenberg M. (2006) Natural killer T cells recognize diacylglycerol antigens from pathogenic bacteria. *Nat Immunol* **7**, 978-86.
- Kjer-Nielsen L., Clements C. S., Brooks A. G., Purcell A. W., Fontes M. R., McCluskey J. and Rossjohn J. (2002) The structure of HLA-B8 complexed to an immunodominant viral determinant: peptide-induced conformational changes and a mode of MHC class I dimerization. *J Immunol* **169**, 5153-60.
- Kjer-Nielsen L., Clements C. S., Purcell A. W., Brooks A. G., Whisstock J. C., Burrows S. R., McCluskey J. and Rossjohn J. (2003) A structural basis for the selection of dominant alphabeta T cell receptors in antiviral immunity. *Immunity* **18**, 53-64.
- Kjer-Nielsen L., Patel O., Corbett A. J., Le Nours J., Meehan B., Liu L., Bhati M., Chen Z., Kostenko L., Reantragoon R., Williamson N. A., Purcell A. W., Dudek N. L., McConville M. J., O'Hair R. A., Khairallah G. N., Godfrey D. I., Fairlie D. P., Rossjohn J. and McCluskey J. (2012) MR1 presents microbial vitamin B metabolites to MAIT cells. *Nature* **491**, 717-23.
- Kloetzel P. M. and Ossendorp F. (2004) Proteasome and peptidase function in MHC-class-I-mediated antigen presentation. *Curr Opin Immunol* **16**, 76-81.
- Kohler G. and Milstein C. (1975) Continuous cultures of fused cells secreting antibody of predefined specificity. *Nature* **256**, 495-7.
- Koning F., Maloy W. L. and Coligan J. E. (1990) The implications of subunit interactions for the structure of the T cell receptor-CD3 complex. *Eur J Immunol* **20**, 299-305.
- Kronenberg M. (2005) Toward an understanding of NKT cell biology: progress and paradoxes. *Annu Rev Immunol* **23**, 877-900.
- Kronig H., Hofer K., Conrad H., Guillaume P., Muller J., Schiemann M., Lennerz V., Cosma A., Peschel C., Busch D. H., Romero P. and Bernhard H. (2009) Allorestricted T lymphocytes with a high avidity T-cell receptor towards NY-ESO-1 have potent anti-tumor activity. *Int J Cancer* **125**, 649-55.
- Kuball J., Dossett M. L., Wolf M., Ho W. Y., Voss R. H., Fowler C. and Greenberg P. D. (2007) Facilitating matched pairing and expression of TCR chains introduced into human T cells. *Blood* **109**, 2331-8.

- Kumar S. and Nussinov R. (1999) Salt bridge stability in monomeric proteins. *J Mol Biol* **293**, 1241-55.
- Ladbury J. E. (1996) Just add water! The effect of water on the specificity of protein-ligand binding sites and its potential application to drug design. *Chem Biol* **3**, 973-80.
- Laemmli U. K. (1970) Cleavage of structural proteins during the assembly of the head of bacteriophage T4. *Nature* **227**, 680-5.
- Laugel B., Cole D. K., Clement M., Wooldridge L., Price D. A. and Sewell A. K. (2011) The multiple roles of the CD8 coreceptor in T cell biology: opportunities for the selective modulation of self-reactive cytotoxic T cells. *J Leukoc Biol* **90**, 1089-99.
- Laugel B., Price D. A., Milicic A. and Sewell A. K. (2007) CD8 exerts differential effects on the deployment of cytotoxic T lymphocyte effector functions. *Eur J Immunol* **37**, 905-13.
- Lefranc M. P. (1990) Organization of the human T-cell receptor genes. *Eur Cytokine Netw* **1**, 121-30.
- Leishman A. J., Naidenko O. V., Attinger A., Koning F., Lena C. J., Xiong Y., Chang H. C., Reinherz E., Kronenberg M. and Cheroutre H. (2001) T cell responses modulated through interaction between CD8alphaalpha and the nonclassical MHC class I molecule, TL. *Science* **294**, 1936-9.
- Leslie A. G. W. (1992) Recent changes to the MOSFLM package for processing film and image plate data, Joint CCP4 + ESF-EAMCB Newsletter on Protein Crystallography, No. 26.
- Li Y., Depontieu F. R., Sidney J., Salay T. M., Engelhard V. H., Hunt D. F., Sette A., Topalian S. L. and Mariuzza R. A. (2010) Structural basis for the presentation of tumor-associated MHC class II-restricted phosphopeptides to CD4+ T cells. *J Mol Biol* **399**, 596-603.
- Li Y., Huang Y., Lue J., Quandt J. A., Martin R. and Mariuzza R. A. (2005a) Structure of a human autoimmune TCR bound to a myelin basic protein self-peptide and a multiple sclerosis-associated MHC class II molecule. *EMBO J* **24**, 2968-79.
- Li Y., Moysey R., Molloy P. E., Vuidepot A. L., Mahon T., Baston E., Dunn S., Liddy N., Jacob J., Jakobsen B. K. and Boulter J. M. (2005b) Directed evolution of human T-cell receptors with picomolar affinities by phage display. *Nat Biotechnol* **23**, 349-54.
- Liddy N., Bossi G., Adams K. J., Lissina A., Mahon T. M., Hassan N. J., Gavaret J., Bianchi F. C., Pumphrey N. J., Ladell K., Gostick E., Sewell A. K., Lissin N. M., Harwood N. E., Molloy P. E., Li Y., Cameron B. J., Sami M., Baston E. E., Todorov P. T., Paston S. J., Dennis R. E., Harper J. V., Dunn S. M., Ashfield R., Johnson A., McGrath Y., Plesa G., June C. H., Kalos M., Price D. A., Vuidepot A., Williams D. D., Sutton D. H. and Jakobsen B. K. (2012) Monoclonal TCR-redirectioned tumor cell killing. *Nat Med* **18**, 980-7.
- Lindenthal C. and Elsinghorst E. A. (1999) Identification of a glycoprotein produced by enterotoxigenic Escherichia coli. *Infect Immun* **67**, 4084-91.
- Linke R., Klein A. and Seimetz D. (2010) Catumaxomab: clinical development and future directions. *MAbs* **2**, 129-36.
- Liu C. P., Crawford F., Marrack P. and Kappler J. (1998) T cell positive selection by a high density, low affinity ligand. *Proc Natl Acad Sci U S A* **95**, 4522-6.

- Liu X., Peralta E. A., Ellenhorn J. D. and Diamond D. J. (2000) Targeting of human p53-overexpressing tumor cells by an HLA A*0201-restricted murine T-cell receptor expressed in Jurkat T cells. *Cancer Res* **60**, 693-701.
- Luz J. G., Huang M., Garcia K. C., Rudolph M. G., Apostolopoulos V., Teyton L. and Wilson I. A. (2002) Structural comparison of allogeneic and syngeneic T cell receptor-peptide-major histocompatibility complex complexes: a buried alloreactive mutation subtly alters peptide presentation substantially increasing V(beta) Interactions. *J Exp Med* **195**, 1175-86.
- Ma C. S., Tangye S. G. and Deenick E. K. (2010) Human Th9 cells: inflammatory cytokines modulate IL-9 production through the induction of IL-21. *Immunol Cell Biol* **88**, 621-3.
- Macdonald W. A., Chen Z., Gras S., Archbold J. K., Tynan F. E., Clements C. S., Bharadwaj M., Kjer-Nielsen L., Saunders P. M., Wilce M. C., Crawford F., Stadinsky B., Jackson D., Brooks A. G., Purcell A. W., Kappler J. W., Burrows S. R., Rossjohn J. and McCluskey J. (2009) T cell allorecognition via molecular mimicry. *Immunity* **31**, 897-908.
- Madden D. R. (1995) The three-dimensional structure of peptide-MHC complexes. *Annu Rev Immunol* **13**, 587-622.
- Mannon R. B., Kotzin B. L., Nataraj C., Ferri K., Roper E., Kurlander R. J. and Coffman T. M. (1998) Downregulation of T cell receptor expression by CD8(+) lymphocytes in kidney allografts. *J Clin Invest* **101**, 2517-27.
- Manolios N., Kemp O. and Li Z. G. (1994) The T cell antigen receptor alpha and beta chains interact via distinct regions with CD3 chains. *Eur J Immunol* **24**, 84-92.
- Manz B. N., Jackson B. L., Petit R. S., Dustin M. L. and Groves J. (2011) T-cell triggering thresholds are modulated by the number of antigen within individual T-cell receptor clusters. *Proc Natl Acad Sci U S A* **108**, 9089-94.
- Marshall N. B. and Swain S. L. (2011) Cytotoxic CD4 T cells in antiviral immunity. *J Biomed Biotechnol* **2011**, 954602.
- Mason D. (1998) A very high level of crossreactivity is an essential feature of the T-cell receptor. *Immunol Today* **19**, 395-404.
- Maynard J., Petersson K., Wilson D. H., Adams E. J., Blondelle S. E., Boulanger M. J., Wilson D. B. and Garcia K. C. (2005) Structure of an autoimmune T cell receptor complexed with class II peptide-MHC: insights into MHC bias and antigen specificity. *Immunity* **22**, 81-92.
- Mazza C., Auphan-Anezin N., Gregoire C., Guimezanes A., Kellenberger C., Roussel A., Kearney A., van der Merwe P. A., Schmitt-Verhulst A. M. and Malissen B. (2007) How much can a T-cell antigen receptor adapt to structurally distinct antigenic peptides? *EMBO J* **26**, 1972-83.
- Mazza C. and Malissen B. (2007) What guides MHC-restricted TCR recognition? *Semin Immunol* **19**, 225-35.
- McCoy A. J. (2009) Protein Crystallography with Coffee 8th edition. In *BCA Protein Crystallography Summer School 2010*.
- McCoy A. J., Grosse-Kunstleve R. W., Adams P. D., Winn M. D., Storoni L. C. and Read R. J. (2007) Phaser crystallographic software. *J Appl Crystallogr* **40**, 658-674.
- McCoy A. J. and Read R. J. (2010) Experimental phasing: best practice and pitfalls. *Acta Crystallogr D Biol Crystallogr* **66**, 458-69.
- McKeithan T. W. (1995) Kinetic proofreading in T-cell receptor signal transduction. *Proc Natl Acad Sci U S A* **92**, 5042-6.

- Medzhitov R. and Janeway C., Jr. (2000) Innate immune recognition: mechanisms and pathways. *Immunol Rev* **173**, 89-97.
- Metzger T. C. and Anderson M. S. (2011) Control of central and peripheral tolerance by Aire. *Immunol Rev* **241**, 89-103.
- Michaeli Y., Denkberg G., Sinik K., Lantzy L., Chih-Sheng C., Beauverd C., Ziv T., Romero P. and Reiter Y. (2009) Expression hierarchy of T cell epitopes from melanoma differentiation antigens: unexpected high level presentation of tyrosinase-HLA-A2 Complexes revealed by peptide-specific, MHC-restricted, TCR-like antibodies. *J Immunol* **182**, 6328-41.
- Miles J. J., Bulek A. M., Cole D. K., Gostick E., Schauenburg A. J., Dolton G., Venturi V., Davenport M. P., Tan M. P., Burrows S. R., Wooldridge L., Price D. A., Rizkallah P. J. and Sewell A. K. (2010) Genetic and structural basis for selection of a ubiquitous T cell receptor deployed in epstein-barr virus infection. *PLoS Pathog* **6**, e1001198.
- Minami Y., Weissman A. M., Samelson L. E. and Klausner R. D. (1987) Building a multichain receptor: synthesis, degradation, and assembly of the T-cell antigen receptor. *Proc Natl Acad Sci U S A* **84**, 2688-92.
- Mitsuyasu R. T., Anton P. A., Deeks S. G., Scadden D. T., Connick E., Downs M. T., Bakker A., Roberts M. R., June C. H., Jalali S., Lin A. A., Pennathur-Das R. and Hege K. M. (2000) Prolonged survival and tissue trafficking following adoptive transfer of CD4zeta gene-modified autologous CD4(+) and CD8(+) T cells in human immunodeficiency virus-infected subjects. *Blood* **96**, 785-93.
- Molloy P. E., Sewell A. K. and Jakobsen B. K. (2005) Soluble T cell receptors: novel immunotherapies. *Curr Opin Pharmacol* **5**, 438-43.
- Momburg F. and Tan P. (2002) Tapasin-the keystone of the loading complex optimizing peptide binding by MHC class I molecules in the endoplasmic reticulum. *Mol Immunol* **39**, 217-33.
- Moremen K. W., Tiemeyer M. and Nairn A. V. (2012) Vertebrate protein glycosylation: diversity, synthesis and function. *Nat Rev Mol Cell Biol* **13**, 448-62.
- Morgan R. A., Dudley M. E., Wunderlich J. R., Hughes M. S., Yang J. C., Sherry R. M., Royal R. E., Topalian S. L., Kammula U. S., Restifo N. P., Zheng Z., Nahvi A., de Vries C. R., Rogers-Freezer L. J., Mavroukakis S. A. and Rosenberg S. A. (2006) Cancer regression in patients after transfer of genetically engineered lymphocytes. *Science* **314**, 126-9.
- Mosmann T. R., Cherwinski H., Bond M. W., Giedlin M. A. and Coffman R. L. (1986) Two types of murine helper T cell clone. I. Definition according to profiles of lymphokine activities and secreted proteins. *J Immunol* **136**, 2348-57.
- Murphy K. (2012) *Janeway's Immunobiology, 8th Edition*. Garland Science.
- Murphy K., Travers P. and Walport M. (2008) *Janeway's Immunobiology, Seventh Edition*. Garland Science.
- Murphy K. P. and Freire E. (1995) Thermodynamic strategies for rational protein and drug design. *Pharm Biotechnol* **7**, 219-41.
- Murshudov G. N., Vagin A. A. and Dodson E. J. (1997) Refinement of macromolecular structures by the maximum-likelihood method. *Acta Crystallogr D Biol Crystallogr* **53**, 240-55.
- Niedermann G. (2002) Immunological functions of the proteasome. *Curr Top Microbiol Immunol* **268**, 91-136.

- Nikolich-Zugich J., Slifka M. K. and Messaoudi I. (2004) The many important facets of T-cell repertoire diversity. *Nat Rev Immunol* **4**, 123-32.
- Nino-Vasquez J. J., Allicotti G., Borrás E., Wilson D. B., Valmori D., Simon R., Martin R. and Pinilla C. (2004) A powerful combination: the use of positional scanning libraries and biometrical analysis to identify cross-reactive T cell epitopes. *Mol Immunol* **40**, 1063-74.
- Novellino L., Castelli C. and Parmiani G. (2005) A listing of human tumor antigens recognized by T cells: March 2004 update. *Cancer Immunol Immunother* **54**, 187-207.
- Okamoto S., Mineno J., Ikeda H., Fujiwara H., Yasukawa M., Shiku H. and Kato I. (2009) Improved expression and reactivity of transduced tumor-specific TCRs in human lymphocytes by specific silencing of endogenous TCR. *Cancer Res* **69**, 9003-11.
- Palmer E. and Naeher D. (2009) Affinity threshold for thymic selection through a T-cell receptor-co-receptor zipper. *Nat Rev Immunol* **9**, 207-13.
- Panelli M. C., Wunderlich J., Jeffries J., Wang E., Mixon A., Rosenberg S. A. and Marincola F. M. (2000) Phase I study in patients with metastatic melanoma of immunization with dendritic cells presenting epitopes derived from the melanoma-associated antigens MART-1 and gp100. *J Immunother* **23**, 487-98.
- Pang D. J., Neves J. F., Sumaria N. and Pennington D. J. (2012) Understanding the complexity of gammadelta T-cell subsets in mouse and human. *Immunology* **136**, 283-90.
- Parmiani G., De Filippo A., Novellino L. and Castelli C. (2007) Unique human tumor antigens: immunobiology and use in clinical trials. *J Immunol* **178**, 1975-9.
- Pattnaik P. (2005) Surface plasmon resonance: applications in understanding receptor-ligand interaction. *Appl Biochem Biotechnol* **126**, 79-92.
- Perozzo R., Folkers G. and Scapozza L. (2004) Thermodynamics of protein-ligand interactions: history, presence, and future aspects. *J Recept Signal Transduct Res* **24**, 1-52.
- Persaud S. P., Donermeyer D. L., Weber K. S., Kranz D. M. and Allen P. M. (2010) High-affinity T cell receptor differentiates cognate peptide-MHC and altered peptide ligands with distinct kinetics and thermodynamics. *Mol Immunol* **47**, 1793-801.
- Plattner B. L. and Hostetter J. M. (2011) Comparative gamma delta T cell immunology: a focus on mycobacterial disease in cattle. *Vet Med Int* **2011**, 214384.
- Polikarpov I., Teplyakov A. and Oliva G. (1997) The ultimate wavelength for protein crystallography? *Acta Crystallogr D Biol Crystallogr* **53**, 734-7.
- Porcelli S., Yockey C. E., Brenner M. B. and Balk S. P. (1993) Analysis of T cell antigen receptor (TCR) expression by human peripheral blood CD4-8-alpha/beta T cells demonstrates preferential use of several V beta genes and an invariant TCR alpha chain. *J Exp Med* **178**, 1-16.
- Porcelli S. A. and Modlin R. L. (1999) The CD1 system: antigen-presenting molecules for T cell recognition of lipids and glycolipids. *Annu Rev Immunol* **17**, 297-329.
- Price D. A., Sewell A. K., Dong T., Tan R., Goulder P. J., Rowland-Jones S. L. and Phillips R. E. (1998) Antigen-specific release of beta-chemokines by anti-HIV-1 cytotoxic T lymphocytes. *Curr Biol* **8**, 355-8.

- Probst-Kepper M., Hecht H. J., Herrmann H., Janke V., Ocklenburg F., Klempnauer J., van den Eynde B. J. and Weiss S. (2004) Conformational restraints and flexibility of 14-meric peptides in complex with HLA-B*3501. *J Immunol* **173**, 5610-6.
- Provasi E., Genovese P., Lombardo A., Magnani Z., Liu P. Q., Reik A., Chu V., Paschon D. E., Zhang L., Kuball J., Camisa B., Bondanza A., Casorati G., Ponzoni M., Ciceri F., Bordignon C., Greenberg P. D., Holmes M. C., Gregory P. D., Naldini L. and Bonini C. (2012) Editing T cell specificity towards leukemia by zinc finger nucleases and lentiviral gene transfer. *Nat Med* **18**, 807-15.
- Purbhoo M. A., Boulter J. M., Price D. A., Vuidepot A. L., Hourigan C. S., Dunbar P. R., Olson K., Dawson S. J., Phillips R. E., Jakobsen B. K., Bell J. I. and Sewell A. K. (2001) The human CD8 coreceptor effects cytotoxic T cell activation and antigen sensitivity primarily by mediating complete phosphorylation of the T cell receptor zeta chain. *J Biol Chem* **276**, 32786-92.
- Purbhoo M. A., Sutton D. H., Brewer J. E., Mullings R. E., Hill M. E., Mahon T. M., Karbach J., Jager E., Cameron B. J., Lissin N., Vyas P., Chen J. L., Cerundolo V. and Jakobsen B. K. (2006) Quantifying and imaging NY-ESO-1/LAGE-1-derived epitopes on tumor cells using high affinity T cell receptors. *J Immunol* **176**, 7308-16.
- Rabinowitz J. D., Beeson C., Lyons D. S., Davis M. M. and McConnell H. M. (1996) Kinetic discrimination in T-cell activation. *Proc Natl Acad Sci U S A* **93**, 1401-5.
- Ravandi F., Estey E. H., Appelbaum F. R., Lo-Coco F., Schiffer C. A., Larson R. A., Burnett A. K. and Kantarjian H. M. (2012) Gemtuzumab Ozogamicin: Time to Resurrect? *J Clin Oncol*.
- Reich Z., Boniface J. J., Lyons D. S., Borochoy N., Wachtel E. J. and Davis M. M. (1997) Ligand-specific oligomerization of T-cell receptor molecules. *Nature* **387**, 617-20.
- Reiser J. B., Darnault C., Gregoire C., Mosser T., Mazza G., Kearney A., van der Merwe P. A., Fontecilla-Camps J. C., Housset D. and Malissen B. (2003) CDR3 loop flexibility contributes to the degeneracy of TCR recognition. *Nat Immunol* **4**, 241-7.
- Reiser J. B., Darnault C., Guimezanes A., Gregoire C., Mosser T., Schmitt-Verhulst A. M., Fontecilla-Camps J. C., Malissen B., Housset D. and Mazza G. (2000) Crystal structure of a T cell receptor bound to an allogeneic MHC molecule. *Nat Immunol* **1**, 291-7.
- Richman S. A. and Kranz D. M. (2007) Display, engineering, and applications of antigen-specific T cell receptors. *Biomol Eng* **24**, 361-73.
- Robbins P. F., Li Y. F., El-Gamil M., Zhao Y., Wargo J. A., Zheng Z., Xu H., Morgan R. A., Feldman S. A., Johnson L. A., Bennett A. D., Dunn S. M., Mahon T. M., Jakobsen B. K. and Rosenberg S. A. (2008) Single and dual amino acid substitutions in TCR CDRs can enhance antigen-specific T cell functions. *J Immunol* **180**, 6116-31.
- Romero P., Gervois N., Schneider J., Escobar P., Valmori D., Pannetier C., Steinle A., Wolfel T., Lienard D., Brichard V., van Pel A., Jotereau F. and Cerottini J. C. (1997) Cytolytic T lymphocyte recognition of the immunodominant HLA-A*0201-restricted Melan-A/MART-1 antigenic peptide in melanoma. *J Immunol* **159**, 2366-74.

- Rosenberg S. A., Restifo N. P., Yang J. C., Morgan R. A. and Dudley M. E. (2008) Adoptive cell transfer: a clinical path to effective cancer immunotherapy. *Nat Rev Cancer* **8**, 299-308.
- Rosenberg S. A., Yang J. C. and Restifo N. P. (2004) Cancer immunotherapy: moving beyond current vaccines. *Nat Med* **10**, 909-15.
- Rudolph M. G., Luz J. G. and Wilson I. A. (2002) Structural and thermodynamic correlates of T cell signaling. *Annu Rev Biophys Biomol Struct* **31**, 121-49.
- Rudolph M. G., Stanfield R. L. and Wilson I. A. (2006) How TCRs bind MHCs, peptides, and coreceptors. *Annu Rev Immunol* **24**, 419-66.
- Ruppert J., Sidney J., Celis E., Kubo R. T., Grey H. M. and Sette A. (1993) Prominent role of secondary anchor residues in peptide binding to HLA-A2.1 molecules. *Cell* **74**, 929-37.
- Sadovnikova E. and Stauss H. J. (1996) Peptide-specific cytotoxic T lymphocytes restricted by nonself major histocompatibility complex class I molecules: reagents for tumor immunotherapy. *Proc Natl Acad Sci U S A* **93**, 13114-8.
- Sami M., Rizkallah P. J., Dunn S., Molloy P., Moysey R., Vuidepot A., Baston E., Todorov P., Li Y., Gao F., Boulter J. M. and Jakobsen B. K. (2007) Crystal structures of high affinity human T-cell receptors bound to peptide major histocompatibility complex reveal native diagonal binding geometry. *Protein Eng Des Sel* **20**, 397-403.
- Saper M. A., Bjorkman P. J. and Wiley D. C. (1991) Refined structure of the human histocompatibility antigen HLA-A2 at 2.6 Å resolution. *J Mol Biol* **219**, 277-319.
- Sapoznik S., Hammer O., Ortenberg R., Besser M. J., Ben-Moshe T., Schachter J. and Markel G. (2012) Novel anti-melanoma immunotherapies: disarming tumor escape mechanisms. *Clin Dev Immunol* **2012**, 818214.
- Schaft N., Dorrie J., Muller I., Beck V., Baumann S., Schunder T., Kampgen E. and Schuler G. (2006) A new way to generate cytolytic tumor-specific T cells: electroporation of RNA coding for a T cell receptor into T lymphocytes. *Cancer Immunol Immunother* **55**, 1132-41.
- Schatz D. G. (2004) V(D)J recombination. *Immunol Rev* **200**, 5-11.
- Schmid D. A., Irving M. B., Posevitz V., Hebeisen M., Posevitz-Fejfar A., Sarria J. C., Gomez-Eerland R., Thome M., Schumacher T. N., Romero P., Speiser D. E., Zoete V., Michielin O. and Rufer N. (2010) Evidence for a TCR affinity threshold delimiting maximal CD8 T cell function. *J Immunol* **184**, 4936-46.
- Schuster I. G., Busch D. H., Eppinger E., Kremmer E., Milosevic S., Hennard C., Kuttler C., Ellwart J. W., Frankenberger B., Nossner E., Salat C., Bogner C., Borkhardt A., Kolb H. J. and Krackhardt A. M. (2007) Allorestricted T cells with specificity for the FMNL1-derived peptide PP2 have potent antitumor activity against hematologic and other malignancies. *Blood* **110**, 2931-9.
- Sebestyen Z., Schooten E., Sals T., Zaldivar I., San Jose E., Alarcon B., Bobisse S., Rosato A., Szollosi J., Gratama J. W., Willemsen R. A. and Debets R. (2008) Human TCR that incorporate CD3zeta induce highly preferred pairing between TCRalpha and beta chains following gene transfer. *J Immunol* **180**, 7736-46.
- Seder R. A., Boulay J. L., Finkelman F., Barbier S., Ben-Sasson S. Z., Le Gros G. and Paul W. E. (1992) CD8+ T cells can be primed in vitro to produce IL-4. *J Immunol* **148**, 1652-6.
- Segelke B. W. (2001) Efficiency analysis of sampling protocols used in protein crystallization screening. *Journal of Crystal Growth* **232**, 553-562.

- Seimetz D. (2011) Novel monoclonal antibodies for cancer treatment: the trifunctional antibody catumaxomab (removab). *J Cancer* **2**, 309-16.
- Sewell A. K. (2002) Breaking the kinetic window of T-cell activation. *Trends Immunol* **23**, 67.
- Sewell A. K. (2012) Why must T cells be cross-reactive? *Nat Rev Immunol* **12**, 669-77.
- Sherlock O., Dobrindt U., Jensen J. B., Munk Vejborg R. and Klemm P. (2006) Glycosylation of the self-recognizing Escherichia coli Ag43 autotransporter protein. *J Bacteriol* **188**, 1798-807.
- Sherman L. A. and Chattopadhyay S. (1993) The molecular basis of allorecognition. *Annu Rev Immunol* **11**, 385-402.
- Siegel R. W. (2009) Antibody affinity optimization using yeast cell surface display. *Methods Mol Biol* **504**, 351-83.
- Sigal L. J., Crotty S., Andino R. and Rock K. L. (1999) Cytotoxic T-cell immunity to virus-infected non-haematopoietic cells requires presentation of exogenous antigen. *Nature* **398**, 77-80.
- Skipper J. C., Gulden P. H., Hendrickson R. C., Harthun N., Caldwell J. A., Shabanowitz J., Engelhard V. H., Hunt D. F. and Slingsluff C. L., Jr. (1999) Mass-spectrometric evaluation of HLA-A*0201-associated peptides identifies dominant naturally processed forms of CTL epitopes from MART-1 and gp100. *Int J Cancer* **82**, 669-77.
- Sliz P., Michielin O., Cerottini J. C., Luescher I., Romero P., Karplus M. and Wiley D. C. (2001) Crystal structures of two closely related but antigenically distinct HLA-A2/melanocyte-melanoma tumor-antigen peptide complexes. *J Immunol* **167**, 3276-84.
- Smyth M. S. and Martin J. H. J. (2000) X Ray Crystallography. *Molecular Pathology* **53**, 8-14.
- Sommermeier D., Neudorfer J., Weinhold M., Leisegang M., Engels B., Noessner E., Heemskerk M. H., Charo J., Schendel D. J., Blankenstein T., Bernhard H. and Uckert W. (2006) Designer T cells by T cell receptor replacement. *Eur J Immunol* **36**, 3052-9.
- Speiser D. E., Baumgaertner P., Voelter V., Devevre E., Barbey C., Rufer N. and Romero P. (2008) Unmodified self antigen triggers human CD8 T cells with stronger tumor reactivity than altered antigen. *Proc Natl Acad Sci U S A* **105**, 3849-54.
- Stanislowski T., Voss R. H., Lotz C., Sadovnikova E., Willemsen R. A., Kuball J., Ruppert T., Bolhuis R. L., Melief C. J., Huber C., Stauss H. J. and Theobald M. (2001) Circumventing tolerance to a human MDM2-derived tumor antigen by TCR gene transfer. *Nat Immunol* **2**, 962-70.
- Starr T. K., Jameson S. C. and Hogquist K. A. (2003) Positive and negative selection of T cells. *Annu Rev Immunol* **21**, 139-76.
- Stewart-Jones G. B., McMichael A. J., Bell J. I., Stuart D. I. and Jones E. Y. (2003) A structural basis for immunodominant human T cell receptor recognition. *Nat Immunol* **4**, 657-63.
- Stone J. D., Chervin A. S., Aggen D. H. and Kranz D. M. (2012) T cell receptor engineering. *Methods Enzymol* **503**, 189-222.
- Stone J. D., Chervin A. S. and Kranz D. M. (2009) T-cell receptor binding affinities and kinetics: impact on T-cell activity and specificity. *Immunology* **126**, 165-76.

- Storkus W. J., Alexander J., Payne J. A., Dawson J. R. and Cresswell P. (1989) Reversal of natural killing susceptibility in target cells expressing transfected class I HLA genes. *Proc Natl Acad Sci U S A* **86**, 2361-4.
- Szymczak A. L., Workman C. J., Wang Y., Vignali K. M., Dilioglou S., Vanin E. F. and Vignali D. A. (2004) Correction of multi-gene deficiency in vivo using a single 'self-cleaving' 2A peptide-based retroviral vector. *Nat Biotechnol* **22**, 589-94.
- Tanaka K., Mizushima T. and Saeki Y. (2012) The proteasome: molecular machinery and pathophysiological roles. *Biol Chem* **393**, 217-34.
- Tang H., Kuhen K. L. and Wong-Staal F. (1999) Lentivirus replication and regulation. *Annu Rev Genet* **33**, 133-70.
- Tellinghuisen J. (2006) Van't Hoff analysis of K degrees (T): how good...or bad? *Biophys Chem* **120**, 114-20.
- Terry L. A., DiSanto J. P., Small T. N. and Flomenberg N. (1990) Differential expression and regulation of the human CD8 alpha and CD8 beta chains. *Tissue Antigens* **35**, 82-91.
- Teschendorf C., Warrington K. H., Jr., Siemann D. W. and Muzyczka N. (2002) Comparison of the EF-1 alpha and the CMV promoter for engineering stable tumor cell lines using recombinant adeno-associated virus. *Anticancer Res* **22**, 3325-30.
- Thomas R. (2004) Signal 3 and its role in autoimmunity. *Arthritis Res Ther* **6**, 26-27.
- Thomas S., Xue S. A., Bangham C. R., Jakobsen B. K., Morris E. C. and Stauss H. J. (2011) Human T cells expressing affinity-matured TCR display accelerated responses but fail to recognize low density of MHC-peptide antigen. *Blood* **118**, 319-29.
- Tian S., Maile R., Collins E. J. and Frelinger J. A. (2007) CD8+ T cell activation is governed by TCR-peptide/MHC affinity, not dissociation rate. *J Immunol* **179**, 2952-60.
- Tickle I. J., Laskowski R. A. and Moss D. S. (2000) Rfree and the rfree ratio. II. Calculation Of the expected values and variances of cross-validation statistics in macromolecular least-squares refinement. *Acta Crystallogr D Biol Crystallogr* **56**, 442-50.
- Tonegawa S. (1983) Somatic generation of antibody diversity. *Nature* **302**, 575-81.
- Topalian S. L., Kasid A. and Rosenberg S. A. (1990) Immunoselection of a human melanoma resistant to specific lysis by autologous tumor-infiltrating lymphocytes. Possible mechanisms for immunotherapeutic failures. *J Immunol* **144**, 4487-95.
- Topalian S. L., Solomon D. and Rosenberg S. A. (1989) Tumor-specific cytolysis by lymphocytes infiltrating human melanomas. *J Immunol* **142**, 3714-25.
- Townsend A. and Bodmer H. (1989) Antigen recognition by class I-restricted T lymphocytes. *Annu Rev Immunol* **7**, 601-24.
- Townsend A. R., Gotch F. M. and Davey J. (1985) Cytotoxic T cells recognize fragments of the influenza nucleoprotein. *Cell* **42**, 457-67.
- Trautmann A. and Randriamampita C. (2003) Initiation of TCR signalling revisited. *Trends Immunol* **24**, 425-8.
- Treiner E., Duban L., Bahram S., Radosavljevic M., Wanner V., Tilloy F., Affaticati P., Gilfillan S. and Lantz O. (2003) Selection of evolutionarily conserved mucosal-associated invariant T cells by MR1. *Nature* **422**, 164-9.

- Treiner E., Duban L., Moura I. C., Hansen T., Gilfillan S. and Lantz O. (2005) Mucosal-associated invariant T (MAIT) cells: an evolutionarily conserved T cell subset. *Microbes Infect* **7**, 552-9.
- Treiner E. and Lantz O. (2006) CD1d- and MR1-restricted invariant T cells: of mice and men. *Curr Opin Immunol* **18**, 519-26.
- Tsuji T., Yasukawa M., Matsuzaki J., Ohkuri T., Chamoto K., Wakita D., Azuma T., Niiya H., Miyoshi H., Kuzushima K., Oka Y., Sugiyama H., Ikeda H. and Nishimura T. (2005) Generation of tumor-specific, HLA class I-restricted human Th1 and Tc1 cells by cell engineering with tumor peptide-specific T-cell receptor genes. *Blood* **106**, 470-6.
- Turner S. J., Doherty P. C., McCluskey J. and Rossjohn J. (2006) Structural determinants of T-cell receptor bias in immunity. *Nat Rev Immunol* **6**, 883-94.
- Tynan F. E., Burrows S. R., Buckle A. M., Clements C. S., Borg N. A., Miles J. J., Beddoe T., Whisstock J. C., Wilce M. C., Silins S. L., Burrows J. M., Kjer-Nielsen L., Kostenko L., Purcell A. W., McCluskey J. and Rossjohn J. (2005) T cell receptor recognition of a 'super-bulged' major histocompatibility complex class I-bound peptide. *Nat Immunol* **6**, 1114-22.
- Tynan F. E., Reid H. H., Kjer-Nielsen L., Miles J. J., Wilce M. C., Kostenko L., Borg N. A., Williamson N. A., Beddoe T., Purcell A. W., Burrows S. R., McCluskey J. and Rossjohn J. (2007) A T cell receptor flattens a bulged antigenic peptide presented by a major histocompatibility complex class I molecule. *Nat Immunol* **8**, 268-76.
- Uckert W. and Schumacher T. N. (2009) TCR transgenes and transgene cassettes for TCR gene therapy: status in 2008. *Cancer Immunol Immunother* **58**, 809-22.
- Udyavar A., Alli R., Nguyen P., Baker L. and Geiger T. L. (2009) Subtle affinity-enhancing mutations in a myelin oligodendrocyte glycoprotein-specific TCR alter specificity and generate new self-reactivity. *J Immunol* **182**, 4439-47.
- Valitutti S. (2012) The Serial Engagement Model 17 Years After: From TCR Triggering to Immunotherapy. *Front Immunol* **3**, 272.
- Valitutti S., Muller S., Cella M., Padovan E. and Lanzavecchia A. (1995) Serial triggering of many T-cell receptors by a few peptide-MHC complexes. *Nature* **375**, 148-51.
- Valmori D., Fonteneau J. F., Lizana C. M., Gervois N., Lienard D., Rimoldi D., Jongeneel V., Jotereau F., Cerottini J. C. and Romero P. (1998) Enhanced generation of specific tumor-reactive CTL in vitro by selected Melan-A/MART-1 immunodominant peptide analogues. *J Immunol* **160**, 1750-8.
- van Boxel G. I., Stewart-Jones G., Holmes S., Sainsbury S., Shepherd D., Gillespie G. M., Harlos K., Stuart D. I., Owens R. and Jones E. Y. (2009) Some lessons from the systematic production and structural analysis of soluble (alpha)(beta) T-cell receptors. *J Immunol Methods* **350**, 14-21.
- van der Bruggen P., Traversari C., Chomez P., Lurquin C., De Plaen E., Van den Eynde B., Knuth A. and Boon T. (1991) A gene encoding an antigen recognized by cytolytic T lymphocytes on a human melanoma. *Science* **254**, 1643-7.
- van der Merwe P. A. (2001) Surface Plasmon Resonance. In *Protein-ligand interactions: hydrodynamics and calorimetry* (Edited by Chowdry S. H. B.), p. 137-170. Oxford University Press, Oxford.
- van der Merwe P. A. and Davis S. J. (2003) Molecular interactions mediating T cell antigen recognition. *Annu Rev Immunol* **21**, 659-84.

- van der Merwe P. A. and Dushek O. (2011) Mechanisms for T cell receptor triggering. *Nat Rev Immunol* **11**, 47-55.
- van der Veken L. T., Hagedoorn R. S., van Loenen M. M., Willemze R., Falkenburg J. H. and Heemskerk M. H. (2006) Alphabeta T-cell receptor engineered gammadelta T cells mediate effective antileukemic reactivity. *Cancer Res* **66**, 3331-7.
- Varela-Rohena A., Molloy P. E., Dunn S. M., Li Y., Suhoski M. M., Carroll R. G., Milicic A., Mahon T., Sutton D. H., Laugel B., Moysey R., Cameron B. J., Vuidepot A., Purbhoo M. A., Cole D. K., Phillips R. E., June C. H., Jakobsen B. K., Sewell A. K. and Riley J. L. (2008) Control of HIV-1 immune escape by CD8 T cells expressing enhanced T-cell receptor. *Nat Med* **14**, 1390-5.
- Vijayakumar M., Wong K. Y., Schreiber G., Fersht A. R., Szabo A. and Zhou H. X. (1998) Electrostatic enhancement of diffusion-controlled protein-protein association: comparison of theory and experiment on barnase and barstar. *J Mol Biol* **278**, 1015-24.
- Viola A., Schroeder S., Sakakibara Y. and Lanzavecchia A. (1999) T lymphocyte costimulation mediated by reorganization of membrane microdomains. *Science* **283**, 680-2.
- Voskens C. J., Strome S. E. and Sewell D. A. (2009) Synthetic peptide-based cancer vaccines: lessons learned and hurdles to overcome. *Curr Mol Med* **9**, 683-93.
- Voss R. H., Willemsen R. A., Kuball J., Grabowski M., Engel R., Intan R. S., Guillaume P., Romero P., Huber C. and Theobald M. (2008) Molecular design of the Calphabeta interface favors specific pairing of introduced TCRalphabeta in human T cells. *J Immunol* **180**, 391-401.
- Waldmann T. A. (2003) Immunotherapy: past, present and future. *Nat Med* **9**, 269-77.
- Wang J., Lim K., Smolyar A., Teng M., Liu J., Tse A. G., Hussey R. E., Chishti Y., Thomson C. T., Sweet R. M., Nathenson S. G., Chang H. C., Sacchettini J. C. and Reinherz E. L. (1998) Atomic structure of an alphabeta T cell receptor (TCR) heterodimer in complex with an anti-TCR fab fragment derived from a mitogenic antibody. *EMBO J* **17**, 10-26.
- Webb A. I., Dunstone M. A., Chen W., Aguilar M. I., Chen Q., Jackson H., Chang L., Kjer-Nielsen L., Beddoe T., McCluskey J., Rossjohn J. and Purcell A. W. (2004) Functional and structural characteristics of NY-ESO-1-related HLA A2-restricted epitopes and the design of a novel immunogenic analogue. *J Biol Chem* **279**, 23438-46.
- Weidanz J. A., Card K. F., Edwards A., Perlstein E. and Wong H. C. (1998) Display of functional alphabeta single-chain T-cell receptor molecules on the surface of bacteriophage. *J Immunol Methods* **221**, 59-76.
- Weiss A. and Stobo J. D. (1984) Requirement for the coexpression of T3 and the T cell antigen receptor on a malignant human T cell line. *J Exp Med* **160**, 1284-99.
- Wilde S., Sommermeyer D., Frankenberger B., Schiemann M., Milosevic S., Spranger S., Pohla H., Uckert W., Busch D. H. and Schendel D. J. (2009) Dendritic cells pulsed with RNA encoding allogeneic MHC and antigen induce T cells with superior antitumor activity and higher TCR functional avidity. *Blood* **114**, 2131-9.
- Wilkins M. R., Gasteiger E., Bairoch A., Sanchez J. C., Williams K. L., Appel R. D. and Hochstrasser D. F. (1999) Protein identification and analysis tools in the ExPASy server. *Methods Mol Biol* **112**, 531-52.

- Willcox B. E., Gao G. F., Wyer J. R., Ladbury J. E., Bell J. I., Jakobsen B. K. and van der Merwe P. A. (1999a) TCR binding to peptide-MHC stabilizes a flexible recognition interface. *Immunity* **10**, 357-65.
- Willcox B. E., Gao G. F., Wyer J. R., O'Callaghan C. A., Boulter J. M., Jones E. Y., van der Merwe P. A., Bell J. I. and Jakobsen B. K. (1999b) Production of soluble alphabeta T-cell receptor heterodimers suitable for biophysical analysis of ligand binding. *Protein Sci* **8**, 2418-23.
- Wolf E., Hofmeister R., Kufer P., Schlereth B. and Baeuerle P. A. (2005) BiTEs: bispecific antibody constructs with unique anti-tumor activity. *Drug Discov Today* **10**, 1237-44.
- Wong P. and Pamer E. G. (2003) CD8 T cell responses to infectious pathogens. *Annu Rev Immunol* **21**, 29-70.
- Wooh J. W., Kidd R. D., Martin J. L. and Kobe B. (2003) Comparison of three commercial sparse-matrix crystallization screens. *Acta Crystallogr D Biol Crystallogr* **59**, 769-72.
- Wooldridge L., Ekeruche-Makinde J., van den Berg H. A., Skowera A., Miles J. J., Tan M. P., Dolton G., Clement M., Llewellyn-Lacey S., Price D. A., Peakman M. and Sewell A. K. (2012) A single autoimmune T cell receptor recognizes more than a million different peptides. *J Biol Chem* **287**, 1168-77.
- Wooldridge L., Laugel B., Ekeruche J., Clement M., van den Berg H. A., Price D. A. and Sewell A. K. (2010) CD8 controls T cell cross-reactivity. *J Immunol* **185**, 4625-32.
- Wooldridge L., Lissina A., Cole D. K., van den Berg H. A., Price D. A. and Sewell A. K. (2009) Tricks with tetramers: how to get the most from multimeric peptide-MHC. *Immunology* **126**, 147-64.
- Wooldridge L., van den Berg H. A., Glick M., Gostick E., Laugel B., Hutchinson S. L., Milicic A., Brenchley J. M., Douek D. C., Price D. A. and Sewell A. K. (2005) Interaction between the CD8 coreceptor and major histocompatibility complex class I stabilizes T cell receptor-antigen complexes at the cell surface. *J Biol Chem* **280**, 27491-501.
- Wu L. C., Tuot D. S., Lyons D. S., Garcia K. C. and Davis M. M. (2002) Two-step binding mechanism for T-cell receptor recognition of peptide MHC. *Nature* **418**, 552-6.
- Xue S. A., Gao L., Hart D., Gillmore R., Qasim W., Thrasher A., Apperley J., Engels B., Uckert W., Morris E. and Stauss H. (2005) Elimination of human leukemia cells in NOD/SCID mice by WT1-TCR gene-transduced human T cells. *Blood* **106**, 3062-7.
- Zelante T., De Luca A., D'Angelo C., Moretti S. and Romani L. (2009) IL-17/Th17 in anti-fungal immunity: what's new? *Eur J Immunol* **39**, 645-8.
- Zhao P. (2011) The 2009 Nobel Prize in Chemistry: Thomas A. Steitz and the structure of the ribosome. *Yale J Biol Med* **84**, 125-9.
- Zhao Y., Bennett A. D., Zheng Z., Wang Q. J., Robbins P. F., Yu L. Y., Li Y., Molloy P. E., Dunn S. M., Jakobsen B. K., Rosenberg S. A. and Morgan R. A. (2007) High-affinity TCRs generated by phage display provide CD4+ T cells with the ability to recognize and kill tumor cell lines. *J Immunol* **179**, 5845-54.
- Zhukov A. and Karlsson R. (2007) Statistical aspects of van't Hoff analysis: a simulation study. *J Mol Recognit* **20**, 379-85.

- Zinkernagel R. M. and Doherty P. C. (1974) Restriction of in vitro T cell-mediated cytotoxicity in lymphocytic choriomeningitis within a syngeneic or semiallogeneic system. *Nature* **248**, 701-2.
- Zinkernagel R. M. and Doherty P. C. (1997) The discovery of MHC restriction. *Immunol Today* **18**, 14-7.
- Zoeger A., Blau M., Egerer K., Feist E. and Dahlmann B. (2006) Circulating proteasomes are functional and have a subtype pattern distinct from 20S proteasomes in major blood cells. *Clin Chem* **52**, 2079-86.
- Zoete V., Irving M. B. and Michielin O. (2010) MM-GBSA binding free energy decomposition and T cell receptor engineering. *J Mol Recognit* **23**, 142-52.
- Zoete V. and Michielin O. (2007) Comparison between computational alanine scanning and per-residue binding free energy decomposition for protein-protein association using MM-GBSA: application to the TCR-p-MHC complex. *Proteins* **67**, 1026-47.
- Zufferey R., Donello J. E., Trono D. and Hope T. J. (1999) Woodchuck hepatitis virus posttranscriptional regulatory element enhances expression of transgenes delivered by retroviral vectors. *J Virol* **73**, 2886-92.
- Zufferey R., Dull T., Mandel R. J., Bukovsky A., Quiroz D., Naldini L. and Trono D. (1998) Self-inactivating lentivirus vector for safe and efficient in vivo gene delivery. *J Virol* **72**, 9873-80.

APPENDICES

Appendix 1: MEL5, α 24 β 17, HLA-A2 and β 2m sequences

MEL5 soluble α chain 22.5 kDa:

MQKEVEQNSGPLSVPEGAIASLNCTYSDRGSQSFFWYRQYSGKSP~~ELIMFIYS~~
NGDKEDGRFTAQLNKASQYVSLIRDSQPSDSATYLCAVNVAGKSTFGDGT
TLTVKPNIQNPDPAVYQLRDSKSSDKSVCLFTDFDSQTNVSQSKDSDVYITD
KCVLDMRSMDFKSNSAVAWSNKSDFACANAFNNSIIPEDTFFPSP~~ESS~~

MEL5 soluble β chain 27.4 kDa:

MSQTIHQWPATLVQPVGSP~~LSLECT~~VEGTSNPPLYWYRQAAGRGLQLLFYS
VGIGQISSEVPQNLSASRPQDRQFILSSKLLLLSDSGFYLC~~AWSET~~GLGTGELF
FGEGSRLTVLEDLKNVFPPEVAVFEPSEAEISHTQKATLVCLATGFYPDHVEL
SWWVNGKEVHSGVCTDPQPLKEQPALNDSRYALSSRLRV~~SATFWQD~~PRNH
FRCQVQFYGLSENDEWTQDRAKPVTQIVSAEAWGRAD

Mel α 24 β 17 soluble α chain (mutations from MEL5 in bold and underlined) 22.6

kDa:

MQKEVEQNSGPLSVPEGAIASLNCTYSFLGSQSFFWYRQYSGKSP~~ELIMFIYS~~
REGDKEDGRFTAQLNKASQHVSLLIRDSQPSDSATYLCAVNVDGGRLTFGDGT
TTLTVKPNIQNPDPAVYQLRDSKSSDKSVCLFTDFDSQTNVSQSKDSDVYIT
DKCVLDMRSMDFKSNSAVAWSNKSDFACANAFNNSIIPEDTFFPSP~~ESS~~

Mel α 24 β 17 soluble β chain (mutations from MEL5 in bold and underlined) 27.5

kDa:

MSQTIHQWPATLVQPVGSP~~LSLECT~~VEGTSNPPLYWYRQAAGRGPQLLFY
WGPFGQISSEVPQNLSASRPQDRQFILSSKLLLLSDSGFYLC~~AWSET~~GLGMMG
GWQFGEGSRLTVLEDLKNVFPPEVAVFEPSEAEISHTQKATLVCLATGFYPD
HVELSWWVNGKEVHSGVCTDPQPLKEQPALNDSRYALSSRLRV~~SATFWQD~~
PRNHFRQCQVQFYGLSENDEWTQDRAKPVTQIVSAEAWGRAD

HLA-A2 heavy chain 32.0 kDa:

MGSHSMRYFFTSVSRPGRGEPFRFIAVGYVDDTQFVRFSDAASQRMEPRAP
WIEQEGPEYWDGETRQVKAHSQTHRVDLGTLRGYYNQSEAGSHTVQRM
GCDVGSQWRFLRGYHQYAYDGKDYIALKEDLRSWTAADMAAQTTHKHW
EAAHVAEQLRAYLEGTCVEWLRRYLENGKETLQRTDAPKTHMTHHAVSDH
EATLRCWALSFPYPAEITLTWQRDGEDQTQDTELVETRPAGDGTQKWA
VPSGQEQRYTCHVQHEGLPKPLTLRWE

Biotin tagged HLA-A2 heavy chain 33.8 kDa:

MGSHSMRYFFTSVSRPGRGEPFRFIAVGYVDDTQFVRFSDAASQRMEPRAP
WIEQEGPEYWDGETRQVKAHSQTHRVDLGTLRGYYNQSEAGSHTVQRM
GCDVGSQWRFLRGYHQYAYDGKDYIALKEDLRSWTAADMAAQTTHKHW
EAAHVAEQLRAYLEGTCVEWLRRYLENGKETLQRTDAPKTHMTHHAVSDH
EATLRCWALSFPYPAEITLTWQRDGEDQTQDTELVETRPAGDGTQKWA
VPSGQEQRYTCHVQHEGLPKPLTLRWEPLNDIFEAKIEWHE

β 2m 11.9 kDa:

MIQRTPKIQVYSRHPAENGKSNFLNCYVSGFHPSDIEVDLLKNGERIEKVEHS
DLSFSKDWSFYLLYTFEPTTEKDEYACRVNHVTLSPKIVKWDRDM

Appendix 2: TCR/pMHC datasets obtained for 25 complexes in my laboratory

TCR/pMHC complex	Screen	Resolution (Å)	pH	PEG (%)	PEG	Glycerol (%)	Salt ^a
<u>α24β17/A2-ELA</u>	<u>TOPS</u>	<u>3.02</u>	<u>7</u>	<u>15</u>	<u>4000</u>	<u>0</u>	<u>1</u>
<u>α24β17/A2-ELA</u>	<u>TOPS</u>	<u>3.21</u>	<u>7</u>	<u>20</u>	<u>4000</u>	<u>0</u>	<u>1</u>
<u>α24β17/A2-ELA</u>	<u>TOPS</u>	<u>2.99</u>	<u>7.5</u>	<u>15</u>	<u>4000</u>	<u>0</u>	<u>1</u>
<u>α24β17/A2-ELA</u>	<u>TOPS4</u>	<u>2.43</u>	<u>7</u>	<u>20</u>	<u>4000</u>	<u>0</u>	<u>1</u>
<u>α24β17/A2-AAG</u>	<u>TOPS</u>	<u>2.81</u>	<u>7</u>	<u>20</u>	<u>4000</u>	<u>15</u>	<u>0</u>
<u>α24β17/A2-ELA-4A</u>	<u>TOPS</u>	<u>2.46</u>	<u>7.5</u>	<u>20</u>	<u>4000</u>	<u>0</u>	<u>1</u>
<u>α24β17/A2-ELA-4A</u>	<u>TOPS3</u>	<u>2.71</u>	<u>7</u>	<u>15</u>	<u>4000</u>	<u>17.4</u>	<u>0</u>
<u>α24β17/A2-ELA-4A</u>	<u>TOPS4</u>	<u>2.44</u>	<u>7</u>	<u>20</u>	<u>4000</u>	<u>8.7</u>	<u>1</u>
<u>α24β17/A2-ELA-4A</u>	<u>TOPS4</u>	<u>3.08</u>	<u>7</u>	<u>20</u>	<u>4000</u>	<u>4.4</u>	<u>1</u>
<u>α24β17/A2-ELA-7A</u>	<u>PACT</u>	<u>2.7</u>	<u>6.5</u>	<u>20</u>	<u>3350</u>	<u>0</u>	<u>1</u>
<u>α24β17/A2-ELA-7A</u>	<u>TOPS4</u>	<u>2.97</u>	<u>7</u>	<u>20</u>	<u>4000</u>	<u>8.7</u>	<u>1</u>
<u>α24β17/A2-ELA-7A</u>	<u>TOPS4</u>	<u>2.63</u>	<u>7</u>	<u>20</u>	<u>4000</u>	<u>17.4</u>	<u>1</u>
<u>α24β17/A2-EAA</u>	<u>TOPS4</u>	<u>2.1</u>	<u>7.5</u>	<u>15</u>	<u>4000</u>	<u>8.7</u>	<u>1</u>
<u>MEL5/A2-EAA</u>	<u>TOPS</u>	<u>3</u>	<u>6.5</u>	<u>15</u>	<u>4000</u>	<u>15</u>	<u>0</u>
<u>MEL5/A2-EAA</u>	<u>TOPS</u>	<u>3.12</u>	<u>8.5</u>	<u>25</u>	<u>4000</u>	<u>15</u>	<u>0</u>
<u>MEL5/A2-AAG</u>	<u>TOPS</u>	<u>3.16</u>	<u>7.5</u>	<u>25</u>	<u>4000</u>	<u>15</u>	<u>0</u>
P1/A2-CLG	TOPS	2.6	6	15	4000	15	0
SB7/A2-FLY	TOPS	2.56	6.5	15	4000	0	1
868/A2-SLY	TOPS	2.94	6	15	4000	0	1
868/A2-6I	TOPS	2.91	6	15	4000	0	1
868/A2-3F6I8V	TOPS1	2.75	5.5	15	4000	0	1
1E6/A2-ALW	TOPS	2.7	7.5	15	4000	0	1
1E6/A2-ALW	TOPS	2.7	8	15	4000	15	0
1E6/A2-ALW	TOPS	2.56	6	15	4000	15	0
1E6/A2-ALW	TOPS	2.76	7.5	15	4000	20	0
1E6/A2-ALW	TOPS	3.12	7	15	4000	0	1
1E6/A2-ALW	TOPS	3.16	8.5	25	4000	0	1
1E6/A2-ALW	PACT	3.01	7.5	20	3350	0	1
1E6/A2-ALW	PACT	2.78	7.5	20	3350	0	1
1E6/A2-ALW	PACT	2.58	6.5	20	3350	0	1
1E6/A2-ALW	PACT	3.2	7	25	1500	0	0
1E6/A2-ALW	PACT	3.04		20	3350	0	1
1E6/A2-ALW	PACT	2.97	6.5	20	3350	0	1
1E6/A2-RQW	PACT	2.33	6	20	6000	0	1
1E6/A2-YQF	PACT	2.11	7	20	6000	0	1
1E6/A2-YQF	PACT	3.21	5	20	6000	0	1
1E6/A2-WQY	TOPS	2.51	7.5	15	8000	15	0
1E6/A2-WQY	TOPS	1.87	7	25	8000	0	1
1E6/A2-KLP	TOPS	3.09	6	15	8000	0	1
1E6/A2-KLP	TOPS	2.92	6.5	15	4000	0	1
1E6/A2-KLP	TOPS	2.85	6.5	15	8000	0	1
1E6/A2-KLP	TOPS	2.96	7	15	8000	0	1

1E6/A2-YLG	TOPS	<u>2.5</u>	<u>6.5</u>	15	4000	0	1
1E6/A2-YLG	TOPS	2.6	7.5	15	4000	0	1
1E6/A2-MVW	TOPS	<u>2</u>	<u>7.5</u>	15	4000	0	1
1E6/A2-MVW	TOPS	2.46	6	15	4000	0	1
1E6/A2-RQF(I)	TOPS	<u>1.9</u>	<u>7.5</u>	15	4000	0	1
1E6/A2-RQF(I)	TOPS	2	7	15	4000	0	1
1E6/A2/RQF(A)	TOPS	<u>1.9</u>	<u>7</u>	15	4000	0	1
GP100/A2-YLE	JBScreen	2		20	3350	0	1
ILA/A2-ILA	TOPS	<u>3.06</u>	<u>7</u>	20	8000	0	1
ILA/A2-ILA	TOPS	2.57	7	20	8000	0	1
AS01/A2-GLC	TOPS	<u>2.56</u>	<u>6</u>	20	4000	0	1

TCR/pMHC complexes I obtained are in bold and underlined. One dataset represents a full diffraction dataset obtained from one particular crystal growing condition for a given complex and usable to solve, analyze and publish the structure. We often collected several datasets from the same condition for a particular complex but only one is included in the table in order to avoid any redundancy in the analysis.

^a Presence of salt was described as “1” and absence of salt was described as “0”

Appendix 3: Frequency of appearance of the 29 different conditions where we obtained TCR/pMHC complexes

Condition n°	pH	PEG (%)	PEG	Salt ^a	Frequency (%)
1	7.0	25	1500	0	2.0
2	6.0	15	4000	0	3.9
3	6.5	15	4000	0	2.0
4	7.0	15	4000	0	2.0
5	7.5	15	4000	0	2.0
6	8.0	15	4000	0	2.0
7	7.0	20	4000	0	2.0
8	7.5	25	4000	0	2.0
9	8.5	25	4000	0	2.0
10	7.5	15	8000	0	2.0
<u>11</u>	<u>6.5</u>	<u>20</u>	<u>3350</u>	<u>1</u>	<u>5.9</u>
12	7.5	20	3350	1	3.9
13	5.5	15	4000	1	2.0
<u>14</u>	<u>6.0</u>	<u>15</u>	<u>4000</u>	<u>1</u>	<u>5.9</u>
<u>15</u>	<u>6.5</u>	<u>15</u>	<u>4000</u>	<u>1</u>	<u>5.9</u>
<u>16</u>	<u>7.0</u>	<u>15</u>	<u>4000</u>	<u>1</u>	<u>7.8</u>
<u>17</u>	<u>7.5</u>	<u>15</u>	<u>4000</u>	<u>1</u>	<u>11.8</u>
18	6.0	20	4000	1	2.0
<u>19</u>	<u>7.0</u>	<u>20</u>	<u>4000</u>	<u>1</u>	<u>11.8</u>
20	7.5	20	4000	1	2.0
21	8.5	25	4000	1	2.0
22	5.0	20	6000	1	2.0
23	6.0	20	6000	1	2.0
24	7.0	20	6000	1	2.0
25	6.0	15	8000	1	2.0
26	6.5	15	8000	1	2.0
27	7.0	15	8000	1	2.0
28	7.0	20	8000	1	3.9
29	7.0	25	8000	1	2.0

The conditions producing more than 5% of the datasets (conditions n°11, 14, 15, 16, 17 and 19) are in bold and underlined.

^a Presence of salt was described as “1” and absence of salt was described as “0”

Appendix 4: $\alpha 24\beta 17$ TCR/A2-ELA contacts

Peptide	TCR	H-bonds ($\leq 3.2\text{\AA}$)	H-bonds (3.2 \AA -3.4 \AA)	vdW (3.2 \AA – 3.5 \AA)	vdW (3.5 \AA - 4 \AA)
Glu1 ^{Oe2/H2O}	α Gly29 ^{O/H2O}	1	1		2
Glu1 ^{H2O}	α Gln31 ^{H2O}		1		2
Leu2 ^O	α Gln31 ^{Ne2}	1			1
Ala3	α Gln31				2
Ala3	β Leu98			1	
Gly4 ^N	α Gln31 ^{Oe1}	1		2	3
Gly4 ^{H2O}	α Ser32 ^{H2O}	1	1		
Gly4 ^{H2O}	α Asn92 ^{H2O}	1			
Gly4	β Leu98				2
Ile5	α Tyr51				1
Ile5	β Leu98			2	
Ile5	β Met100				1
Gly6 ^N	β Leu98 ^O	1			
Ile7	β Gly97			2	
Ile7 ^{NO}	β Leu98 ^{ON}	2			6
Leu8	β Gly99				1
Thr9	β Thr96				2
MHC	TCR	H-bonds ($\leq 3.2\text{\AA}$)	H-bonds (3.2 \AA -3.4 \AA)	vdW (3.2 \AA – 3.5 \AA)	vdW (3.5 \AA - 4 \AA)
Glu58	α Phe27				4
Gly62	α Asp93				1
Arg65	β Ile56				2
Arg65 ^{NH2}	α Asp93 ^O	1			3
Arg65 ^{Ne}	α Gly94 ^O	1		2	3
Arg65	α Arg96				7
Lys66 ^{H2O}	α Gly29 ^{H2O}	1			
Lys66 ^{H2O}	α Gly31 ^{H2O}		1		1
Lys66 ^{H2O}	α Asp93 ^{H2O}	1			
Lys66	α Gly94				1
Ala69	β Tyr49				1
Ala69	β Ile56				2
Ala69	β Leu98				1
His70	β Leu98				2
Gln72	β Gly51			2	1
Gln72 ^{Oe1}	β Pro52 ^N	1		1	3
Gln72 ^{Oe1}	β Phe53 ^N	1			4
Gln72 ^{Ne2}	β Gly54 ^O		1		
Gln72	β Ile56				2
Thr73	β Gly97			2	
Arg75	β Phe53			2	11
Val76	β Asn30			1	
Val76	β Phe53				3
Glu154	α Tyr51			1	2
Gln155	α Tyr51				3
Gln155	β Gly99				1
Gln155 ^{H2O}	β Met100 ^{H2O}	1			2
Arg157	α Arg52			1	2
Ala158	α Tyr51				2
Tyr159	α Gln31			1	
Thr163 ^{H2O}	α Gln31 ^{H2O}	1			2
Thr163	α Lys66 ^{Nc}		1		
Trp167	α Leu28				3
Trp167	α Gly29				2
Arg170	α Leu28			1	1

Appendix 5: α 24 β 17 TCR/A2-ELA4A contacts

Peptide	TCR	H-bonds ($\leq 3.2\text{\AA}$)	H-bonds (3.2 \AA - 3.4 \AA)	vdW (3.2 \AA - 3.5 \AA)	vdW (3.5 \AA - 4 \AA)
Glu1 ^{Oϵ2/H₂O}	α Gly29 ^{O/H₂O}	1	1		2
Glu1 ^{Oϵ2}	α Gln31 ^{Nϵ2}		1		2
Leu2 ^O	α Gln31 ^{Nϵ2}	1			1
Ala3	α Gln31				2
Ala4 ^N	α Gln31 ^{Oϵ1}	1			6
Ala4 ^{H₂O}	α Ser32 ^{H₂O}	1			
Ala4 ^{H₂O}	α Asn92 ^{H₂O}		1		
Ala4	β Leu98				2
Ile5	α Tyr51				1
Ile5	β Leu98			2	
Ile5	β Met100				1
Gly6 ^N	β Leu98 ^O		1		
Ile7	β Gly97			2	
Ile7 ^{N/O}	β Leu98 ^{O/N}	2			7
Thr9	β Thr96			1	
MHC	TCR	H-bonds ($\leq 3.2\text{\AA}$)	H-bonds (3.2 \AA - 3.4 \AA)	vdW (3.2 \AA - 3.5 \AA)	vdW (3.5 \AA - 4 \AA)
Glu58	α Phe27				4
Gly62	α Asp93				1
Arg65	β Ile56				2
Arg65 ^{NH₂}	α Asp93 ^{O/Oδ2}	1	1SB		3
Arg65	α Arg96				8
Lys66 ^{H₂O}	α Gly29 ^{H₂O}	1			
Lys66	α Gln31				1
Lys66	α Gly94				3
Lys68 ^{H₂O}	β Ile56 ^{H₂O}	1			
Ala69	β Tyr49				1
Ala69	β Leu98				2
His70	β Leu98				1
Gln72	β Gly51			2	1
Gln72 ^{Oϵ1}	β Pro52 ^N	1		1	3
Gln72 ^{Oϵ1}	β Phe53 ^N	1			5
Gln72 ^{Nϵ2}	β Gly54 ^O		1		1
Gln72	β Ile56				2
Thr73	β Gly97			1	1
Arg75	β Phe53			2	15
Val76	β Asn30				1
Val76	β Phe53				2
Glu154 ^{Oϵ1/Oϵ2}	α Tyr51 ^{OH}	2			7
Gln155	α Tyr51				4
Gln155	β Gly99				1
Gln155 ^{H₂O}	β Met100 ^{H₂O}	1			2
Ala158	α Tyr51				2
Tyr159	α Gln31				1
Thr163 ^{H₂O}	α Gln31 ^{H₂O}	1			2
Trp167	α Leu28				4
Trp167	α Gly29				2
Arg170	α Leu28				3

SB: salt bridge

Appendix 6: α 24 β 17 TCR /A2-ELA7A contacts

Peptide	TCR	H-bonds ($\leq 3.2\text{\AA}$)	H-bonds (3.2 \AA - 3.4 \AA)	vdW (3.2 \AA - 3.5 \AA)	vdW (3.5 \AA - 4 \AA)
Glu1 ^{Oϵ2}	α Gly29 ^O		1	1	1
Glu1 ^{Oϵ2}	α Gln31 ^{Nϵ2}	1			1
Leu2 ^O	α Gln31 ^{Nϵ2}	1			2
Ala3	α Gln31				4
Ala3	β Leu98			1	
Gly4 ^N	α Gln31 ^{Oϵ1}	1		2	3
Gly4	β Leu98				2
Ile5	β Leu98			1	1
Ala6 ^N	β Leu98 ^O	1			2
Ala7	β Gly97				2
Ala7 ^{N/O}	β Leu98 ^{O/N}	2			6
Leu8	β Thr96				1
Leu8	β Leu98				1
Leu8	β Gly99				1
Thr9	β Thr96			1	1
MHC	TCR	H-bonds ($\leq 3.2\text{\AA}$)	H-bonds (3.2 \AA - 3.4 \AA)	vdW (3.2 \AA - 3.5 \AA)	vdW (3.5 \AA - 4 \AA)
Arg44 ^{H2O}	β Ser58 ^{H2O}	1			
Glu58	α Phe27				4
Gly62	α Asp93				1
Arg65	β Ile56				2
Arg65 ^{H2O}	β Ser58 ^{H2O/H2O}	2			
Arg65 ^{NH2}	α Asp93 ^O	1			3
Arg65 ^{Nϵ}	α Gly94 ^O	1		1	3
Arg65	α Arg96			1	6
Lys66	α Gly94				2
Lys66	α Leu98				1
Lys68	β Ile56				1
Ala69	β Tyr49				1
Ala69	β Leu98			1	
His70	β Leu98				1
Gln72	β Gly51			2	1
Gln72 ^{Oϵ1}	β Pro52 ^N	1		1	3
Gln72 ^{Oϵ1}	β Phe53 ^N	1			8
Gln72 ^{Nϵ1}	β Gly54 ^O	1			4
Gln72	β Ile56				2
Arg75	β Phe53			1	13
Val76	β Asn30				1
Val76	β Phe53			1	1
Glu154	α Tyr51				3
Gln155	α Tyr51				3
Gln155	β Gly99				1
Gln155 ^{H2O}	β Met100 ^{H2O}	1			3
Ala158	α Tyr51				2
Tyr159	α Gln31				1
Thr163 ^{H2O}	α Gln31 ^{H2O}	1			3
Trp167	α Gly29				2
Arg170	α Leu28			1	1

Appendix 7: $\alpha 24\beta 17$ TCR /A2-EAA contacts

Peptide	TCR	H-bonds ($\leq 3.2\text{\AA}$)	H-bonds (3.2 \AA - 3.4 \AA)	vdW (3.2 \AA - 3.5 \AA)	vdW (3.5 \AA - 4 \AA)
Glu1 ^{Oe2}	α Gly29 ^O	1		1	2
Glu1 ^{Oe2}	α Gln31 ^{Ne2}		1SB		2
Ala2 ^O	α Gln31 ^{Ne2}	1			
Ala3	α Gln31				2
Ala3	β Leu98			1	
Gly4 ^N	α Gln31 ^{Oe1}	1		1	3
Gly4	β Leu98				2
Ile5	α Gln31				1
Ile5	α Ser32				1
Ile5	α Tyr51				2
Ile5	β Leu98			2	
Gly6 ^N	β Leu98 ^O	1			2
Ile7	β Gly97			1	1
Ile7 ^{NO}	β Leu98 ^{ON}	2		1	5
Thr9	β Thr96				1
MHC	TCR	H-bonds ($\leq 3.2\text{\AA}$)	H-bonds (3.2 \AA - 3.4 \AA)	vdW (3.2 \AA - 3.5 \AA)	vdW (3.5 \AA - 4 \AA)
Glu58	α Phe27			1	3
Gly62	α Asp93				1
Arg65 ^{NH2}	α Asp93 ^O	1		1	3
Arg65 ^{Ne}	α Gly94 ^O	1		2	3
Arg65	α Arg96			2	14
Arg65	β Ile56				1
Arg65	β Ser57				3
Lys66	α Gln31				1
Lys66	α Gly94				1
Lys66	β Leu98				1
Lys68	β Ile56				1
Ala69	β Tyr49			1	
Ala69	β Leu98				2
His70	β Leu98				2
Gln72	β Gly51			2	2
Gln72 ^{Oe1}	β Pro52 ^N	1		1	3
Gln72 ^{Oe1}	β Phe53 ^N	1			6
Gln72 ^{Ne2}	β Gly54 ^O		1		3
Gln72	β Ile56			1	2
Arg73	β Gly97			1	1
Arg75	β Phe53			1	17
Val76	β Asn30				1
Val76	β Phe53				2
Val76	β Thr96				1
Glu154	α Tyr51			1	2
Gln155	α Tyr51				6
Gln155	β Gly99				1
Gln155	β Met100				3
Arg157	α Arg52				2
Ala158	α Tyr51				1
Tyr159	α Gln31			1	
Thr163	α Gln31				3
Trp167	α Leu28				2
Trp167	α Gly29				2
Arg170	α Leu28				1

SB: salt bridge

Appendix 8: $\alpha 24\beta 17$ TCR /A2-AAG contacts

Peptide AAG bulged	TCR	H-bonds ($\leq 3.2\text{\AA}$)	H-bonds (3.2 \AA - 3.4 \AA)	vdW (3.2 \AA - 3.5 \AA)	vdW (3.5 \AA - 4 \AA)
Ala1 ^O	α Gln31 ^{Ne2}		1		
Ala2	α Gln31			3	4
Ala2	β Leu98				2
Gly3 ^N	α Gln31 ^{Oe1/Ne2}	1	1	2	2
Gly3	β Leu98			3	2
Gly3	β Gly99				1
Ile4	α Gln31				3
Ile4	α Ser32				1
Ile4	α Tyr51				1
Ile4	β Leu98			1	1
Gly5 ^N	β Leu98 ^O	1			2
Ile6	β Thr96				1
Ile6	β Gly97			2	
Ile6 ^{N/O}	β Leu98 ^{O/N}	2		2	7
Thr8	β Thr96			2	
Peptide AAG stretched	TCR	H-bonds ($\leq 3.2\text{\AA}$)	H-bonds (3.2 \AA - 3.4 \AA)	vdW (3.2 \AA - 3.5 \AA)	vdW (3.5 \AA - 4 \AA)
Ala2 ^O	α Gln31 ^{Ne2}	1			3
Gly3	α Gln31				2
Gly3	β Leu98				1
Ile4 ^N	α Gln31 ^{Oe1}	1		2	2
Ile4	α Asn92			1	1
Ile4	α Gly94				1
Ile4	α Gly95				1
Ile4	β Leu98				5
Gly5 ^N	β Leu98 ^O		1	2	
Ile6	β Gly97				2
Ile6 ^{N/O}	β Leu98 ^{O/N}	2		1	6
Thr8	β Thr96			2	
MHC	TCR	H-bonds ($\leq 3.2\text{\AA}$)	H-bonds (3.2 \AA - 3.4 \AA)	vdW (3.2 \AA - 3.5 \AA)	vdW (3.5 \AA -4 \AA)
Glu58	α Phe27				3
Gly62	α Asp93				1
Arg65 ^{NH2}	α Asp93 ^{O/Oe1}	1	1SB	1	3
Arg65 ^{Ne}	α Gly94 ^O	1		1	6
Arg65	α Arg96			3	10
Arg65	β Ile56				1
Arg65	β Ser57				3
Lys66	α Gln31				1
Lys66	α Gly94				2
Lys66	β Leu98				1
Lys68	β Ile56			1	1
Ala69	β Tyr49				1
Ala69	β Ile56				1
Ala69	β Leu98			1	1
His70	β Leu98			1	
Gln72	β Gly51			2	2
Gln72 ^{Oe1}	β Pro52 ^N		1	1	3
Gln72 ^{Oe1}	β Phe53 ^N	1		1	6
Gln72 ^{Ne2}	β Gly54 ^O	1			5
Gln72	β Ile56			1	1
Arg75	β Phe53			5	16
Val76	β Asn30			1	1
Val76	β Phe53			1	1
Glu154	α Tyr51				4

Gln155	α Tyr51				5
Gln155	β Gly99				1
Gln155	β Met100				3
Ala158	α Tyr51				2
Tyr159	α Gln31			1	3
Thr163	α Lys67				1
Glu166 ^{Nϵ1/Nϵ2}	α Lys67 ^{Nϵ}	1	1SB	1	
Trp167	α Gly29				2
Arg170	α Leu28				1

SB: salt bridge

Appendix 9: MEL5 TCR /A2-EAA contacts

Peptide	TCR	H-bonds ($\leq 3.2\text{\AA}$)	H-bonds (3.2 \AA - 3.4 \AA)	vdW (3.2 \AA - 3.5 \AA)	vdW (3.5 \AA - 4 \AA)
Glu1 ^{Oe2}	α Gly29 ^O		1		3
Glu1 ^{Oe2}	α Gln31 ^{Ne2}		1SB		1
Ala2 ^O	α Gln31 ^{Ne2}		1		
Ala3	α Gln31				1
Gly4 ^N	α Gln31 ^{Oe1}	1		2	4
Gly4	α Asn92				1
Gly4	β Leu98			1	3
Ile5	α Gln31			1	2
Ile5	α Ser32				1
Ile5	α Asn92				1
Ile5	β Leu98				2
Ile5	β Gly99			1	2
Gly6 ^N	β Leu98 ^O	1			2
Ile7	β Gly97				2
Ile7 ^{N/O}	β Leu98 ^{O/N}	2		1	8
Ile7	β Gly99				1
Leu8	β Gly99			1	1
Thr9	β Thr96				1
MHC	TCR	H-bonds ($\leq 3.2\text{\AA}$)	H-bonds (3.2 \AA - 3.4 \AA)	vdW (3.2 \AA - 3.5 \AA)	vdW (3.5 \AA - 4 \AA)
Gly62	α Ala94			1	4
Arg65 ^{Ne/NH2}	α Ala94 ^O	1	1	3	3
Arg65	α Lys96				3
Arg65	β Tyr49			1	5
Arg65 ^{NH1}	β Glu59 ^{Oe2}		1SB		2
Lys66	α Gln31			1	
Lys66	β Leu98				1
Lys68	β Tyr49				2
Lys68	β Ser57				1
Ala69	β Leu98				3
His70	β Leu98				1
Gln72	β Val51				2
Gln72	β Gln55			1	
Thr73	β Gly97				1
Arg75	β Gln55				1
Val76	β Asn30			1	3
His151	α Tyr51				1
Glu154	α Tyr51				3
Gln155	α Tyr51				6
Gln155	β Gly99			1	2
Gln155 ^{Oe1}	β Thr100 ^N		1	1	4
Ala158	α Tyr51			1	1
Tyr159	α Gln31			1	2
Thr163	α Gln31				3
Glu166 ^{Oe2}	α Arg28 ^{NH2}		1SB		4
Trp167	α Arg28				1
Trp167	α Gly29				2

SB: salt bridge

Appendix 10: MEL5 TCR /A2-AAG contacts

Peptide AAG bulged	TCR	H-bonds ($\leq 3.2\text{\AA}$)	H-bonds (3.2 \AA - 3.4 \AA)	vdW (3.2 \AA - 3.5 \AA)	vdW (3.5 \AA - 4 \AA)
Ala2	α Gln31				1
Ala2	β Leu98				1
Gly3 ^N	α Gln31 ^{Oe1}	1		1	3
Gly3	β Leu98			1	4
Ile4	β Leu98			1	
Ile4	β Gly99			2	2
Gly5 ^N	β Leu98 ^O	1			2
Ile6	β Gly97				2
Ile6 ^{N/O}	β Leu98 ^{O/N}	2			5
Leu7	β Gly99				2
Thr8	β Thr96				2
Peptide AAG stretched	TCR	H-bonds ($\leq 3.2\text{\AA}$)	H-bonds (3.2 \AA - 3.4 \AA)	vdW (3.2 \AA - 3.5 \AA)	vdW (3.5 \AA - 4 \AA)
Ala2 ^O	α Gln31 ^{Oe1}	1			
Gly3	β Leu98				1
Ile4	α Gln31			2	6
Ile4	β Leu98			1	3
Gly5 ^N	β Leu98 ^O	1		2	1
Gly5	β Gly99				1
Ile6	β Gly97				2
Ile6 ^{N/O}	β Leu98 ^{O/N}	2			6
Leu7	β Gly99				2
Thr8	β Thr96				2
MHC	TCR	H-bonds ($\leq 3.2\text{\AA}$)	H-bonds (3.2 \AA - 3.4 \AA)	vdW (3.2 \AA - 3.5 \AA)	vdW (3.5 \AA - 4 \AA)
Gly62	α Ala94			1	3
Arg65 ^{Ne}	α Ala94 ^O	1		2	5
Arg65	α Gly95				1
Arg65	α Lys96				4
Arg65	β Tyr49			2	3
Arg65 ^{NH1}	β Glu59 ^{Oe1}	1			
Lys66	β Leu98				1
Ala69	β Leu98			1	1
His70	β Leu98				1
Gln72	β Val51			1	1
Gln72	β Gln55				1
Thr73	β Gly97			1	1
Arg75 ^{NH1}	β Gln55 ^{Oe1}			1	
Val76	β Asn30			1	2
Glu154	α Tyr51				3
Gln155	α Tyr51			1	5
Gln155	β Gly99			1	2
Gln155 ^{Oe1}	β Thr100 ^N	1		1	3
Ala158	α Tyr51				1
Tyr159	α Gln31				1
Thr163	α Gly29				1
Thr163 ^{Oy1}	α Gln31 ^{Ne2}	1			2
Glu166 ^{Oe2}	α Arg28 ^{NH2}		1SB		

SB: salt bridge

Appendix 11: Detailed analysis of Mel5/A2-AAG, Mel5/A2-EAA, α 24 β 17/A2-AAG and α 24 β 17/A2-EAA buried surface area and contacts

TCR-MHC	MEL5/A2-AAG bulged	MEL5/A2-AAG stretched	MEL5/A2-EAA	α 24 β 17/A2-AAG bulged	α 24 β 17/A2-AAG stretched	α 24 β 17/A2-EAA
Total No. contacts ^a	4/1/55	4/1/55	3/2/73	6/2/114	6/2/114	5/0/112
No. MHC α 1 helix contacts ^a	2/0/34	2/0/34	2/1/40	5/1/90	5/1/90	5/0/87
No. MHC α 2 helix contacts ^a	2/1/21	2/1/21	1/1/33	1/1/24	1/1/24	0/0/25
No. V $_{\alpha}$ contacts ^a	2/1/30	2/1/30	2/1/40	3/2/51	3/2/51	2/0/53
CDR1 $_{\alpha 27-32}$ ^a	1/1/4	1/1/4	0/1/14	0/0/11	0/0/11	0/0/14
CDR2 $_{\alpha 50-54}$ ^a	0/0/10	0/0/10	0/0/12	0/0/11	0/0/11	0/0/12
FW $_{\alpha 67-71}$ ^a	0/0/0	0/0/0	0/0/0	1/1/2	1/1/2	0/0/0
CDR3 $_{\alpha 89-100}$ ^a	1/0/16	1/0/16	2/0/14	2/1/27	2/1/27	2/0/27
No. V $_{\beta}$ contacts ^a	2/0/25	2/0/25	1/1/33	3/0/63	3/0/63	3/0/59
CDR1 $_{\beta 27-32}$ ^a	0/0/3	0/0/3	0/0/4	0/0/2	0/0/2	0/0/1
CDR2 $_{\beta 49-59}$ ^a	1/0/9	1/0/9	0/1/15	3/0/53	3/0/53	3/0/46
CDR3 $_{\beta 91-106}$ ^a	1/0/13	1/0/13	1/0/14	0/0/8	0/0/8	0/0/12
BSA ^b (\AA^2)	789/831	788/837	804/880	980/964	980/971	913/920
TCR-peptide	MEL5/A2-AAG bulged	MEL5/A2-AAG stretched	MEL5/A2-EAA	α 24 β 17/A2-AAG bulged	α 24 β 17/A2-AAG stretched	α 24 β 17/A2-EAA
Total No. contacts ^a	4/0/29	4/0/29	6/1/43	6/0/42	5/0/32	6/1/31
No. V $_{\alpha}$ contacts ^a	1/0/5	1/0/8	3/1/17	3/0/16	2/0/13	3/1/15
CDR1 $_{\alpha 27-32}$ ^a	1/0/5	1/0/8	3/1/15	3/0/15	2/0/9	3/1/13
CDR2 $_{\alpha 50-54}$ ^a	0/0/0	0/0/0	0/0/0	0/0/1	0/0/0	0/0/2
CDR3 $_{\alpha 89-100}$ ^a	0/0/0	0/0/0	0/0/2	0/0/0	0/0/4	0/0/0
No. V $_{\beta}$ contacts ^a	3/0/24	3/0/21	3/0/26	3/0/26	3/0/19	3/0/16
CDR3 $_{\beta 91-106}$ ^a	3/0/24	3/0/21	3/0/26	3/0/26	3/0/19	3/0/16
BSA ^c (\AA^2)	240/415	162/383	308/374	251/431	255/407	313/382

^a Number of hydrogen bonds (H-bond) ($\leq 4\text{\AA}$) / salt bridges ($\leq 4\text{\AA}$) / van der Waals (vdW) (3.2-4 \AA) contacts calculated with CONTACT program from the CCP4 package

^b Buried surface area (BSA) (\AA^2) of V $_{\alpha}$ -MHC / V $_{\beta}$ -MHC calculated with PISA program from the CCP4 package

^c Buried surface area (BSA) (\AA^2) of V $_{\alpha}$ -peptide / V $_{\beta}$ -peptide calculated with PISA program from the CCP4 package

Appendix 12: MEL5 β wt, MEL5 β 5, MEL5 β 9, MEL5 β 12, MEL5 β 13, MEL5 β 15 and MEL5 β 17 sequences for lentiviral expression

Mutations from MEL5 β wt are in bold and underlined.

MEL5 β wt:

MLCSLLALLLGTFFGVRSQTIHQWPATLVQPVGSPSLECTVEGTSNPPLYW
YRQAAGRGLQLLFYSVGIGQISSEVPQNLSASRPQDRQFILSSKLLLLSDSGF
YLCAWSETGLGTGELFFGEGSRLTVLEDLKNVFPPEVAVFEPSEAEISHTQK
ATLVCLATGFYDPDHVELSWVNGKEVHSGVCTDPQPLKEQPALNDSRYCL
SSRLRVSAATFWQNPRNHFRQCQVQFYGLSENDEWTQDRAKPVTQIVSAEAW
GRADCGFTSESYQQGVLSATILYEILLGKATLYAVLVSALVLMAMVKRKDA
GVLESGSG

MEL5 β 5:

MLCSLLALLLGTFFGVRSQTIHQWPATLVQPVGSPSLECTVEGTSNPPLYW
YRQAAGRGLQLLFYSVGIGQISSEVPQNLSASRPQDRQFILSSKLLLLSDSGF
YLCAWSETGL**GMGGWQ**FGEGSRLTVLEDLKNVFPPEVAVFEPSEAEISHTQ
KATLVCLATGFYDPDHVELSWVNGKEVHSGVCTDPQPLKEQPALNDSRYC
LSSRLRVSAATFWQNPRNHFRQCQVQFYGLSENDEWTQDRAKPVTQIVSAEAW
GRADCGFTSESYQQGVLSATILYEILLGKATLYAVLVSALVLMAMVKRKDA
GVLESGSG

MEL5 β 9:

MLCSLLALLLGTFFGVRSQTIHQWPATLVQPVGSPSLECTVEGTSNPPLYW
YRQAAGRGLQLLFYSVGIGQISSEVPQNLSASRPQDRQFILSSKLLLLSDSGF
YLCAWSETGL**GVGGWE**FGEGSRLTVLEDLKNVFPPEVAVFEPSEAEISHTQ
KATLVCLATGFYDPDHVELSWVNGKEVHSGVCTDPQPLKEQPALNDSRYC
LSSRLRVSAATFWQNPRNHFRQCQVQFYGLSENDEWTQDRAKPVTQIVSAEAW
GRADCGFTSESYQQGVLSATILYEILLGKATLYAVLVSALVLMAMVKRKDA
GVLESGSG

MEL5 β 12:

MLCSLLALLLGTFFGVRSQTIHQWPATLVQPVGSPSLECTVEGTSNPPLYW
YRQAAGRGLQLLFYSVGIGQISSEVPQNLSASRPQDRQFILSSKLLLLSDSGF
YLCAWSETGL**NLGGWF**FGEGSRLTVLEDLKNVFPPEVAVFEPSEAEISHTQ
KATLVCLATGFYDPDHVELSWVNGKEVHSGVCTDPQPLKEQPALNDSRYC
LSSRLRVSAATFWQNPRNHFRQCQVQFYGLSENDEWTQDRAKPVTQIVSAEAW
GRADCGFTSESYQQGVLSATILYEILLGKATLYAVLVSALVLMAMVKRKDA
GVLESGSG

MEL5 β13:

MLCSLLALLLGTFFGVRSQTIHQWPATLVQPVGSPSLECTVEGTSNPPLYW
YRQAAGRGLQLLFYSVGIGQISSEVPQNLSASRPQDRQFILSSKLLLLSDSGF
YLCAWSETGLNVSGWFFGEGSRLTVLEDLKNVFPPEVAVFEPSEAEISHTQK
ATLVCLATGFYDPDHVELSWVWNGKEVHSGVCTDPQPLKEQPALNDSRYCL
SSRLRVSATFWQNPRNHFRQCQVQFYGLSENDEWTQDRAKPVTQIVSAEAW
GRADCGFTSESYQQGVLSATILYEILLGKATLYAVLVSALVLMAMVKRKDA
GVLESGSG

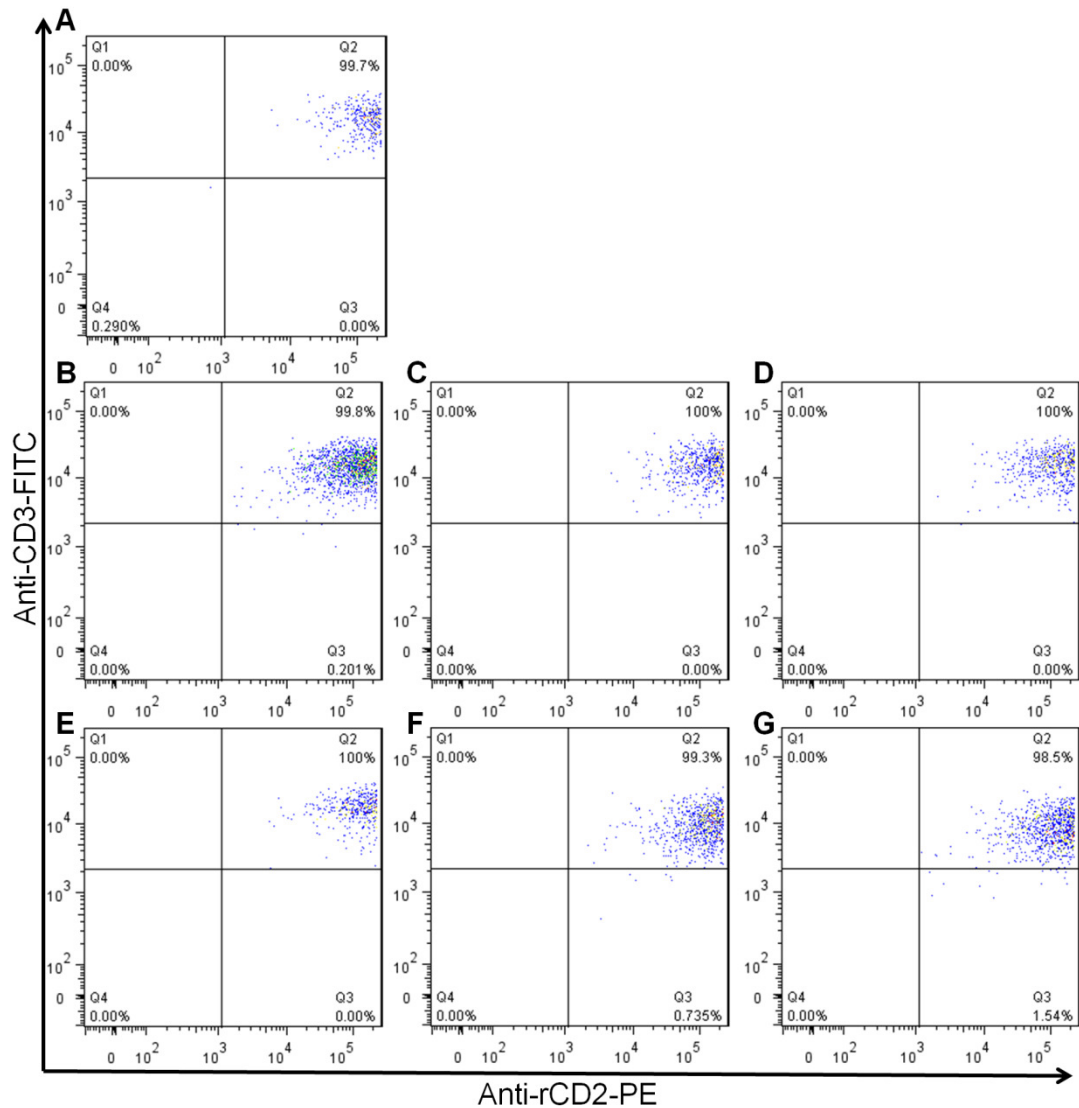
MEL5 β15:

MLCSLLALLLGTFFGVRSQTIHQWPATLVQPVGSPSLECTVEGTSNPPLYW
YRQAAGRGPQLLFYYGPFGQISSEVPQNLSASRPQDRQFILSSKLLLLSDSGF
YLCAWSETGLGMGGWQFGEGSRLTVLEDLKNVFPPEVAVFEPSEAEISHTQ
KATLVCLATGFYDPDHVELSWVWNGKEVHSGVCTDPQPLKEQPALNDSRYC
LSSRLRVSATFWQNPRNHFRQCQVQFYGLSENDEWTQDRAKPVTQIVSAEAW
GRADCGFTSESYQQGVLSATILYEILLGKATLYAVLVSALVLMAMVKRKDA
GVLESGSG

MEL5 β17:

MLCSLLALLLGTFFGVRSQTIHQWPATLVQPVGSPSLECTVEGTSNPPLYW
YRQAAGRGPQLLFYWGPFGQISSEVPQNLSASRPQDRQFILSSKLLLLSDSG
FYLCWSETGLGMGGWQFGEGSRLTVLEDLKNVFPPEVAVFEPSEAEISHT
QKATLVCLATGFYDPDHVELSWVWNGKEVHSGVCTDPQPLKEQPALNDSRY
CLSSRLRVSATFWQNPRNHFRQCQVQFYGLSENDEWTQDRAKPVTQIVSAEA
WGRADCGFTSESYQQGVLSATILYEILLGKATLYAVLVSALVLMAMVKRK
DAGVLESGSG

Appendix 13: Anti-CD3 sorting of transduced Jurkat TCR negative GLuc



Jurkat TCR negative GLuc transduced with rCD2 and (A) MEL5, (B) MEL5 β 5, (C) MEL5 β 9, (D) MEL5 β 12, (E) MEL5 β 13, (F) MEL5 β 15 and (G) MEL5 β 17 were sorted as described in **Chapter 2** with anti-CD3 antibodies. Staining with anti-CD3-FITC and anti-rCD2-PE followed by FACS analysis revealed that the populations were 100% double positive.